

***Air-sea Exchange of CO₂ over the
Antarctic Seasonal Ice Zone***

by

Helen Mary Beggs, Bsc (Hons), MSc

Submitted in fulfilment of the requirements for the degree of
Doctor of Philosophy

Antarctic CRC

and

Institute of Antarctic and Southern Ocean Studies

University of Tasmania

Hobart

Australia

December, 1995

for Brad

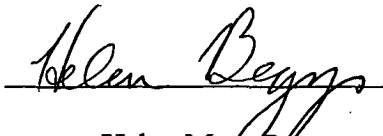


"Looking towards the sun in the vessel's wake, the leads formed a mesh of waterways - chains of silver which linked together burnished lakes, like jewels on the bosom of the world."

*Frank Hurley,
Shackleton's Argonauts*

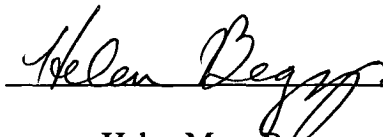
DECLARATION

This is to certify that the material comprising this thesis has never been accepted for any other degree or award in any tertiary institution and, to the best of my knowledge and belief, is solely the work of the author and contains no material previously published or written by another person, except where due reference is made in the text.


Helen Mary Beggs

AUTHORITY OF ACCESS

This thesis may be made available for loan and limited copying in accordance with the Copyright Act 1968.


Helen Mary Beggs

ABSTRACT

The Antarctic Seasonal Ice Zone (ASIZ) is potentially a large contemporary sink for anthropogenic CO₂ due to the formation of bottom water along the Antarctic coast. However, south of 55°S, the lack of measurements of the fugacity of CO₂ in surface seawater ($f\text{CO}_2$), or the concentration and ratio of stable carbon isotopes of atmospheric CO₂, has meant that it has been difficult to determine whether the ASIZ acts as a net source or sink for atmospheric CO₂. This study contributes to, and is largely based on, new measurement programmes of oceanic $f\text{CO}_2$ and the concentration and $^{13}\text{C}/^{12}\text{C}$ ratio of atmospheric CO₂ over the region of the Southern Ocean between Australia and the Antarctic continent, with particular emphasis on data from regions of pack ice.

Using $f\text{CO}_2$ data from six voyages of the *RSV Aurora Australis*, it was estimated that between 1 October 1992 and 31 March 1993 the ocean south of 55°S, between 60°E and 150°E, sequestered 0.025 ± 0.013 Gt C over an area of ocean equivalent to 19% of the maximum area of open water south of 55°S. The CO₂ sink was most pronounced west of 105°E (0.026 ± 0.013 Gt C), where it was associated with intense summer phytoplankton blooms following the melting of sea-ice.

In conjunction with the sampling of oceanic $f\text{CO}_2$, flasks were regularly filled on the ship with dry air and later analysed for levels of CO₂ and its $^{13}\text{C}/^{12}\text{C}$ ratio. This provided the opportunity to observe atmospheric variations directly forced by fluctuations in $f\text{CO}_2$, temperature, and the $^{13}\text{C}/^{12}\text{C}$ ratio of dissolved inorganic carbon (DIC) in the surface ocean.

Sea surface temperature and $^{13}\text{C}/^{12}\text{C}$ -DIC effects are transmitted to the atmosphere by gross air-sea fluxes of CO₂ in the absence of net exchange. Over the ice-free region of the Southern Ocean between 44°S and 60°S, from 85°E to 160°E, atmospheric $^{13}\text{CO}_2/^{12}\text{CO}_2$ values were dominated by a linear dependence on sea surface temperature (0.0041 ± 0.0003 ‰ °C⁻¹), due to the “equilibrium” isotopic fractionation of CO₂ during air-sea exchange. During late spring and summer, over the region of the ASIZ

south of 60°S, between 60°E and 105°E, the effect of sea surface temperature on atmospheric $^{13}\text{CO}_2/^{12}\text{CO}_2$ values was overwhelmed by the effect of high marine productivity on $^{13}\text{C}/^{12}\text{C}$ -DIC.

It is demonstrated that the impact of net air-sea flux of $^{13}\text{CO}_2$ on atmospheric ratios of $^{13}\text{CO}_2/^{12}\text{CO}_2$ can be measured more easily than the impact of net CO_2 flux on atmospheric mixing ratios of CO_2 . Long-term changes in sea surface temperature and productivity over the ASIZ, and therefore net ocean uptake, can be more accurately determined from isotopic ratios of $^{13}\text{CO}_2/^{12}\text{CO}_2$ in baseline air samples from a coastal Antarctic station, than from mixing ratios of CO_2 in the same samples.

ACKNOWLEDGMENTS

My thanks go to my supervisors, Garth Paltridge, Roger Francey and Bronte Tilbrook, for their support and encouragement. I would also like to thank Bill Budd for many fruitful discussions regarding the thesis, and Patrick Monfray, Peter Rayner and Pieter Tans for their advice regarding the mass balance modeling. Kathy Haskard very generously helped with the calculation of errors.

This project is the culmination of the efforts of many people, and has drawn upon the resources and data sets of many organizations, to all of whom I am very grateful. Roger Francey and Paul Steele of CSIRO Division of Atmospheric Research supplied the air sampling pump and flasks to be used on the *RSV Aurora Australis*, and analysed air samples for the concentration of CO₂ and its ¹³C/¹²C ratio, with the help of Colin Allison, Ray Langenfelds and Emily Welch. Bronte Tilbrook of CSIRO Division of Oceanography provided the *f*CO₂ continuous monitoring system and much of the oceanic *f*CO₂ data used in this thesis. Mark Pretty assisted with the construction and calibration of the *f*CO₂ system, and David Beardsmore of CSIRO Division of Atmospheric Research calibrated the gas standards used with this experiment. Simon Wright of the Australian Antarctic Division provided chlorophyll *a* data, and Phil Reid and the Australian Bureau of Meteorology provided GASP wind speed data. Brad Phillips and Jonathan Reeve of the Australian Antarctic Division developed and operated the meteorological data logging system on the ship. The help of the officers and crew of *RSV Aurora Australis* and logistic support provided by the Australian Antarctic Division is gratefully acknowledged. I would like to acknowledge the support and financial assistance of the Antarctic CRC, CSIRO Climate Change Research Programme, National Greenhouse Advisory Committee and the Department of the Environment, Sport and Territories.

NOMENCLATURE

- A' = area of ice-free ocean over the region of interest (m^2),
 A = area of open ocean over reservoir a (m^2),
 C = mixing ratio of CO_2 sample at ambient atmospheric pressure (ppmv)
 C_i = mixing ratio of CO_2 sample in IRGA sample cell at pressure p_i (ppmv),
 C_o = mixing ratio of CO_2 gas in the dried equilibrator air stream at 1 atm total pressure (ppmv),
 $C_m(T_o)$ = partial pressure of CO_2 in the undried equilibrator air stream at 1 atm total pressure and temperature T_o (μatm),
 C_a = mixing ratio of CO_2 gas in the dried atmosphere at 20 m a.s.l. and at 1 atm total pressure (ppmv),
 $C_a(z)$ = mixing ratio of CO_2 at height z above sea level over the sampling site (ppmv),
 C_b = CO_2 mixing ratio in the atmosphere above the sampling site unaffected by net air-sea gas exchange (ppmv),
 p_i = pressure in IRGA sample cell (atm),
 p = ambient atmospheric pressure (atm),
 $p_{\text{H}_2\text{O}}$ = saturated vapour pressure of seawater in the equilibrator (atm),
 $p\text{CO}_2$ = partial pressure of CO_2 (μatm),
 T_o = absolute temperature of seawater in equilibrator,
 T_m = absolute temperature of the surface ocean,
 S_m = salinity of the surface ocean (ppt),
 $f\text{CO}_2$ = fugacity of CO_2 (μatm),
 $\Delta f\text{CO}_2 = f_m - f_a$ (μatm),
 f_m = fugacity of CO_2 in the surface ocean (μatm),
 f_a = fugacity of CO_2 in the sea level atmosphere at the sea surface temperature (μatm),
 F = net ocean-to-air flux of CO_2 ($\text{g C m}^{-2} \text{d}^{-1}$),
 N = net transfer of CO_2 from the surface ocean to the atmosphere (g C d^{-1})
 Φ_{ma} = gross ocean-to-air transfer of CO_2 (g C d^{-1}),

- Φ_{am} = gross air-to-ocean transfer of CO_2 (g C d^{-1}),
 K = air-sea gas exchange coefficient for CO_2 ($\text{mol C m}^{-2} \text{ d}^{-1} \mu\text{atm}^{-1}$),
 σ_m = solubility of CO_2 at the sea surface temperature ($\text{mol C m}^{-3} \mu\text{atm}^{-1}$),
 V_p = gas transfer piston velocity of CO_2 gas across the air-sea interface (cm h^{-1}),
 X = proportionality factor where $V_p = X W^2 (\text{Sc}/660)^{-1/2}$ (Wanninkhof, 1992),
 = 0.31 ± 0.15 for “instantaneous” 10 m wind speeds over the open ocean
 (Wanninkhof, 1992; Wanninkhof, pers. com.),
 Sc = Schmidt number,
 W = “instantaneous” or short-term averaged surface wind speed at a height of 10
 m a.s.l. (m s^{-1}),
 W_{ship} = hourly mean wind speeds measured at 32 m a.s.l. from the *RSV Aurora*
Australis, and corrected to 10 m a.s.l. by multiplying by 0.92 (m s^{-1}),
 W_{GASP} = six-hourly surface wind speeds from the Australian Bureau of Meteorology’s
 Global Assimilation and Prediction System analyses (m s^{-1}),
 $P(W)$ = Rayleigh probability function for instantaneous 10 m wind speeds,
 $O(W)$ = observed frequency distribution of wind speed W ,
 R_a = ratio of $^{13}\text{C}/^{12}\text{C}$ in atmospheric CO_2 at 20 m a.s.l.,
 R_m = ratio of $^{13}\text{C}/^{12}\text{C}$ in total dissolved inorganic carbon in the surface ocean,
 R_a^e = the ratio of $^{13}\text{C}/^{12}\text{C}$ in gaseous CO_2 that would be in equilibrium with the
 surface ocean
 = $(\alpha_{ma}/\alpha_{am})R_m$,
 α_{am} = the isotopic fractionation (kinetic) between the atmosphere and the surface
 ocean,
 α_{ma} = the isotopic fractionation (kinetic and thermodynamic) between the surface
 ocean and the atmosphere,
 α_{ma}/α_{am} = the $^{13}\text{C}/^{12}\text{C}$ equilibrium fractionation factor of gaseous CO_2 with respect to
 total dissolved inorganic carbon in seawater
 = $(0.98947 \pm 0.00005) + (0.104 \pm 0.003) \times 10^{-3} \text{ SST}$ (Zhang et al., 1995),
 SST = sea surface temperature ($^{\circ}\text{C}$),

ϵ_{am} = isotopic shift that occurs during air-sea exchange of CO_2 due to kinetic fractionation

$$= (\alpha_{am} - 1) \times 1000 \text{ (‰)},$$

$$\delta^{13}\text{C} = \frac{(^{13}\text{C}/^{12}\text{C})_s - (^{13}\text{C}/^{12}\text{C})_{\text{PDB}}}{(^{13}\text{C}/^{12}\text{C})_{\text{PDB}}} \times 1000 \text{ (‰)},$$

δ_a = $\delta^{13}\text{C}$ of atmospheric CO_2 at 20 m a.s.l. above the sampling site

$$= (R_a/R_{\text{PDB}} - 1) \times 1000 \text{ (‰)},$$

$\delta_a(z)$ = $\delta^{13}\text{C}$ of atmospheric CO_2 at height z above sea level over the sampling site (‰),

δ_b = $\delta^{13}\text{C}$ of atmospheric CO_2 above the sampling site unaffected by gross air-sea gas exchange (‰),

δ_a^e = $\delta^{13}\text{C}$ of gaseous CO_2 that would be in equilibrium with the sea surface

$$= [(0.98947 + 0.104 \times 10^{-3} \text{ SST})(1 + \delta_m/1000) - 1] \times 1000 \text{ ‰},$$

δ_m = $\delta^{13}\text{C}$ of dissolved inorganic carbon in the surface ocean (‰),

^{13}N = net transfer of $^{13}\text{CO}_2$ gas from the ocean to the atmosphere ($\text{g } ^{13}\text{C d}^{-1}$),

$^{13}N_R$ = change in the atmospheric isotopic ratio, R_a , with time, due to air-sea exchange (d^{-1}),

$^{13}N_\delta$ = change in atmospheric $\delta^{13}\text{C}$ with time, due to exchange of CO_2 gas with the ocean (‰ d^{-1}),

z_N = effective mixing height of a perturbation in atmospheric CO_2 mixing ratios caused by net air-sea carbon exchange (m)

$$= \int (C_a(z)/C_a) dz \text{ by definition,}$$

z_G = effective mixing height of a perturbation in atmospheric $\delta^{13}\text{C}$ caused by gross air-sea carbon exchange (m)

$$= \int (\delta_a(z)/\delta_a) dz \text{ by definition,}$$

M_a = mass of atmospheric CO_2 in a volume of horizontal surface area, A , centred on the sampling site, and height z_N (g C),

$D(z_N)$ = effective vertical diffusion coefficient of CO_2 gas at a height z_N

$$= f(N, C_a - C_b) \text{ (g C m}^{-2} \text{ d}^{-1} \text{ ppmv}^{-1}\text{)},$$

$D(z_G)$ = effective vertical diffusion coefficient of CO_2 gas at a height z_G

$$= f(G, C_b(\delta_a - \delta_b)) \text{ (g C m}^{-2} \text{ d}^{-1} \text{ ppmv}^{-1}\text{)},$$

$$G = \varepsilon_{am}(f_m - f_a) + f_m(\delta_a^e - \delta_a) (‰ \mu\text{atm}),$$

$$H = \text{effective diffusion coefficient of CO}_2 \text{ gas in the north-south direction} \\ (\text{g C m}^{-2} \text{ d}^{-1} \text{ ppmv}^{-1}),$$

$$\Delta\delta_a = \text{anomaly in atmospheric } \delta^{13}\text{C} \text{ at 20 m a.s.l. at the sampling site due to marine} \\ \text{productivity} \\ = \delta_a - \delta_a' (‰),$$

$$\delta_a' = \text{atmospheric } \delta^{13}\text{C} \text{ that would be at 20 m a.s.l. at the sampling site for no} \\ \text{algal production in the ocean mixed layer (‰)},$$

$$\Delta\delta_m = \text{anomaly in } \delta^{13}\text{C} \text{ of total dissolved inorganic carbon in the surface ocean at} \\ \text{the sampling site due to marine productivity} \\ = \delta_m - \delta_m' (‰),$$

$$\delta_m' = \delta^{13}\text{C} \text{ of total dissolved inorganic carbon in the surface ocean at the sampling} \\ \text{site for no algal production in the ocean mixed layer (‰)}.$$

LIST OF ILLUSTRATIONS

- Fig. 1.1** The Southern Ocean giving the approximate location of the Antarctic Polar Front (dotted line) and the northern limit of the pack ice (dashed line) (after Tréguer and Jacques, 1992). Shown here in bold type are all stations south of 40°S where atmospheric CO₂ mixing ratios are measured from air samples. Of these, Atmospheric ¹³CO₂/¹²CO₂ ratios are measured from air sampled at Cape Grim, Macquarie Is., Mawson and South Pole. (Figure courtesy of J. Cox, Australian Antarctic Division.) 1-4
- Fig. 1.2** Summary of four commonly used relationships between the gas transfer piston velocity, V_p , and wind speed (at 10 m a.s.l.), for air-sea exchange of CO₂ at 20°C. 1-13
- Fig. 2.1** Schematic of system used to measure the f CO₂ of surface waters. 2-3
- Fig. 2.2** The version of the “Weiss” type equilibrator column used on *RSV Aurora Australis* after 17 October 1992 (after Butler et al. (1988)). 2-5
- Fig. 2.3.** Valve switching sequence over a 180 minute cycle. 2-6
- Fig. 3.1** Hourly averaged values of Δf CO₂ (oceanic f CO₂ - atmospheric f CO₂) measured from the *RSV Aurora Australis* along transects south of 55°S during (a) 15-22 October 1991, 21-28 October 1992, (b) 5-17 November 1992 and 24-30 November 1993, (c) 1-20 December 1993, (d) 10-31 January 1993 and 9-31 January 1994, (e) 1-28 February 1993 and 1-26 February 1994, (f) 1-31 March 1993, and (g) 1-27 April 1993. The solid grey lines denote ice shelves and the dashed lines represent the mean position of the ice edge for those particular months. 3-6
- Fig. 3.2** Hourly averaged Δf CO₂ values measured in the region south of 55°S, between 60°E and 126°E, plotted against concentrations of Chlorophyll a in surface water samples. 3-9
- Fig. 3.3** Hourly averaged Δf CO₂ values measured from the *RSV Aurora Australis* during 15 October 1991 to 26 February 1994 over the region 55° - 70°S, 60° - 150°E, plotted against hourly mean values of sea surface temperature at the water inlet (7.5 m depth). 3-11

- Fig. 4.1** Frequency of occurrence of mean hourly wind speeds measured from *RSV Aurora Australis*, and the corresponding Rayleigh distribution function, for the period 10 January to 31 March 1993 and 9 January to 26 February 1994 over the region 55° - 70°S, 60° - 150°E. 4-5
- Fig. 4.2** Frequency of occurrence of surface wind speeds from six-hourly GASP analyses and the corresponding Rayleigh distribution for the period 1 January to 31 March 1993, over the region 55° - 70°S, 60° - 150°E. 4-6
- Fig. 4.3** Net sea-to-air transfer of CO₂ for (a) October 1992, (b) November 1992, (c) December 1992, (d) January 1993, (e) February 1993, and (f) March 1993. The gas transfer for each 2.5°×2.5° grid square was estimated using the six-hourly surface wind speed outputs of the GASP analyses. Negative values indicate net uptake of carbon dioxide by the surface ocean. 4-13
- Fig. 5.1** Sites where baseline air was sampled from 20 m a.s.l. aboard the *RSV Aurora Australis*, during the period 17 October 1992 to 28 February 1994. 5-2
- Fig. 5.2** Hourly averaged $\Delta f\text{CO}_2$ values measured from the *RSV Aurora Australis* over the region 60° - 160°E, for cruises between 17 October 1992 and 28 February 1994. 5-4
- Fig. 5.3** Atmospheric CO₂ mixing ratios obtained from flasks of air collected aboard the *RSV Aurora Australis* and normalised to 55°S along the same transect for (a) Spring (17 October - 22 November 1992, 2 - 8 October 1993), (b) Summer (5 January - 26 February 1993, 19 November - 27 December 1993, 2 January - 28 February 1994), and (c) Autumn (2 - 28 March 1993, 9 April - 8 May 1993). The filled symbols correspond to cruises into the ASIZ to the west of 105°E, and the unfilled symbols denote cruises east of 105°E. 5-7
- Fig. 5.4** Atmospheric $\delta^{13}\text{C}$ values obtained from air samples collected aboard the *RSV Aurora Australis* and normalised to 55°S along the same transect for (a) Spring (17 October to 22 November 1992, 2 to 8 October 1993), (b) Summer (5 January to 26 February 1993, 19 November to 27 December 1993, 2 January to 28 February 1994), and (c) Autumn (2 to 28 March 1993, 9 April to 8 May 1993). The filled symbols correspond to cruises into the ASIZ to the west of 105°E and the unfilled symbols denote cruises east of 105°E. 5-10

- Fig. 5.5** The deviation in atmospheric CO_2 from its concentration at 55°S , against $\Delta f\text{CO}_2$ normalised to 55°S , for transects between 44°S and 60°S during 17 October 1992 to 28 February 1994. The dashed lines represent the linear regressions (Y on X and X on Y) and the solid line the geometric mean functional regression (Teissier, 1948; Ricker, 1973). 5-11
- Fig. 5.6** Simple zonally averaged atmosphere-ocean model of transfer of CO_2 between the ocean mixed layer and the portion of the atmosphere affected by net air-sea exchange, over an ice-free region of the Southern Ocean of area A , centred on the air sampling site. See pages 5-12 and 5-14 for an explanation of the symbols. 5-13
- Fig. 5.7** Simple illustration of the effective vertical mixing height, z_N , of an anomaly in CO_2 mixing ratio $C_a - C_b$, where C_b is unaffected by net air-sea exchange. 5-13
- Fig. 5.8** The deviation in $\Delta f\text{CO}_2$ from its value at 55°S along the same transect. Fugacities were measured from the *RSV Aurora Australis* during 17 October 1992 to 28 February 1994. 5-16
- Fig. 5.9** Atmospheric $\delta^{13}\text{C}$ normalised to 55°S against normalised sea surface temperatures, for sampling sites between 44°S and 60°S . The dashed lines represent the linear regressions (Y on X and X on Y) and the solid line the geometric mean functional regression (Teissier, 1948; Ricker, 1973). 5-21
- Fig. 5.10** Simple illustration of the effective vertical mixing height, z_G , of an anomaly in atmospheric $\delta^{13}\text{C}$, $\delta_a - \delta_b$, where δ_b is unaffected by fractionation during gross air-sea exchange of CO_2 . 5-22
- Fig. 5.11** The deviation in sea surface temperature from its value at 55°S along the same transect. Sea surface temperatures at 7.5 m depth were measured from the *RSV Aurora Australis* during 17 October 1992 to 28 February 1994. 5-25
- Fig. 5.12** Atmospheric $\delta^{13}\text{C}$ normalised to 55°S , against normalised values of $G/C_a(55^\circ\text{S})$, from sites between 44°S and 60°S . Values of $G = \epsilon_{am}\Delta f\text{CO}_2 + f_m(\delta_a^e - \delta_a)$ were calculated from measurements of δ_a at each sample site, hourly averaged measurements of f_m and SST, and with an assumed value of $\delta_m = 1.8 \text{ ‰}$, and ϵ_{am} of -2.2 ‰ . The dashed lines represent the linear regressions (Y on X and X on Y) and the solid line the geometric mean functional regression (Teissier, 1948; Ricker, 1973). 5-26

Fig. 5.13 Atmospheric $\delta^{13}\text{C}$, normalised to 55°S and detrended for the effect of sea surface temperature ($\delta_a - \delta_a(55^\circ\text{S}) - [0.0041(\text{SST} - \text{SST}(55^\circ\text{S})) - 0.002]$), during (a) Spring (17 October to 22 November 1992, 2 to 8 October 1993), (b) Summer (5 January to 26 February 1993, 19 November to 27 December 1993, 2 January to 28 February 1994), and (c) Autumn (2 to 28 March 1993, 9 April to 8 May 1993). The filled symbols correspond to cruises into the ASIZ to the west of 105°E and the unfilled symbols denote cruises east of 105°E .

5-33

Fig. A.1 Southern Ocean transects on *RSV Aurora Australis* where oceanic fugacity of CO_2 , f_m , was recorded continuously during the periods (a) 4 to 26 October, 1991; (b) 19 October to 1 November, 1992; and 12 to 22 November, 1992; (c) 5 to 22 January, 1993; 24 February to 8 March, 1993; (d) 15 January to 7 February, 1993; (e) 7 to 25 February, 1993; (f) 12 to 28 March, 1993; 9 to 25 April, 1993; and 4 to 8 May, 1993; (g) 7 August to 8 October, 1993; (h) 19 November to 28 December, 1993; and (i) 2 January to 1 March, 1994. Air samples were collected between one and three degrees of latitude along the cruise tracks, except in Figures (d) and (e) where air was sampled at the sites marked with the larger circles.

A-5

Fig. B.1 Average area of open water in each $2.5^\circ \times 2.5^\circ$ grid square, over the region south of 55°S , between 60°E and 150°E , for (a) October, 1992; (b) November, 1992; (c) December, 1992; (d) January, 1993; (e) February, 1993; and (f) March, 1993. These values were obtained from U.S. Navy/NOAA Joint Ice Center weekly sea-ice maps.

B-4

Fig. B.2 Mean $\Delta f\text{CO}_2$ for each $2.5^\circ \times 2.5^\circ$ grid square south of 55°S , between 60°E and 150°E , for (a) October, 1991 and 1992; (b) November, 1992 and 1993; (c) December, 1993; (d) January, 1993 and 1994; (e) February, 1993 and 1994; and (f) March, 1993.

B-7

Fig. B.3 Mean GASP wind speeds for each $2.5^\circ \times 2.5^\circ$ grid square south of 55°S , between 60°E and 150°E , for (a) October, 1992; (b) November, 1992; (c) December, 1992; (d) January, 1993; (e) February, 1993; and (f) March, 1993. The average monthly wind speed for each grid point was calculated using six-hourly surface wind speeds from GASP analyses.

B-11

Fig. B.4 Hourly averaged surface ocean measurements of (a) sea surface temperature, (b) chlorophyll *a* concentration and (c) $f\text{CO}_2$ from the *RSV Aurora Australis* transect 19 November to 3 December 1993.

B-13

- Fig. B.5** Hourly averaged surface ocean measurements of (a) sea surface temperature, (b) chlorophyll *a* concentration and (c) $f\text{CO}_2$ from the *RSV Aurora Australis* transect 4 to 28 December 1993. B-14
- Plate 2.1** The Australian icebreaker *RSV Aurora Australis* in Prydz Bay. 2-1
- Plate 2.2** Instrumentation on the *RSV Aurora Australis* used for measuring $f\text{CO}_2$, including an equilibrator column (right) and infra-red gas analyser (left). 2-2
- Plate 2.3** Air sampling on the *RSV Aurora Australis* using a CSIRO Division of Atmospheric Research FPU pump unit. 2-18

LIST OF TABLES

Table 1.1 Published oceanic $p\text{CO}_2$ measurements south of 55°S . Numerically, $f\text{CO}_2$ is close to $p\text{CO}_2$. Where “sea ice” is entered under “Region” this means that at some stage $p\text{CO}_2$ measurements were made in an area of pack ice. Partial pressures expressed as fugacities are marked with a *.	1-17
Table 4.1 Monthly average area of open ocean, and net ocean-to-atmosphere transfer of CO_2 (calculated using GASP wind speeds), for the region of the Southern Ocean bounded by 55° - 60°S , or 60° - 70°S , and (a) 60° - 150°E , (b) 60° - 105°E , and (c) 105° - 150°E . The error is given in terms of the standard deviation, with the values in brackets being the standard deviation in the net transfer without the contribution from the error in X .	4-9
Table 4.2 Uncertainty in values used in equation 4.1 to calculate net carbon transfer. Each error is one standard deviation, with analytical errors in bold type, and interpolation errors in normal type.	4-14
Table 4.3 Average areas of open ocean, and estimates of the minimum net sea-to-air transfer of CO_2 (calculated using GASP wind speeds), for the region of the Southern Ocean bounded by 55° - 60°S , or 60° - 70°S , and (a) 60° - 150°E , (b) 60° - 105°E , and (c) 105° - 150°E . It is assumed that there was zero net flux over a grid square if at least 50% of it was covered by sea ice.	4-16
Table 4.4 Net ocean-to-atmosphere flux of CO_2 per unit area over the Antarctic Seasonal Ice Zone. Values marked “W” were calculated using the relationship for air-sea gas transfer velocity from Wanninkhof (1992), and those marked “T” were calculated using the relationship in Takahashi (1989). The errors presented here were calculated without taking into account the uncertainty attached to using the Wanninkhof (1992) relationship.	4-17
Table A.1 Summary of air samples from the <i>RSV Aurora Australis</i> used in this thesis.	A-6

TABLE OF CONTENTS

ABSTRACT	i
ACKNOWLEDGEMENTS	iii
NOMENCLATURE	iv
LIST OF ILLUSTRATIONS	viii
LIST OF TABLES	xiii
TABLE OF CONTENTS	xiv
1 INTRODUCTION	1-1
1.1 Overview	1-1
1.2 The Antarctic Seasonal Ice Zone	1-7
1.3 Estimating net air-sea transfer of CO ₂ over the ASIZ	1-8
1.3.1 Air-sea gas exchange coefficients for CO ₂ , <i>K</i>	1-9
1.3.2 Measurements of oceanic <i>f</i> CO ₂ over the ASIZ	1-15
1.4 Net air-sea transfer of ¹³ CO ₂ and its effect on atmospheric ¹³ CO ₂ / ¹² CO ₂ over the ASIZ	1-18
2 METHOD	2-1
2.1 Introduction	2-1
2.2 Measurement of oceanic <i>f</i> CO ₂	2-2
2.2.1 Equilibrator	2-4
2.2.2 Valve switching	2-6
2.2.3 Gas Standards	2-7
2.2.4 Infra-red Gas Analyser	2-7
2.2.5 Control and Monitoring	2-8
2.3 Other shipboard measurements necessary for calculating oceanic <i>f</i> CO ₂	2-9
2.3.1 Sea surface temperature	2-9
2.3.2 Sea surface salinity	2-10
2.3.3 Atmospheric pressure	2-10
2.3.4 Sea surface wind speed	2-11
2.3.5 Navigational data	2-11
2.4 Calculation of oceanic <i>f</i> CO ₂	2-11
2.4.1 Correction for pressure variation in the IRGA cell	2-12
2.4.2 Correction for IRGA drift	2-12
2.4.3 Correction for drying the air stream	2-13
2.4.4 Conversion from <i>p</i> CO ₂ to <i>f</i> CO ₂	2-14
2.4.5 Correction of the measured <i>f</i> CO ₂ for warming of the seawater	2-15

2.5	Measurement of atmospheric CO ₂ mixing ratios	2-17
2.5.1	Air sampling on the ship	2-17
2.5.2	Gas chromatography analysis of air samples	2-18
2.6	Calculation of atmospheric $f\text{CO}_2$	2-19
2.7	Measurement of atmospheric $\delta^{13}\text{C}$	2-20
2.8	Measurement of chlorophyll a	2-21
3	$\Delta f\text{CO}_2$ OVER THE ANTARCTIC SEASONAL ICE ZONE	3-1
3.1	Introduction	3-1
3.2	Observations of $\Delta f\text{CO}_2$ in the ASIZ	3-2
3.3	Relationship between $\Delta f\text{CO}_2$ and Chlorophyll a	3-8
3.4	Relationship between $\Delta f\text{CO}_2$ and sea surface temperature	3-10
3.5	Conclusions	3-12
4	NET AIR-SEA TRANSFER OF CO₂ OVER THE ANTARCTIC SEASONAL ICE ZONE	4-1
4.1	Introduction	4-1
4.2	Net air-sea transfer calculated using shipboard wind speeds	4-2
4.3	Net air-sea transfer calculated using GASP wind speeds	4-5
4.3.1	Error estimates	4-14
4.3.2	Effect on flux estimates from reduction of fetch by sea-ice	4-15
4.4	Comparisons with fluxes from different studies	4-17
4.5	Conclusions	4-21
5	INFLUENCE OF THE SOUTHERN OCEAN ON THE CONCENTRATION AND $^{13}\text{C}/^{12}\text{C}$ OF ATMOSPHERIC CO₂	5-1
5.1	Introduction	5-1
5.2	Observations of atmospheric CO ₂ mixing ratios and $\delta^{13}\text{C}$ over the Southern Ocean	5-2
5.3	Effect of $\Delta f\text{CO}_2$ on atmospheric CO ₂ over the Southern Ocean	5-10
5.4	Effect of $\Delta f\text{CO}_2$ on atmospheric $\delta^{13}\text{C}$ over the Southern Ocean	5-18
5.5	Effect of sea surface temperature on atmospheric $\delta^{13}\text{C}$ over the Southern Ocean	5-20
5.6	Effect of marine productivity on atmospheric $\delta^{13}\text{C}$ over the ASIZ	5-30
5.7	Conclusions	5-36
6	SUMMARY	6-1
A	SOUTHERN OCEAN CRUISES	A-1
B	SOUTHERN OCEAN DATA	B-1
B.1	Southern Ocean sea-ice data	B-1
B.2	$\Delta f\text{CO}_2$ data over the ASIZ	B-4
B.3	GASP wind speeds over the ASIZ	B-8
B.4	Chlorophyll a , SST and $f\text{CO}_2$ data from a spring Southern Ocean cruise	B-11
	REFERENCES	REF-1

CHAPTER ONE:

INTRODUCTION

1.1 OVERVIEW

Over the past two hundred years anthropogenic emissions of carbon dioxide by fossil fuel burning, cement production, changes in land use and biomass burning have increased the concentration of carbon dioxide (CO₂) in the atmosphere by approximately 80 ppm. However, the amount of CO₂ remaining in the atmosphere is only about half of the cumulative loading due to human sources, suggesting that natural sinks are currently sequestering anthropogenic CO₂. Both the oceans and terrestrial ecosystems can absorb CO₂ and store large quantities of carbon, but the amount of anthropogenic CO₂ being sequestered by either system, and how future climatic change will affect these carbon sinks, is still unknown. These are key issues in estimating how the carbon cycle might respond to continued greenhouse gas emissions.

In 1989 and 1990 approximately 7.6 ± 1.5 Gt (10^{15} g) of carbon per year was added to the atmosphere in the form of CO₂ from fossil fuel combustion, cement production and changes in land use (Houghton et al., 1992). Global atmospheric measurements in 1991 showed that of this amount, about 3.8 ± 0.1 Gt C yr⁻¹ were found in the atmosphere as CO₂, and carbon cycle models suggest about 2.0 ± 0.8 Gt C yr⁻¹ was taken up by the oceans (Houghton et al., 1992). The carbon imbalance, or “missing sink”, is estimated as 1.8 ± 1.7 Gt C yr⁻¹, and may be partially caused by terrestrial biospheric processes sequestering CO₂ via forest regeneration, and fertilization arising from the effects of both CO₂ and nitrogen (Houghton et al., 1992). However, at the present time there is still considerable uncertainty over the amount of CO₂ taken up by the oceans (Tans et al., 1995).

Approximately 900 Gt C resides in the surface ocean, and 36400 Gt C in the deep ocean, which is very large compared with the 750 Gt C residing in the atmosphere (Sundquist, 1993). Carbon mainly enters and leaves the ocean as CO_2 gas, via exchange at the sea surface. The natural gross carbon fluxes into or out of the ocean are estimated to be about 70 Gt C yr^{-1} (Sundquist, 1993). A further 0.3 to 0.5 Gt C yr^{-1} enters the oceans via rivers (Sarmiento and Sundquist, 1992).

Anthropogenically produced atmospheric CO_2 provides a relatively small perturbation to the natural cycle of air-sea gas exchange, with an estimated net flux into the oceans of approximately 2 Gt C yr^{-1} (Sundquist, 1993).

The net flux of CO_2 across the air-sea interface cannot be directly measured, but is estimated as a product of the air-sea exchange coefficient for CO_2 , K , and the difference between the fugacities of CO_2 in air and seawater, $\Delta f\text{CO}_2$ (Section 1.3). Although it is generally accepted that K depends on the solubility of CO_2 in seawater, and on turbulence at the ocean surface, and hence on wind speed, there is currently no consensus on how to formulate that wind speed dependence (Subsection 1.3.1). In addition to this uncertainty in K , is the uncertainty in $\Delta f\text{CO}_2$. Whereas the seasonal variability of surface water $f\text{CO}_2$ in some oceanic areas, including the North and South Atlantic and the North Pacific, has been measured, that of other areas, including the South Pacific Ocean, the North and South Indian Oceans, and the Southern Ocean, has not been satisfactorily documented (Tans et al., 1990; Poisson et al., 1993).

Of particular importance to an understanding of the future global carbon budget, is the determination of net air-sea transfer of CO_2 over the Antarctic Seasonal Ice Zone (ASIZ). The ASIZ has the potential to be a significant net sink for anthropogenic carbon over time-scales of centuries, due to the thermohaline mixing that occurs between the surface and deep ocean in this region, caused by salt-rejection from freezing of sea-ice in winter (Budd, 1980). How rapidly the ASIZ is able to sequester anthropogenic CO_2 relies on both the rate of deep mixing and on the net flux of CO_2 across the air-sea interface. The air-sea gas exchange coefficient over ice-free regions of the ASIZ may be relatively high due to high solubility of CO_2 (caused by low sea surface temperatures (Skirrow, 1975)) and strong wind speeds (Section 1.3). It is also

reasonable to suspect that the fugacity of CO_2 in surface waters might be relatively low over the ASIZ, due to spring/summer ice-edge algal blooms removing dissolved CO_2 from surface waters (Section 1.2). A high value of K and very negative values of $\Delta f\text{CO}_2$ would result in strong net uptake of atmospheric CO_2 by the ASIZ over seasonal time-scales. However, due to the lack of oceanic $f\text{CO}_2$ data over this region, particularly in areas of pack ice and during winter months (Subsection 1.3.2), it is not known if the ASIZ is a contemporary net source or sink for atmospheric CO_2 . The most appropriate formulation for the gas exchange coefficient over the ASIZ is also subject to uncertainty because of variable wind fetch due to the presence of sea-ice (Subsection 1.3.1).

The reason for the Antarctic Seasonal Ice Zone potentially playing such an important role in the global carbon cycle is that over time-scales of years the mixed layer of most of the world's ocean is in approximate chemical equilibrium with the atmosphere (Broecker and Peng, 1974) and a global change in net air-sea exchange of CO_2 would not by itself influence the long-term removal of atmospheric CO_2 into the oceans. The removal of atmospheric CO_2 due to increased solubility in the ocean mixed layer is limited to about $1 \text{ ppm } ^\circ\text{C}^{-1}$ because of the buffering effect of the ocean carbonate system (Broecker and Peng, 1974; Bacastow, 1979). Over centuries, removal of atmospheric CO_2 by the oceans must involve vertical redistribution of ocean carbon, either by marine biota (Section 1.2), by altered ocean circulation and ocean chemistry (reviewed by Broecker and Peng, 1993), or by increased wind speeds over cooling and sinking seawater in polar regions (Keir, 1993).

There are only eight stations monitoring atmospheric CO_2 concentration south of 40°S (Figure 1.1), and this has meant that it has been very difficult to determine the size of the Southern Ocean carbon sink from inversions of atmospheric CO_2 mixing ratios (e.g. Law et al., 1992; Conway et al., 1994). Conway et al. (1994) performed a two-dimensional model analysis of the mixing ratios from the global NOAA/CMDL flask sampling network, which indicated that the region south of 30°S was a net sink for atmospheric CO_2 that had increased from approximately 0.5 Gt C yr^{-1} during

1981-1988 to approximately 1.5 Gt C yr^{-1} during 1989-1992. However, the analysis used no mixing ratios from stations between Cape Grim (40.68°S , 144.69°E) and Palmer Station (64.92°S , 296.00°E), and the meridional gradient over the Southern Ocean was assumed to be nearly flat between Amsterdam Island (37.95°S , 77.53°E) and Palmer Station. Local anomalies in air-sea flux of CO_2 around Amsterdam Island or Cape Grim would have had a particularly strong effect on estimates of the total net sink south of 30°S . Nevertheless, it would appear that the results of Conway et al. (1992) suggest that over the period 1981 to 1992 the Southern Ocean experienced large interannual variations in net ocean uptake of CO_2 .

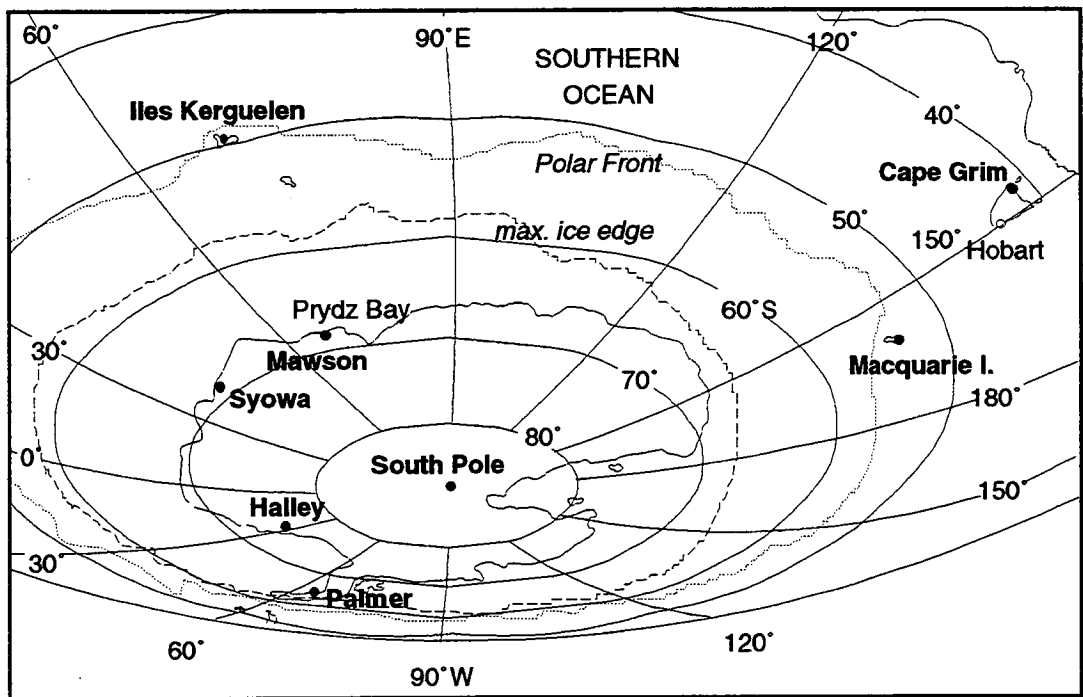


Fig. 1.1 The Southern Ocean giving the approximate location of the Antarctic Polar Front (dotted line) and the northern limit of the pack ice (dashed line) (after Tréguer and Jacques, 1992). Shown here in bold type are all stations south of 40°S where atmospheric CO_2 mixing ratios are measured from air samples. Of these, Atmospheric $^{13}\text{CO}_2/^{12}\text{CO}_2$ ratios are measured from air sampled at Cape Grim, Macquarie Is., Mawson and South Pole. (Figure courtesy of J. Cox, Australian Antarctic Division.)

Although historical or interannual changes in net uptake of atmospheric CO₂ by the Southern Ocean are beyond the scope of this thesis, it will investigate contemporary (1991-1994) air-sea exchange of CO₂ over the region of the Southern Ocean south of 44°S, between 60°E and 160°E, with particular emphasis on the seasonal ice zone. Measurements of $\Delta f\text{CO}_2$, collected on six voyages into the ASIZ by *RSV Aurora Australis*, from October 1991 to February 1994, are presented in Chapter 3. The data represents a significant contribution to $\Delta f\text{CO}_2$ values collected within areas of Antarctic pack ice (Section 1.3.2), and in Chapter 4 are used to calculate net air-sea transfer of CO₂ over the region of the Southern Ocean south of 55°S, between 60°E and 150°E, for the months October 1992 to March 1993. Extra information on air-sea gas exchange over the Southern Ocean is supplied in Chapter 5 by measurements of the CO₂ mixing ratio and $^{13}\text{CO}_2/^{12}\text{CO}_2$ in 360 air samples collected on Southern Ocean cruises by the *RSV Aurora Australis*, from October 1992 to February 1994.

The $^{13}\text{CO}_2/^{12}\text{CO}_2$ ratios provide different information on air-sea gas exchange compared with the atmospheric concentrations of CO₂. This is due to the fact that the net flux of $^{13}\text{CO}_2$ gas across the air-sea interface depends not only on the net air-sea flux of CO₂ gas, but also: (i) kinetic fractionation during gross air-to-sea exchange of CO₂; (ii) kinetic and thermodynamic fractionation during gross sea-to-air flux of CO₂; (iii) the ratio of $^{13}\text{C}/^{12}\text{C}$ in atmospheric CO₂; and (iv) the ratio of $^{13}\text{C}/^{12}\text{C}$ in dissolved inorganic carbon in the surface ocean (Section 1.4). The relationship between observations of atmospheric CO₂ concentration and $\Delta f\text{CO}_2$ is compared in Chapter 5 with the relationship between observations of $^{13}\text{C}/^{12}\text{C}$ in atmospheric CO₂ and sea surface temperature to demonstrate the difference between the effect of net air-sea gas exchange on the concentration of CO₂ in surface air and the effect of gross air-sea exchange on its isotopic ratio. In particular, atmospheric measurements over a highly productive region of the ASIZ are used to investigate the relative impact of marine productivity on atmospheric CO₂ mixing ratios and $^{13}\text{CO}_2/^{12}\text{CO}_2$.

The different fractionations associated with air-terrestrial biosphere and air-sea exchanges (Section 1.4) mean that variations in the atmospheric $^{13}\text{C}/^{12}\text{C}$ ratio can be used to constrain the sources and sinks of anthropogenic carbon dioxide (e.g. Pearman

and Hyson, 1986; Keeling et al., 1989; Enting and Mansbridge, 1991). However, global inversions of the concentration and $^{13}\text{C}/^{12}\text{C}$ ratio of atmospheric CO_2 using atmospheric transport models (e.g. Enting et al., 1995; Ciais et al., 1995a) have been constrained in their estimates of the net Southern Ocean carbon sink, by using $^{13}\text{CO}_2/^{12}\text{CO}_2$ data from only two sites south of 40°S , Cape Grim and South Pole. Recently, Ciais et al. (1995b) added CSIRO Division of Atmospheric Research CO_2 mixing ratio and $^{13}\text{CO}_2/^{12}\text{CO}_2$ data from Macquarie Island (54.50°S , 158.95°E) and Mawson station (67.60°S , 62.88°E) to the data from the global NOAA/CMDL sampling network, and from inverse modeling estimated that the net ocean sink south of 30°S was -1.1 Gt C during 1992 and -0.9 Gt C during 1993. Problems still arose from the lack of data from the Southern Ocean, in that their model run for 1993 inferred a substantial terrestrial sink south of 40°S , peaking at 50°S where there is very little land. Ciais et al. (1995b) hypothesised that the problem might have been partly caused by the sparse data coverage at high southern latitudes.

The meridional gradients in atmospheric $^{13}\text{CO}_2/^{12}\text{CO}_2$ presented in Chapter 5, along with their relationship with sea surface temperatures, will supply a valuable extra constraint on estimates of contemporary sources and sinks for anthropogenic carbon over the Southern Ocean made from inversions of the concentration and $^{13}\text{C}/^{12}\text{C}$ of atmospheric CO_2 .

The application of simultaneous shipboard observations of $f\text{CO}_2$, sea surface temperature, and atmospheric CO_2 concentrations and isotopic ratios to the investigation of air-sea exchange of carbon has only recently become feasible due to improvements in the measuring of $^{13}\text{C}/^{12}\text{C}$ made by the CSIRO Division of Atmospheric Research (Allison et al., 1994; Francey et al., 1994; Francey et al., 1995a). The absence of any significant anthropogenic or terrestrial sources of atmospheric CO_2 , make the ASIZ an ideal region to study air-sea gas exchange directly from atmospheric and ocean measurements (Section 1.4).

1.2 THE ANTARCTIC SEASONAL ICE ZONE

The Antarctic Seasonal Ice Zone is the region of the Southern Ocean over which seasonal sea-ice melts back nearly to the coast in summer and reforms in winter. At its maximum extent, sea-ice covers approximately $20 \times 10^{12} \text{ m}^2$ of the Southern Ocean, but recedes to about $4 \times 10^{12} \text{ m}^2$ cover in the austral summer (Sakshaug and Skjoldal, 1989). The ice edge is always south of the Antarctic Polar Front (Muench, 1990), which is defined for this study as following the 3°C isotherm at 100 m depth (Jacques and Fukuchi, 1994; Figure 1.1).

The $f\text{CO}_2$ of surface water is strongly influenced by the biological fixation of carbon via photosynthesis in phytoplankton. An important feature of the ASIZ affecting its ability to absorb atmospheric CO_2 is the effect of melting sea ice on phytoplankton growth. Algal blooms are particularly vigorous along the melting ice edge where low density surface waters, arising from melting sea ice, provide a stable, nutrient-rich surface layer for phytoplankton growth (Sakshaug and Skjoldal, 1989). Away from sea ice, Southern Ocean open waters are often mixed to 75 m depth or more by strong winds, and the frequency of phytoplankton blooms is correspondingly low, as algae are mixed below the photic zone (Sakshaug and Skjoldal, 1989).

The region of the Southern Ocean over which net air-sea fluxes were calculated in this study ($> 55^\circ\text{S}$, $60^\circ\text{-}150^\circ\text{E}$) includes Prydz Bay and the Adélie Shelf and is south of the Polar Front (Figure 1.1). Prydz Bay is fed by the largest glacier in Antarctica, the Lambert Glacier. Another important feature of the study region is the distinct difference in maximum ice extent west of 105°E compared with east of this longitude. From 60°E to 105°E the average ice edge was at 58°S during September, and at 67°S during February (1979-87) (Parkinson, 1992). From 105°E to 150°E the average ice edge retreated from 62.5°S to 65°S between September and February of the same years (Parkinson, 1992). Hence, the study region includes two different cases of the seasonal ice zone, with rapid and extensive melt of the sea-ice west of 105°E each November and December, and little melt over the region east of 105°E . It will be shown in Chapter 3 that the western region ($> 55^\circ\text{S}$, $60^\circ\text{-}105^\circ\text{E}$) has much lower

average $f\text{CO}_2$ in the surface ocean (and therefore higher productivity) than the eastern region ($> 55^\circ\text{S}$, $105^\circ\text{-}150^\circ\text{E}$).

1.3 ESTIMATING NET AIR-SEA TRANSFER OF CO_2 OVER THE ASIZ

The amount of CO_2 sequestered or emitted by a body of water may be expressed as the net transfer of CO_2 from the surface ocean to the atmosphere, N , and is given by the difference between larger, one-way fluxes:

$$\begin{aligned} N (\text{g C d}^{-1}) &= -\Phi_{am} + \Phi_{ma} \\ &= A'F \end{aligned} \quad (1.1)$$

where

$$\begin{aligned} \Phi_{am} &= \text{gross air-to-ocean transfer (g C d}^{-1}\text{),} \\ \Phi_{ma} &= \text{gross ocean-to-air transfer (g C d}^{-1}\text{),} \\ A' &= \text{area of ice-free ocean (m}^2\text{),} \\ F &= \text{net ocean-to-air flux of CO}_2 \text{ (g C m}^{-2} \text{ d}^{-1}\text{).} \end{aligned}$$

It is assumed here that there is no air-sea gas exchange over ocean which is covered by 100% sea ice.

The equation for the net flux of carbon dioxide from the ocean to the atmosphere, F , is given below (Broecker and Peng, 1982):

$$F (\text{g C m}^{-2} \text{ d}^{-1}) = 12K \Delta f\text{CO}_2 \quad (1.2)$$

where

$$\begin{aligned} K &= \text{air-sea gas exchange coefficient for CO}_2 \text{ (mol C m}^{-2} \text{ d}^{-1} \mu\text{atm}^{-1}\text{),} \\ \Delta f\text{CO}_2 &= f_m - f_a, \\ f_m &= \text{fugacity of CO}_2 \text{ in the surface ocean (}\mu\text{atm),} \\ f_a &= \text{fugacity of CO}_2 \text{ in the atmosphere at sea level and the sea surface} \\ &\quad \text{temperature (}\mu\text{atm).} \end{aligned}$$

The factor of 12 in equation 1.2 has been used to convert moles of carbon to grams of carbon.

The “fugacity” of CO₂ gas, $f\text{CO}_2$, is numerically close to the partial pressure of CO₂, $p\text{CO}_2$, but takes into account the non-ideal nature of the gas (Weiss, 1974). Air is saturated with water vapour at the air-sea interface, and the value of atmospheric $f\text{CO}_2$ used to calculate $\Delta f\text{CO}_2$ is for water saturated air at the temperature of the surface water (Siegenthaler, 1986). The $\Delta f\text{CO}_2$ determines the potential for gas flux, and the gas transfer coefficient, K , determines to what extent the gas transfer will actually occur. A negative $\Delta f\text{CO}_2$ indicates CO₂ uptake by the ocean and a positive value indicates a CO₂ source to the atmosphere.

1.3.1 Air-sea gas exchange coefficient for CO₂, K

The air-sea gas exchange coefficient is given by (Broecker and Peng, 1982):

$$K = 0.24 \sigma_m V_p \quad (1.3)$$

where

$$\begin{aligned} \sigma_m &= \text{solubility of CO}_2 \text{ at the sea surface temperature (mol C m}^{-3} \text{ } \mu\text{atm}^{-1}\text{),} \\ V_p &= \text{gas transfer piston velocity of CO}_2 \text{ gas across the air-sea interface} \\ &\quad \text{(cm h}^{-1}\text{).} \end{aligned}$$

The factor of 0.24 in equation 1.3 has been used to convert the gas transfer velocity from cm h⁻¹ to m d⁻¹.

The solubility of CO₂ in seawater is a function of sea temperature and salinity. For seawater at 1 atm pressure, salinity of 34 ppt, and -1°C, CO₂ is twice as soluble compared to seawater at 20°C (Weiss, 1974). In most studies of the air-sea flux of CO₂ it is the bulk temperature of the mixed layer which is measured, at a few metres below the sea surface, rather than the actual thin surface layer. The surface of the ocean (or ‘skin’) exhibits a temperature gradient within the upper 1 mm, or so, on

average 0.3°C cooler than the bulk mixed layer (e.g. Woodcock, 1941; Hasse, 1971). This cooler surface temperature results in higher CO₂ solubility in the skin compared with the bulk mixed layer, and therefore one obtains a higher estimate of air-sea flux when calculating the air-sea gas exchange coefficient (equation 1.3) using the skin temperature than when using the bulk mixed layer temperature. Robertson and Watson (1992) and Van Skoy et al. (1995) have made estimates of the increase in global ocean uptake of CO₂ due to the thermal skin effect of 0.7 Gt C yr⁻¹ and 0.39 Gt C yr⁻¹, respectively. Unfortunately, skin temperatures were not available for most of the cruises covered in this thesis, and therefore the bulk mixed layer temperature is used for the sea surface temperature in all calculations.

For moderately or slightly soluble gases, the rate of gas exchange is controlled by turbulence at the air-water interface (Liss and Merlivat, 1986). The gas transfer piston velocity can approximately be represented as a function of turbulence at the air-water interface by (Liss and Merlivat, 1986):

$$V_p = Sc^n f(\text{turbulence}) \quad (1.4)$$

where

Sc = Schmidt number (Jähne et al., 1987a),

n = -0.5 to -1.0 (Liss and Merlivat, 1986).

The Schmidt number can be approximated by a third order polynomial in sea surface temperature (Jähne et al., 1987a), with Sc decreasing as the temperature increases. For the case where n is -0.5 then $Sc^{-0.5}$ at -1°C is equal to 0.55 $Sc^{-0.5}$ at 20°C, which nearly cancels the effect of the temperature dependence of the solubility on the air-sea flux.

The major source of turbulence at the air-sea interface is wind stress (Wanninkhof et al., 1985), and therefore the gas transfer velocity is a function of wind speed.

However, there is considerable uncertainty regarding the most appropriate relationship to use (e.g. Liss and Merlivat, 1986; Takahashi, 1989; Wanninkhof, 1992). The wind-speed dependence of the gas transfer velocity has been estimated in the laboratory

using wind tunnels and wind-wave tanks (e.g. Merlivat and Memery, 1983; Jähne et al., 1987b; Wanninkhof and Bliven, 1991), in the field using conservative tracers in lakes or the open ocean (e.g. Wanninkhof et al., 1985; Upstill-Goddard et al., 1990; Wanninkhof et al., 1993), and using ^{14}C (e.g. Broecker et al., 1985) and radon gas measurements over the ocean (e.g. Peng et al., 1979; Smethie et al., 1985). No single wind tunnel study has yet managed to cover the full range of wind speeds from 0 to 20 m s^{-1} (Liss and Merlivat, 1986), and there are few results from lake or ocean experiments which give air-sea gas transfer velocities for wind speeds exceeding 13 m s^{-1} (Watson et al., 1991).

Liss and Merlivat (1986) extrapolated lacustrine measurements by Wanninkhof et al. (1985), for an enlarged set of values of wind speed, based on knowledge obtained from models and wind tunnel experiments. Liss and Merlivat (1986) normalised all data to a Schmidt number of $S_c = 600$, corresponding to CO_2 at 20°C in fresh water, then used a Schmidt Number power dependence of $-2/3$ for wind speeds less than 3.6 m s^{-1} (smooth surface regime), and $-1/2$ for all higher speeds (breaking waves). They obtained three relationships for the gas transfer piston velocity at 20°C :

$$\begin{aligned} V_p (\text{cm h}^{-1}) &= 0.17 W & (W \leq 3.6) \\ V_p (\text{cm h}^{-1}) &= 2.85 W - 9.65 & (3.6 < W \leq 13) \\ V_p (\text{cm h}^{-1}) &= 5.9 W - 49.3 & (W > 13) \end{aligned} \tag{1.5}$$

where

$$W = \text{surface wind speed at a height of 10 m a.s.l. (m s}^{-1}\text{)}.$$

These three relationships for V_p are widely used in the literature to calculate the net air-sea flux of carbon dioxide over the Southern Ocean (e.g. Murphy et al., 1991; Robertson and Watson, 1995; Metzl et al., 1995).

Smethie et al. (1985) developed a relationship for gas exchange based on analyses of gas transfer data obtained by a radon deficit method in the Equatorial Atlantic. In this relationship, it is assumed that no gas transfer takes place between zero and

3 m s⁻¹ wind speed (at 19.5 m height) and that gas transfer is linearly dependent on wind speeds greater than 3 m s⁻¹. Takahashi (1989) revised the Smethie et al. (1985) relationship to intercept the global average gas transfer velocity obtained from the bomb-¹⁴C inventory in the ocean. He derived the following relationship for the CO₂ gas transfer velocity for seawater at 20°C:

$$\begin{aligned} V_p(\text{cm h}^{-1}) &= 0 & (W < 3) \\ V_p(\text{cm h}^{-1}) &= 5.8 (W - 3) & (W > 3) \end{aligned} \quad (1.6)$$

The relationship of Takahashi (1989) has a significantly stronger dependence on wind speed than that of Liss and Merlivat (1986) (Figure 1.2). Wanninkhof (1992) accounted for some of the difference with the following argument. For a non-linear relationship between gas transfer and wind speed, the variance of wind speed during the measurement interval can have a significant influence on the calculated gas transfer velocity. Most experimental results suggest that the relationship has a positive curvature, so gas transfer velocities measured over long time periods with variable winds will be higher than if transfer velocities are measured instantaneously, or under steady wind conditions for the same average wind speed. Gas transfer velocities obtained with ¹⁴C correspond to average long-term winds, while gas transfer measurements in wind tunnels are performed under steady wind conditions. The Liss and Merlivat relationship is based on gas transfer velocities measured over 1-2 days on a small lake. Because of the short time interval of measurement, the gas transfer-wind speed relationship of Liss and Merlivat may yield low gas transfer values if long-term averaged winds over the ocean are used. On the other hand, the relationship of Takahashi (1989) has been fit through long-term bomb-¹⁴C invasion rates over the ocean. This relationship will yield anomalously high values if used for short-term or steady winds.

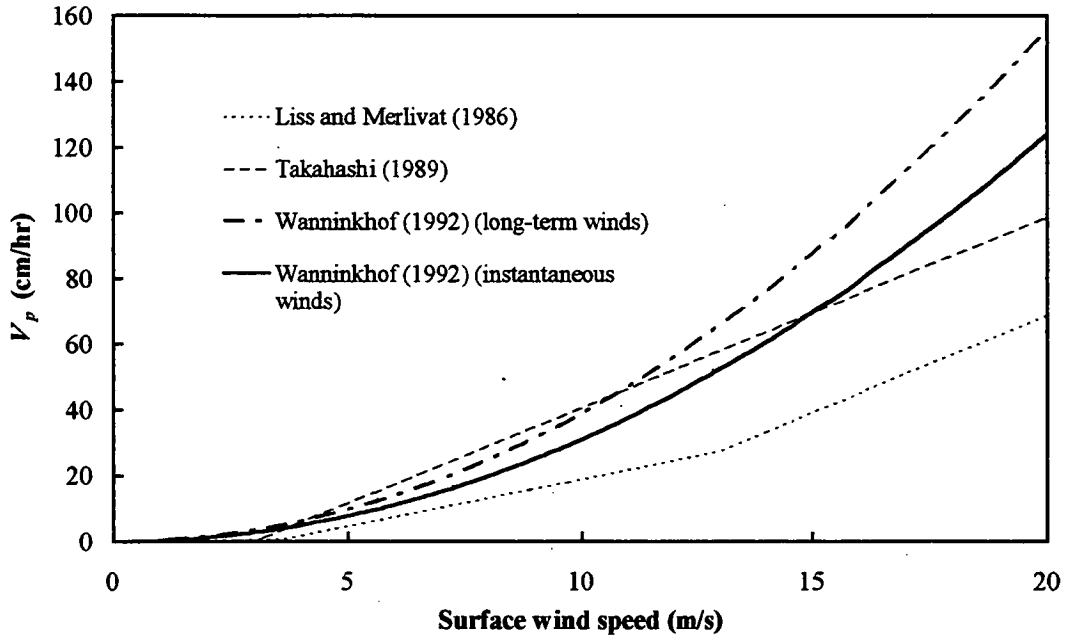


Fig. 1.2 Summary of four commonly used relationships between the gas transfer piston velocity, V_p , and wind speed (at 10 m a.s.l.), for air-sea exchange of CO_2 at 20°C .

Wanninkhof (1992) determined two different equations for the gas transfer velocity from long term climatological wind speeds and short term or steady wind speeds. Including the Schmidt number dependence, his equation for the CO_2 gas transfer velocity for long term averaged wind speeds, $V_p(\text{av})$, is

$$V_p(\text{av}) (\text{cm h}^{-1}) = 0.39 W_{\text{av}}^2 (\text{Sc}/660)^{-1/2} \quad (1.7)$$

where

$$\begin{aligned} W_{\text{av}} &= \text{long term averaged wind speed at 10 m a.s.l. (m s}^{-1}\text{),} \\ \text{Sc} &= 660 \text{ for } \text{CO}_2 \text{ in seawater at } 20^\circ\text{C (Jähne et al., 1987a).} \end{aligned}$$

The gas transfer velocity for short term or steady winds, such as spot measurements using shipboard anemometers, is (Wanninkhof, 1992):

$$V_p (\text{cm h}^{-1}) = 0.31 W^2 (\text{Sc}/660)^{-1/2} \quad (1.8)$$

Equation 1.7 yields transfer velocities close to those of Takahashi (1989) for wind speeds below about 13 m s^{-1} , while equation 1.8 yields transfer velocities between the Liss and Merlivat and Takahashi estimates for wind speeds below 15 m s^{-1} (Figure 1.2).

Other factors besides wind stress can also influence air-sea gas exchange over the ASIZ.

In areas of ocean partially covered by sea-ice the gas transfer velocity is affected by the finite distance over which a wave field can develop - the “fetch” (Wanninkhof, 1992). Work in wind-wave tanks has indicated that fetch has an influence on gas transfer, especially at lower wind speeds (Jähne et al., 1989; Wanninkhof and Bliven, 1991). Larger lakes also show higher average gas transfer values at a particular wind speed compared with smaller lakes (Wanninkhof, 1992), and the fetch dependence is most pronounced at higher wind speeds (Upstill-Goddard et al., 1990; Wanninkhof, 1992). Over parts of the ASIZ, where pack ice breaks up the ocean surface into polynyas and leads, it is expected that the average gas transfer velocity will be less than it would be over the open ocean for the same sea surface temperature and wind speed.

Chemical enhancement of CO_2 exchange occurs by reaction of CO_2 with water or hydroxide ions in the surface boundary, increasing the concentration gradient of the diffusing species in the water boundary layer and, thereby, the gas transfer (Bolin, 1960). All experimental and theoretical evidence points to negligible enhancement at gas transfer velocities corresponding to steady winds above 5 to 7 m s^{-1} , especially for low sea surface temperatures (Broecker and Peng, 1974; Hoover and Berkshire, 1969; Liss, 1973; Wanninkhof, 1992). For the ASIZ, where monthly mean wind speeds almost always exceed 5 m s^{-1} (Appendix B: Figure B.3), chemical enhancement is expected to have no significant effect on the gas transfer velocities.

1.3.2 Measurements of oceanic $f\text{CO}_2$ over the ASIZ

Most of the carbon in seawater is in the form of HCO_3^- and $\text{CO}_3^{=}$ ions and less than 1% is present as carbon dioxide gas. The chemical equilibria between the dissolved carbonate species can be written as follows (Broecker and Peng, 1982):



where

$\text{CO}_{2,\text{aq}}$ = dissolved CO_2 including H_2CO_3 .

Two parameters that can readily be measured in seawater are the total dissolved inorganic carbon (DIC) concentration,

$$\text{DIC} = [\text{CO}_{2,\text{aq}}] + [\text{HCO}_3^-] + [\text{CO}_3^{=}] , \quad (1.10)$$

and the pressure of CO_2 gas in air equilibrated with this water,

$$p\text{CO}_2 (\mu\text{atm}) = [\text{CO}_{2,\text{aq}}]/\sigma \quad (1.11)$$

where

$[\text{CO}_{2,\text{aq}}]$ = concentration of dissolved CO_2 including H_2CO_3 (mol C m^{-3}),

σ = solubility of CO_2 in seawater at the sea temperature
($\text{mol C m}^{-3} \mu\text{atm}^{-1}$).

The parameter used in this study is the fugacity of CO_2 gas, $f\text{CO}_2$, as this takes into account the non-ideal nature of carbon dioxide, whereas a partial pressure assumes an ideal gas. The difference between oceanic $f\text{CO}_2$ and $p\text{CO}_2$ is most pronounced in cold waters, $f\text{CO}_2$ being as much as 2 μatm lower than $p\text{CO}_2$ at -1.8°C (Weiss and Price, 1980). The fugacity of carbon dioxide is defined as

$$f\text{CO}_2 (\mu\text{atm}) = \phi p\text{CO}_2 \quad f\text{CO}_2/p\text{CO}_2 \rightarrow 1 \text{ as } p \rightarrow 0 \quad (1.12)$$

where

- ϕ = a function of pressure and water temperature (Weiss, 1974; Subsection 2.4.4),
- p = total pressure (atm).

Variations of sea surface $f\text{CO}_2$, are controlled by dynamic processes (mixing in the surface layer), thermodynamic processes (variation of temperature and salinity), exchanges of CO_2 between the atmosphere and the ocean, and biological processes (primary production, remineralisation). It has been possible to estimate values of sea surface $f\text{CO}_2$ over many regions of the world's oceans using monthly mean sea surface temperature fields (e.g. Tans et al., 1990; Metzl et al., 1995), but there is no clear relationship between these parameters south of about 50°S (Poisson et al., 1993; Takahashi et al., 1993; Metzl et al., 1995). Unless more sophisticated relationships are developed to determine $f\text{CO}_2$ from not only sea surface temperature, but other parameters such as chlorophyll a from ocean colour maps, the most reliable method for determining surface ocean fugacities over the ASIZ is to sample seawater from a ship.

Few cruises have been made south of 55°S to measure $p\text{CO}_2$ or $f\text{CO}_2$, and even fewer have sampled in areas of pack ice. Table 1.1 presents a summary of oceanic $p\text{CO}_2$ and $f\text{CO}_2$ measurements south of 55°S published to date. It can be seen that there is no published $p\text{CO}_2$ data for the ASIZ for the months April to September. When comparing $p\text{CO}_2$ data measured using various techniques, one should bear in mind that there are discrepancies between $p\text{CO}_2$ measured with infra-red gas analysers and those calculated from titration data, as the latter depend on knowing the equilibrium constants for CO_2 .

Region	Time Period	Oceanic $p\text{CO}_2$ (μatm)	Sampling method	Reference
57° - 62.5°S, 0° - 4°E (sea ice)	Oct - Nov '81	313 - 340	titration	Takahashi and Chipman (1982)
55° - 66°S, 20° - 80°E	Feb - Mar '93	256 - 370*	equilibrator with gas chromatograph	Robertson and Watson (1995)
55° - 65°S, 30° - 90°E	Feb '87	300 - 380	equilibrator with gas chromatograph	Metzl et al. (1991)
55° - 69°S, 40° - 150°E	Nov - Mar, '87-'92.	260 - 360	equilibrator with infra red gas analyser	Hashida et al. (1994)
65° - 68.5°S, 63° - 78°E (sea ice)	austral summer '79 - '80	195 - 490	titration	Milne and Smith (1980)
55° - 63°S, 60° - 100°E GEOSECS Indian exp.	Feb '78	310 - 340		Takahashi and Chipman (1982)
55° - 66°S, 62° - 87°E	4 Jan '91 - 1 Apr '91	315 - 355*	equilibrator with infra red gas analyser	Poisson et al. (1993)
56.6° - 65°S, 150°E	17 Dec '93 - 13 Jan '84	346 - 373	equilibrator with infra red gas analyser	Inoue and Sugimura (1988)
63° - 65°S, 115° - 150°E	13 - 18 Jan '84	338 - 366	equilibrator with infra red gas analyser	Inoue and Sugimura (1988)
55° - 65°S, 115°E	18 - 23 Jan '84	340 - 358	equilibrator with infra red gas analyser	Inoue and Sugimura (1988)
55° - 70°S, 170° - 190°E GEOSECS Pacific exp.	Feb - Mar '74	280 - 310		Takahashi and Chipman (1982)
55° - 58°S, 193° - 203°E	Mar - Apr '84	undersaturated by $> -20 \mu\text{atm}$	equilibrator with gas chromatograph	Murphy et al. (1991)
55° - 60°S, 235° - 256°E	Feb - Mar '89	slightly oversaturated	equilibrator with gas chromatograph	Murphy et al. (1991)
59° - 69°S, 272°E (to ice edge)	5 Nov - 17 Dec '92	214 - 350	equilibrator with gas chromatograph	Robertson and Watson (1995)
60° - 63°S, 292° - 297°E METEOR expedition	21 Jan - Feb '90	320 - 355	equilibrator with gas chromatograph	Chipman et al. (1992)
55° - 62°S, 295° - 299°E ANTX/1	Nov - Dec '91	242 - 346	equilibrator with infra red gas analyser	Schneider and Morlang (1995)
60° - 64°S, 313° - 325°E METEOR expedition	Feb '90	230 - 325	equilibrator with gas chromatograph	Chipman et al. (1992)
55° - 76°S, 290° - 360°E (sea ice)	Nov - Dec, '83 - '90.	220 - 390	various cruises and methods	Takahashi et al. (1993)
55° - 63°S, 290° - 345°E GEOSECS Atlantic exp.	Jan '73	280 - 320		Takahashi and Chipman (1982)
55° - 60°S, 6°W (sea ice)	24 Oct - 21 Nov '92	344 - 375	equilibrator with gas chromatograph	de Baar et al. (1995)
60° - 70°S, 20°W - 2°E Atlantic Long Lines (AJAX) expedition	24 Jan - 2 Feb '84	215 - 390	equilibrator with gas chromatograph	Chipman et al. (1986), Takahashi et al. (1993)

Table 1.1 Published oceanic $p\text{CO}_2$ measurements south of 55°S. Numerically, $f\text{CO}_2$ is close to $p\text{CO}_2$. Where "sea ice" is entered under "Region" this means that at some stage $p\text{CO}_2$ measurements were made in an area of pack ice. Partial pressures expressed as fugacities are marked with a *.

1.4 NET AIR-SEA TRANSFER OF $^{13}\text{CO}_2$ AND ITS EFFECT ON ATMOSPHERIC $^{13}\text{CO}_2/^{12}\text{CO}_2$ OVER THE ASIZ

The isotopic composition of carbon dioxide (ratio of $^{13}\text{CO}_2$ to $^{12}\text{CO}_2$) is expressed as the per mill difference in the isotopic ratio between a CO_2 sample and a calcium carbonate standard, the Pee Dee Belemnite ("PDB"; Craig, 1957):

$$\delta^{13}\text{C} (\text{‰}) = \frac{(^{13}\text{C}/^{12}\text{C})_s - (^{13}\text{C}/^{12}\text{C})_{\text{PDB}}}{(^{13}\text{C}/^{12}\text{C})_{\text{PDB}}} \times 1000 \quad (1.13)$$

where

$$(^{13}\text{C}/^{12}\text{C})_s = \text{the ratio of } ^{13}\text{C} \text{ to } ^{12}\text{C} \text{ in the sample of } \text{CO}_2 \text{ gas.}$$

During uptake of atmospheric CO_2 by plants the lighter isotopes are preferred. The result of fractionation during photosynthesis is that, on average, biospheric material is depleted in ^{13}C by about 17 ‰ relative to air, (Craig, 1953; Farquar et al., 1982).

There is no significant fractionation associated with the return of biospheric carbon to the atmosphere, either by respiration, decay or combustion, so that atmospheric $\delta^{13}\text{C}$ becomes more negative as a result of the addition of CO_2 to the atmosphere of terrestrial biospheric origin (Keeling, 1961).

The other major carbon exchange on seasonal-to-century timescales involves the oceans. Air-to-ocean transfer of gaseous CO_2 involves kinetic fractionation of approximately 2 ‰, whereas ocean-to-air transfer of carbon involves kinetic and thermodynamic fractionation of CO_2 of about -8.5 ‰ at 20°C (Mook et al., 1974).

The resulting influence on atmospheric $\delta^{13}\text{C}$ from exchange with the ocean is therefore generally small compared with the effect from terrestrial biota and fossil fuel (Francey, 1985; Pearman and Hyson, 1986).

The region studied in this thesis - the Southern Ocean south of 44°S, between 60°E and 160°E, and in particular the region of the ASIZ (60° - 70°S, 60° - 150°E), is remote from terrestrial or anthropogenic sources of CO_2 . Therefore, the seasonal variations in $\delta^{13}\text{C}$ of atmospheric CO_2 over the ASIZ to be presented in Chapter 5, are

not a result of air-terrestrial biosphere exchange, but must be due to exchange of CO₂ with the ocean surface and to atmospheric transport of ¹³CO₂ - depleted air from the north.

The net transfer of ¹³CO₂ from the ocean to the atmosphere, ¹³N, may be expressed in a similar fashion to the net sea-to-air transfer of CO₂ in equation 1.1 (after Tans et al., 1993):

$$^{13}N (\text{g } ^{13}\text{C d}^{-1}) = -\alpha_{am}\Phi_{am}R_a + \alpha_{ma}\Phi_{ma}R_m \quad (1.14)$$

where

α_{am} = the isotopic fractionation (kinetic) between the atmosphere and the surface ocean (Heimann and Keeling, 1989, p. 263),

α_{ma} = the isotopic fractionation (kinetic and thermodynamic) between the surface ocean and the atmosphere (Heimann and Keeling, 1989, p. 263),

R_a = ratio of ¹³C/¹²C in atmospheric CO₂,

R_m = ratio of ¹³C/¹²C in DIC in the surface ocean.

The ¹³C/¹²C equilibrium fractionation factor of gaseous CO₂ with respect to total dissolved inorganic carbon in seawater is defined as $\alpha_{eq} = \alpha_{ma}/\alpha_{am}$ (Heimann and Keeling, 1989, p. 263). This equilibrium fractionation factor was empirically determined to be a function of sea surface temperature, SST (°C), (for 5°C < SST < 25°C), such that (Zhang et al., 1995):

$$\alpha_{ma}/\alpha_{am} = (0.98947 \pm 0.00005) + (0.104 \pm 0.003) \times 10^{-3} \text{ SST}, \quad (1.15)$$

which agrees closely with the relationship obtained by Mook et al. (1974) for the equilibrium fractionation factor between gaseous CO₂ and dissolved bicarbonate in seawater.

Substituting equation 1.1 into 1.14 and defining R_a^e to be the $^{13}\text{C}/^{12}\text{C}$ isotopic composition of gaseous CO_2 that would be in equilibrium with the sea surface (Tans et al., 1993), where

$$R_a^e = (\alpha_{ma}/\alpha_{am})R_m, \quad (1.16)$$

gives

$$^{13}N (\text{g C d}^{-1}) = \alpha_{am}NR_a + \alpha_{am}\Phi_{ma}(R_a^e - R_a) \quad (1.17)$$

Equation 1.17 separates the net air-sea transfer of $^{13}\text{CO}_2$ into an “equilibrium” flux ($\alpha_{am}NR_a$) proportional to the net air-sea transfer of CO_2 , and a “disequilibrium” flux ($\alpha_{am}\Phi_{ma}(R_a^e - R_a)$) proportional to the ocean-to-air gross CO_2 flux, Φ_{ma} , and the isotopic disequilibrium between the atmosphere and the ocean, $R_a^e - R_a$ (Tans et al., 1993; Ciais et al., 1995a).

The net transfer of $^{13}\text{CO}_2$ gas from the ocean to the atmosphere, ^{13}N , cannot be measured directly, but the rate of change in the ratio of atmospheric $^{13}\text{CO}_2$ to $^{12}\text{CO}_2$ can be measured. Therefore, following the chain rule of differentiation, ^{13}N may be expressed in terms of the ratio of $^{13}\text{C}/^{12}\text{C}$ in atmospheric CO_2 , R_a , and the mass of atmospheric CO_2 , M_a , such that

$$^{13}N = M_a ^{13}N_R + R_a N \quad (1.18)$$

where

$$^{13}N_R = \text{the change in the atmospheric isotopic ratio, } R_a, \text{ due to air-sea exchange (d}^{-1}\text{)}.$$

Substituting equation 1.18 into equation 1.17, one obtains

$$M_a ^{13}N_R = N(\alpha_{am} - 1)R_a + \Phi_{ma}\alpha_{am}(R_a^e - R_a) \quad (1.19)$$

Equation 1.19 may be more conveniently expressed by defining $\delta_k = [(R_k - R_{\text{PDB}})/R_{\text{PDB}}] \times 1000 \text{ ‰}$ (as in equation 1.13) and $\epsilon_k = [\alpha_k - 1] \times 1000 \text{ ‰}$. After dividing through by $R_{\text{PDB}}/1000$, and approximating the multiplicative factors $\alpha_{am} = 0.998$ and $(\delta_a/1000) + 1$ to 1 (Tans et al., 1993), equation 1.19 may be rewritten to give the rate at which $\delta^{13}\text{C}$ changes in the atmosphere, due to exchange of CO_2 gas with the ocean, $^{13}N_\delta (\text{‰ d}^{-1})$:

$$M_a \text{ } ^{13}N_\delta = N \epsilon_{am} + \Phi_{ma}(\delta_a^e - \delta_a) \quad (1.20)$$

where

$$\begin{aligned} \delta_a &= \delta^{13}\text{C of atmospheric CO}_2 \text{ (‰)}, \\ \epsilon_{am} &= \text{kinetic fractionation of CO}_2 \text{ as it passes from air to seawater (‰)} \\ &= -2.23 \pm 0.2 \text{‰ at } 5^\circ\text{C, and } -2.02 \pm 0.2 \text{‰ at } 21^\circ\text{C (Zhang et al., 1995),} \\ \delta_a^e &= \delta^{13}\text{C of gaseous CO}_2 \text{ that would be in equilibrium with the sea surface (‰)} \\ &= [(0.98947 + 0.104 \times 10^{-3} \text{ SST})(1 + \delta_m/1000) - 1] \times 1000 \text{ ‰ from} \\ &\quad \text{equations 1.15 and 1.16,} \\ \delta_m &= \delta^{13}\text{C of DIC in the surface ocean (‰)}. \end{aligned}$$

As in equation 1.17, equation 1.20 separates the change in atmospheric $\delta^{13}\text{C}$ due to air-sea exchange into a “net flux term”, $N \epsilon_{am}$, and a “gross flux term”, $\Phi_{ma}(\delta_a^e - \delta_a)$. The net flux term reflects the relatively small kinetic fractionation in atmospheric $\delta^{13}\text{C}$ associated with net air-sea transfer of carbon ($\epsilon_{am} \approx -2 \text{ ‰}$, $N \propto f_m - f_a$). The gross flux term reflects the large gross flux ($\Phi_{ma} \propto f_m$), the isotopic disequilibrium between DIC in the surface ocean and atmospheric CO_2 (Tans et al., 1993), and the temperature dependence of the fractionation between DIC to gaseous CO_2 (equation 1.15). The gross flux term in equation 1.20 can become significant if $\delta_a^e - \delta_a$ is non-zero.

Isotopic disequilibrium between the atmosphere and surface ocean ($\delta_a^e \neq \delta_a$) may occur due to a number of factors. Globally, the average ratio of $^{13}\text{C}/^{12}\text{C}$ in atmospheric CO_2 is steadily decreasing due to the burning of fossil fuel, but because there is a finite

residence time for CO_2 in the ocean, anthropogenic changes in globally averaged δ_m lag globally averaged δ_a (Francey et al., 1995b). In 1990, the world's atmosphere and surface ocean were out of isotopic equilibrium by an average of about 0.43 ‰ (Tans et al., 1993).

On a smaller scale, rapid mixing in the atmosphere prevents the establishment of atmosphere-ocean equilibrium. In this case, regional disequilibrium will occur due to the thermodynamic fractionation of CO_2 as it leaves the ocean (Mook et al., 1974) and from any additional changes in δ_m unrelated to variation in δ_a , such as marine biological productivity and respiration or decay (Tans et al., 1993). Algal growth results in increased levels of $\delta^{13}\text{C}$ -DIC in the same waters, since carbon-12 is taken up preferentially by phytoplankton, with the average DIC - phytoplankton fractionation being -22 ‰ (Tans et al., 1993).

Over the Southern Ocean, if $\delta^{13}\text{C}$ -DIC in the surface ocean is altered by factors unrelated to the kinetic fractionation associated with net air-sea exchange, such as upwelling of DIC, fractionation from algal uptake of DIC, or changes in sea surface temperature, then any gross air-sea exchange of CO_2 will significantly alter local levels of atmospheric $\delta^{13}\text{C}$. It will be demonstrated in this thesis that with current measurement techniques it is possible to measure the impact of gross air-sea flux on atmospheric $\delta^{13}\text{C}$ more easily than the impact of net air-sea flux on atmospheric CO_2 mixing ratios. In particular, over a relatively unproductive region of the Southern Ocean the strong sea surface temperature dependence of atmospheric $^{13}\text{CO}_2/^{12}\text{CO}_2$ will be measured, and over a highly productive region of the ASIZ, the effect that changes in $\delta^{13}\text{C}$ -DIC of the surface ocean may have on $\delta^{13}\text{C}$ of atmospheric CO_2 will be demonstrated.

CHAPTER TWO:

METHOD

2.1 INTRODUCTION

This chapter describes the methods and equipment used to measure the fugacity of carbon dioxide in the ocean and atmosphere. The instruments described in Sections 2.2 and 2.5.1 were installed on the *RSV Aurora Australis* (Plate 2.1) during the austral winter of 1992. Sampling and analysis techniques for measuring the concentration and stable carbon isotopic ratio ($\delta^{13}\text{C}$) of atmospheric CO_2 , and concentration of Chlorophyll *a* in surface waters, are also described.



Plate 2.1 The Australian icebreaker *RSV Aurora Australis* in Prydz Bay.

2.2 MEASUREMENT OF OCEANIC $f\text{CO}_2$

The fugacity of CO_2 in surface seawater, f_m , was measured on *RSV Aurora Australis* by infrared analysis of air equilibrated with seawater (Plate 2.2). The technique used was similar to that of Takahashi (1961) and Copin-Montégut (1985), and employed a “Weiss” type equilibrator and a LICOR 6252 Infrared Gas Analyser (IRGA). A schematic of the system is shown in Figure 2.1. During a three hour cycle two standards, an air sample, and air equilibrated with surface waters were analysed.

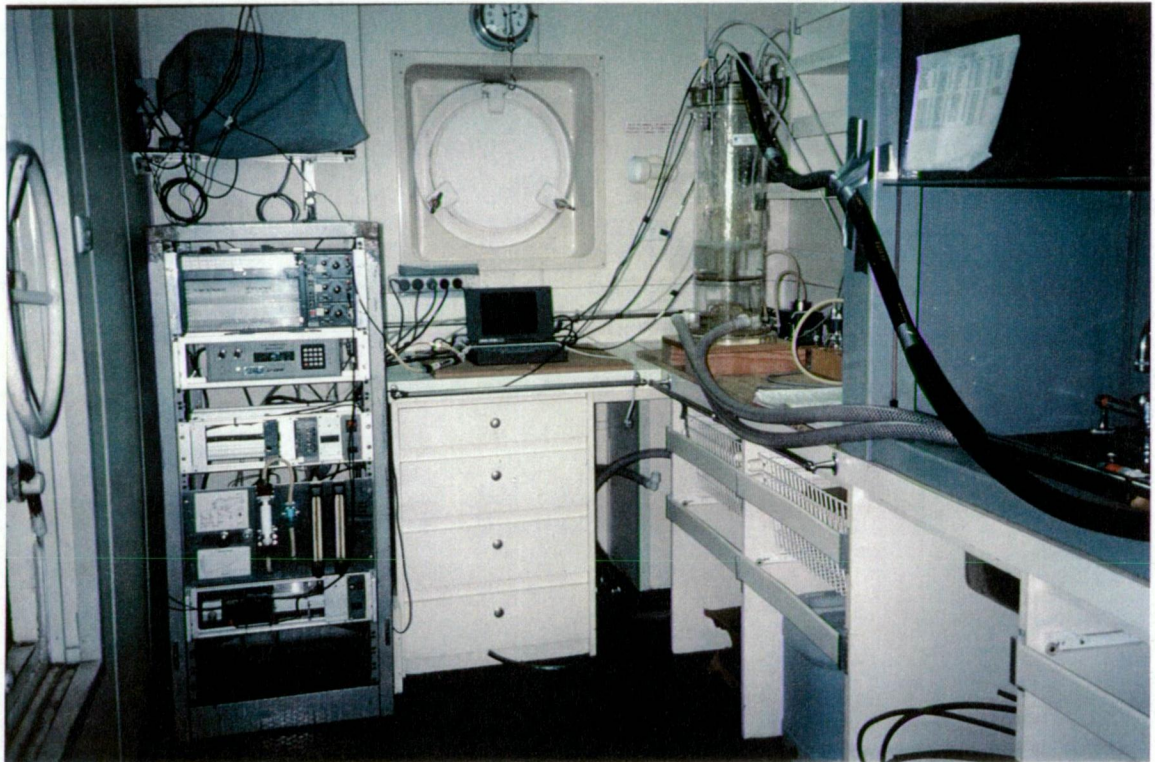


Plate 2.2 Instrumentation on the *RSV Aurora Australis* used for measuring $f\text{CO}_2$, including an equilibrator column (right) and infra-red gas analyser (left).

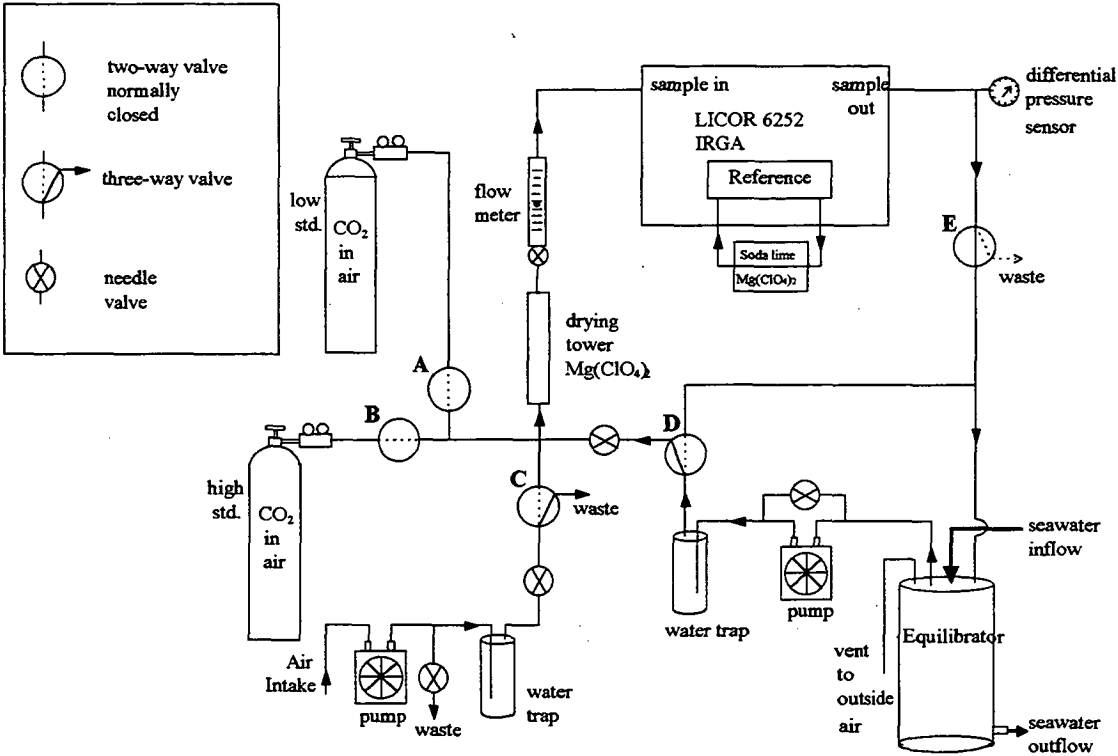


Fig. 2.1 Schematic of system used to measure the $f\text{CO}_2$ of surface waters.

2.2.1 Equilibrator

The perspex equilibrator column is similar to that designed by Dr. Ray Weiss and used by Butler et al. (1988). The major differences being a slightly smaller equilibration chamber (19 cm ID \times 47.5 cm H) and a modified drain (Figure 2.2). The volume of water in the base of the equilibrator chamber is approximately 2.5 litres and the headspace in the column is about 11 litres in volume. Seawater was pumped from an inlet at 7.5 m depth near the bow of the ship and warmed between 0.5°C and 2°C before reaching the equilibrator column. A warming of 2°C only occurred when the ship was in pack ice. The seawater flowed into the equilibrator at 6 to 10 litre min⁻¹ and passed through a “shower head” (containing 232 holes of 0.5 mm diameter), whereupon it rained down inside the column in a dense spray and drained through the bottom of the equilibrator column. The interior of the column was kept at atmospheric pressure by venting it to outside air. Air from the equilibrator head space was circulated in a closed loop at 350 ml min⁻¹ using a KNF Neuberger series N010 diaphragm vacuum pump. Three 4-wire platinum resistance temperature detectors (RTDs) were placed in the equilibrator column to measure the absolute temperature of the air-space, T_1 , waste water, T_2 , and spray, T_3 (Figure 2.2). Foam insulation was wrapped around the equilibrator during normal operation to minimise heat exchange with the lab air.

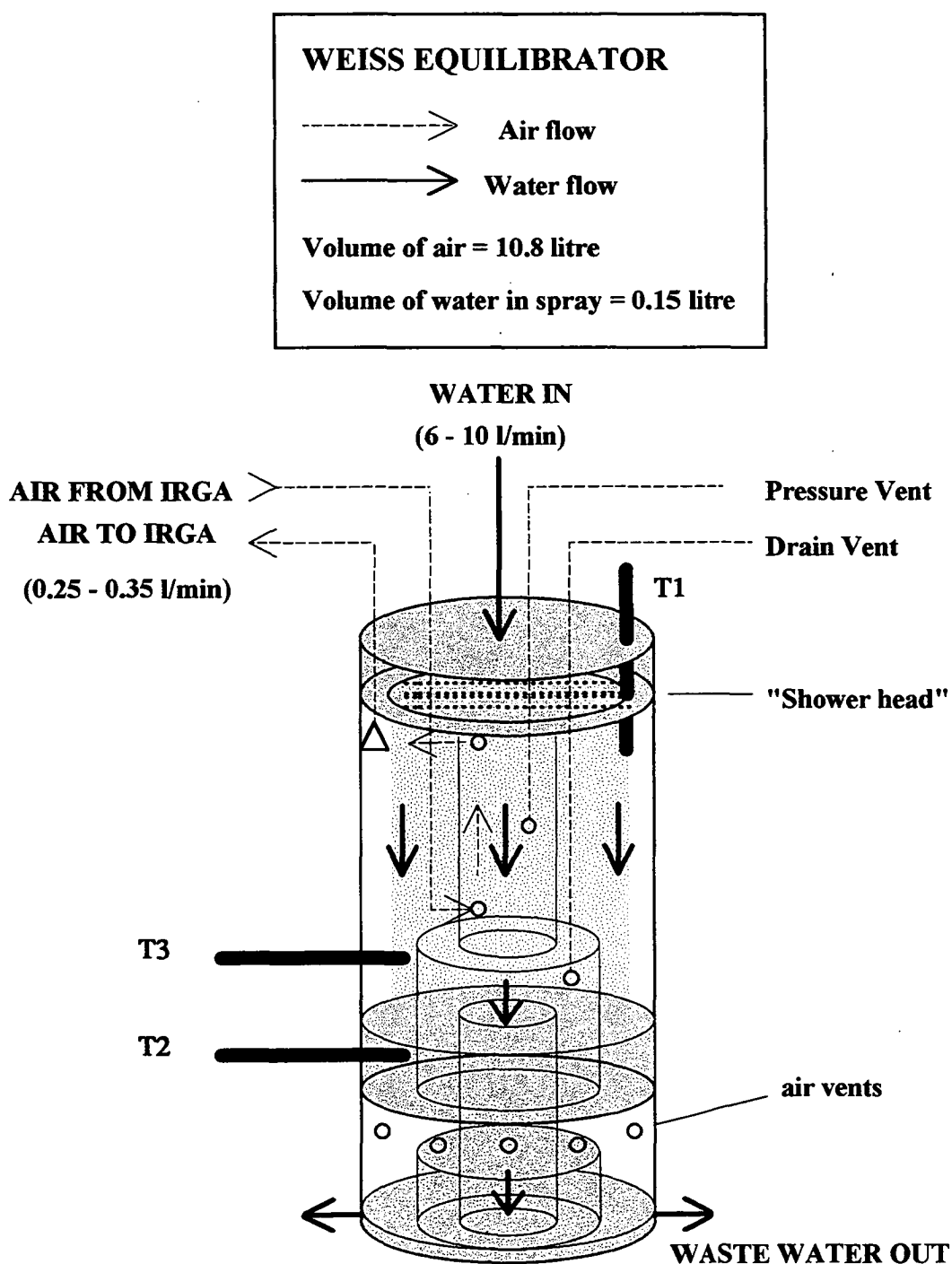
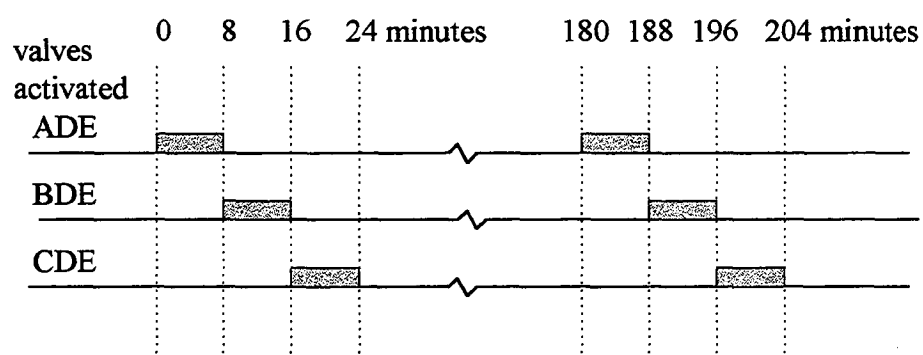


Fig. 2.2 The version of the "Weiss" type equilibrator column used on *RSV Aurora Australis* after 17 October 1992 (after Butler et al. (1988)).

2.2.2 Valve switching

Every three hours, two different calibration gases (CO₂ in air mixtures), and outside air, were dried using Dehydrite® (magnesium perchlorate) and switched into the IRGA for eight minutes each, by way of solenoids controlled by the Data Electronics DT50 Datataker. All gases flowing into the IRGA were maintained at about 350 ml min⁻¹. The sequence in which the valves A to E (Figure 2.1) were activated during a three hour cycle is shown in Figure 2.3.



3 hour cycle

Low standard (LOSPAN) - activate valves ADE, 0-8 minutes

High standard (HISPAN) - activate valves BDE, 8-16 minutes

Air sample - activate valves CDE, 16-24 minutes

Seawater - no valves activated, 24-180 minutes

Fig. 2.3. Valve switching sequence over a 180 minute cycle.

2.2.3 Gas Standards

Two CO₂-in-air standards were used to quantify the CO₂ concentration in the head-space gas and correct for drift in the infra-red gas analyser. The calibration gases were obtained from CIG (Commonwealth Industrial Gases Ltd) and were calibrated against standards which are held at the CSIRO Division of Atmospheric Research (DAR) (Beardsmore et al., 1995). These standards have in turn been calibrated against a suite of WMO X85 Secondary Standard CO₂-in-air mixtures held at CSIRO DAR. The calibrations were made at the beginning and end of use of the cylinders and agreement was typically better than 0.1 ppmv. The CO₂ mixing ratios of the low and high concentration calibration gases used on cruises between 1 October 1991 and 8 March 1993 were 321.4 ppmv and 351.1 ppmv; from 12 March to 8 May 1993 they were 329.7 ppmv and 365.0 ppmv; and from 7 August 1993 to 1 March 1994 they were 333.7 ppmv and 370.91 ppmv (D. Beardsmore, pers. com.).

2.2.4 Infra-red Gas Analyser

A LI-COR[®] 6252 non-dispersive infra-red CO₂ gas analyser (IRGA) measured the mixing ratio of CO₂ in the dried equilibrator air. Analysis of the zero gas and various standards in the range of 300 to 375 ppmv agreed to within 0.3 ppmv, indicating the output of the IRGA was reasonably linear.

The IRGA was run in "absolute mode". Soda lime and magnesium perchlorate were used to remove CO₂ and H₂O vapour from the reference cell. The zero was set using CO₂-free nitrogen and was checked periodically. The drift in the zero setting of the IRGA was typically less than 1 ppm over a month of field measurements.

The manufacturers specify the noise level of the LI-6252 IRGA as being approximately 0.2 ppmv peak-to-peak (at 350 ppmv) when using a one second signal averaging.

2.2.5 Control and Monitoring

A Datataker 50 data logger (Data Electronics Pty. Ltd.) controlled the valve switching and recorded the output signal current of the IRGA, the differential pressure in the gas lines at the exit of the IRGA sample cell, and the temperatures inside the equilibrator column at three locations. All data were collected as four minute averages of readings taken every second. For each cycle the first four minutes of data for the standards, outside air, and air from the equilibration chamber were not recorded. This allowed time to flush the lines of gases used in the previous analysis. All averaged values recorded by the Datataker were output to a PC compatible computer every four minutes through an RS232C port.

The pressure differential between the IRGA sensor cell and the outside air was measured by a Druck Model PDCR 810 differential pressure sensor located in the IRGA outlet gas line (Figure 2.1). The sensor was used to correct for any differences in the pressure of the standard gases relative to the ambient air and equilibrator headspace gases. The Druck pressure sensor was calibrated before each season and has a resolution of ± 0.05 hPa and an accuracy of ± 0.5 hPa.

Changes in atmospheric pressure can result in some drift in the span of the IRGA. In order to minimise drift, a barometric sensor (Vaisala PTA 427) with an analog output was connected to an auxiliary input of the IRGA. The sensor was calibrated using a high precision resonant sensor barometer (Druck Model DPI 141) that has been calibrated against the Australian Bureau of Meteorology Barometric Standards, and was accurate to ± 0.5 hPa.

Platinum RTD's (4-wire, $\alpha = 0.00385 \text{ } \Omega/^{\circ}\text{C}$) measured the temperature of water in the equilibrator. The RTD's were calibrated at a National Association of Testing Authorities (NATA) calibration facility located at CSIRO Division of Oceanography. The calibrations were used to characterise each RTD and repeated calibrations

indicated the temperature could be routinely measured to an accuracy of better than $\pm 0.03^\circ\text{C}$.

2.3 OTHER SHIPBOARD MEASUREMENTS NECESSARY FOR CALCULATING OCEANIC $f\text{CO}_2$

Section 2.2 described the measurement of the mixing ratio of CO_2 in the dried equilibrator air, temperatures in the equilibrator and differential pressure in the IRGA sample cell. However, in order to calculate the fugacity of CO_2 at the ocean surface, it is necessary to know the temperature and salinity of seawater at the water inlet, and the atmospheric pressure in the ship's laboratory. If instantaneous air-sea fluxes of carbon dioxide are to be determined from the oceanic $f\text{CO}_2$ values, then it is also necessary to measure the absolute wind speed from the ship.

2.3.1 Sea surface temperature

An uncontaminated seawater supply line, with inlet located in the bow of the *RSV Aurora Australis* at 7.5 m below sea level, supplied surface water to the equilibrator. The temperature of the surface seawater was continuously measured using a 4-wire PT100 RTD probe located at the inlet of the uncontaminated seawater line, about 150 mm back from the ship's hull. The signal from the probe was recorded with a Yokogawa Model 7563 Digital Thermometer with a specified accuracy of $\pm 0.05^\circ\text{C}$. These temperatures were logged with a resolution of $\pm 0.01^\circ\text{C}$ on the ship's data logging system (NOQALMS) at once per minute until 4 February 1993, and once every 20 seconds after that date. Laboratory tests performed at the Antarctic Division on 27 November 1992 indicated that the thermometer's accuracy over 24 hours was $\pm 0.0005^\circ\text{C}$ at 23°C with a 200 ms integration time. The temperature of the RTD was regularly checked against CTD temperatures measured near the inlet and agreement between the two measurements was typically better than $\pm 0.03^\circ\text{C}$.

2.3.2 Sea Surface Salinity

The salinity of the surface seawater was measured continuously with a thermosalinograph (Applied Microsystems Ltd. Model STD-12) mounted inline with the uncontaminated seawater supply line. The sampling rate was once every 10 seconds with salinity values being recorded once every minute on the NOQALMS system until 4 Feb'93/0916 UT after which time it was logged once every 20 seconds.

The accuracy of the thermosalinograph system, as specified by the manufacturer, is ± 0.01 ‰. The thermosalinograph was calibrated for salinity using measurements made on discrete water samples taken from the uncontaminated seawater line. The salinity of the water samples was measured at CSIRO Division of Oceanography using a Yeo-Cal salinometer which was calibrated routinely against IAPSO seawater standards. The calibrations indicate that in January to March 1993 the maximum standard deviation in the thermosalinograph salinities was ± 0.1 ‰. The thermosalinograph was calibrated on 19 July 1993 using a quantity of seawater of known salinity and found to have a mean standard deviation of ± 0.05 ‰ (pers. com., J. Reeve).

The maximum standard deviation in our calculated fugacities from uncertainty in the salinity values was ± 0.005 μatm , which is negligible compared with other errors.

2.3.3 Atmospheric pressure

A Vaisala Pressure Transducer (Model DPA21) was situated 18 m above sea level beside the ship's bridge. The pressure resolution was 0.1 hPa with an accuracy of ± 0.5 hPa. Logging rate on the NOQALMS system was once a minute until 4 February 1993 after which time it was logged once every 20 seconds and spot values taken every 4 minutes. As the ship's laboratory containing the equilibrator and IRGA was located

at sea level, the barometric pressure was converted from 18 m height to sea level using the hydrostatic equation combined with the equation of state for dry air (Gill, 1982). The difference in atmospheric pressures from sea level to 18 m a.s.l. was typically 2.2 hPa.

2.3.4 Sea Surface Wind speed

Relative wind speed and direction were measured at 32 m above sea level by a Belfort Instrument Co. Model 123 HD propeller anemometer. Wind values (direction and speed) were vector averaged over a 10 second period to reduce effects of pitch and roll. The standard deviation in the relative wind speed was $\pm 10\%$, with a resolution of 0.1 knot. The wind direction standard deviation was $\pm 5^\circ$ with a resolution of 0.1° . The true wind speed was calculated using the ship's heading (standard deviation $\pm 2^\circ$) and speed through the water (standard deviation $\pm 10\%$). Hence, the wind speed quoted in this thesis is the wind speed relative to the ocean surface. The 10 second average true wind speed was logged on the NOQALMS system once a minute until 4 February 1993 after which time it was logged once every 20 seconds.

2.3.5 Navigational data

A Magnavox MX1107 GPS and Transit Satellite receiver was used to measure latitude and longitude to an accuracy of ± 300 m. Latitude and longitude were logged every 20 seconds to the NOQALMS system.

2.4 CALCULATION OF OCEANIC $f\text{CO}_2$

The output of the IRGA is in the form of the mole fraction of CO_2 in $\mu\text{mol mol}^{-1}$, which is equivalent to the mixing ratio of CO_2 in ppmv. The unit adopted in this study is the fugacity of CO_2 in the air or seawater at one atmosphere total pressure, $f\text{CO}_2$.

expressed in microatmospheres (Subsection 1.3.2). The values reported are the fugacities of CO₂ in equilibrium with seawater at one atmosphere total pressure and at the sea surface temperature.

2.4.1 Correction for pressure variation in the IRGA cell

The infra-red gas analyser measures mixing ratios of CO₂ in the sensor cell, C_i (ppmv), which are proportional to the partial pressure of CO₂ in the cell. Applying Dalton's Law (Gordon, 1973), it follows that the mixing ratio of the CO₂ sample at ambient atmospheric pressure, p (atm), is given by:

$$C(\text{ppmv}) = C_i \frac{p}{p_i} \quad 2.1$$

where

$$p_i = \text{pressure in IRGA sample cell (atm).}$$

For the measurements made in this study, the pressure in the IRGA cell was typically 0.7 hPa greater for sample gases than for reference gases. The pressure correction was of the order of about 0.07 % for samples near 1 atmosphere pressure.

The output current of the IRGA sample cell, I_i (mA), is proportional to C_i . Following equation 2.1, the output current scaled to one atmosphere total pressure is given by:

$$I(\text{mA}) = I_i \frac{1}{p_i} \quad 2.2$$

2.4.2 Correction for IRGA drift

Changes in pressure and temperature cause the output signal of the infra-red gas analyser to drift with time. To correct for this drift, calibration gases were switched

into the IRGA every three hours (Subsection 2.2.3) and a linear interpolation with time was applied between the calibration gas analyses. Let I_1 and I_2 represent the IRGA output current response to the two calibration gases, scaled to one atmosphere total pressure using equation 2.2, and corrected for the drift between calibrations. The maximum drift in I_1 and I_2 over the three hour period between calibrations was equivalent to a change in CO_2 concentration of about 0.3 ppmv.

The output of the IRGA being linear over the expected range of concentrations (Subsection 2.2.4) allowed the mixing ratio of CO_2 in dried air from the equilibrator at one atmosphere pressure, C_o , to be calculated as follows:

$$C_o \text{ (ppmv)} = \frac{C_2 - C_1}{I_2 - I_1} (I_o - I_1) + C_1 \quad 2.3$$

where

C_1 = CO_2 mixing ratio of the lower concentration calibration gas at one atmosphere (ppmv),

C_2 = CO_2 mixing ratio of the higher concentration calibration gas at one atmosphere (ppmv),

I_o = IRGA output current response to the mixing ratio of CO_2 in dried air from the equilibrator corrected to 1 atm total pressure (mA).

From a study of CO_2 mixing ratios in dried air sampled under baseline conditions on the ship and analysed on the IRGA the maximum standard deviation in C_o was estimated to be ± 1 ppmv.

2.4.3 Correction for drying the air stream

The output of the infra-red gas analyser is sensitive to water vapour as well as to CO_2 , and therefore it was necessary to remove moisture from the air stream by using a

drying tower filled with Dehydrite[®]. When water vapour is removed from the air stream, the concentrations of all the remaining gases are increased in proportion to the original water vapour pressure in the air stream, p_{H_2O} . The gas phase in the equilibrator is saturated with respect to water vapour, and therefore the partial pressure of CO₂ (at 1 atm) in the undried equilibrator air stream, $C_m(T_o)$, is given in terms of the corresponding dried mixing ratio, C_o , by (Weiss and Price, 1980):

$$C_m(T_o) (\mu\text{atm}) = C_o (1 - p_{H_2O}(T_o)) \quad 2.4$$

where

$p_{H_2O}(T_o)$ = saturated vapour pressure of seawater in the equilibrator (atm),

T_o = absolute temperature of seawater in equilibrator.

The seawater vapour pressure, p_{H_2O} , was calculated from the absolute temperature of seawater in the equilibrator, T_o , and salinity, S (‰) (Weiss and Price (1980)):

$$\ln p_{H_2O} = 24.4543 - 67.4509 (100 / T_o) - 4.8489 \ln(T_o / 100) - 0.000544 S \quad 2.5$$

The calculated standard deviation in p_{H_2O} was less than ± 0.0001 atm, which is negligible compared with the standard deviation in $C_m(T_o)$. The standard deviation in $C_m(T_o)$ was therefore ± 1 ppmv.

2.4.4 Conversion from $p\text{CO}_2$ to $f\text{CO}_2$

An expression for the fugacity of a non-ideal gas in seawater (Weiss, 1974) was used to convert partial pressure values ($C_m(T_o)$) to the equivalent fugacity of CO₂ at the equilibrator temperature, $f_m(T_o)$:

$$f_m(T_o) (\mu\text{atm}) = C_m(T_o) \exp[(\beta(T_o) + 2\chi(T_o))p/RT_o] \quad 2.6$$

where

p = total pressure, which in this case is 1 atm,

R = 82.05601 cm³ atm mol⁻¹ K⁻¹.

For CO₂ in seawater (Weiss, 1974):

$$\beta(T_o) = -1636.75 + 12.0408 T_o - 3.27957 \times 10^{-2} T_o^2 + 3.16528 \times 10^{-5} T_o^3 \quad 2.7$$

$$\chi(T_o) = 57.7 - 0.118 T_o \quad 2.8$$

The units for β and χ are both cm³ mol⁻¹. For a standard deviation in $C_m(T_o)$ of ± 1 μ atm, the corresponding standard deviation in $f_m(T_o)$ was approximately ± 1 μ atm.

2.4.5 Correction of the measured $f\text{CO}_2$ for warming of the seawater

In the absence of external exchange, the $f\text{CO}_2$ of seawater increases with increasing temperature. This variation of $f\text{CO}_2$ is due to the modification of the equilibrium position with temperature of the carbonate system and also of other weak acids systems, such as borate (Copin-Montégut, 1988). In this study, seawater warmed between 0.5°C and 2.0°C between the ship's inlet and the equilibrator and a correction had to be applied to account for the warming.

For a change in temperature of up to 1°C, Weiss et al. (1982) proposed a relationship for the temperature dependence of $f\text{CO}_2$ which is not strongly dependent on the choice of dissociation constants. For larger temperature variations, however, the equation of Weiss et al. (1982) must be integrated and in this case the deviation between $f\text{CO}_2$ computed from their formula and $f\text{CO}_2$ computed from DIC and total alkalinity depends on the equilibrium constants used (Copin-Montégut, 1988). Copin-Montégut (1988) found that the Weiss et al. formula does not fit all the values of $f\text{CO}_2$ calculated using the dissociation constants for carbonic acid in seawater computed by Dickson and Millero (1987). Copin-Montégut (1988, 1989) established a new formula to calculate

$f\text{CO}_2$ in seawater at one temperature, given that the fugacity at another temperature is known, which used the dissociation constants for carbonic acid in seawater taken from Dickson and Millero (1987) and ensures a smaller deviation than the Weiss et al. (1982) equation for any temperature variation. Therefore the Copin-Montégut (1988, 1989) relationship is chosen in this study.

The fugacity of CO_2 at the inlet to the uncontaminated seawater supply, $f_m(T_m)$, is expressed in terms of the $f\text{CO}_2$ of seawater in the equilibrator, $f_m(T_o)$, as (Copin-Montégut, 1988; 1989):

$$\ln f_m(T_m) = \frac{a(T_m)}{a(T_o)} \ln[f_m(T_o) / b(T_o)] + \ln b(T_m) \quad 2.9$$

where

$$\begin{aligned} T_m &= \text{absolute temperature of seawater at the inlet to the ship's} \\ &\quad \text{uncontaminated seawater supply,} \\ T_o &= \text{absolute temperature of seawater in the equilibrator (from T3 in} \\ &\quad \text{Figure 2.2),} \\ a(T) &= 1 + \alpha (T - 273.16), \\ b(T) &= 1 + \gamma (T - 273.16) + \eta (T - 273.16)^2 + \iota (T - 273.16)^3, \\ T &= \text{absolute temperature,} \\ \alpha &= -(1127 + 4.7S) \times 10^{-6}, \\ \gamma &= (3695 + 10.6S) \times 10^{-5}, \\ \eta &= (375 + 3.4S) \times 10^{-6}, \\ \iota &= (0.92 - 0.134S) \times 10^{-6}, \\ S &= \text{salinity (‰).} \end{aligned}$$

The above values of the coefficients, α , γ , η and ι , were taken from Copin-Montégut (1989), and are appropriate for waters where the ratio of DIC to total alkalinity is in

the range 0.83 to 0.93. The ratios of DIC to total alkalinity were within this range in GEOSECS data from the Southern Ocean (Takahashi et al., 1980).

The standard deviation in $f_m(T_m)$ was approximately $\pm 1 \mu\text{atm}$.

2.5 MEASUREMENT OF ATMOSPHERIC CO₂ MIXING RATIOS

2.5.1 Air sampling on the ship

Air samples were collected over the Southern Ocean in 0.5 litre glass flasks supplied by CSIRO Division of Atmospheric Research (DAR). The flasks were prepared at DAR by first cleaning with alcohol and distilled water, after which they were oven dried at 110°C for 3–4 hours, then flushed for one hour with high purity cylinder air before sealing (Francey et al., 1995a). Subsequently, the flasks were flushed and filled with clean, dry air at around 80 kPa above ambient pressure before shipment to Hobart.

The flasks were filled on *RSV Aurora Australis* using a DAR FPU pump unit (Plate 2.3; Francey et al., 1995a), employing a KNF Neuberger diaphragm pump, with the air entering the pump via a drying tower filled with Dehydrite[®]. Each flask was flushed at the sampling site for 10 minutes prior to filling, then the flask sealed with the air sample at 70 kPa above ambient pressure. Until 5 January 1993 air sampling took place with the pump unit located on the deck of the *RSV Aurora Australis* and the 2 m inlet tube held out over the side of the ship. The cleanest air was obtained by sampling on either port or starboard side of the uppermost deck, forward of the ship's stack (Plate 2.1). On 1 January 1993 Dekoron[®] tubing was installed from either side of the uppermost deck, and the FPU pump unit connected to either tube via quick connects and operated in the laboratory immediately below this deck. The height of the air inlets above sea level was ≈ 20 m. Air was sampled only when the relative wind speed exceeded 5 m s^{-1} and relative wind direction was within $\pm 135^\circ$ of the ship's bow. Data from only four out of 360 flasks meeting these criteria had to be discarded due to contamination over the study period.

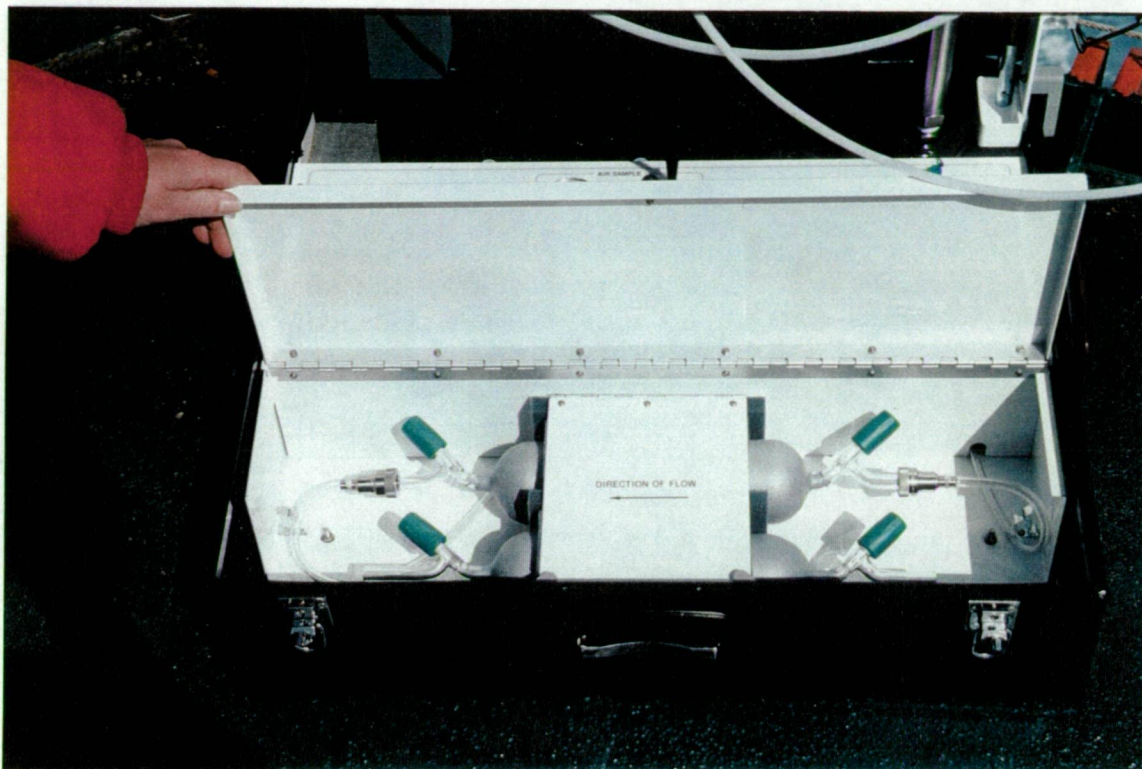


Plate 2.3 Air sampling on the *RSV Aurora Australis* using a CSIRO Division of Atmospheric Research FPU pump unit.

2.5.2 Gas Chromatography analysis of air samples

All atmospheric CO₂ mixing ratios used in this thesis were obtained by analysis of the 0.5 litre flasks of air using a CARLE Series 400 gas chromatograph located at the CSIRO Division of Atmospheric Research Aspendale laboratories (Francey et al., 1995a). The calibration scale used was the WMO X85 mole fraction scale from a suite of gas standards held at CSIRO DAR. The standards are traceable to the WMO Central CO₂ laboratory operated by C. D. Keeling of the Scripps Institute of Oceanography, via the Climate Monitoring and Diagnostics Laboratory (CMDL) of NOAA. The external precision of the gas chromatograph for routine flask analyses was ± 0.02 % (Francey et al., 1995a).

2.6 CALCULATION OF ATMOSPHERIC $f\text{CO}_2$

In order to calculate $\Delta f\text{CO}_2$, and hence air-sea flux of CO_2 (Section 1.3), it is necessary to determine the fugacity of carbon dioxide in the atmosphere at the air-sea interface, f_a . Past researchers have determined f_a using air pumped from an inlet on the ship's bow and processed with the same shipboard equipment used for measurement of f_m . In this study, air was sampled from the bow of the *RSV Aurora Australis* every three hours, dried using Dehydrite® and input into the LI6252 infrared gas analyzer in the same fashion as the air from the equilibrator. However, whereas the external precision of gas chromatograph CO_2 mixing ratios from glass flasks filled with air along each cruise transect was approximately ± 0.07 ppmv, and the agreement between flask pairs typically better than 0.1 ppmv, the standard deviation in mixing ratios derived from the LI6252 IRGA was approximately ± 1 ppmv. Because of the much higher accuracy of the gas chromatograph, the atmospheric fugacity, f_a , was calculated from the gas chromatograph atmospheric CO_2 mixing ratios, C_a , averaged over each transect. The standard deviation in C_a for a particular transect was at most ± 0.5 ppmv which is less than the standard deviation in IRGA mixing ratios. Using equations 2.4 and 2.6, and assuming that the air at the air-sea interface was 100% water saturated air at the air-sea interface at the same temperature as the bulk sea surface temperature, T_m (Wanninkhof and Thoning, 1993), the following relationship is obtained for atmospheric fugacity of CO_2 at the air-sea interface at 1 atm total pressure (Weiss, 1974):

$$f_a(T_m) (\mu\text{atm}) = \langle C_a \rangle (1 - p_{\text{H}_2\text{O}}) \exp[\beta(T_m) + 2\chi(T_m)]p / RT_m] \quad 2.10$$

where

$$\begin{aligned} \langle C_a \rangle &= \text{Average } \text{CO}_2 \text{ mixing ratio in dried air samples collected at 20 m} \\ &\quad \text{above sea level, processed by the CARLE Series 400 gas} \\ &\quad \text{chromatograph and converted to 1 atm total pressure (ppmv),} \\ p &= \text{total atmospheric pressure} = 1 \text{ atm.} \end{aligned}$$

The standard deviation in $f_a(T_m)$ was at most approximately $\pm 0.5 \mu\text{atm}$. Hence, the maximum standard deviation in $\Delta f\text{CO}_2 (= f_m - f_a)$ was approximately $\sqrt{0.5^2 + 1^2} \mu\text{atm} = \pm 1.1 \mu\text{atm}$.

2.7 MEASUREMENT OF ATMOSPHERIC $\delta^{13}\text{C}$

After a portion of air from each 0.5 litre flask was analyzed for greenhouse gas concentrations by the CARLE Series 400 gas chromatograph at GASLAB, the remaining air was input into a Finnigan MAT MT Box-C gas preparation system in order to extract pure CO_2 gas (Francey et al., 1995a). The pure CO_2 gas was then fed into a MAT 252 dual-inlet isotope-ratio mass spectrometer (Finnigan MAT GmbH, Bremen).

In the ion source of the mass spectrometer, CO_2 molecules are ionized by an electron beam generated by a heated tungsten filament, and an accelerating potential propels the positive ions down the analyzer tube into the curved sector located in a magnetic field. Holding the strength of the magnetic field and the accelerating potential constant, the trajectory of the ions passing through the magnetic field becomes a function of the mass and energy of the ions. The major species of CO_2 , 44 ($^{12}\text{C}^{16}\text{O}^{16}\text{O}$), 45 ($^{13}\text{C}^{16}\text{O}^{16}\text{O}$, $^{12}\text{C}^{17}\text{O}^{16}\text{O}$) and 46 ($^{13}\text{C}^{17}\text{O}^{16}\text{O}$, $^{12}\text{C}^{17}\text{O}^{17}\text{O}$), are resolved into three separate ion beams on the basis of their mass, each striking separate Faraday cup collectors (Allison et al., 1994). Alternating injections of the sample, and a “working” reference CO_2 gas from a variable volume reservoir, permit accurate determination of the relative ion beam ratio 45/44 (Francey et al., 1995a). Much of the high precision of the MAT252 mass spectrometer system is linked to the isotopic composition of the “working” reference gas being close to that of the air samples to be analysed (Allison et al., 1994; Francey et al., 1995a). After a number of corrections are made to the 45/44 ratio (Allison and Francey, 1995; Francey et al., 1995a) the ratio of $^{13}\text{C}/^{12}\text{C}$ in the CO_2 sample is determined relative to the reference gas (Allison et al, 1993).

To allow comparison with data from other laboratories, the $\delta^{13}\text{C}$ values relative to the working reference gas were converted to the international "PDB" reference scale (equation 1.13). The basis of the reference scale is CO_2 derived from the CaCO_3 of the rostrum of a Cretaceous belemnite (*Belemnitella americana*) collected in the Pee Dee formation of Southern Carolina, USA, and is no longer available (Allison et al., 1994). This study uses NBS19, with an IAEA recommended value of $\delta^{13}\text{C} = +1.95 \text{ ‰}$ relative to the hypothetical Vienna-PDB (VPDB), as the reference material through which measurements are related to VPDB (Allison et al., 1993).

The external precision of the $\delta^{13}\text{C}$ measurements from routine flask analyses using the MAT252 mass spectrometer was approximately $\pm 0.01 \text{ ‰}$ (Francey et al., 1989a).

2.8 MEASUREMENT OF CHLOROPHYLL *a*

During the 19 November to 28 December 1993 cruise, a seawater sample was collected from the 7.5 m uncontaminated seawater inlet every four hours that the ship was underway. The water was then filtered through a Whatman glass microfibre GF/F filter and stored in liquid nitrogen. Later, at the Australian Antarctic Division, the pigments on these filters were extracted into 3 ml of pure methanol in an ultrasonicator and separated from the filter material in a centrifuge (Wright and Shearer, 1984). The liquid was pipetted off and analysed for chlorophyll *a* in a GBC UV/VIS 916 spectrophotometer. This work was performed cooperatively with Dr. Simon Wright of the Australian Antarctic Division.

The chlorophyll *a* analyses for the 5 January to 8 March 1993 cruise were performed somewhat differently to the above method, although results should be comparable (Simon Wright, pers. com.). The extraction medium was methanol buffered with 2% V/V of 0.5 M ammonium acetate and the samples were analysed for all pigments,

including chlorophyll α , by injecting 50 μ l of the sonicated and centrifuged liquid into an HITACHI F1000 fluorescence spectrophotometer with an excitation wavelength of 430 nm. The output peaks were transferred to a personal computer and the peak areas integrated using "Maxima" software. The photometric equations used were from Geoffrey and Humphrey (1975).

CHAPTER THREE:

$\Delta f\text{CO}_2$ OVER THE ANTARCTIC

SEASONAL ICE ZONE

3.1 INTRODUCTION

A significant uncertainty in the global carbon budget can be attributed to our lack of knowledge of the role played by the Antarctic Seasonal Ice Zone (ASIZ) in the removal of carbon dioxide from the atmosphere (Section 1.1). The rate of exchange of carbon dioxide between the ocean and atmosphere is a function of sea surface temperature, wind speed, sea ice cover, and of the difference in fugacities of CO_2 across the interface, $\Delta f\text{CO}_2$ (Section 1.3). There are few measurements of the fugacity of CO_2 in surface seawater south of 55°S (Table 1.1), roughly corresponding to the most northerly extent of the Antarctic sea ice (Parkinson, 1992). Hence, it is not known if the ASIZ is currently a net source or sink for atmospheric CO_2 .

This chapter presents $\Delta f\text{CO}_2$ data collected on six voyages by the *RSV Aurora Australis* south of 55°S , between 60°E to 150°E , from 15 October 1992 to 26 February 1994 (Tilbrook and Beggs, 1996). The measurements represent a significant contribution to $\Delta f\text{CO}_2$ data collected within areas of Antarctic pack ice, and are used in Chapter 4 to estimate the monthly net uptake of atmospheric carbon dioxide by the region $55^\circ - 70^\circ\text{S}$, $60^\circ - 150^\circ\text{E}$, over the months October 1992 to March 1993.

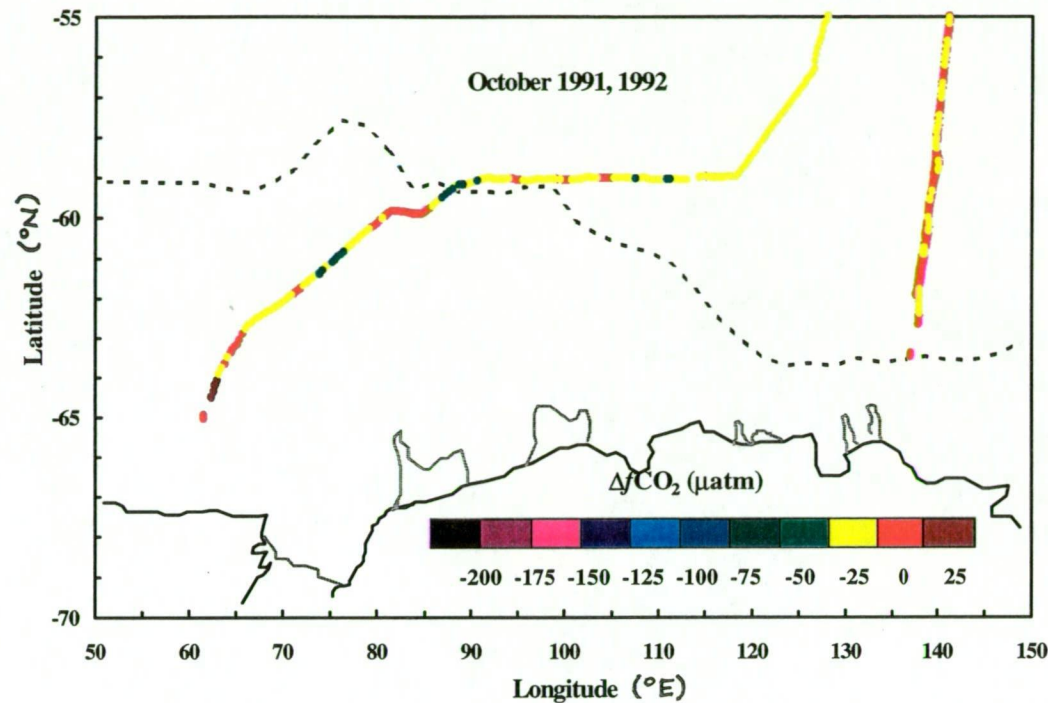
Relationships between $\Delta f\text{CO}_2$, surface chlorophyll a concentrations and sea surface temperatures are investigated, in order to demonstrate the high productivity of surface waters south of 60°S , between 60°E and 105°E .

3.2 OBSERVATIONS OF $\Delta f\text{CO}_2$ IN THE ASIZ

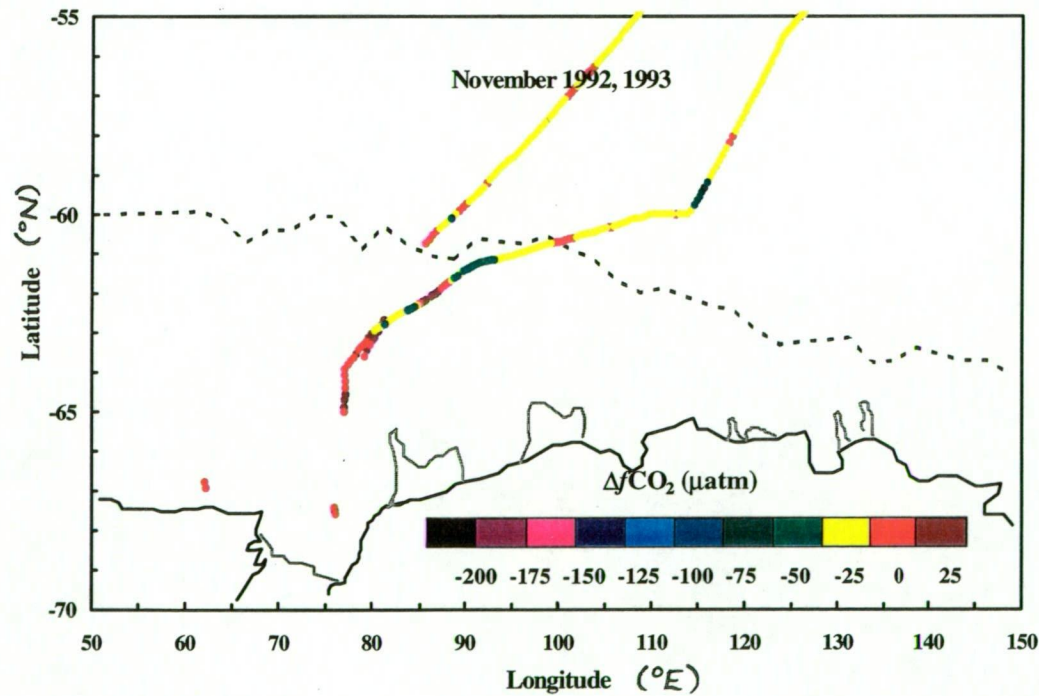
The fugacity of carbon dioxide in surface seawater, f_m , was continuously measured on six cruises between Hobart and Antarctica aboard the Australian icebreaker, *RSV Aurora Australis*, from 4 October 1991 to 28 February 1994 (Sections 2.2-2.4). The transects are shown in Appendix A: Figure A.1. Every one to three degrees of latitude along the transects, 0.5 litre glass flasks were filled with baseline air and later analysed at CSIRO Division of Atmospheric Research to obtain the mixing ratio of CO_2 in air at 20 m a.s.l. (Section 2.5). The CO_2 mixing ratios in air were converted to atmospheric $f\text{CO}_2$, f_a (Section 2.6), and were then used to calculate the difference in fugacity of CO_2 across the air-sea interface ($\Delta f\text{CO}_2 = f_m - f_a$). Atmospheric $f\text{CO}_2$ was found to vary by less than 1 μatm during each cruise, and $\Delta f\text{CO}_2$ changes generally reflected variations in the fugacity of CO_2 in surface waters.

Figure 3.1 presents hourly averaged values of $\Delta f\text{CO}_2$ collected south of 55°S , during the months October to April. An hourly average was chosen in order to smooth any short term variations in the gas analyser output on the ship. Negative values indicate a potential sink for atmospheric CO_2 , and positive values a potential source of CO_2 to the atmosphere.

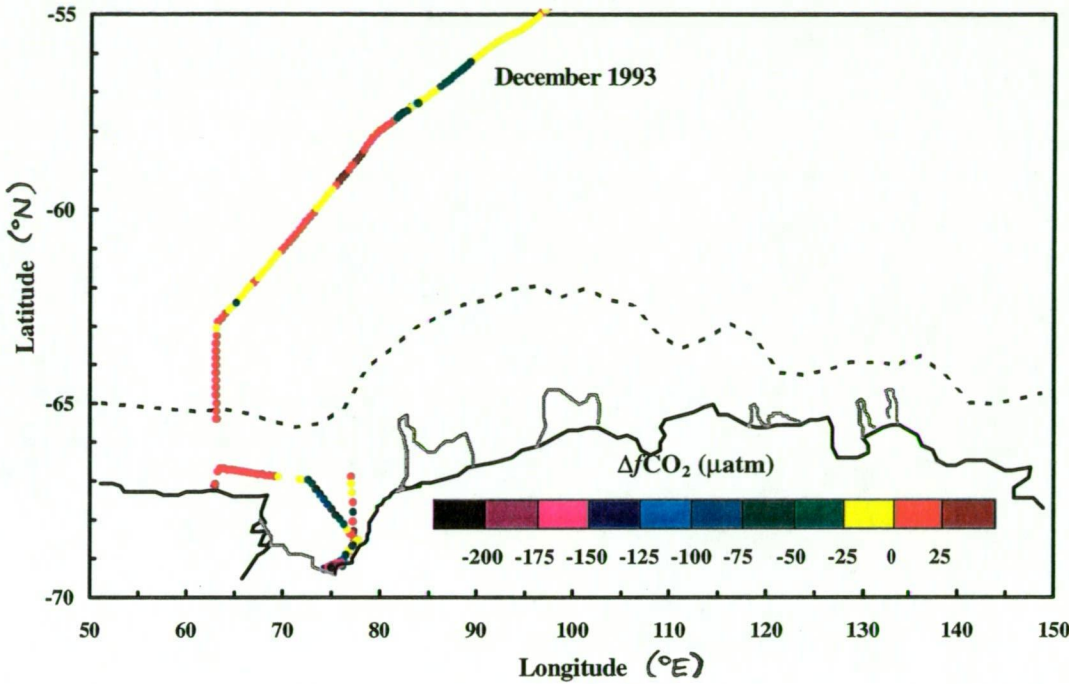
(a)



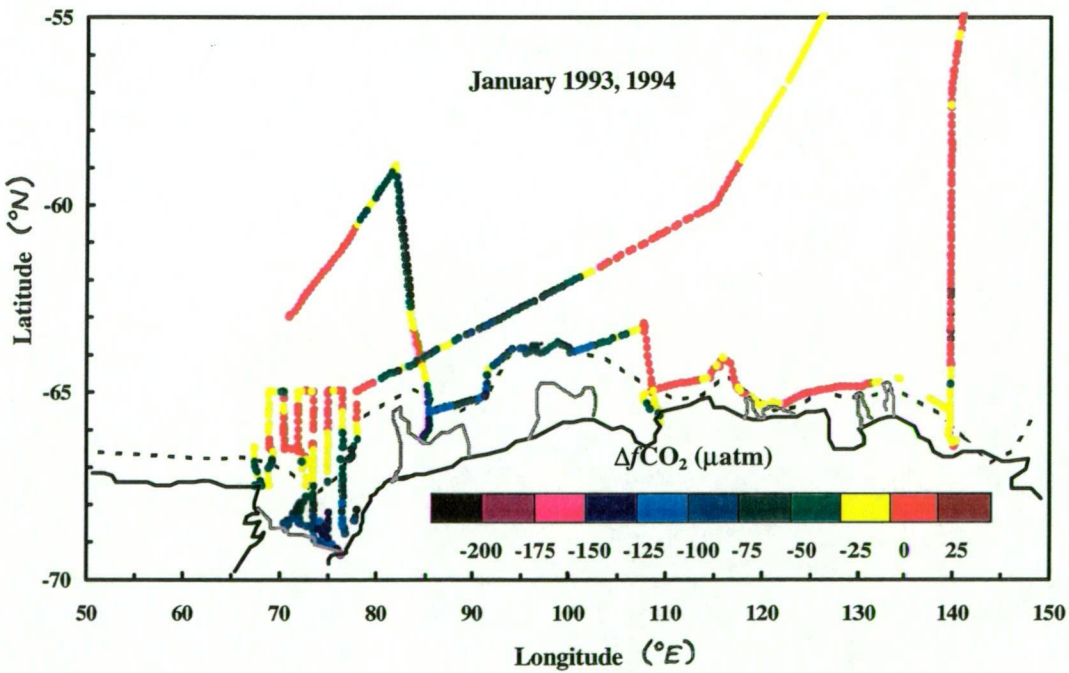
(b)



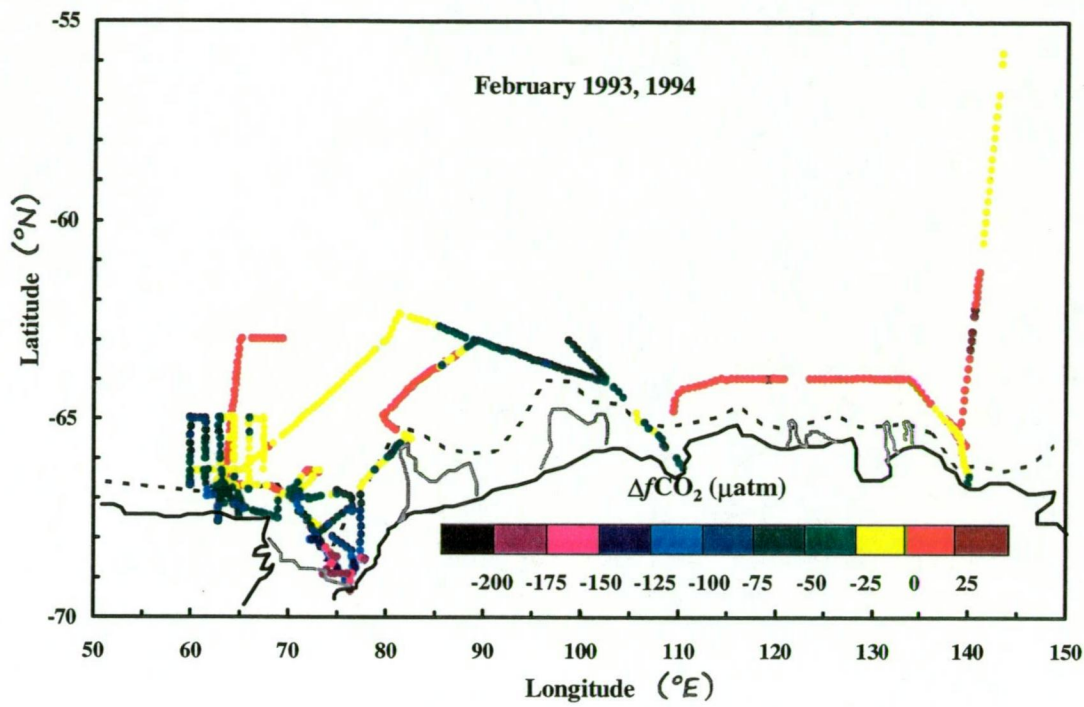
(c)



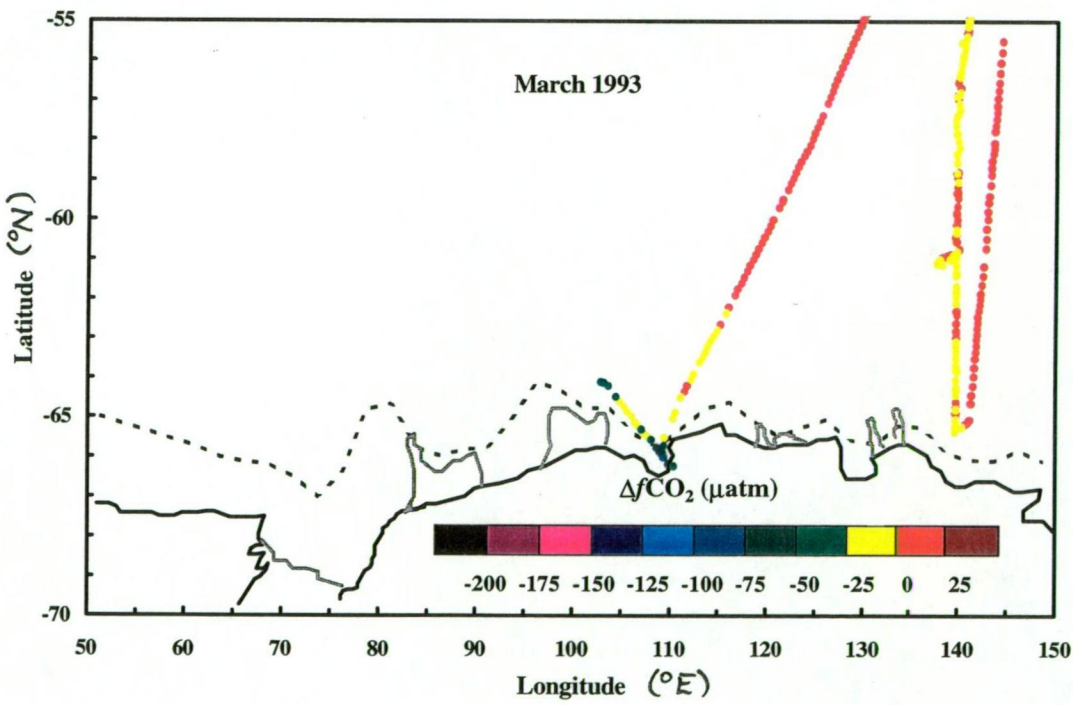
(d)



(e)



(f)



(g)

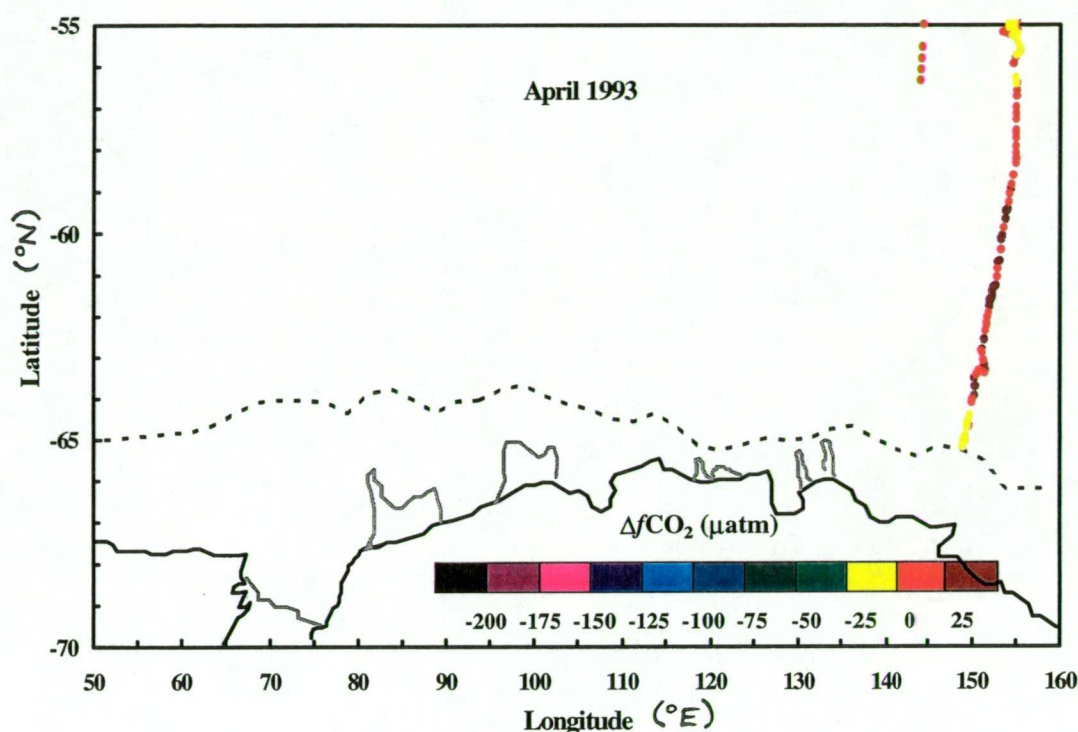


Fig. 3.1 Hourly averaged values of $\Delta f\text{CO}_2$ (oceanic $f\text{CO}_2$ - atmospheric $f\text{CO}_2$) measured from the *RSV Aurora Australis* along transects south of 55°S during (a) 15-22 October 1991, 21-28 October 1992, (b) 5-17 November 1992 and 24-30 November 1993, (c) 1-20 December 1993, (d) 10-31 January 1993 and 9-31 January 1994, (e) 1-28 February 1993 and 1-26 February 1994, (f) 1-31 March 1993, and (g) 1-27 April 1993. The solid grey lines denote ice shelves and the dashed lines represent the mean position of the ice edge for those particular months.

In October and November (Figures 3.1(a)-(b)), a high proportion of $\Delta f\text{CO}_2$ data was measured in regions of up to 9/10 pack ice, and $\Delta f\text{CO}_2$ values were generally between $\pm 25 \mu\text{atm}$. In January and February, there was a distinct contrast between hourly averaged $\Delta f\text{CO}_2$ values measured west of 105°E ($-201 \mu\text{atm} < \Delta f\text{CO}_2 < 23 \mu\text{atm}$, mean = $-43 \mu\text{atm}$) compared with east of 105°E ($-75 \mu\text{atm} < \Delta f\text{CO}_2 < 32 \mu\text{atm}$, mean = $2 \mu\text{atm}$) (Figures 3.1(d)-(e)), with a range of values in Prydz Bay (67° - 70°S, 70° - 79°E) of $-201 \mu\text{atm} < \Delta f\text{CO}_2 < 4 \mu\text{atm}$ (mean = $-89 \mu\text{atm}$). Instantaneous values of $\Delta f\text{CO}_2$ as low as $-246 \mu\text{atm}$ ($f_m = 109 \mu\text{atm}$) were measured at 69.26°S, 74.98°E on 4 December 1993, in ice-free seas close to the Amery Ice Shelf. The same waters had a

sea surface temperature of -0.61°C and a relatively high chlorophyll *a* concentration of 14.03 mg m^{-3} , implying a very high phytoplankton biomass. The sea-ice in Prydz Bay had broken up some time between 4 and 11 November 1993. An oceanic $f\text{CO}_2$ of $109 \text{ } \mu\text{atm}$ is lower than other reported partial pressures south of 55°S (Table 1.1), the lowest previous measurement being $195 \text{ } \mu\text{atm}$ measured during the summer of 1979-80 in pack-ice at 67.6°S , 62.9°E (Milne and Smith, 1980).

The low summertime oceanic fugacities measured in Prydz Bay and in the vicinity of ice shelves (shown in Figure 3.1 as solid grey lines) may be attributable to high phytoplankton productivity in shallow waters near continental margins (Comiso et al., 1993). Close to the Antarctic continent, phytoplankton blooms may be enhanced by meltwater stratification, or possibly by dissolved trace elements such as iron derived from shelf sediments and glacial melt (Sullivan et al., 1993). Over the study region, summertime values of $\Delta f\text{CO}_2$ less than $-25 \text{ } \mu\text{atm}$ were predominantly measured over the Antarctic shelf, in waters shallower than about 500 m (Figures 3.1(d)-(f)).

North of the shelf-break, between 80°E and 105°E , the negative $\Delta f\text{CO}_2$ values measured during January and February (Figures 3.1(d) and (e)) may have resulted from phytoplankton blooms at the ice edge (Smith and Nelson, 1986; Sakshaug and Skjoldal, 1989) as it retreated during late spring and early summer (Figures 3.1(a)-(d)). The seasonal ice zone covered only about 3° of latitude between 120°E and 150°E , whereas it extended over 10° to 14° of latitude north of Prydz Bay (Figures 3.1(a)-(g)). From November to January, sea-ice melted over a much greater area of ocean in the western region (60° - 105°E), compared with the eastern half of the study region (105° - 150°E). Ice-edge algal blooms had a larger area over which to develop west of 105°E , and therefore a greater probability of significant development during the spring/summer. The relatively negative values of $\Delta f\text{CO}_2$ (as low as $-100 \text{ } \mu\text{atm}$) measured to the north-east of Prydz Bay in the region south of 59°S , between 80°E and 105°E , correspond to a relatively high pigment region (0.4 to 1.2 mg m^{-3}) on CZCS (Coastal Zone Colour Scanner) maps (Comiso et al., 1993).

Hashida et al. (1994) also report low partial pressures of CO_2 in surface waters ($-95 \mu\text{atm} < \Delta p\text{CO}_2 < -5 \mu\text{atm}$) between 82°E and 102°E , from four transects during February to March (1989-92) along approximately 63°S .

3.3 RELATIONSHIP BETWEEN $\Delta f\text{CO}_2$ AND CHLOROPHYLL a

The fugacity of CO_2 in surface waters is influenced by the biological fixation of dissolved inorganic carbon via photosynthesis in phytoplankton. Chlorophyll a is present in all photosynthetic algae and the concentration of chlorophyll a is routinely used as a convenient measure of the current approximate abundance of phytoplankton in a water sample (e.g. Jacques and Fukuchi, 1994). In this study, chlorophyll a is used to indicate where phytoplankton blooms were present, and as a qualitative indication of the importance of biological production on levels of $f\text{CO}_2$ in the surface ocean (Schneider and Morlang, 1995).

The relationship between observations of low oceanic $f\text{CO}_2$ and high chlorophyll a in the ASIZ is demonstrated in Figure 3.2, which gives the hourly averaged $\Delta f\text{CO}_2$ values measured in the region $55^\circ - 70^\circ\text{S}$, $60^\circ - 126^\circ\text{E}$, plotted against values of chlorophyll a obtained from surface water samples (Section 2.8). The chlorophyll a concentrations for the period 17 January to 7 February 1993 were obtained by averaging measurements from water samples taken from Niskin bottles filled at 1 m and 10 m depths at each site. Over this period, the depth of the mixed layer was less than 25 m, and the standard deviation of the difference between the 1 m and 10 m samples was $\pm 0.6 \text{ mg chl } a \text{ m}^{-3}$ ($n = 81$), from a total range of chlorophyll a concentrations of 0.002 to 4.03 mg m^{-3} . The average of the chlorophyll a measurements at 1 m and 10 m depths was taken to be representative of chlorophyll a concentrations in the mixed layer at each sampling site. Chlorophyll a concentrations for 24 November to 20 December 1993 were measured from water samples taken from the same seawater intake (at 7.5 m) used to measure oceanic $f\text{CO}_2$. Values were particularly elevated (up to $17.2 \text{ mg Chl } a \text{ m}^{-3}$) in the southern-most region of Prydz Bay, south of 69°S (See Appendix B: Figures B.4 and B.5).

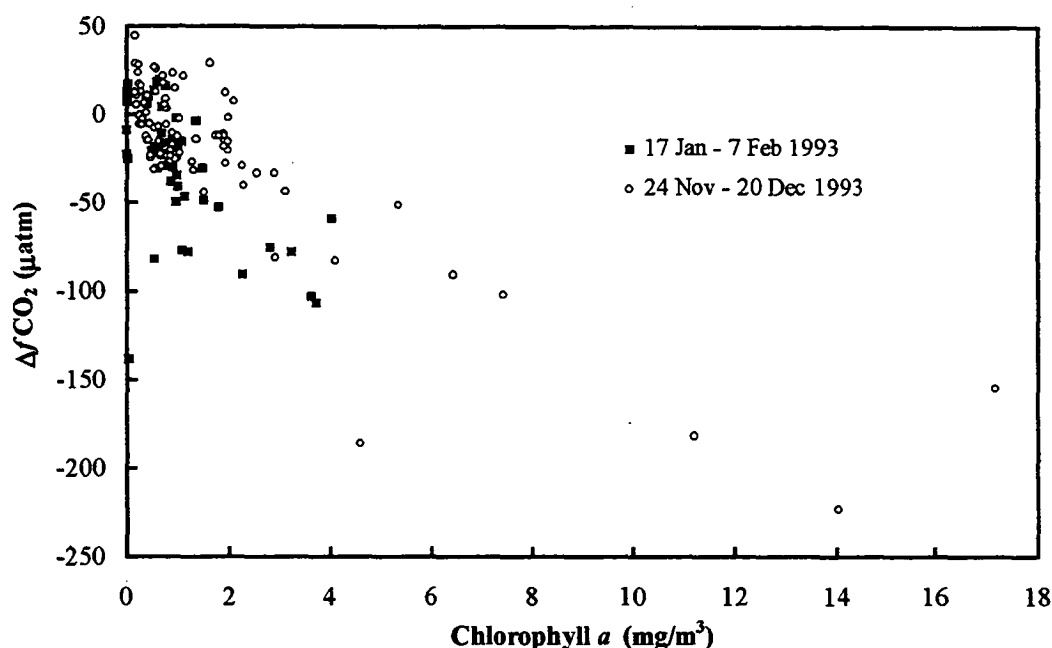


Fig. 3.2 Hourly averaged $\Delta f\text{CO}_2$ values measured in the region south of 55°S , between 60°E and 126°E , plotted against concentrations of Chlorophyll a in surface water samples.

Samples collected between 24 November and 20 December 1993 show $\Delta f\text{CO}_2$ strongly anti-correlated with chlorophyll a concentrations ($r^2 = 0.72$, $n = 86$) (Section B.4), with the slope of the linear regression, $d(\Delta f\text{CO}_2)/d(\text{Chl } a)$, equaling $-14 \pm 1 \mu\text{atm}/(\text{mg Chl } a \text{ m}^{-3})$. During the period 17 January to 7 February 1993, the anti-correlation was less strong ($r^2 = 0.37$, $n = 57$), and $d(\Delta f\text{CO}_2)/d(\text{Chl } a)$ was $-23 \pm 4 \mu\text{atm}/(\text{mg Chl } a \text{ m}^{-3})$. The stronger anti-correlation in the November/December period may result from more recent development of ice edge algal blooms (Sakshaug and Skjoldal, 1989) compared with January/February, since the sea-ice over the study region began to retreat in October 1993. The regression coefficient of $d(\Delta f\text{CO}_2)/d(\text{Chl } a)$ obtained for the November/December period is similar to the $-18 \mu\text{atm}/(\text{mg Chl } a \text{ m}^{-3})$ regression slope from measurements of $p\text{CO}_2$ and chlorophyll a taken during December 1991 in the South Atlantic, between 40°S and 62°S (Schneider and Morlang, 1995).

Although negative correlations between $\Delta f\text{CO}_2$ and chlorophyll a concentrations in highly productive regions ($> 1 \text{ mg Chl } a \text{ m}^{-3}$) are due to the utilization of dissolved

inorganic carbon in surface waters by phytoplankton, low fugacity does not necessarily imply a high chlorophyll *a* content in the same waters. The fugacity of CO₂ in the surface ocean, corrected for ocean mixing, air-sea gas exchange and changes in sea temperature, is a rough indicator of the total uptake of DIC in the surface water by phytoplankton from the start of the spring blooms. Chlorophyll *a* concentration, on the other hand, is influenced not only by vertical mixing and advection, but also by zooplankton grazing, sedimentation, light limitation, and the composition of the phytoplankton population (Schneider and Morlang, 1995).

3.4 RELATIONSHIP BETWEEN $\Delta f\text{CO}_2$ AND SEA SURFACE TEMPERATURE

The effect of a change in seawater temperature, on the fugacity of CO₂ has been described in detail in Subsection 2.4.5. The fugacity is temperature dependent due to the temperature dependence of the dissociation constants of carbonic acid and solubility of CO₂ in seawater (Weiss, 1974). For example, laboratory tests have shown that in waters with a salinity of 35 ‰, DIC concentration of 1917 $\mu\text{mol kg}^{-1}$ and temperatures between -2°C and 10°C, the difference between oceanic $f\text{CO}_2$ and its value at 20°C increases at approximately 6 $\mu\text{atm } ^\circ\text{C}^{-1}$ (Goyet et al., 1993).

In the complex ocean system of the ASIZ, a poor correlation exists between hourly mean $\Delta f\text{CO}_2$ and hourly averaged sea surface temperature over the region 55° - 70°S, 60° - 150°E (Figure 3.3). During the summer months, r^2 values were 0.06 ($n = 1882$) for January 1993 and 1994, 0.30 ($n = 1534$) for February 1993 and 1994, and 0.005 ($n = 384$) for December 1993. During the spring months, the r^2 values were 0.03 ($n = 426$) for October 1991 and 1992, and 0.005 ($n = 498$) for November 1992 and 1993. The summertime lack of correlation with temperatures less than about 2°C agrees with Southern Ocean studies by Poisson et al. (1993), Takahashi (1993), Robertson and Watson (1995) and Schneider and Morlang (1995), and is due to coastal and ice edge algal blooms in this region affecting oceanic $f\text{CO}_2$ levels more strongly than temperature. This hypothesis is supported by the

strong anti-correlations shown in Figure 3.2 between $\Delta f\text{CO}_2$ and chlorophyll *a* concentrations in surface waters of the ASIZ during early summer (24 November to 20 December 1993). An increase in chlorophyll *a* concentration of 1 mg m^{-3} resulted in a decrease in $\Delta f\text{CO}_2$ of $-14 \pm 1 \text{ } \mu\text{atm}$ during this period, whereas an increase in sea surface temperatures over the same region caused an approximate increase in $\Delta f\text{CO}_2$ of between $5 \text{ } \mu\text{atm } ^\circ\text{C}^{-1}$ and $11 \text{ } \mu\text{atm } ^\circ\text{C}^{-1}$ (Copin-Montégut, 1988; Copin-Montégut, 1989). Therefore, strong increases in productivity would have swamped the sea surface temperature effect on oceanic $f\text{CO}_2$.

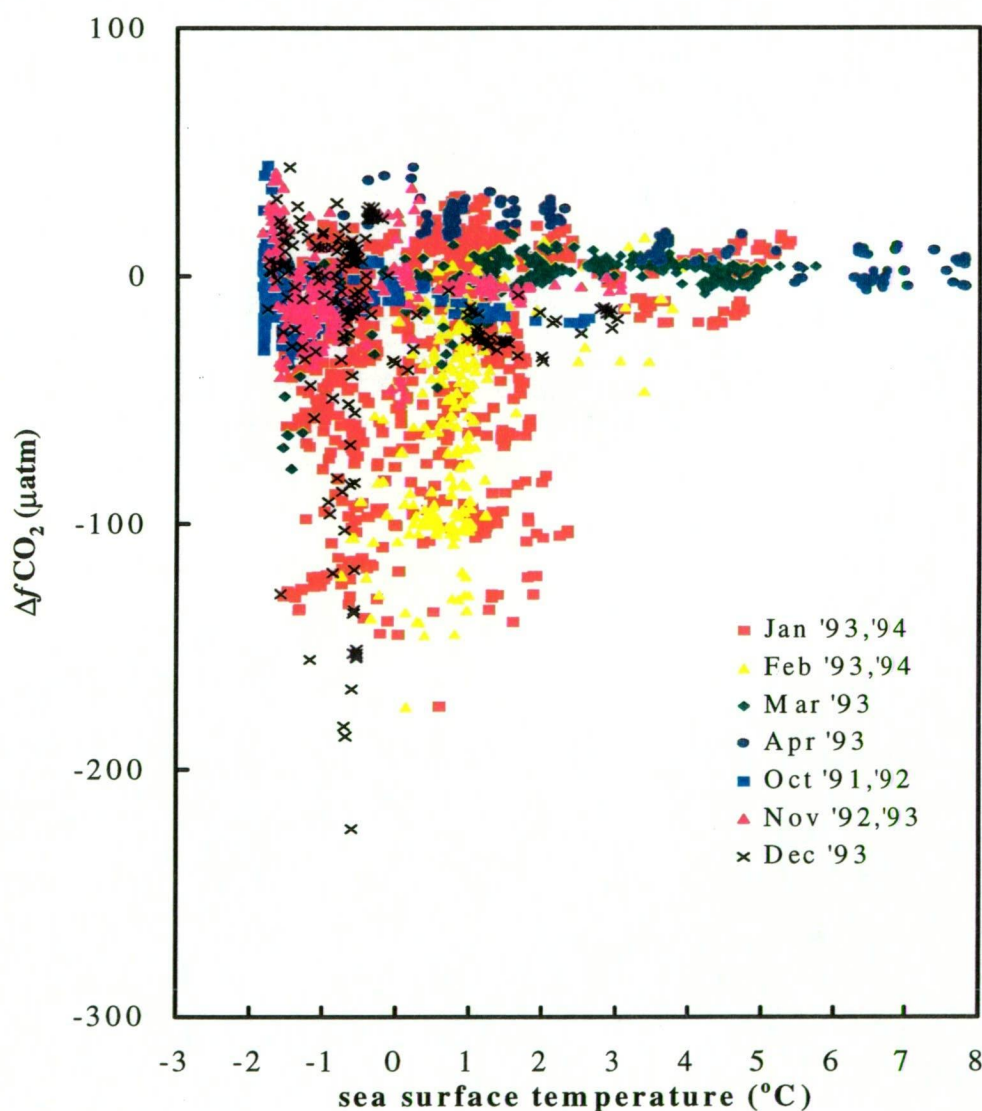


Fig. 3.3 Hourly averaged $\Delta f\text{CO}_2$ values measured from the *RSV Aurora Australis* during 15 October 1991 to 26 February 1994 over the region $55^\circ - 70^\circ\text{S}$, $60^\circ - 150^\circ\text{E}$, plotted against hourly mean values of sea surface temperature at the water inlet (7.5 m depth).

3.5 CONCLUSIONS

Evidence was presented for a seasonal oceanic sink for carbon dioxide in the Antarctic Seasonal Ice Zone from 60°E to 105°E, based on measurements of the fugacity of CO₂ in surface waters taken on six voyages from 4 October 1991 to 28 February 1994, covering the coast of Antarctica from 60°E to 150°E. Extensive ocean sampling during January to February, particularly in areas of pack ice, indicated that the region 55° - 70°S, 60° - 105°E, experienced much lower oceanic fugacities compared with the ocean to the east (55° - 70°S, 105° - 150°E). Hourly average $\Delta f\text{CO}_2$ values in the western region ranged from -201 μatm to 23 μatm , with a mean of -43 μatm , whereas over the eastern region the range was -75 μatm to 32 μatm , with an average $\Delta f\text{CO}_2$ value of 2 μatm . The zonal contrast in oceanic $f\text{CO}_2$ values during the summer is partially due to the difference in the area of seasonal pack ice over the two regions. A larger area of ice melting during early summer provides a greater opportunity for algal blooms to develop. However, much of the seasonal ice zone west of 105°E experienced little or no depletion in $f\text{CO}_2$ of the surface ocean by late February 1993, in spite of the retreat of the ice edge. It would appear, then, that the retreating sea-ice did not generate phytoplankton blooms in all of the study region, possibly due to iron limitation.

Particularly low levels of oceanic $f\text{CO}_2$ (as low as 109 μatm) were measured in southern Prydz Bay (> 69°S) from early December to mid-February, linked to intense algal blooms during that time, with measured surface chlorophyll *a* concentrations reaching 17.2 mg m⁻³. During early summer, over the region 55°-70°S, 60°-126°E, $\Delta f\text{CO}_2$ measurements were strongly anti-correlated with chlorophyll *a* ($r^2 = 0.72$, $n = 87$), but poorly correlated with sea surface temperature. Hence, phytoplankton productivity was the predominant cause of low fugacities in surface waters measured during summer over this region of the ASIZ.

CHAPTER FOUR:

NET AIR-SEA TRANSFER OF CO₂

OVER THE ANTARCTIC SEASONAL ICE ZONE

4.1 INTRODUCTION

In this chapter the $\Delta f\text{CO}_2$ data obtained in the Antarctic Seasonal Ice Zone (Chapter 3) are used to estimate the net rate of air-sea transfer of carbon dioxide over the region of the Southern Ocean south of 55°S, between 60°E and 150°E. In order to determine the effect that choice of wind speed data set and interpolation of $\Delta f\text{CO}_2$ data has on estimates of net transfer, two different methods are used to calculate net air-sea flux. The first uses hourly averaged surface wind speeds measured from *RSV Aurora Australis*, and the second, six-hourly “spot” surface wind speeds from the Australian Bureau of Meteorology’s Global Assimilation and Prediction System (GASP) analyses. These transfer estimates are then compared against those calculated by other workers using similar methods.

The net flux of CO₂ from the surface ocean to the atmosphere, F , may be defined from equations 1.2, 1.3 and 1.8 as

$$F (\text{g C m}^{-2} \text{ d}^{-1}) = 2.88 \sigma_m X W^2 (\text{Sc}/660)^{-1/2} \Delta f\text{CO}_2 \quad (4.1)$$

where

$$\begin{aligned} X &= \text{“proportionality factor”} \\ &= 0.31 \text{ for “instantaneous” 10 m wind speeds over the open ocean} \\ &\text{(Wanninkhof, 1992).} \end{aligned}$$

Wanninkhof’s (1992) equation for gas transfer velocity (equation 1.8) is considered the most appropriate relationship for this study, as in this chapter we will use short-term averaged, or “spot”, surface wind speeds over the open ocean. The equation for gas

transfer velocity used by Liss and Merlivat (1986) (equation 1.5) was developed using data from fetch limited systems (lakes and wind-wave tanks), and if applied to the open ocean would lead to net flux estimates as much as 50% lower than those expected using the Wanninkhof (1992) equation (figure 1.2). The relationship used by Tans et al. (1990) (equation 1.6), a curve fitted through the long-term bomb- ^{14}C invasion rates over the ocean (Takahashi, 1989), applies to long-term averaged wind speeds and might yield anomalously high values if applied to short-term averaged wind speeds (Wanninkhof, 1992).

In this study, the solubility of CO_2 in surface seawater, σ_m , was calculated by substituting hourly averaged sea surface temperatures (Subsection 2.3.1) and salinities (Subsection 2.3.2) into the solubility relationship in Weiss (1974). The Schmidt number, Sc , was calculated using the same hourly averaged sea surface temperatures (Jähne et al., 1987a).

4.2 NET AIR-SEA TRANSFER CALCULATED USING SHIPBOARD WIND SPEEDS

The first method adopted to calculate the net carbon sea-to-air transfer is similar to that used by Robertson and Watson (1995) and Metzl et al. (1995), and follows their assumption that shipboard measurements of wind speed are representative of surface wind speeds over the study region. The values chosen in this case for W in equation 4.1 were hourly wind speeds (W_{ship}), obtained by averaging one second measurements of wind speed from an anemometer mounted 32 m above sea level on the *RSV Aurora Australis* (Subsection 2.3.4). The wind speeds were corrected to 10 m a.s.l. using the wind profile equation for conditions of neutral stability, assuming a smooth ocean surface (Fleagle and Businger, 1980), by multiplying the hourly wind speeds measured at 32 m a.s.l. by a factor of 0.92.

The best spatial coverage of ship data for the study region ($55^\circ - 70^\circ\text{S}$, $60^\circ - 150^\circ\text{E}$) was during the months January to March (Figure 3.1), for which there were 2092 hours of data. The rate of sea-to-air transfer of CO_2 over this region was estimated for

the period 1 January to 31 March 1993 by first averaging all “instantaneous fluxes” (equation 4.1). The instantaneous fluxes were calculated from hourly mean values of wind speed (corrected to 10 m a.s.l.), sea surface temperature, salinity and $\Delta f\text{CO}_2$, measured from the *RSV Aurora Australis* during 10 January to 31 March 1993 and 9 January to 26 February 1994 in waters south of 55°S. The average of all the hourly fluxes was then multiplied by the mean area of open water over the study region during the period 1 January to 31 March 1993 to obtain an estimate for the net amount of CO_2 transferred from the ocean surface to the atmosphere. The area of ice-free ocean over the study region was estimated from weekly sea-ice maps from the U.S. Navy/NOAA Joint Ice Center. For the three month period 1 January to 31 March 1993 the ocean south of 55°S, between 60°E and 150°E, was a net sink for atmospheric CO_2 , with an estimated sea-to-air transfer of $-15.2 \times 10^3 \text{ Gt C/90 d}$ ($1 \text{ Gt C} = 10^{15} \text{ g C} = (10^{15}/12) \text{ mol C}$) over a mean area of open ocean $6.00 \pm 0.05 \times 10^{12} \text{ m}^2$.

There are a number of problems with the method used above to estimate net air-sea fluxes. Wanninkhof's (1992) relationship between short-term 10 m wind speeds and gas transfer (equation 1.8) was derived for a global wind speed distribution over the open ocean, approximated by the Rayleigh probability function, $P(W)$ (Wentz et al., 1984):

$$P(W) = \frac{W \exp(-W^2 / 2\Delta W^2)}{2\Delta W^2} \quad (4.2)$$

where

$$\begin{aligned} \Delta W &= W_{\text{av}}(2/\pi)^{1/2}, \\ W_{\text{av}} &= \text{average surface wind speed.} \end{aligned}$$

Choice of a proportionality factor, X , of 0.31 to calculate net transfer (equation 4.1) was based on the assumption that the frequency of occurrence of hourly mean wind speeds measured from the ship followed a Rayleigh distribution. Although it was found that the distribution of shipboard wind speeds approached a Rayleigh probability function more closely as the number of observations increased, the shipboard wind speeds for the period 10 January to 31 March 1993 and 9 January to 26 February 1994

(1891 data points), chosen as the sampling period with greatest spatial coverage of the study region, did not quite approximate a Rayleigh distribution function (Figure 4.1). Hence, a more appropriate value of the proportionality factor to be used with the shipboard wind speeds, X_{ship} , would have been (Wanninkhof, 1992):

$$X_{ship} = 0.31 \frac{\sum [P(W_{ship}) W_{ship}^2]}{\sum [O(W_{ship}) W_{ship}^2]} = 0.29 \quad (4.3)$$

where

$O(W_{ship})$ = observed frequency distribution of hourly mean wind speeds measured on the ship.

Using $X = 0.29$ in equation 4.1 gives a corrected value of net sea-to-air transfer over the study region of -14.1×10^{-3} Gt C/90 d.

There is an additional problem with estimating net transfer in the ASIZ by averaging instantaneous net fluxes and multiplying by the area of open water. This method gives equal weighting to each hourly flux value, irrespective of whether the ship at this point is sampling in 9/10 pack ice or open ocean, and does not take into account the length of time the ship is in a region. During summer months the estimate of net carbon transfer may be biased towards too negative a value, since ice edge algal blooms may cause oceanic $f\text{CO}_2$ to be significantly lower within pack ice than in open waters north of the ASIZ (Chapter 3). If the ship has spent a significant amount of time within pack ice then averaging the hourly net fluxes over a period of time such as one month will overemphasise the negative $\Delta f\text{CO}_2$ measured in the vicinity of melting ice. An alternative method for estimating net air-sea carbon transfer is used in the following section.

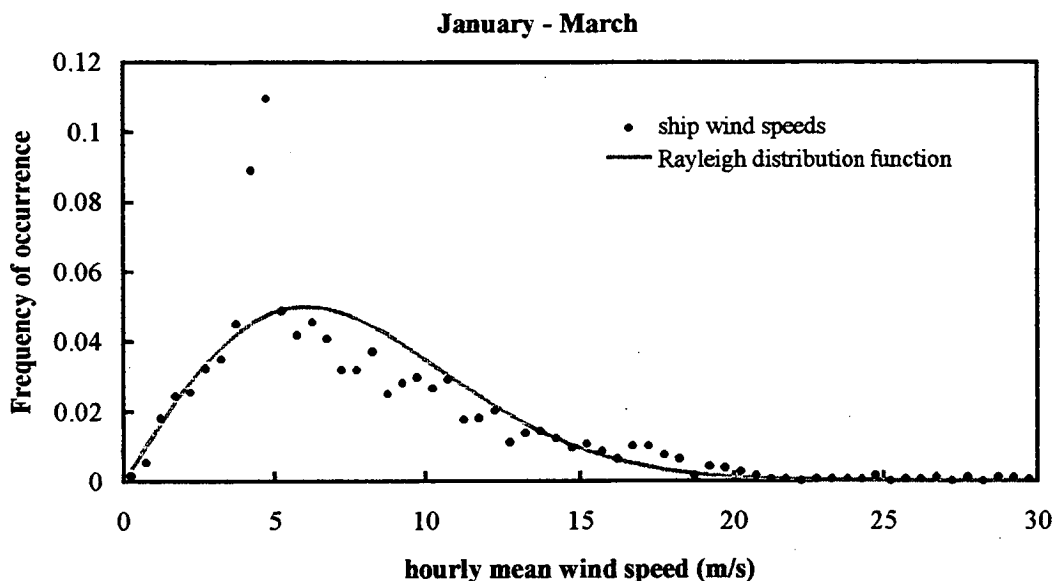


Fig. 4.1 Frequency of occurrence of mean hourly wind speeds measured from *RSV Aurora Australis*, and the corresponding Rayleigh distribution function, for the period 10 January to 31 March 1993 and 9 January to 26 February 1994 over the region 55° - 70°S, 60° - 150°E.

4.3 NET AIR-SEA TRANSFER CALCULATED USING GASP WIND SPEEDS

The method for calculating net carbon transfer used in the previous section is satisfactory given sufficient spatial and temporal data coverage of the region of interest and no sea-ice. However, wind speed can vary on shorter time scales than oceanic variables such as $f\text{CO}_2$. Thus, the spatial interpolation of hourly mean wind speeds measured from the ship is likely to contribute greater uncertainty to the calculated monthly fluxes than spatially interpolating and averaging oceanic parameters over a month.

The interpolation error may be reduced by using satellite wind speed data over a fine grid to calculate net transfer. Unfortunately, surface wind speeds are not measured by the Special Sensor Microwave Imager (SSM/I) or the Active Microwave Instrument (AMI) south of about 60°S (Halpern et al., 1994b). An alternative set of wind speeds over the ASIZ are the six-hourly surface wind speeds from the Australian Bureau of

Meteorology's Global Assimilation and Prediction System (GASP) analyses, W_{GASP} . The GASP model uses spot measurements from satellites, ships and stations in the few hours preceding each six-hourly analysis, spatially averaged over $2.24^\circ \times 3.75^\circ$ grid squares. The "surface" in this case corresponds to the height where atmospheric pressure is 0.991 times the pressure at sea level. South of 55°S , sea level pressures are generally below one atmosphere. Surface GASP wind speeds over our study region correspond to a height between sea level and 60 m a.s.l., and hence may be used to approximate the 10 m a.s.l. wind speeds to within an error of $\pm 13\%$, assuming an adiabatic atmosphere (Fleagle and Businger, 1980).

Due to the large number of data points (75600 six-hourly wind speeds), the frequency distribution of six-hourly surface wind speeds from GASP analyses over all grid points of the study region during 1 January to 31 March 1993 closely follows a Rayleigh probability distribution (Figure 4.2). When calculating net flux from GASP wind speeds over the region $55^\circ - 70^\circ\text{S}$, $60^\circ - 150^\circ\text{E}$, the appropriate value for the proportionality factor in equation 4.1 is therefore Wanninkhof's (1992) value of 0.31.

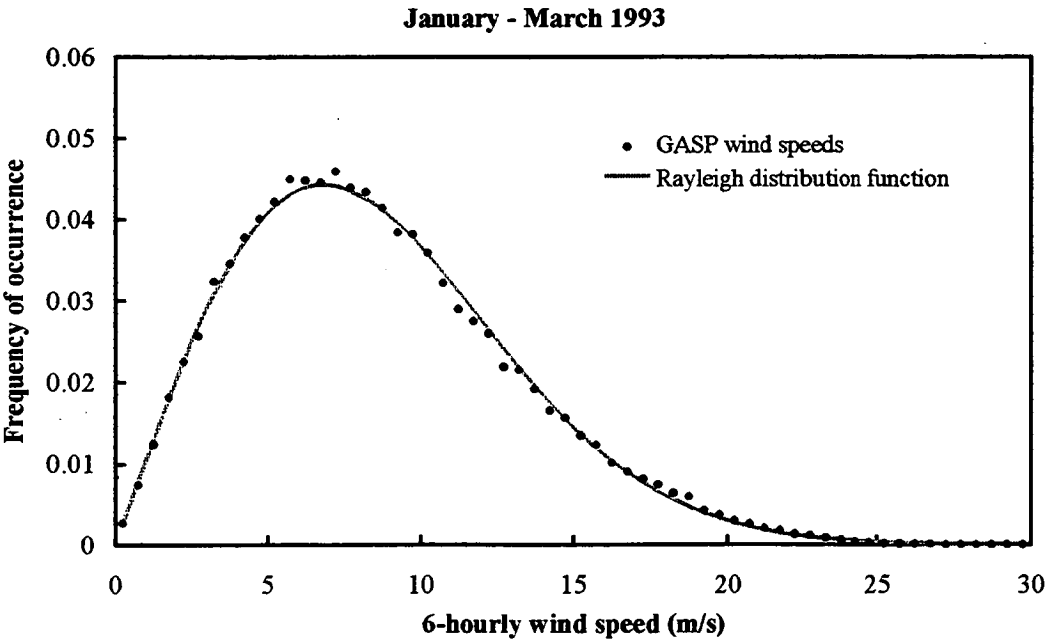


Fig. 4.2 Frequency of occurrence of surface wind speeds from six-hourly GASP analyses and the corresponding Rayleigh distribution for the period 1 January to 31 March 1993, over the region $55^\circ - 70^\circ\text{S}$, $60^\circ - 150^\circ\text{E}$.

In order to take into account the variability of $\Delta f\text{CO}_2$ in the vicinity of sea-ice, and the variation in wind speed, the study region was gridded into $2.5^\circ \times 2.5^\circ$ grid squares. Estimates of the monthly average area of open water in each grid square were obtained from U.S. Navy/NOAA Joint Ice Center weekly sea-ice maps (Appendix B: Figure B.1). The 6-hourly GASP wind speeds were transformed from the $2.24^\circ \times 3.75^\circ$ grid to the $2.5^\circ \times 2.5^\circ$ grid by a simple one-to-one correspondence for corresponding grid squares and linear interpolation for non-overlapping grid squares. The monthly net flux of CO_2 over each grid square was calculated by substituting monthly averaged values of W_{GASP}^2 , $\Delta f\text{CO}_2$, sea surface temperature and salinity into equation 4.1. The flux was then multiplied by the area of open water in each grid square to give the net carbon transfer. In this case, there was sufficient data coverage of the study region to enable estimates of net transfer to be made for the months October 1992 to March 1993.

Sea surface temperature, salinity and $\Delta f\text{CO}_2$ measurements from the ship were interpolated between grid squares for each month (Appendix B: Figure B.2). Data within a grid square were averaged for each month and a standard deviation calculated for the grid point. If no data were available for a grid point, data from adjacent months were used, and a standard deviation again calculated. If no data were available in adjacent months the data were linearly interpolated from adjacent grid points at the same latitude. The interpolation error attached to mean values of $\Delta f\text{CO}_2$, sea surface temperature and salinity in each grid square was taken to be the maximum standard deviation for any grid square in the same 2.5° latitude band. Over the study region, the high spatial variability in $\Delta f\text{CO}_2$ (Figure 3.1) meant that it was considered wiser to use a mean value for the same grid square from an adjacent month than to interpolate between measurements made hundreds of kilometers from the grid square. As well as the interpolation error, the uncertainty in net transfer calculated for each month includes contributions from measurement errors, and the uncertainty in the “proportionality factor”, X (see Subsection 4.3.1).

For the three month period 1 January to 31 March 1993, the net sea-to-air transfer of atmospheric CO₂, calculated from GASP wind speeds, was $-14.3 \pm 7 (0.2) \times 10^{-3}$ Gt C/90 d over a mean area of open ocean $6.00 \pm 0.05 \times 10^{12}$ m² (Table 4.1(a)). The net transfer estimate based on GASP wind speed data is 94% of the value calculated in Section 4.2 using shipboard wind speeds, or 102% of the value corrected for using a non-Rayleigh distribution of W_{ship} . The relatively close agreement between the fluxes is not due to agreement between the wind speed data sets used to calculate the two transfer estimates. The average of all shipboard wind speeds (corrected to 10 m a.s.l.), measured during the period 10 January to 31 March 1993 and 9 January to 26 February 1994, was 7.0 m s^{-1} , whereas the average of all the GASP wind speeds for the period 1 January to 31 March 1993 over the same study region was 8.6 m s^{-1} . The ratio of mean W_{GASP}^2 to mean W_{ship}^2 was 1.40, and therefore the net transfer estimate from GASP wind speeds should have been 140% of the net transfer calculated using shipboard wind speeds. The difference between the methods used to interpolate $\Delta f\text{CO}_2$, sea surface temperature and salinity appears to have counteracted the effect of the difference in wind speeds on net transfer.

The calculation of monthly fluxes allows an investigation of seasonal variation in air-sea exchange, while the interpolation of ship's data over the grid permits a study of zonal and meridional variations in net transfer (Table 4.1).

(a) 60° - 150°E

Period	55°-60°S Area of open water (10 ¹² m ²)	55°-60°S Net transfer (10 ⁻³ GtC/period)	> 60°S Area of open water (10 ¹² m ²)	> 60°S Net transfer (10 ⁻³ GtC/period)
October 1992	2.82 ± 0.04	-2.75 ± 1.3 (0.2)	1.00 ± 0.04	0.16 ± 0.09 (0.04)
November 1992	2.98 ± 0.04	-5.93 ± 2.9 (0.3)	1.42 ± 0.04	-0.22 ± 0.14 (0.08)
December 1992	2.99 ± 0.04	-2.55 ± 1.3 (0.2)	2.52 ± 0.04	0.25 ± 0.18 (0.12)
January 1993	2.99 ± 0.04	-2.74 ± 1.3 (0.2)	2.93 ± 0.04	-2.54 ± 1.3 (0.3)
February 1993	2.99 ± 0.04	-3.74 ± 1.8 (0.2)	3.05 ± 0.04	-1.46 ± 0.7 (0.2)
March 1993	2.99 ± 0.04	-1.24 ± 0.6 (0.2)	3.05 ± 0.04	-2.57 ± 1.3 (0.2)
Total	2.96 ± 0.04	-18.95 ± 9.2 (1.3)	2.33 ± 0.04	-6.38 ± 3.7 (0.9)

(b) 60° - 105°E ("Western region")

Period	55°-60°S Area of open water (10 ¹² m ²)	55°-60°S Net transfer (10 ⁻³ GtC/period)	> 60°S Area of open water (10 ¹² m ²)	> 60°S Net transfer (10 ⁻³ GtC/period)
October 1992	1.32 ± 0.02	-1.26 ± 0.6 (0.09)	0.17 ± 0.03	-0.14 ± 0.07 (0.03)
November 1992	1.48 ± 0.02	-4.48 ± 2.2 (0.3)	0.50 ± 0.03	-0.58 ± 0.29 (0.07)
December 1992	1.50 ± 0.02	-2.18 ± 1.1 (0.2)	1.21 ± 0.03	-0.76 ± 0.38 (0.08)
January 1993	1.50 ± 0.02	-2.05 ± 1.0 (0.2)	1.51 ± 0.03	-3.65 ± 1.8 (0.3)
February 1993	1.50 ± 0.02	-3.55 ± 1.7 (0.2)	1.57 ± 0.03	-2.36 ± 1.2 (0.2)
March 1993	1.50 ± 0.02	-1.95 ± 1.0 (0.2)	1.54 ± 0.03	-3.03 ± 1.5 (0.2)
Total	1.47 ± 0.02	-15.5 ± 7.6 (1.2)	1.08 ± 0.03	-10.52 ± 5.2 (0.9)

(c) 105° - 150°E ("Eastern region")

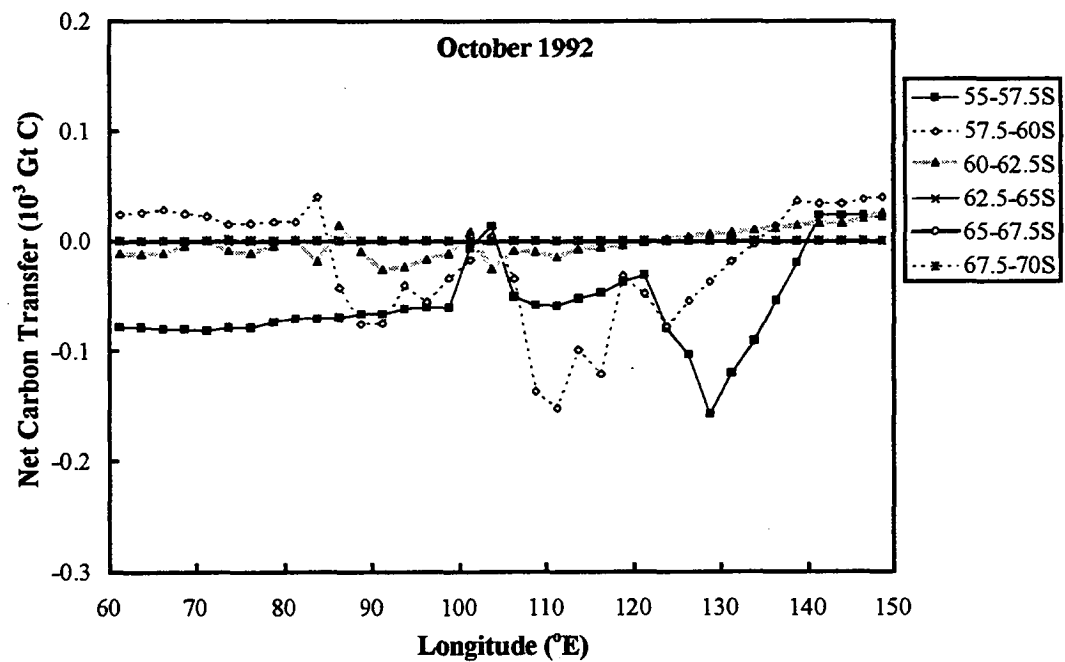
Period	55°-60°S Area of open water (10 ¹² m ²)	55°-60°S Net transfer (10 ⁻³ GtC/period)	> 60°S Area of open water (10 ¹² m ²)	> 60°S Net transfer (10 ⁻³ GtC/period)
October 1992	1.50 ± 0.02	-1.49 ± 0.7 (0.1)	0.83 ± 0.03	0.30 ± 0.15 (0.03)
November 1992	1.50 ± 0.02	-1.45 ± 0.7 (0.1)	0.92 ± 0.03	0.36 ± 0.18 (0.03)
December 1992	1.50 ± 0.02	-0.37 ± 0.2 (0.1)	1.31 ± 0.03	1.01 ± 0.50 (0.09)
January 1993	1.50 ± 0.02	-0.68 ± 0.3 (0.08)	1.42 ± 0.03	1.11 ± 0.55 (0.10)
February 1993	1.50 ± 0.02	-0.19 ± 0.1 (0.09)	1.48 ± 0.03	0.90 ± 0.44 (0.06)
March 1993	1.50 ± 0.02	0.71 ± 0.4 (0.05)	1.51 ± 0.03	0.47 ± 0.24 (0.06)
Total	1.50 ± 0.02	-3.47 ± 2.5 (0.6)	1.24 ± 0.03	4.15 ± 2.1 (0.4)

Table 4.1 Monthly average area of open ocean, and net ocean-to-atmosphere transfer of CO₂ (calculated using GASP wind speeds), for the region of the Southern Ocean bounded by 55°-60°S, or 60°-70°S, and (a) 60°-150°E, (b) 60°-105°E, and (c) 105°-150°E. The error is given in terms of the standard deviation, with the values in brackets being the standard deviation in the net transfer without the contribution from the error in X.

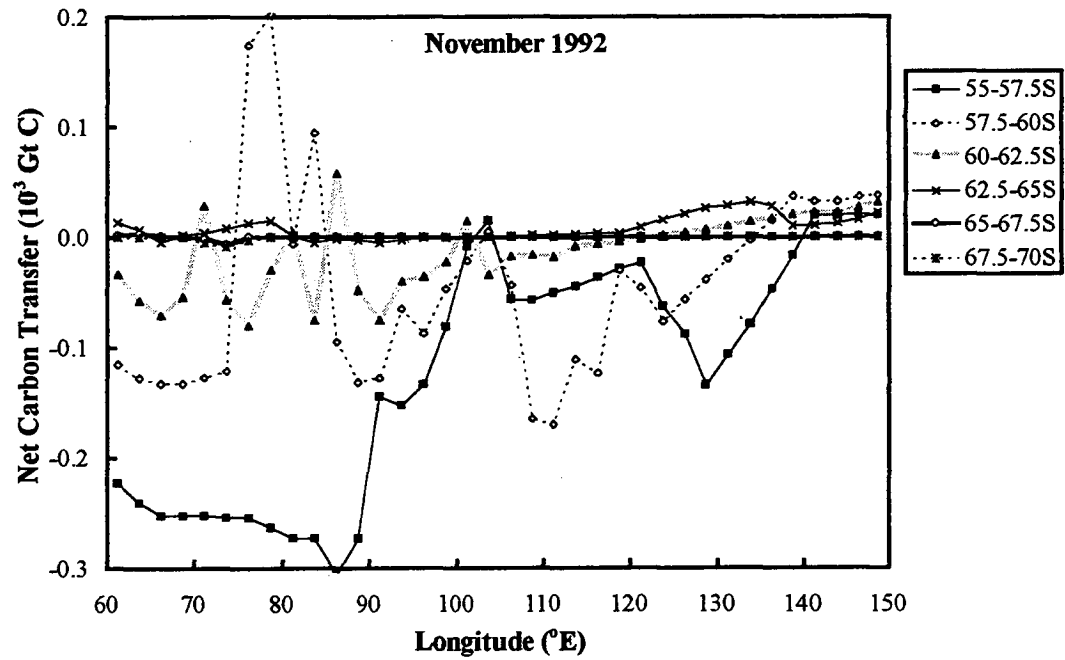
During October 1992 the ocean east of 105°E was a slightly greater sink compared with the western region (Figure 4.3(a)), due to less ice cover over the eastern region. Figure 4.3(b) shows the advent of the spring ice edge blooms in the increased carbon uptake by the ocean in the region 55° - 57.5°S, 60° - 100°E during November 1992. During December 1992 to March 1993, east of 105°E the average net sea-to-air transfer of CO₂ was small and mainly positive, whereas west of 105°E the net transfer was more variable and negative, with the ocean a stronger net sink for carbon (Figures 4.3(c)-(f)). The same pattern is evident in each of the monthly net transfer values for December 1992 to March 1993, presented in Table 4.1 for (b) 60° - 105°E, and (c) 105° - 150°E. For the period 1 October 1992 to 31 March 1993 the ocean south of 55°S, between 60°E and 105°E, was a net sink for atmospheric CO₂ of $-26 \pm 13 \times 10^{-3}$ Gt C/182 d (Table 4.1(b)), and a net source of $1 \pm 5 \times 10^{-3}$ Gt C/182 d for 105° - 150°E (Table 4.1(c)). The errors quoted here are one standard deviation, and were estimated from the root sum square of the standard deviations of the transfer estimates in each grid square. The calculation of errors associated with the net transfer values is discussed in Subsection 4.3.1.

As well as strong zonal variation in the uptake of atmospheric CO₂ by the ocean, there was also high meridional variability. Net transfer of CO₂ over the latitude bands 55° - 60°S and 60° - 70°S are compared in Table 4.1(a). The region 55° - 60°S, 60° - 150°E, was a stronger sink for atmospheric CO₂ during 1 October 1992 to 31 March 1993 ($-19 \pm 9 \times 10^{-3}$ Gt C/182 d) compared with the ocean to the south of 60°S for the same longitudes ($-6 \pm 4 \times 10^{-3}$ Gt C/182 d). The higher rate of carbon transfer in the 55° - 60°S region is due to: (i) stronger wind speeds over this region compared to further south (Appendix B: Figure B.3); (ii) the ocean surface over the region 60° - 70°S, 105° - 150°E, being supersaturated with CO₂ gas (Table 4.1(c)); and (iii) the slightly greater area of open ocean over 55° - 60°S compared with 60° - 70°S (Table 4.1(a)). When estimating net air-sea fluxes of CO₂ over the ASIZ from limited data sets, it is therefore important to account for the high spatial variability in $\Delta f\text{CO}_2$, and in particular, the disproportionately large contribution to the estimate of net transfer made by small errors in $\Delta f\text{CO}_2$ over the region 55° - 60°S, due to strong wind speeds.

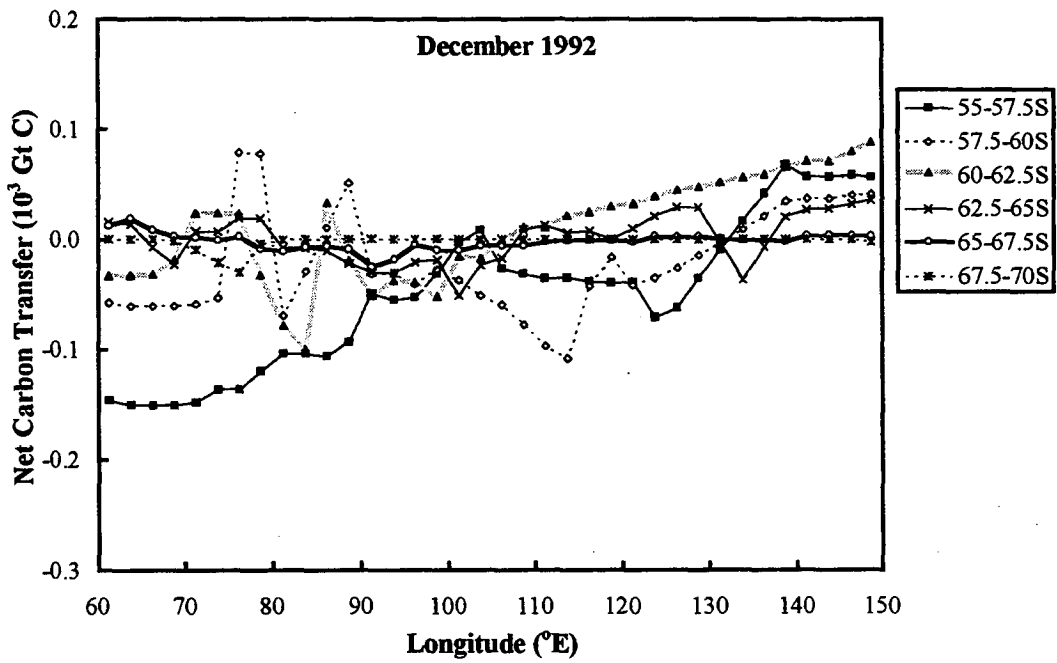
(a)



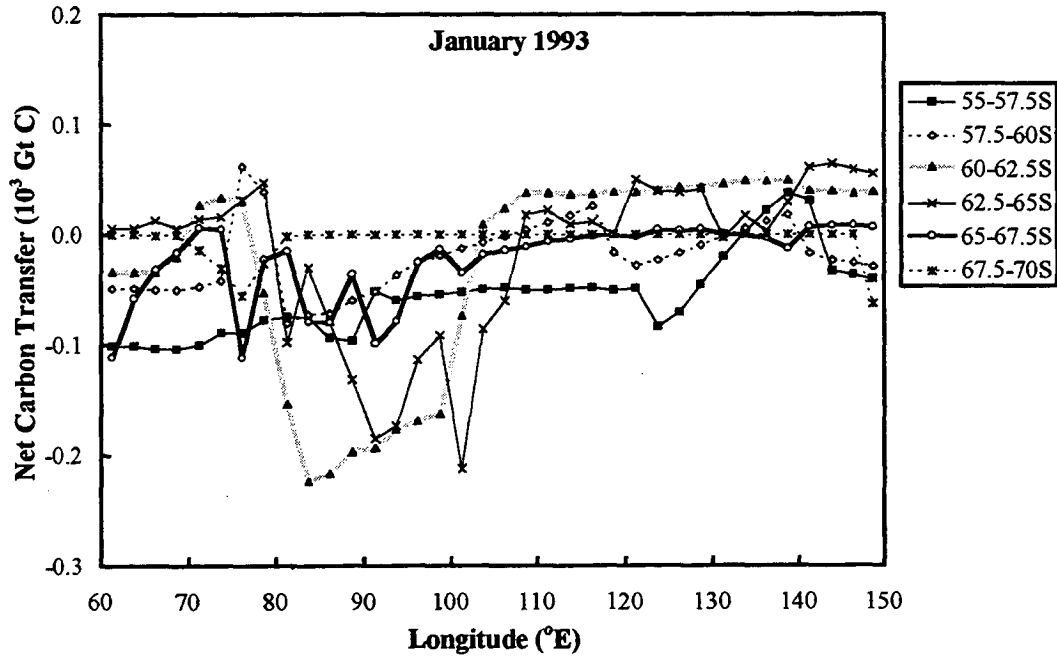
(b)



(c)



(d)



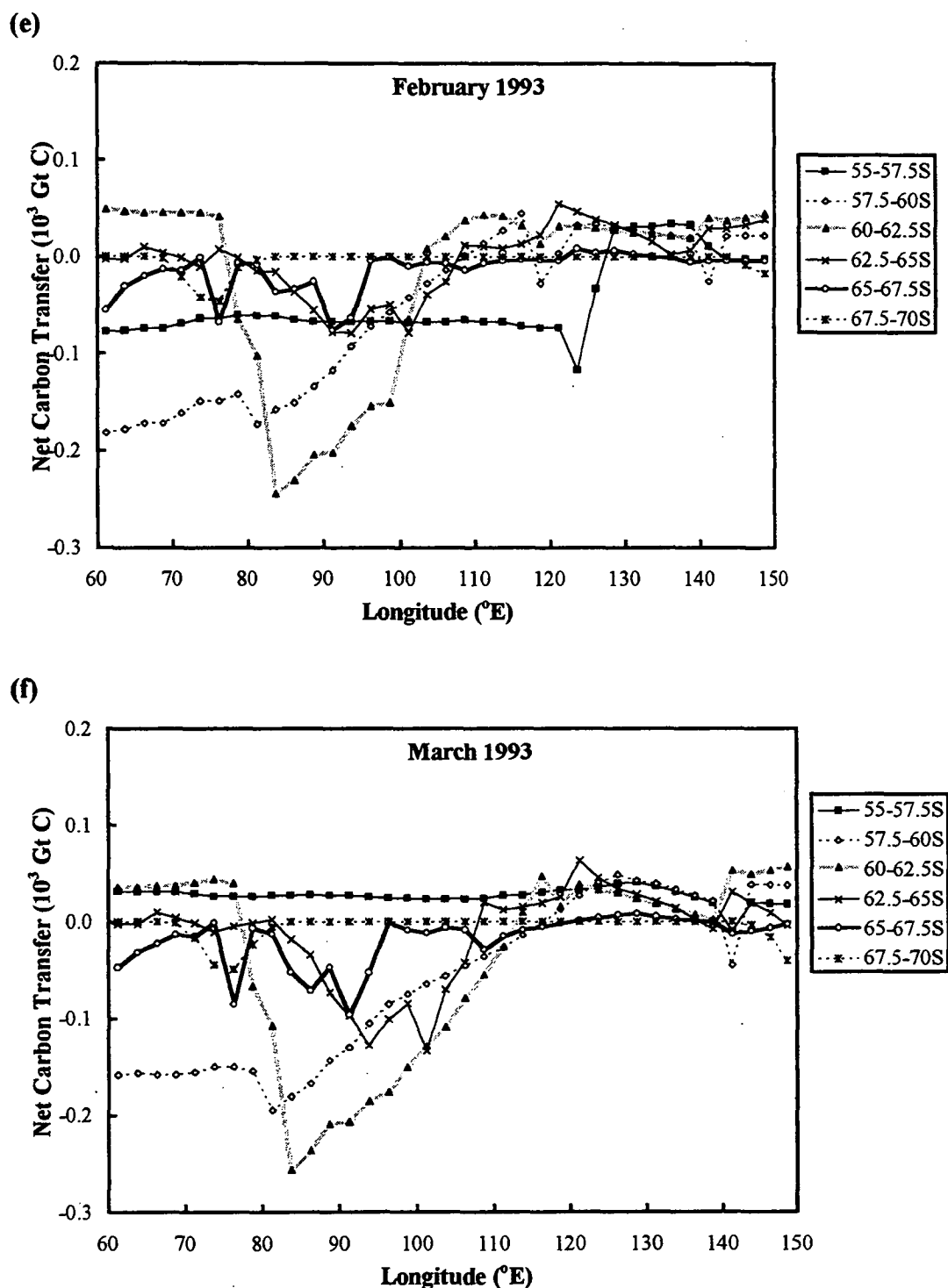


Fig. 4.3 Net sea-to-air transfer of CO_2 for (a) October 1992, (b) November 1992, (c) December 1992, (d) January 1993, (e) February 1993, and (f) March 1993. The gas transfer for each $2.5^{\circ} \times 2.5^{\circ}$ grid square was estimated using the six-hourly surface wind speed outputs of the GASP analyses. Negative values indicate net uptake of carbon dioxide by the surface ocean.

4.3.1 Error Estimates

The error estimates given in Table 4.1 are the standard deviations in net transfer due to both analytical and interpolation errors. The analytical error includes random errors due to measurement and uncertainty in the equations used. Measurement errors are described in Sections 2.3 to 2.5. The interpolation error is the error estimate attached to a data value in a particular grid square from either averaging measured values over that grid square, or from interpolating from other grid squares or other months. In this study it is taken to be the maximum standard deviation for any grid square in the same 2.5° latitude band.

The estimated errors in the parameters used in the calculation of net transfer are listed in Table 4.2, with the analytical errors in bold type, and the interpolation errors in normal type. The area of open water is represented in Table 4.2 by A' .

Parameter	Error Estimate	Units
A'	0.14'	m^2
σ_m	$((5.2 \times 10^{-6})^2 + \text{Var}(\sigma_m))^{1/2}$	$\text{mol m}^{-3} \mu\text{atm}^{-1}$
X	0.15	
W	0.13W	m s^{-1}
Sc	$(1.1^2 + \text{Var}(Sc))^{1/2}$	
f_m	$(1 + \text{Var}(f_m))^{1/2}$	μatm
f_a	$(0.02^2 + 0.5^2)^{1/2}$	μatm

Table 4.2 Uncertainty in values used in equation 4.1 to calculate net carbon transfer. Each error is one standard deviation, with analytical errors in bold type, and interpolation errors in normal type.

The uncertainty in the “proportionality factor” (0.31 ± 0.15 (Wanninkhof, pers. com.)) dominates the analytical errors in net transfer. Over the ASIZ the uncertainty may be even larger due to the reduction in ocean turbulence by sea-ice (Subsection 1.3.1). The effect on air-sea flux from the reduction in wind fetch by sea-ice is discussed in more detail in the following subsection.

4.3.2 Effect on flux estimates from reduction of fetch by sea-ice

The gas transfer velocity is affected by the wind fetch, with a lower transfer velocity for smaller fetch (Subsection 1.3.1). As regions of open water in the ASIZ grow with the summer melt, the average fetch increases and the proportionality factor appropriate to this region should also increase until it approaches a value for infinite fetch of 0.31 (Wanninkhof, 1992). Even if it were possible to apply an accurate relationship between gas transfer velocity, wind speed and area to any one polynya, it would be difficult to determine a precise estimate of the total net gas flux over the grid square in question due to the variation in size of polynyas. Over any one grid square which has some sea ice coverage, there is a large variation in the areas (and fetch) of individual polynyas and leads, and therefore a variation in appropriate proportionality factors.

Suppose one takes the extreme case that there is no net air-sea transfer of CO_2 over a grid square if it is at least 50% covered by sea-ice. i.e.

$$\begin{aligned} N_j(\text{min}) &= 0 && \text{if } A_j' < 0.5A_j, \\ &= N_j && \text{if } A_j' \geq 0.5A_j, \end{aligned} \quad (4.4)$$

where

A_j' = area of open water in the j th grid square,

A_j = total surface area of the j th grid square,

$N(\text{min})$ = Minimum sea-to-air transfer of CO_2 over the study region, taking into account the effect of sea-ice on the gas transfer velocities,

$$= \sum_j N_j'.$$

The effect of applying the above approximate fetch correction to net transfer estimates over the study region is shown in Table 4.3, which lists values of $N(\text{min})$. Between 55°S and 60°S , the estimates of net transfer are not altered by applying the fetch correction (equation 4.4). South of 60°S , between 60°E and 105°E , net transfer changes from $-10.52 \times 10^3 \text{ Gt C/182 d}$ (Table 4.1(b)) to $-8.54 \times 10^3 \text{ Gt C/182 d}$ (Table 4.3(b)), with little change over the region between 105°E and 150°E . The reduction in fetch by sea-ice makes very little difference to estimates of net ocean

uptake over the study region (55° - 70° S, 60° - 150° E), decreasing the net uptake from 25.33×10^{-3} Gt C/182 d to 23.26×10^{-3} Gt C/182 d.

(a) 60° - 150° E

Period	55° - 60° S Area of open water (10^{12} m ²)	55° - 60° S Minimum net transfer (10^{-3} GtC/period)	$> 60^{\circ}$ S Area of open water (10^{12} m ²)	$> 60^{\circ}$ S Minimum net transfer (10^{-3} GtC/period)
October 1992	2.82 ± 0.04	-2.76	1.00 ± 0.04	0.20
November 1992	2.98 ± 0.04	-5.93	1.42 ± 0.04	-0.07
December 1992	2.99 ± 0.04	-2.55	2.52 ± 0.04	0.64
January 1993	2.99 ± 0.04	-2.74	2.93 ± 0.04	-1.83
February 1993	2.99 ± 0.04	-3.74	3.05 ± 0.04	-1.19
March 1993	2.99 ± 0.04	-1.24	3.05 ± 0.04	-2.06
Total	2.96 ± 0.04	-18.95	2.33 ± 0.04	-4.31

(b) 60° - 105° E ("Western Section")

Period	55° - 60° S Area of open water (10^{12} m ²)	55° - 60° S Minimum net transfer (10^{-3} GtC/period)	$> 60^{\circ}$ S Area of open water (10^{12} m ²)	$> 60^{\circ}$ S Minimum net transfer (10^{-3} GtC/period)
October 1992	1.32 ± 0.02	-1.27	0.17 ± 0.03	0.00
November 1992	1.48 ± 0.02	-4.48	0.50 ± 0.03	-0.37
December 1992	1.50 ± 0.02	-2.18	1.21 ± 0.03	-0.37
January 1993	1.50 ± 0.02	-2.05	1.51 ± 0.03	-3.04
February 1993	1.50 ± 0.02	-3.55	1.57 ± 0.03	-2.14
March 1993	1.50 ± 0.02	-1.95	1.54 ± 0.03	-2.62
Total	1.47 ± 0.02	-15.5	1.08 ± 0.03	-8.54

(c) 105° - 150° E ("Eastern Section")

Period	55° - 60° S Area of open water (10^{12} m ²)	55° - 60° S Minimum net transfer (10^{-3} GtC/period)	$> 60^{\circ}$ S Area of open water (10^{12} m ²)	$> 60^{\circ}$ S Minimum net transfer (10^{-3} GtC/period)
October 1992	1.50 ± 0.02	-1.49	0.83 ± 0.03	0.20
November 1992	1.50 ± 0.02	-1.45	0.92 ± 0.03	0.30
December 1992	1.50 ± 0.02	-0.37	1.31 ± 0.03	1.02
January 1993	1.50 ± 0.02	-0.68	1.42 ± 0.03	1.21
February 1993	1.50 ± 0.02	-0.19	1.48 ± 0.03	0.94
March 1993	1.50 ± 0.02	0.71	1.51 ± 0.03	0.56
Total	1.50 ± 0.02	-3.47	1.24 ± 0.03	4.23

Table 4.3 Average areas of open ocean, and estimates of the minimum net sea-to-air transfer of CO₂ (calculated using GASP wind speeds), for the region of the Southern Ocean bounded by 55° - 60° S, or 60° - 70° S, and (a) 60° - 150° E, (b) 60° - 105° E, and (c) 105° - 150° E. It is assumed that there was zero net flux over a grid square if at least 50% of it was covered by sea ice.

4.4 COMPARISONS WITH FLUXES FROM DIFFERENT STUDIES

In order to compare methods for estimating air-sea gas transfer over the ASIZ, net flux estimates made in this and other studies are listed in Table 4.4.

Source	Period	Region	Area of open water (10^{12} m^2)	Net CO ₂ flux per unit area ($10^{-2} \text{ gC m}^{-2} \text{ d}^{-1}$)
Robertson and Watson (1995) (ship wind speeds)	Nov. - Dec.'92, Feb. - Mar.'93 (120 days)	>50°S, 80°W-80°E	9.3	-7.0 ± 0.4 (W)
This study (GASP wind speeds)	Nov. - Dec.'92, Feb. - Mar.'93 (120 days)	>55°S, 60°E-150°E	5.50	-2.65 ± 0.23 (W)
Metzl et al. (1995) (ship wind speeds)	Jan. - May ('91-'93) (151 days)	>50°S, 20°E-110°E	≈ 9	-2.1 (W)
This study (GASP wind speeds)	Jan. - Mar.'93 (90 days)	>55°S, 60°E-150°E	6.00	-2.65 ± 0.24 (W) -2.57 (T)
Takahashi (1989) (monthly climatological wind speeds)	Year ('72-'81, '84-'85, '88-'89) (365 days)	>55°S	≈ 32	-3.6 (T)
This study (GASP wind speeds)	Oct.'92 - Mar.'93 (182 days)	>55°S, 60°E-150°E	5.29	-2.63 ± 0.23 (W) -2.43 (T)
Tans et al. (1990) (monthly climatological wind speeds)	Jan. - Apr. ('72-'81, '84-'85, '88-'89) (120 days)	>50°S	≈ 45	-2.3 (T)

Table 4.4 Net ocean-to-atmosphere flux of CO₂ per unit area over the Antarctic Seasonal Ice Zone. Values marked "W" were calculated using the relationship for air-sea gas transfer velocity from Wanninkhof (1992), and those marked "T" were calculated using the relationship in Takahashi (1989). The errors presented here were calculated without taking into account the uncertainty attached to using the Wanninkhof (1992) relationship.

Robertson and Watson (1995) calculated a flux per unit area of $-7.0 \pm (0.4) \times 10^{-2} \text{ g C m}^{-2} \text{ d}^{-1}$ (1 S.E., $n = 497$) for a region of the Southern Ocean south of 50°S , between 80°W and 80°E , of area $9.3 \times 10^{12} \text{ m}^2$. Their estimate was made using data from two cruises of the *RRS Discovery* during November to December 1992 and February to March 1993. Robertson and Watson (1995) used hourly wind speeds measured from the ship and Wanninkhof's (1992) relationship for gas transfer velocity to calculate the net flux. The error in parentheses does not include the uncertainty in the gas transfer velocity relationship.

The gas flux estimate from GASP wind speeds for the region $55^\circ - 70^\circ\text{S}$, $60^\circ - 150^\circ\text{E}$, averaged over the same four months sampled by Robertson and Watson, was $-2.65 \pm 1.4 (0.23) \times 10^{-2} \text{ g C m}^{-2} \text{ d}^{-1}$ over an area of open ocean of $5.50 \times 10^{12} \text{ m}^2$ (Table 4.1(a)). This is only 38% of Robertson and Watson's (1995) flux estimate. Robertson and Watson's (1995) study region extended northwards to 50°S , was mainly westwards of our study region, and did not penetrate into pack ice. The difference between the two flux estimates may be due to high variability in $\Delta f\text{CO}_2$ over the Southern Ocean, strong wind speeds between 50°S and 55°S , or to higher wind speeds being measured on the two cruises aboard *RRS Discovery* compared with those from GASP analyses for the same period. The mean wind speed from GASP analyses over the region $55^\circ - 70^\circ\text{S}$, $60^\circ - 150^\circ\text{E}$, for the period 1 November to 31 December 1992 and 1 February to 31 March 1993, was 8.9 m s^{-1} .

Metzl et al. (1995) employed a similar method to Robertson and Watson (1995) to measure $\Delta f\text{CO}_2$ and calculate net carbon transfer over the Southern Indian Ocean. They used hourly averaged ship wind speeds from 14 cruises in 1991, 1992 and 1993, and Wanninkhof's (1992) relationship for gas transfer velocity (equation 1.8) to estimate hourly net fluxes over the region from 50°S to the ice edge, between 20°E and 110°E . For the 15 month period January to May (1991-1993) Metzl et al. (1995) estimated an average net ocean-to-air flux of $-2.1 \times 10^{-2} \text{ g C m}^{-2} \text{ d}^{-1}$ over roughly the same surface area ($9 \times 10^{12} \text{ m}^2$) as Robertson and Watson's (1995) flux of $-7.0 \pm (0.4) \times 10^{-2} \text{ g C m}^{-2} \text{ d}^{-1}$. The difference between these two fluxes again implies either strong zonal variations in $\Delta f\text{CO}_2$ south 50°S , much stronger carbon uptake by this region

during November and December than in January to May, or that wind speeds were typically lower during the 15 month period studied by Metzl et al (1995) than the 4 month period investigated by Robertson and Watson (1995).

Over the period 1 January to 31 March 1993, the estimate of average net flux calculated using GASP wind speeds (Section 4.3) was $-2.65 \pm 1.3 (0.24) \times 10^{-2}$ g C m⁻² d⁻¹ (Table 4.1(a)) over an area of open ocean of 6.00×10^{12} m². Our estimate is 126% of the average flux per unit area calculated by Metzl et al. (1995) over ice-free waters. Neither Metzl et al. (1995) or Robertson and Watson (1995) used $\Delta f\text{CO}_2$ measurements within areas of pack ice in their flux calculations. As we have seen in Section 3.2, these regions may experience low levels of oceanic $f\text{CO}_2$ during spring/summer months due to ice edge algal blooms. Hence, they may make a significant contribution to the total air-sea transfer of CO₂, despite the relatively small area of open water. This may be part of the reason for the comparatively higher estimate of net carbon flux over our study region compared with the estimate made by Metzl et al. (1995). However, it is also possible that the average wind speed measured by Metzl et al. (1995) during January to May (1991-1993) was lower than the mean GASP wind speed over our study region for January to March 1993 (8.6 m s⁻¹).

Takahashi (1989) gridded $\Delta p\text{CO}_2$ observations over a $2^\circ \times 2^\circ$ grid and used these in conjunction with monthly climatological wind speeds (Esbensen and Kushnir, 1981) and equation 1.6 to calculate the annual net flux south of 55°S (-3.6×10^{-2} g C m⁻² d⁻¹ over an approximate area 32×10^{12} m²). The estimate of average net flux from GASP wind speeds, for the period 1 October 1992 to 31 March 1993, was $-2.63 \pm 1.3 (0.23) \times 10^{-2}$ g C m⁻² d⁻¹ over an area of open ocean 5.29×10^{12} m² (Table 4.1). This flux estimate is 73% of Takahashi's (1989) value for annual net flux per unit area. What caused the difference in flux estimates? Takahashi (1989) used a different relationship (equation 1.6) than was used in this study (equation 1.8) to calculate gas transfer velocity from wind speed. However, this can account for very little of the discrepancy. Using Takahashi's equation to calculate gas transfer velocity from monthly averaged GASP wind speeds produced a net flux estimate of -2.43×10^{-2} g C m⁻² d⁻¹ over the period 1 October 1992 to 31 March 1993, which is similar to the estimate using

Wanninkhof's equation. It is most likely that the difference in flux estimates between the two studies is due to both the different sampling regions (Takahashi using $\Delta p\text{CO}_2$ data mainly from the Atlantic Ocean and little from the Indian Ocean) and the flux estimate from GASP wind speeds not including values for April to September. Winter fluxes over the ASIZ may be significant, in spite of increasing ice cover, due to high wind speeds, and this may be partially responsible for Takahashi's higher flux estimate.

Tans et al. (1990) used the Takahashi (1989) relationship for gas transfer velocity, with the Esbensen and Kushnir (1981) monthly climatological wind speeds, to estimate that the average net flux south of 50°S , over an area approximately $45 \times 10^{12} \text{ m}^2$, was $-2.3 \times 10^{-2} \text{ g C m}^{-2} \text{ d}^{-1}$ during the period 1 January to 30 April. Over the period 1 January to 31 March 1993, the flux estimate from GASP wind speeds was $-2.65 \pm 1.3 (0.24) \times 10^{-2} \text{ g C m}^{-2} \text{ d}^{-1}$ over an area of open ocean of $6.00 \times 10^{12} \text{ m}^2$ (Table 4.1(a)), which is 115% of the net flux per unit area calculated by Tans et al. (1990). Using Takahashi's equation to calculate gas transfer velocity from monthly averaged GASP wind speeds produced a net flux estimate of $-2.57 \times 10^{-2} \text{ g C m}^{-2} \text{ d}^{-1}$ over the period 1 January to 31 March 1993, which is 112% of the Tans et al. (1990) flux estimate for the period 1 January to 31 April over a number of years. The small discrepancy here may be attributed to the difference in sampling regions and of wind speeds.

Agreement between fluxes, even from studies employing similar measurement techniques and equations, does not necessarily imply that anyone has yet calculated a sensible value for the amount of atmospheric CO_2 sequestered by the ASIZ. Estimates of flux for May to September are particularly uncertain due to lack of $\Delta f\text{CO}_2$ data south of 55°S (Table 1.1) and the maximum extent of the ice edge occurring in October. There is uncertainty in the correct wind speed dependence to use when calculating air-sea flux of CO_2 , and better techniques need to be developed for interpolating sparsely distributed oceanic $f\text{CO}_2$ data over the ASIZ. In addition, further work needs to be done on measuring the "skin temperature effect" on air-sea CO_2 flux (Subsection 1.3.1). Robertson et al. (1995) estimated that the skin effect would have contributed a further $-1.8 \times 10^{-2} \text{ g C m}^{-2} \text{ d}^{-1}$ to their net flux estimate of

$-7.0 \pm 0.4 \times 10^{-2} \text{ g C m}^{-2} \text{ d}^{-1}$ over their study region south of 50°S for the period November to December 1992 and February to March 1993 (Table 4.4). If this same skin effect contribution may be applied to the study region $55^{\circ} - 70^{\circ}\text{S}$, $60^{\circ} - 150^{\circ}\text{E}$, then it would significantly increase the net flux into the ocean from $-2.65 \times 10^{-2} \text{ g C m}^{-2} \text{ d}^{-1}$ to $-4.45 \times 10^{-2} \text{ g C m}^{-2} \text{ d}^{-1}$ over the same four month period.

4.5 CONCLUSIONS

Measurements of the fugacity of CO_2 in surface waters, taken on six voyages of the *RSV Aurora Australis* (15 October 1991 to 26 February 1994), have been used to calculate the monthly net transfer of CO_2 between the ocean and atmosphere in the Antarctic Seasonal Ice Zone. Two different methods were employed in these gas transfer calculations, one using surface wind speeds measured on the ship and corrected to 10 m a.s.l., and the other using six-hourly surface wind speeds from GASP analyses. Both methods employed the relationship for gas transfer velocity from “instantaneous” or steady 10 m wind speeds formulated by Wanninkhof (1992).

Over the period 1 January to 31 March 1993 the net transfer estimates for the region $55^{\circ} - 70^{\circ}\text{S}$, $60^{\circ} - 150^{\circ}\text{E}$, from ship and GASP wind speeds were $-15.2 \times 10^{-3} \text{ Gt C/90 d}$ and $-14.3 \times 10^{-3} \text{ Gt C/90 d}$, respectively, over an average area of open water of $6.00 \times 10^{12} \text{ m}^2$. The close agreement between these two fluxes does not imply that the two different methods used here to estimate gas transfer will always necessarily give similar results. From the difference between the two wind speed data sets it would have been expected that the net transfer estimate obtained using GASP wind speeds would have been 140% of the transfer calculated from shipboard wind speeds. The observed close agreement between the two transfer estimates was due to the difference in data interpolation techniques almost canceling out the effect of using different wind speed data sets.

Between 1 October 1992 and 31 March 1993 the ocean south of 55°S , between 60°E and 150°E (average area $5.29 \times 10^{12} \text{ m}^2$), sequestered $-25 \pm 13 \times 10^{-3} \text{ Gt C/182 d}$

(calculated using surface wind speeds from GASP analyses). The reduction in gas transfer velocity by the wave-damping effect of sea-ice made very little difference to the total transfer value, with an estimate of -23×10^{-3} Gt C/182 d, assuming no net flux over a grid square at least 50% covered by sea-ice.

There were distinctive zonal and meridional variations in net air-sea transfer of CO₂ over the study region. The ocean sink was most pronounced west of 105°E ($-26 \pm 13 \times 10^{-3}$ Gt C/182 d over an area 2.55×10^{12} m²), where it was associated with summer phytoplankton blooms (Chapter 3).

Over the northern region (55° - 60°S, 60° - 150°E: 2.96×10^{12} m² of open water), the ocean sequestered $-19 \pm 9 \times 10^{-3}$ Gt C during 1 October 1992 to 31 March 1993, and only $-6.4 \pm 3.7 \times 10^{-3}$ Gt C south of 60°S (2.33×10^{12} m² of open water). During December 1992 to February 1993, the ocean south of 60°S was a relatively small net sink for atmospheric CO₂ compared with the region 55°S to 60°S, mainly due to higher surface wind speeds over the northern region and to oceanic *f*CO₂ generally exceeding atmospheric fugacities over the south-eastern region 60° - 70°S, 105° - 150°E.

The estimates for average air-sea flux per unit area, calculated in this study using GASP wind speeds, agreed relatively closely with flux estimates for the Southern Ocean made by Takahashi (1989), Tans et al. (1990), and Metzl et al. (1995). There was less agreement with flux estimates made by Robertson and Watson (1995), with their calculated mean flux per unit area over the ocean south of 50°S, between 80°W and 80°E, being nearly three times the flux estimate from GASP wind speeds for the same four month period (November to December 1992 and February to March 1993). Fluxes from GASP wind speeds were calculated using the same equations as were used by Robertson and Watson (1995) and Metzl et al. (1995). The higher estimate from Robertson and Watson (1995) may indicate that surface Δf CO₂ was more negative in their study region and/or that shipboard wind speeds measured during their two cruises were atypically high and did not follow a Rayleigh distribution due to the shortness of the sampling period.

Care should be taken when interpolating or extrapolating from $\Delta f\text{CO}_2$ and wind speed data over the Antarctic Seasonal Ice Zone due to the high spatial and temporal variability in both parameters throughout this region. More oceanic $f\text{CO}_2$ data is required south of 55°S , particularly during autumn and winter months when high wind speeds over areas of open water may cause strong net air-sea fluxes of CO_2 .

CHAPTER FIVE:

INFLUENCE OF THE SOUTHERN OCEAN ON THE CONCENTRATION AND $^{13}\text{C}/^{12}\text{C}$ OF ATMOSPHERIC CO_2

5.1 INTRODUCTION

South of Australia, the lack of land masses supporting significant plant, animal or human populations means that changes in the concentration of atmospheric CO_2 and its $^{13}\text{C}/^{12}\text{C}$ ratio observed over the Southern Ocean must be due to either atmospheric transport from northern regions or to exchange with the ocean. Valuable information on air-sea exchange of CO_2 may be obtained from a study of surface ocean measurements of $f\text{CO}_2$ and temperature from the Southern Ocean, combined with measurements of atmospheric CO_2 mixing ratios and $\delta^{13}\text{C}$ along the same transects.

This chapter presents measurements of atmospheric CO_2 mixing ratios and $\delta^{13}\text{C}$ obtained from six cruises by the *RSV Aurora Australis* between Tasmania and the Antarctic coast (60°E to 150°E), during the period 17 October 1992 and 28 February 1994. Relationships between the atmospheric and oceanic observations are investigated and compared with theory. It will be demonstrated that the $\delta^{13}\text{C}$ values from atmospheric samples give different information about air-sea exchange and oceanic parameters to that provided by the CO_2 mixing ratios from the same atmospheric samples.

5.2 OBSERVATIONS OF ATMOSPHERIC CO₂ MIXING RATIOS AND $\delta^{13}\text{C}$ OVER THE SOUTHERN OCEAN

Since March 1991, air samples have been collected aboard *RSV Aurora Australis* (Subsection 2.5.1) and analysed for the mixing ratio and $\delta^{13}\text{C}$ of CO₂ in the atmosphere (Sections 2.5.2 and 2.7). The air sampling programme is the first shipboard survey of $\delta^{13}\text{C}$ in the Southern Ocean atmosphere. The high precision of the mixing ratio and $\delta^{13}\text{C}$ data (Sections 2.5.2 and 2.7) has provided the opportunity to observe changes in the atmosphere directly forced by fluctuations in properties of the local ocean surface.

In this chapter, atmospheric measurements are presented from 360 flasks filled at 20 m a.s.l. on six cruises between Hobart and Antarctica, from 17 October 1992 to 28 February 1994 (Appendix A: Table A.1). Sampling sites are shown in Figure 5.1. Values of the atmospheric CO₂ mixing ratio, C_a , and $\delta^{13}\text{C}$ of atmospheric CO₂, δ_a , used in this work therefore refer to spot measurements at 20 m a.s.l. Atmospheric data collected prior to October 1992 are not used in the analysis due to inferior data quality.

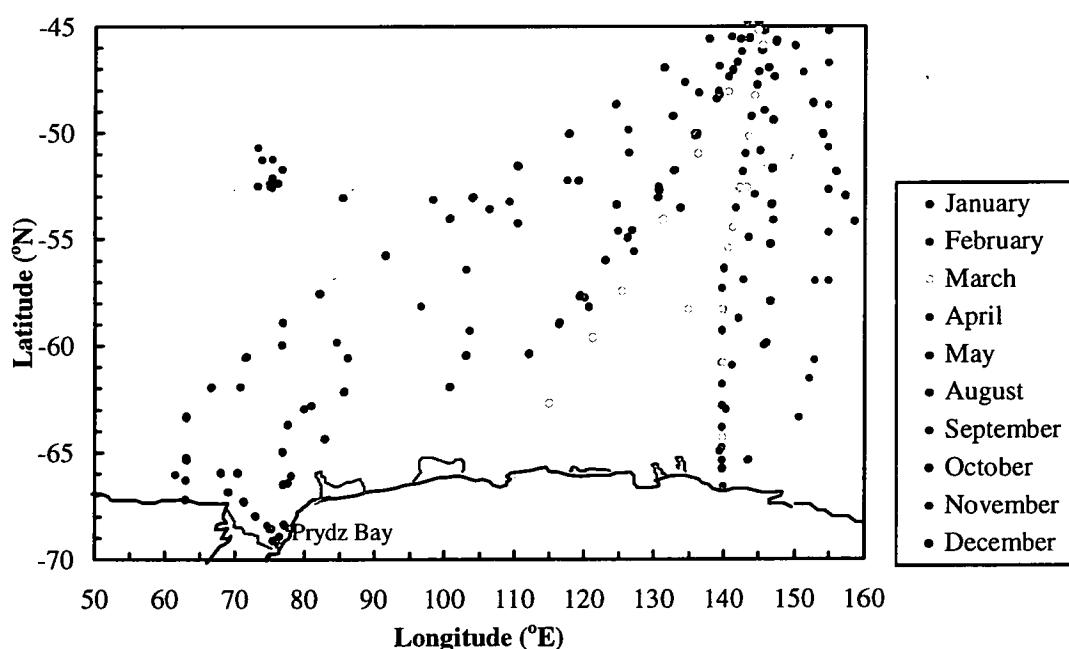


Fig. 5.1 Sites where baseline air was sampled from 20 m a.s.l. aboard the *RSV Aurora Australis*, during the period 17 October 1992 to 28 February 1994.

In order to identify variations in C_a and δ_a , caused by air-sea gas exchange over the immediate ocean, it was necessary to remove seasonal and interannual variations in these parameters caused by atmospheric mixing.

Over seasonal time scales, the Southern Ocean atmospheric boundary layer may be considered to be well-mixed with respect to carbon dioxide (Law et al., 1992). Short-term variations in C_a and δ_a , observed over the Southern Ocean, are therefore likely to be due to exchange of CO_2 with the ocean. Normalising values of C_a and δ_a to measurements from a Southern Ocean site experiencing minimal air-sea gas exchange removes seasonal and interannual variations caused by large-scale atmospheric mixing. In this way, measurements from transects at different times can be combined, and the effects of variations in the surface ocean more clearly isolated.

The first step was to identify a latitude where seasonal variability in air-sea gas flux, and sea-ice influences on atmospheric CO_2 and its $^{13}\text{C}/^{12}\text{C}$ ratio, are minimal. The latitude chosen was 55°S , since $\Delta f\text{CO}_2$ was observed to be closer to zero at 55°S , and experience less natural variability, compared with other latitudes during the study period (Figure 5.2). At 55°S , there was minimal impact on atmospheric CO_2 concentrations from net exchange with the local ocean, and therefore any observed variation in C_a was more likely to be due to atmospheric transport. Along the cruise tracks, this latitude was north of the maximum ice edge but south of the Polar Front (Figure 1.1), and hence was within the Permanently Open Ocean Zone (POOZ). Surface waters of the POOZ are less productive than the Polar Frontal Zone to the north or the ASIZ to the south (Tréguer and Jacques, 1992). Hence, $\delta^{13}\text{C}$ -DIC in surface water at 55°S along the transects would have been relatively constant throughout the year. Atmospheric $\delta^{13}\text{C}$ measured at 55°S was therefore less likely to be affected by changes in oceanic $f\text{CO}_2$ and $^{13}\text{C}/^{12}\text{C}$ of DIC compared with other latitudes sampled. To a first order approximation, normalising values of C_a and δ_a to 55°S suppresses seasonal and interannual variations.

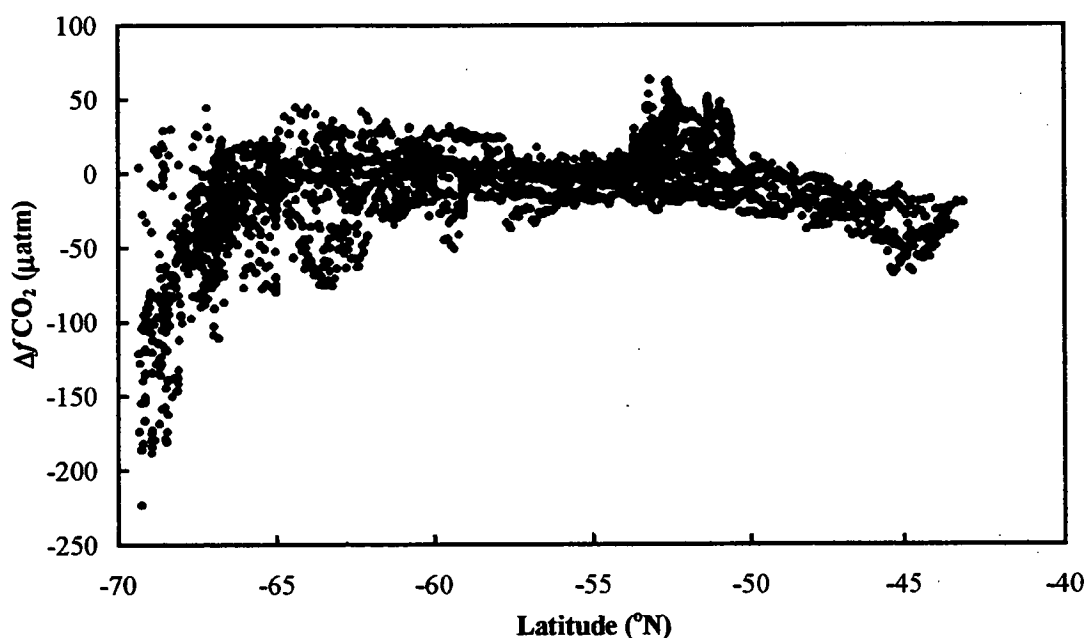


Fig. 5.2 Hourly averaged $\Delta f\text{CO}_2$ values measured from the *RSV Aurora Australis* over the region $60^\circ - 160^\circ\text{E}$, for cruises between 17 October 1992 and 28 February 1994.

Some smoothing was necessary to characterise the normalising value at 55°S for each transect. A spline (Enting et al., 1993), with 50% attenuation every 5° of latitude, was fitted to values of C_a and δ_a versus latitude for each cruise. As the air samples were collected every one to three degrees of latitude along each transect, 5° was considered the optimum latitude interval to use in the splines. The results of the analysis were not sensitive to the attenuation latitude interval chosen. The mixing ratios and $\delta^{13}\text{C}$ of atmospheric CO_2 along each transect were normalised to the spline fitted value at 55°S , to obtain values of $C_a - C_a(55^\circ\text{S})$ and $\delta_a - \delta_a(55^\circ\text{S})$.

Figure 5.3 presents atmospheric CO₂ mixing ratios normalised to 55°S along the same cruise transect, $C_a - C_a(55^\circ\text{S})$, to isolate the effect of net air-sea exchange.

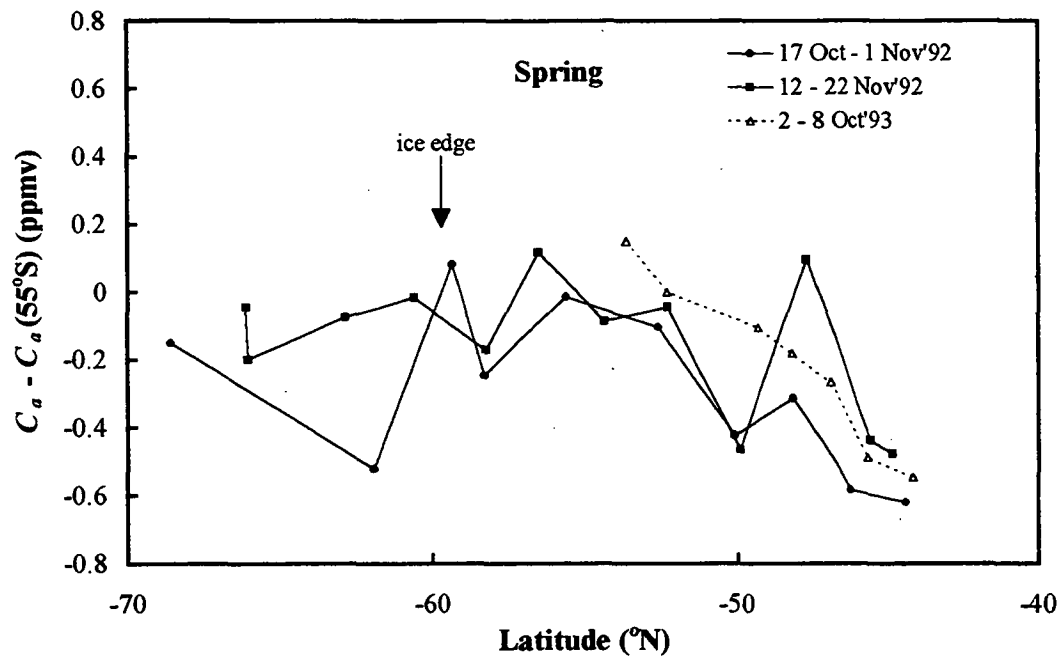
Measurements from the same sampling site have been averaged. Agreement between pairs of flasks filled at the same site was good, with the average difference between CO₂ mixing ratio pairs being 0.09 ppmv (0.025%). The external measurement precision of the Carle Series 400 gas chromatograph for routine flask analyses was $\pm 0.02\%$ (Francey et al., 1995a).

Normalised CO₂ mixing ratios increased from north to south over the region from 44°S to 55°S, between 85°E and 160°E, during all months sampled except January 1993 (Figure 5.3). This meridional trend in $C_a - C_a(55^\circ\text{S})$ suggests net uptake of atmospheric CO₂ by the ocean between 44°S and 55°S, with higher uptake at lower latitudes.

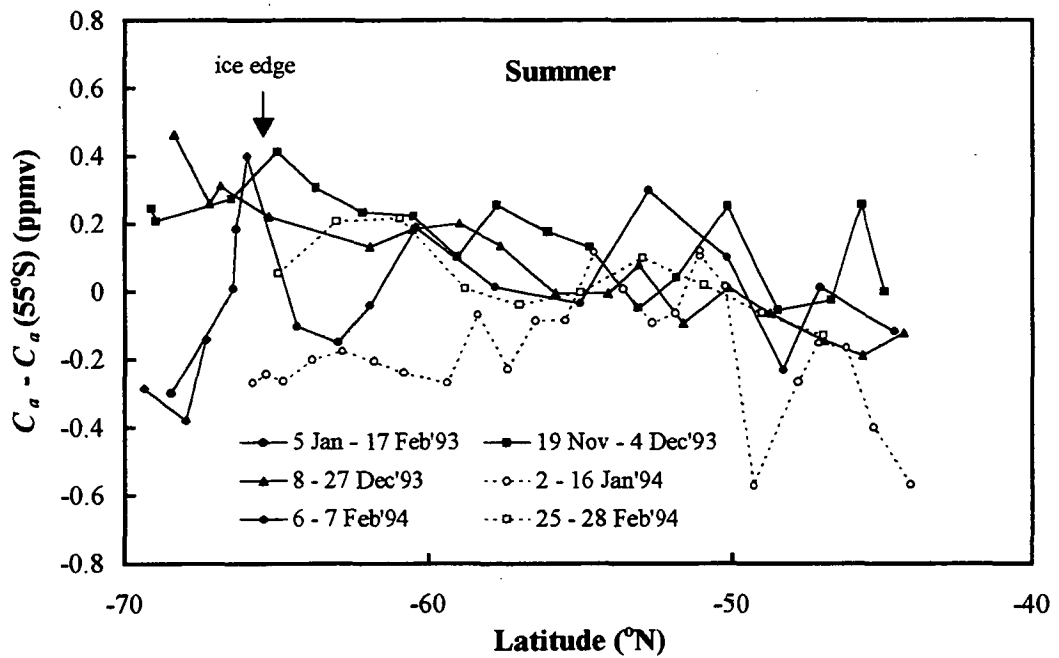
The relationship between shipboard measurements of atmospheric CO₂ mixing ratios and $\Delta f\text{CO}_2$, over this ice-free region of the Southern Ocean, is demonstrated in Section 5.3.

There appears to be a wide scatter in summertime values of $C_a - C_a(55^\circ\text{S})$ south of 55°S, between 60°E and 105°E (solid symbols in Figure 5.3(b)), with high values during November to early January, and below average $C_a - C_a(55^\circ\text{S})$ values during January to February. The large variation in mixing ratios may be due to the wide variation in net air-sea transfer of CO₂ over the same region (Figures 4.3(d) - (e)). The decrease in ice cover late in the summer coincided with below average levels of $C_a - C_a(55^\circ\text{S})$ over Prydz Bay (Figure 5.3(b)). This sudden decrease in $C_a - C_a(55^\circ\text{S})$ agrees with the estimates of stronger net ocean uptake of atmospheric CO₂ south of 60°S, 60° - 105°E, during January and February 1993, compared with earlier months (Table 4.1(b)).

(a)



(b)



(c)

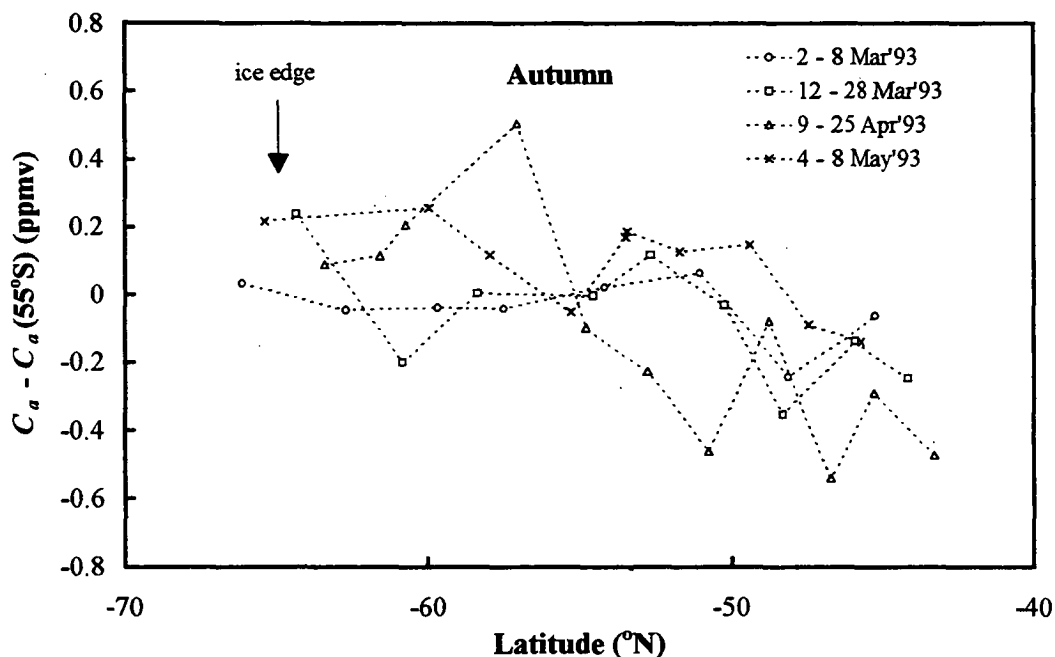
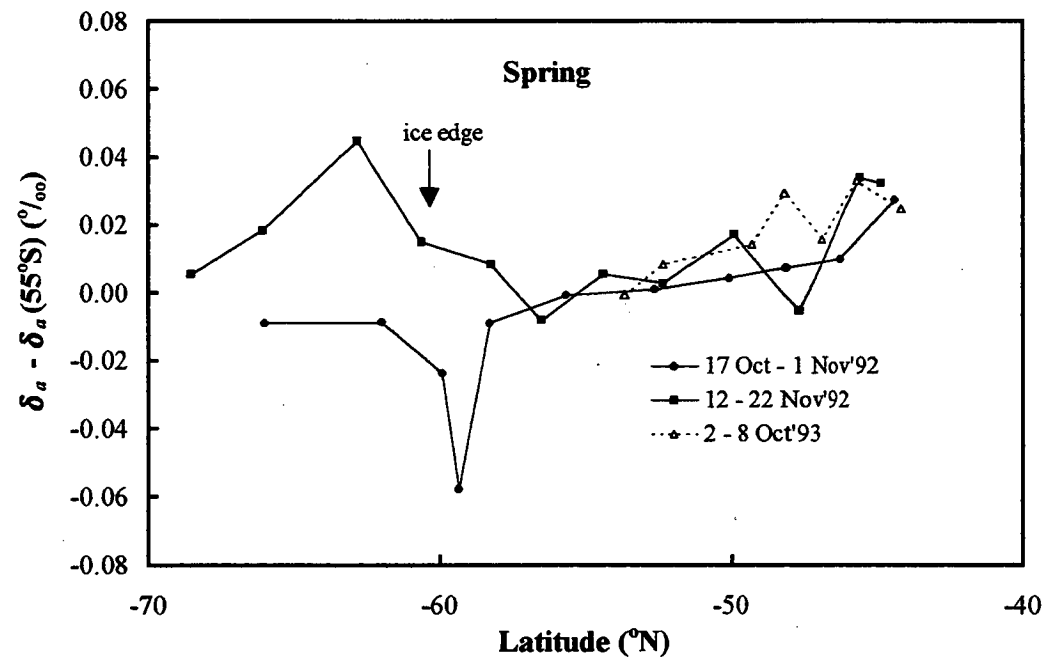


Fig. 5.3 Atmospheric CO₂ mixing ratios obtained from flasks of air collected aboard the *RSV Aurora Australis* and normalised to 55°S along the same transect for (a) Spring (17 October - 22 November 1992, 2 - 8 October 1993), (b) Summer (5 January - 26 February 1993, 19 November - 27 December 1993, 2 January - 28 February 1994), and (c) Autumn (2 - 28 March 1993, 9 April - 8 May 1993). The filled symbols correspond to cruises into the ASIZ to the west of 105°E, and the unfilled symbols denote cruises east of 105°E.

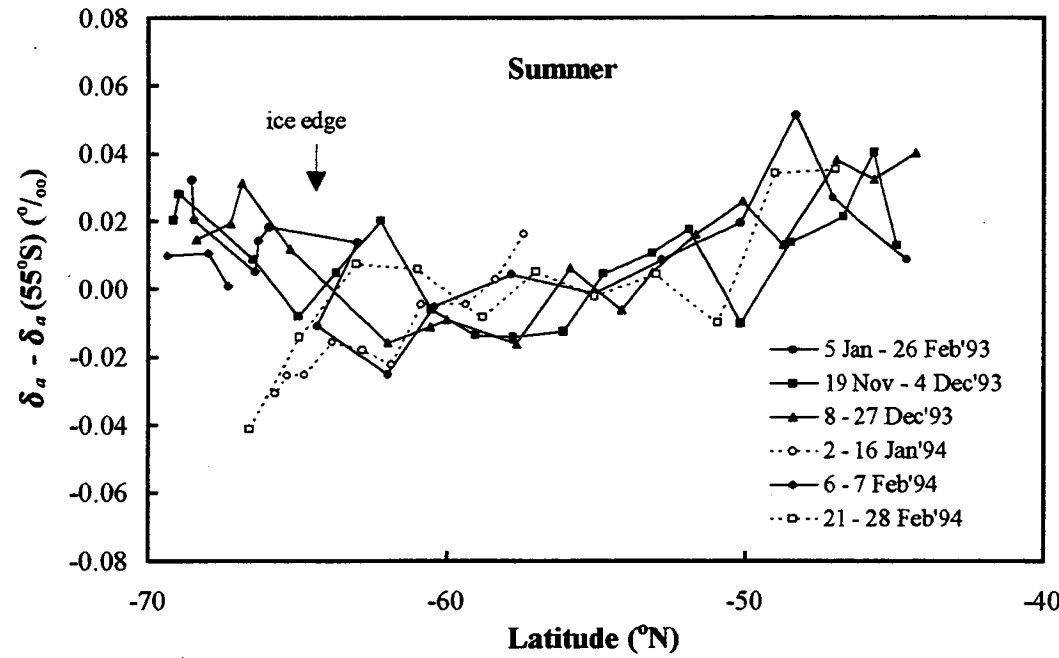
Figure 5.4 presents values of atmospheric $\delta^{13}\text{C}$ normalised to 55°S along the same cruise transect, $\delta_a - \delta_a(55^\circ\text{S})$, to isolate the effect of air-sea exchange. As in Figure 5.3, measurements from the same sampling site have been averaged. Excellent agreement was obtained between pairs of flasks filled at the same site, with the average difference between $\delta^{13}\text{C}$ pairs being 0.01 ‰ , which is the external measurement precision ($\pm 0.01\text{ ‰}$) of the MAT252 mass spectrometer (Francey et al., 1995a).

From shipboard observations, the most northerly extent of sea-ice for the transects used in this analysis was 60°S . Between Tasmania (44°S) and 60°S , values of $\delta_a - \delta_a(55^\circ\text{S})$ appeared to decrease from north to south (Figure 5.4). The decrease in atmospheric $\delta^{13}\text{C}$ with latitude south will be shown in Section 5.4 to be due to the temperature dependence of the fractionation of the stable carbon isotopes between gaseous CO_2 and dissolved inorganic carbon (Mook et al., 1974). South of 60°S and east of 105°E , summertime $\delta_a - \delta_a(55^\circ\text{S})$ values appeared to continue to decrease from north to south, whereas south of 60°S and west of 105°E , summertime $\delta_a - \delta_a(55^\circ\text{S})$ values increased with latitude (Figure 5.4(b)), due to a combination of net uptake of CO_2 by the ocean in this region, and increased ratios of $^{13}\text{C}/^{12}\text{C}$ of DIC in the surface ocean. These phenomena will be investigated in Sections 5.3 and 5.5, respectively.

(a)



(b)



(c)

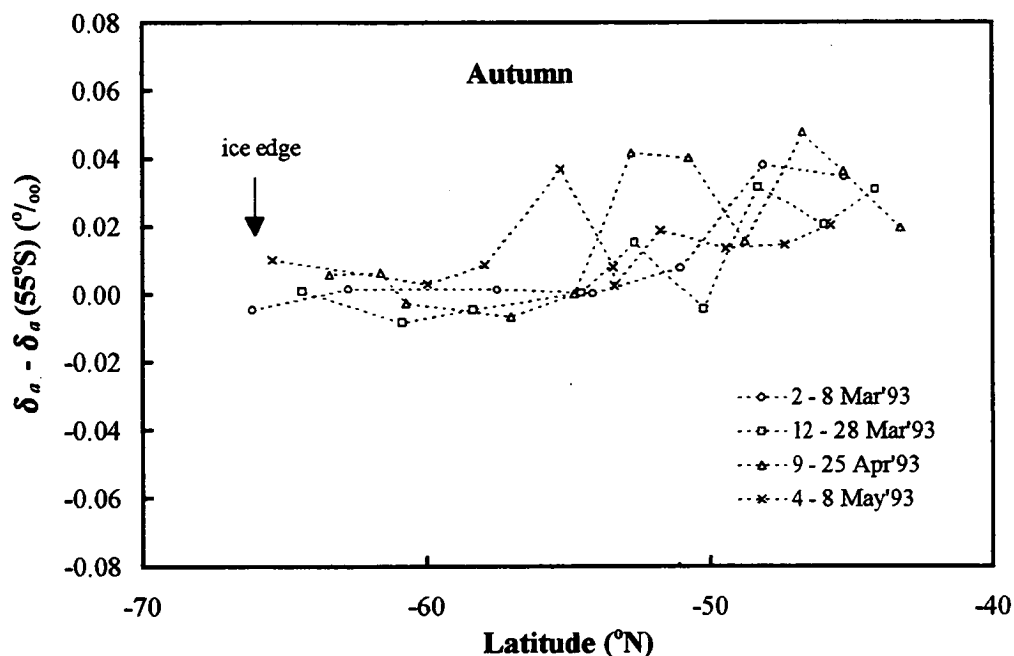


Fig. 5.4 Atmospheric $\delta^{13}\text{C}$ values obtained from air samples collected aboard the *RSV Aurora Australis* and normalised to 55°S along the same transect for (a) Spring (17 October to 22 November 1992, 2 to 8 October 1993), (b) Summer (5 January to 26 February 1993, 19 November to 27 December 1993, 2 January to 28 February 1994), and (c) Autumn (2 to 28 March 1993, 9 April to 8 May 1993). The filled symbols correspond to cruises into the ASIZ to the west of 105°E and the unfilled symbols denote cruises east of 105°E .

5.3 EFFECT OF $\Delta f\text{CO}_2$ ON ATMOSPHERIC CO_2 OVER THE SOUTHERN OCEAN

The net amount of CO_2 that enters the atmosphere from exchange with the ocean surface is proportional to $\Delta f\text{CO}_2$ (equations 1.1 and 1.2). It is not surprising, then, that over ice-free areas of the Southern Ocean (44° - 60°S) there appears to be a linear relationship between atmospheric CO_2 mixing ratios (normalised to 55°S to suppress seasonal and interannual variations - Section 5.2), and hourly averaged values of $\Delta f\text{CO}_2$ in the vicinity of the air sampling site, also normalised to 55°S (Figure 5.5).

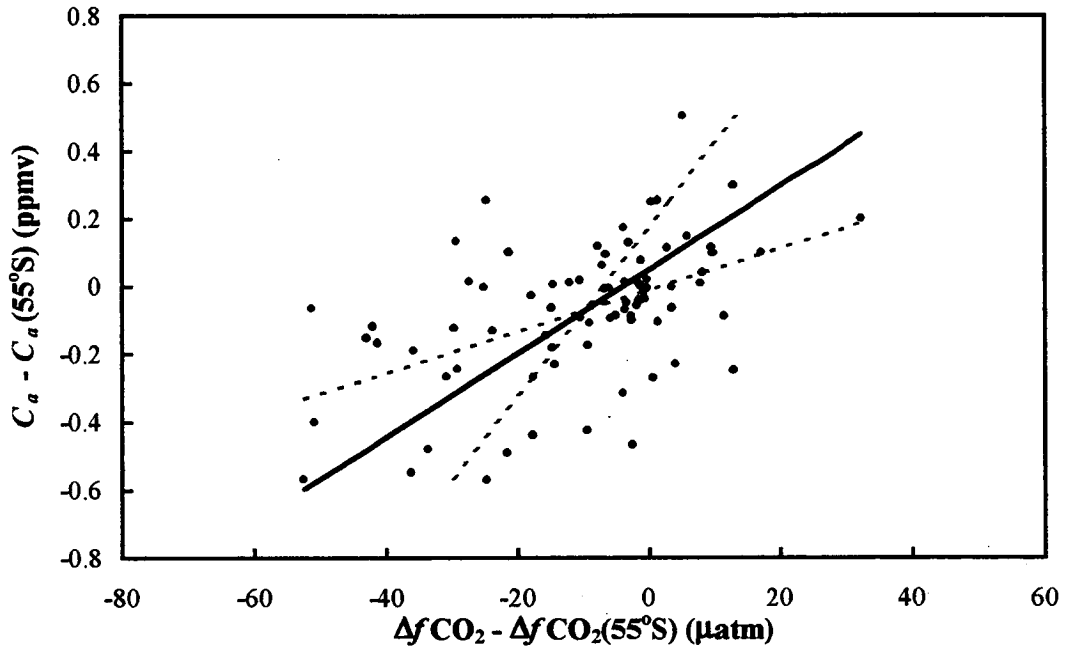


Fig. 5.5 The deviation in atmospheric CO₂ from its concentration at 55°S, against ΔfCO₂ normalised to 55°S, for transects between 44°S and 60°S during 17 October 1992 to 28 February 1994. The dashed lines represent the linear regressions (Y on X and X on Y) and the solid line the geometric mean functional regression (Teissier, 1948; Ricker, 1973).

A line can be fitted to the data in Figure 5.5 using a geometric mean functional regression (Teissier, 1948; Ricker, 1973), giving

$$C_a - C_a(55^\circ\text{S}) = (0.012 \pm 0.001)(\Delta f\text{CO}_2 - \Delta f\text{CO}_2(55^\circ\text{S})) + (0.05 \pm 0.02)$$

$$r^2 = 0.25, n = 82 \quad (5.1)$$

It is appropriate in this case to use the geometric mean functional regression since the variation in both atmospheric CO₂ mixing ratios and ΔfCO₂ is mostly natural, rather than predominantly caused by measurement error (Ricker, 1973). Note that the difference in linear regression coefficients (slopes of dashed lines in Figure 5.5) is an indication of the correlation between the two variables, $C_a - C_a(55^\circ\text{S})$ and $\Delta f\text{CO}_2 - \Delta f\text{CO}_2(55^\circ\text{S})$. For a perfect correlation, both linear regressions would have the same slope (Ricker, 1973).

From equation 5.1, the slope of the geometric regression is given by:

$$\frac{d(C_a - C_a(55^\circ\text{S}))}{d(\Delta f\text{CO}_2 - \Delta f\text{CO}_2(55^\circ\text{S}))} = 0.012 \pm 0.001 \quad (5.2)$$

Equation 5.2 indicates that there was a definite linear relationship between atmospheric CO₂ mixing ratios (normalised to suppress seasonal and interannual variation) and normalised hourly averaged $\Delta f\text{CO}_2$, since the standard error in the slope (0.001) was only 9% of the total gradient. The usefulness of this equation can best be explored by setting up a simple model for carbon mass balance between the surface ocean and the atmosphere.

In the Southern Ocean troposphere, atmospheric transport in the zonal direction is relatively rapid so that most structure is in the meridional direction (Plumb and Mahlman, 1987; Law et al., 1992). In the surface ocean, temperatures and fugacities are also likely to vary more with latitude than with longitude. Therefore, a simple zonally averaged box model may be set up as illustrated in Figure 5.6, encompassing the region of the atmosphere affected by air-sea gas exchange (a) and the ocean mixed layer (m). Reservoir a is bounded to the south by reservoir s , to the north by reservoir n , and above by reservoir b . The box is centred on the air sampling site, and is of horizontal surface area, A , and “effective mixing height”, z_N . The effective mixing height of a perturbation in atmospheric CO₂ caused by net air-sea exchange, z_N , is defined here for any atmospheric profile of CO₂ mixing ratios, $C_a(z)$ (Figure 5.7), such that:

$$\int (C_a(z) - C_b) dz = (C_a - C_b) z_N \quad (5.3)$$

where

- C_a = mixing ratio of atmospheric CO₂ at 20 m a.s.l. over the sample site
 \approx mean CO₂ mixing ratio in reservoir a (ppmv),
- C_b = CO₂ mixing ratio in the atmosphere above reservoir a unaffected by net air-sea gas exchange (ppmv).

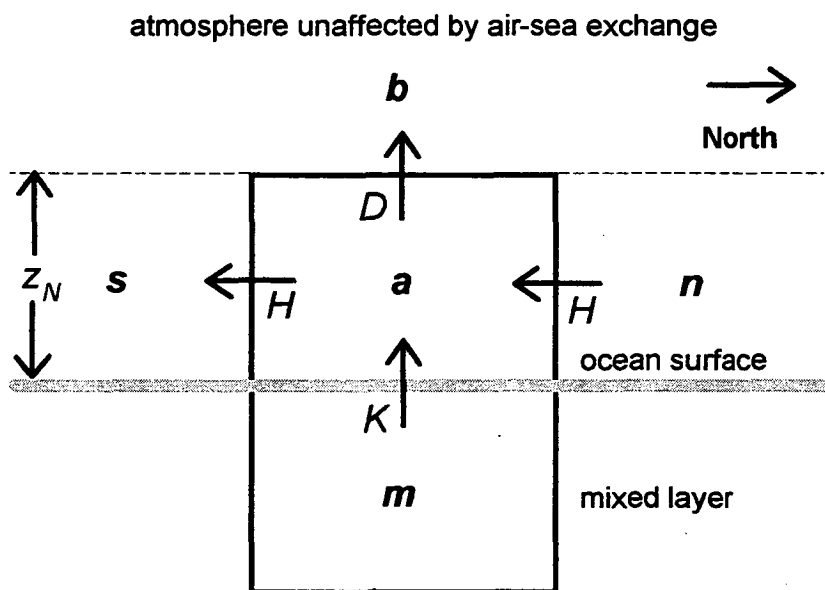


Fig. 5.6 Simple zonally averaged atmosphere-ocean model of transfer of CO₂ between the ocean mixed layer and the portion of the atmosphere affected by net air-sea exchange, over an ice-free region of the Southern Ocean of area A , centred on the air sampling site. See pages 5-12 and 5-14 for an explanation of the symbols.

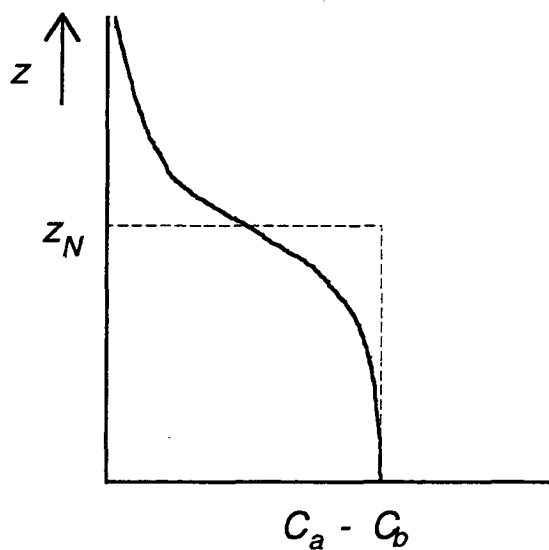


Fig. 5.7 Simple illustration of the effective vertical mixing height, z_N , of an anomaly in CO₂ mixing ratio $C_a - C_b$, where C_b is unaffected by net air-sea exchange.

In effect, equation 5.3 defines the effective mixing height such that a perturbation in atmospheric CO₂ mixing ratios due to net air-sea transfer is constant ($= C_a - C_b$) from sea level to the effective mixing height, and zero above this height. The rate of transfer of CO₂ gas across the boundary between reservoirs a and b may be expressed in terms of an “effective vertical diffusion coefficient”, D , which depends solely on the effective mixing height, z_N , and therefore on the vertical atmospheric profile of CO₂. The vertical atmospheric profile in turn reflects both the source of CO₂ from the ocean and the vertical diffusion of the gas through the atmosphere.

Only areas of open ocean will be considered in this analysis. Atmospheric and oceanic data from transects between 44°S and 60°S are used, as these were through ice-free regions.

The rate at which carbon accumulates in the portion of the atmosphere affected by air-sea exchange (reservoir a), from exchange of CO₂ gas with the ocean (equations 1.1 and 1.2), exchange of CO₂ gas with the atmosphere above a (reservoir b) and from meridional mixing is given by

$$\frac{dM_a}{dt} = 12AK \Delta f\text{CO}_2 - AD(z_N) (C_a - C_b) + A_v H(C_n - C_a) - A_v H(C_a - C_s) \quad (5.4)$$

where

- M_a = mass of carbon in reservoir a (g C),
- A = an area of open water centred on the sampling site (m²),
- K = air-sea gas exchange coefficient (mol C m⁻² d⁻¹ μatm⁻¹),
- $D(z_N)$ = reservoir a to reservoir b CO₂ exchange coefficient
= effective vertical diffusion coefficient of CO₂ gas at a height z_N
(g C m⁻² d⁻¹ ppmv⁻¹),
- z_N = height of reservoir a (m)
= function of the vertical profile of atmospheric CO₂ mixing ratios such that equation 5.3 is satisfied,
- A_v = vertical area of reservoir a in the zonal direction (m²),

- H = effective diffusion coefficient of CO₂ gas in the N-S direction
(g C m⁻² d⁻¹ ppmv⁻¹),
- C_n = mixing ratio of atmospheric CO₂ in the boundary layer north of
reservoir a (ppmv),
- C_s = mixing ratio of atmospheric CO₂ in the boundary layer south of
reservoir a (ppmv).

Equation 5.4 may be simplified by making the approximation that atmospheric CO₂ mixing ratios vary linearly between reservoir n and reservoir s and therefore $C_a = (C_n + C_s)/2$, and

$$\frac{dM_a}{dt} = 12AK \Delta f\text{CO}_2 - AD(z_N) (C_a - C_b). \quad (5.5)$$

Mixing ratios of CO₂ in the region of the atmosphere unaffected by net air-sea exchange, C_b , are relatively constant with latitude over the Southern Ocean, compared with mixing ratios within reservoir a , which are affected by air-sea exchange on short time-scales. Making the approximation that the air-sea gas exchange coefficient, K , and effective vertical diffusion coefficient, $D(z_N)$, are also constant with latitude over the Southern Ocean, then at 55°S (from equation 5.5):

$$\frac{dM_a(55^\circ\text{S})}{dt} = 12AK \Delta f\text{CO}_2(55^\circ\text{S}) - AD(z_N) (C_a(55^\circ\text{S}) - C_b) \quad (5.6)$$

where

$M_a(55^\circ\text{S})$ = mass of carbon in the atmospheric boundary layer, over a
horizontal area, A (g C),

$C_a(55^\circ\text{S})$ = mixing ratio of atmospheric CO₂ at 20 m a.s.l. and 55°S along the
cruise track

≈ mean CO₂ mixing ratio in reservoir a , over a horizontal area, A ,
centred at 55°S along the cruise track (ppmv).

Subtracting equation 5.6 from 5.5 gives:

$$\frac{d(M_a - M_a(55^\circ\text{S}))}{dt} = 12AK(\Delta f\text{CO}_2 - \Delta f\text{CO}_2(55^\circ\text{S})) - AD(z_N)(C_a - C_a(55^\circ\text{S})) \quad (5.7)$$

If, between 44°S and 60°S , the change in $\Delta f\text{CO}_2 - \Delta f\text{CO}_2(55^\circ\text{S})$ with time is relatively small compared with the change in $\Delta f\text{CO}_2 - \Delta f\text{CO}_2(55^\circ\text{S})$ with latitude (Figure 5.8), then $d(M_a - M_a(55^\circ\text{S}))/dt$ is close to zero (steady state), and

$$C_a - C_a(55^\circ\text{S}) \approx (12K/D(z_N)) (\Delta f\text{CO}_2 - \Delta f\text{CO}_2(55^\circ\text{S})) \quad (5.8)$$

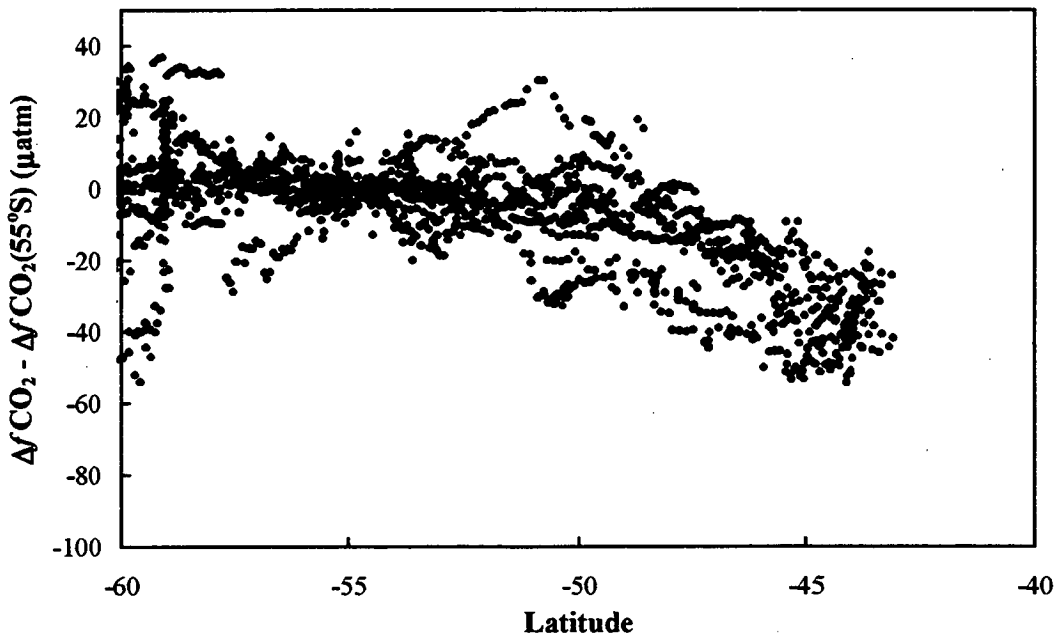


Fig. 5.8 The deviation in $\Delta f\text{CO}_2$ from its value at 55°S along the same transect. Fugacities were measured from the *RSV Aurora Australis* during 17 October 1992 to 28 February 1994.

Supposing that the dependence of $D(z_N)$ on surface wind speed is similar to that of K , then $K/D(z_N)$ should be relatively constant in time and space. If this is the case, then when all measurements between 44°S and 60°S are combined, one expects a linear relationship between $C_a - C_a(55^\circ\text{S})$ and hourly mean values of $\Delta f\text{CO}_2 - \Delta f\text{CO}_2(55^\circ\text{S})$, as seen in Figure 5.5. The correlation (r^2) between $C_a - C_a(55^\circ\text{S})$ and $\Delta f\text{CO}_2 - \Delta f\text{CO}_2(55^\circ\text{S})$ was 0.25, supporting in some degree the assumption of steady state and equation 5.8. Hence, equations 5.1 and 5.8 imply that

$$12K/D(z_N) \approx 0.012 \pm 0.001, \quad (5.9)$$

with the relatively small standard error indicating the natural spatial and temporal variation in the ratio of the air-sea gas exchange coefficient, K , to the effective vertical diffusion coefficient, $D(z_N)$.

In the real world, monthly and annual mean surface wind speeds vary significantly with latitude over the Southern Ocean (e.g. Halpern, 1993; Halpern et al., 1994a, 1994b), with a peak in magnitude at around 55°S. However, it is difficult to effectively incorporate wind speed into the simple atmosphere-ocean model without prior knowledge of the appropriate time interval and area (A) over which to average the surface wind speeds. Attempts were made to calculate K using first hourly averaged shipboard wind speeds and then SSMI 10 m 1988-91 mean wind speeds (Halpern et al., 1994a) without any improvement in accuracy of the estimate of $K/D(z_N)$.

It has been shown in this section that normalised atmospheric CO_2 mixing ratios measured at 20 m a.s.l., from cruises over the Southern Ocean north of the ASIZ, are dominated by net exchanges of carbon with the ocean. Equation 5.9 provides a mean value of the air-sea exchange coefficient over the Southern Ocean during the study period, provided that a value of the effective diffusion coefficient can be determined. Alternatively, equation 5.1 permits an average value of $\Delta f\text{CO}_2$ to be determined from measurements of $C_a - C_a(55^\circ\text{S})$ over the Southern Ocean.

The following three sections demonstrate the extra information on oceanic parameters that may be obtained from shipboard measurements of the ratio of $^{13}\text{C}/^{12}\text{C}$ in atmospheric CO_2 .

5.4 EFFECT OF $\Delta f\text{CO}_2$ ON ATMOSPHERIC $\delta^{13}\text{C}$ OVER THE SOUTHERN OCEAN

In the previous section it was illustrated that a substantial proportion of the variation in atmospheric CO_2 mixing ratios may be linked to variation in hourly mean $\Delta f\text{CO}_2$ values at the sampling site (Figure 5.5). It is useful to determine how much of the variation in atmospheric $\delta^{13}\text{C}$ over the Southern Ocean (Figure 5.4) was also a result of changes in $\Delta f\text{CO}_2$.

The component of the rate of change of atmospheric $\delta^{13}\text{C}$ at 20 m a.s.l. caused by kinetic isotopic fractionation associated with net air-sea exchange of CO_2 , $d\delta_a(\text{net})/dt$, may be given by (equation 1.20):

$$\frac{d\delta_a(\text{net})}{dt} (\text{‰ d}^{-1}) = (\epsilon_{am}/M_a) \frac{dM_a(\text{net})}{dt} \quad (5.10)$$

where

ϵ_{am} = isotopic shift that occurs during air-sea exchange of CO_2 due to kinetic fractionation (‰),

$\frac{dM_a(\text{net})}{dt}$ = the component of the rate of change of the mass of atmospheric CO_2 in reservoir a due to net air-sea exchange (g C d^{-1})
= N .

Defining $M_a = M_{\text{air}}C_a$, where M_{air} = mass of air in reservoir a , then

$$\frac{dM_a(\text{net})}{dt} = M_{\text{air}} \frac{dC_a(\text{net})}{dt} \quad (5.11)$$

Substituting equation 5.11 into equation 5.10 gives

$$\frac{d\delta_a(net)}{dt} = \frac{\epsilon_{am}}{C_a} \frac{dC_a(net)}{dt} \quad (5.12)$$

If $\Delta C_a(net)$ represents the variation in atmospheric CO₂ mixing ratio at the sampling site due to net air-sea exchange over an interval Δt , then the variation in atmospheric $\delta^{13}\text{C}$ at the same site due to fractionation associated with net exchange of CO₂ with the ocean over the same period, $\Delta\delta_a(net)$, will be given by

$$\Delta\delta_a(net) = (\epsilon_{am}/C_a) \Delta C_a(net) \quad (5.13)$$

The maximum peak-to-peak variation in atmospheric CO₂ mixing ratios, measured for any one transect between 17 October 1992 and 28 February 1994, was 0.7 ± 0.2 ppmv. The maximum and minimum values were measured from samples collected on 29 January and 17 February 1993 while the ship was in Prydz Bay (Figure 5.3(b)), during a period of extremely low fugacities in the surface ocean (Figures 3.1(d) and (e)).

Choosing a value for ϵ_{am} of -2.23 ± 0.2 ‰ at 5°C (Zhang et al., 1995) and $C_a = 354.6 \pm 0.2$ ppmv (average CO₂ mixing ratio from January 1993 samples), then the expected change in atmospheric $\delta^{13}\text{C}$ from fractionation linked to net air-sea exchange, associated with a change in the atmospheric CO₂ mixing ratio of 0.7 ± 0.2 ppmv, would be 0.004 ± 0.013 ‰ (from equation 5.13). The difference in atmospheric $\delta^{13}\text{C}$ values in flasks of air collected on 29 January and 17 February 1993 was 0.003 ± 0.009 ‰, which is comparable to the 0.004 ± 0.013 ‰ expected if kinetic fractionation associated with net air-sea exchange alone was affecting the $^{13}\text{C}/^{12}\text{C}$ ratios. However, the maximum scatter in atmospheric $\delta^{13}\text{C}$, observed along any one transect through the Prydz Bay region 60° - 70°S, 60° - 105°E, was 0.06 ± 0.01 ‰ (Figure 5.4(b)). This observed variation in δ_a along one transect was a factor of 15 times greater than that expected from fractionation during net air-sea gas exchange alone, implying that

atmospheric $\delta^{13}\text{C}$ is influenced by other, much stronger, factors over the Southern Ocean than net exchange of CO_2 .

5.5 EFFECT OF SEA SURFACE TEMPERATURE ON ATMOSPHERIC $\delta^{13}\text{C}$ OVER THE SOUTHERN OCEAN

Keeling et al. (1989) predicted that there should be a meridional trend in atmospheric $\delta^{13}\text{C}$ over the Southern Ocean, caused by the temperature dependence of isotopic fractionation during air-sea exchange of CO_2 (Section 1.4). They used the temperature dependence to explain the more negative observations of atmospheric $\delta^{13}\text{C}$ at the South Pole compared with mid-southern latitude observations. In Section 5.4, it was shown that the effect of $\Delta f/\text{CO}_2$ on values of atmospheric $\delta^{13}\text{C}$ was weak compared with the total observed isotopic variation over the Southern Ocean. It is the aim of this section to determine the relative dependence of atmospheric $\delta^{13}\text{C}$ on sea surface temperature, SST, at the sampling site.

Geometric mean functional regression was performed on values of $\delta_a - \delta_a(55^\circ\text{S})$ against normalised SST (Teissier, 1948; Ricker, 1973) (Figure 5.9). The measurements were normalised to 55°S to suppress seasonal and interannual variations, so that all transects might be combined (Section 5.2). Between 44°S and 60°S (ice-free waters), the geometric mean regression to $\delta_a - \delta_a(55^\circ\text{S})$ versus $\text{SST} - \text{SST}(55^\circ\text{S})$ was

$$\begin{aligned} \delta_a - \delta_a(55^\circ\text{S}) &= (0.0041 \pm 0.0003)(\text{SST} - \text{SST}(55^\circ\text{S})) - (0.002 \pm 0.002) \\ r^2 &= 0.39, \quad n = 92 \end{aligned} \quad (5.14)$$

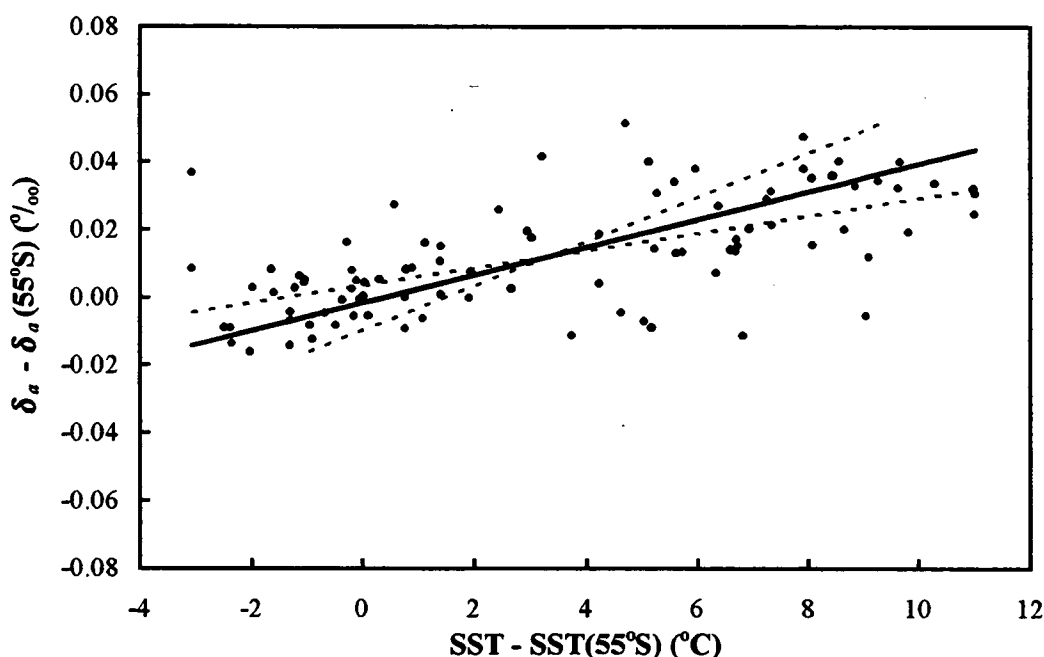


Fig. 5.9 Atmospheric $\delta^{13}\text{C}$ normalised to 55°S against normalised sea surface temperatures, for sampling sites between 44°S and 60°S . The dashed lines represent the linear regressions (Y on X and X on Y) and the solid line the geometric mean functional regression (Teissier, 1948; Ricker, 1973).

Hence, between 44°S and 60°S , the meridional gradient in sea surface temperature changed atmospheric $\delta^{13}\text{C}$ at 20 m a.s.l. by $0.0041 \pm 0.0003 \text{ ‰ } ^\circ\text{C}^{-1}$. This linear relationship with SST has many applications in atmospheric inverse modeling of the net carbon sink over the Southern Ocean, where measurements of atmospheric $\delta^{13}\text{C}$ from stations are very scarce (Chapter 1).

The implications of equation 5.14 can be determined by setting up a similar zonally averaged box model for $^{13}\text{CO}_2$ mass balance in the atmospheric boundary layer, as was set up for CO_2 (Figure 5.6). Again, atmospheric and oceanic data from transects between 44°S and 60°S are used in the analysis. The box is centred on the air sampling site, and is of horizontal surface area, A , and “effective mixing height”, z_G . The height, z_G , is defined as the effective mixing height of a perturbation in atmospheric $^{13}\text{CO}_2/^{12}\text{CO}_2$ caused by fractionation during gross air-sea exchange of CO_2 (Section 1.4), and is defined for any atmospheric profile of $\delta^{13}\text{C}$, $\delta_a(z)$ (Figure 5.10), such that:

$$\int (\delta_a(z) - \delta_b) dz = (\delta_a - \delta_b) z_G \quad (5.15)$$

where

- δ_a = atmospheric $\delta^{13}\text{C}$ at 20 m a.s.l. above the sample site
 \approx mean $\delta^{13}\text{C}$ in reservoir a , centred on the sampling site (‰),
 δ_b = $\delta^{13}\text{C}$ in the region of the atmosphere above the sampling site that is unaffected by fractionation associated with gross air-sea exchange (‰).

In effect, equation 5.15 defines the effective mixing height, z_G , such that a perturbation in $\delta^{13}\text{C}$ due to fractionation during gross air-sea transfer is constant ($= \delta_a - \delta_b$) from sea level to the effective mixing height, and zero above this height. Variation in the degree of fractionation associated with gross transfer of CO_2 from the ocean into reservoir a results in a change in z_G . The “effective vertical diffusion coefficient” from reservoir a to b in this case depends solely on z_G , and therefore on the vertical atmospheric profile of $^{13}\text{CO}_2/^{12}\text{CO}_2$, rather than the vertical profile of CO_2 , as was the case with $D(z_N)$.

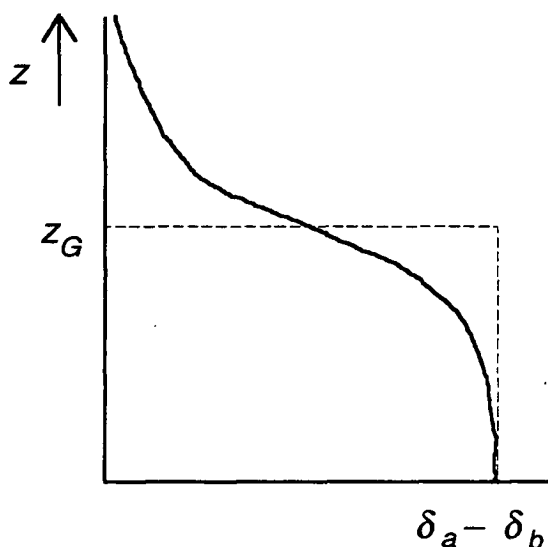


Fig. 5.10 Simple illustration of the effective vertical mixing height, z_G , of an anomaly in atmospheric $\delta^{13}\text{C}$, $\delta_a - \delta_b$, where δ_b is unaffected by fractionation during gross air-sea exchange of CO_2 .

Assume that over the region $44^\circ - 60^\circ\text{S}$, $60^\circ - 160^\circ\text{E}$, the troposphere is well-mixed zonally (Plumb and Mahlman, 1987; Law et al., 1992), and temperatures, fugacities and $\delta^{13}\text{C}$ -DIC in the surface ocean vary much more with latitude than with longitude. The rate of change of $\delta^{13}\text{C}$ in reservoir a is a result of fractionation during gross exchange of CO_2 gas with the ocean (equation 1.20) and net exchange with reservoirs b , n and s , and may be expressed (after equation 5.4) as

$$M_a \frac{d\delta_a}{dt} = 12AK[\epsilon_{am}(f_m - f_a) + f_m(\delta_a^e - \delta_a)] - AD(z_G) C_b(\delta_a - \delta_b) + A_n HC_a(\delta_n - \delta_a) - A_s HC_s(\delta_a - \delta_s) \quad (5.16)$$

where

$$\begin{aligned} \delta_a^e &= \text{atmospheric } \delta^{13}\text{C} \text{ that would be in equilibrium with the sea surface} \\ &= [(1 + \delta_m/1000)((0.98947 \pm 0.00005) + (0.104 \pm 0.003) \times 10^{-3} \text{ SST}) - 1] \times 1000 \text{ } \text{‰} \text{ (from equations 1.15 and 1.16),} \end{aligned}$$

$$\delta_m = \text{mean } \delta^{13}\text{C-DIC} \text{ in the ocean mixed layer, over a horizontal area, } A, \text{ centred on the sampling site (‰),}$$

$$D(z_G) = \text{effective vertical diffusion coefficient of } \text{CO}_2 \text{ gas at a height } z_G \text{ (g C m}^{-2} \text{ d}^{-1} \text{ ppmv}^{-1}),$$

$$\begin{aligned} z_G &= \text{height of reservoir } a \text{ (m)} \\ &= \text{function of the vertical profile of atmospheric } \delta^{13}\text{C} \text{ (and therefore of fractionation associated with gross air-sea exchange) such that equation 5.15 is satisfied,} \end{aligned}$$

$$\delta_n = \delta^{13}\text{C} \text{ in the atmosphere to the north of reservoir } a \text{ (‰),}$$

$$\delta_s = \delta^{13}\text{C} \text{ in the atmosphere to the south of reservoir } a \text{ (‰).}$$

Equation 5.16 may be simplified by making the approximation that atmospheric $\delta^{13}\text{C}$ varies linearly between reservoir n and reservoir s , and therefore $\delta_a = (\delta_n + \delta_s)/2$, and approximating C_a with C_s , then

$$M_a \frac{d\delta_a}{dt} = 12AKG - AD(z_G) C_b(\delta_a - \delta_b) \quad (5.17)$$

where

$$G = \epsilon_{am}(f_m - f_a) + f_m(\delta_a^e - \delta_a) \text{ (‰ } \mu\text{atm}).$$

Isotopic ratios of CO_2 in the portion of the atmosphere unaffected by gross air-sea exchange, δ_b , are relatively constant with latitude over the Southern Ocean, compared with values of $\delta^{13}\text{C}$ within reservoir a , which are affected on short time-scales by fractionation during gross air-sea exchange (Section 1.4). Making the approximation that the air-sea gas exchange coefficient, K , and effective vertical diffusion coefficient, $D(z_G)$, are also constant with latitude over the Southern Ocean, then at 55°S (from equation 5.17):

$$M_a(55^\circ\text{S}) \frac{d\delta_a(55^\circ\text{S})}{dt} = 12AKG(55^\circ\text{S}) - AD(z_G) C_b [\delta_a(55^\circ\text{S}) - \delta_b] \quad (5.18)$$

where

$$G(55^\circ\text{S}) = \varepsilon_{am} \Delta f\text{CO}_2(55^\circ\text{S}) + f_m(55^\circ\text{S}) (\delta_a^e(55^\circ\text{S}) - \delta_a(55^\circ\text{S})).$$

Subtracting equation 5.18 from 5.17 gives:

$$\begin{aligned} M_a \frac{d\delta_a}{dt} - M_a(55^\circ\text{S}) \frac{d\delta_a(55^\circ\text{S})}{dt} \\ = 12AK(G - G(55^\circ\text{S})) - AD(z_G) C_b (\delta_a - \delta_a(55^\circ\text{S})) \end{aligned} \quad (5.19)$$

One can approximate C_b by $C_a(55^\circ\text{S})$, since at 55°S along any transect $\Delta f\text{CO}_2 \approx 0$ (Figure 5.2), and therefore net air-sea transfer of CO_2 was relatively small. By definition, C_b is the mixing ratio of atmospheric CO_2 unaffected by air-sea gas exchange.

If, between 44°S and 60°S , the change in $G - G(55^\circ\text{S})$ with time is relatively small compared with the change in $G - G(55^\circ\text{S})$ with latitude, then the L.H.S. of equation 5.19 will be close to zero (steady state), and

$$\delta_a - \delta_a(55^\circ\text{S}) \approx (12K/D(z_G))(G - G(55^\circ\text{S}))/C_a(55^\circ\text{S}) \quad (5.20)$$

Over the ice-free region of the Southern Ocean $44^\circ - 60^\circ\text{S}$, $52^\circ - 80^\circ\text{E}$, $\delta^{13}\text{C-DIC}$ in the surface ocean was equal to approximately $1.8 \pm 0.3 \text{ ‰}$ during early 1991 (Francois et al., 1993). Globally, $\delta^{13}\text{C-DIC}$ in the surface ocean changes relatively slowly with time at approximately -0.015 ‰ yr^{-1} (Francey et al., 1995b), due to the release of fossil fuel carbon. In the atmosphere, over the region $44^\circ - 60^\circ\text{S}$, $60^\circ - 150^\circ\text{E}$, during 1992-94 $\delta_a - \delta_a(55^\circ\text{S})$ varied more with latitude than with time or longitude (Figure 5.4). Figure 5.11 demonstrates that $\text{SST} - \text{SST}(55^\circ\text{S})$ also changed relatively little with time or longitude compared with its change with latitude. Therefore, $G - G(55^\circ\text{S})$, which is predominantly a function of δ_m , δ_a and SST, changed less with time than with latitude. In addition, if $K/D(z_G)$ was relatively constant in time and space, then combining all measurements from sites between 44°S and 60°S should produce a linear relationship between $\delta_a - \delta_a(55^\circ\text{S})$ and $(G - G(55^\circ\text{S}))/C_a(55^\circ\text{S})$ (equation 5.20). Since G is linearly dependent on δ_a^e , and therefore on SST, it follows from equation 5.20 that $\delta_a - \delta_a(55^\circ\text{S})$ is linearly dependent on sea surface temperature, as was shown in Figure 5.9 and equation 5.14.

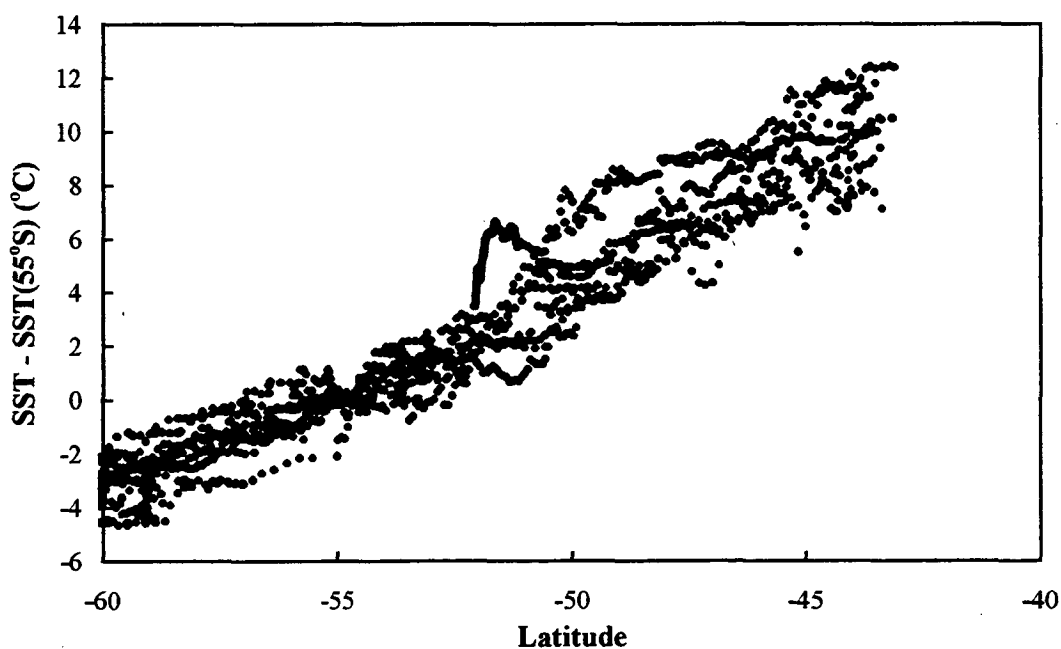


Fig. 5.11 The deviation in sea surface temperature from its value at 55°S along the same transect. Sea surface temperatures at 7.5 m depth were measured from the *RSV Aurora Australis* during 17 October 1992 to 28 February 1994.

Figure 5.12 presents values of $\delta_a - \delta_a(55^\circ\text{S})$ versus $(G - G(55^\circ\text{S}))/C_a(55^\circ\text{S})$ for sites where air was sampled between 44°S and 60°S . Values of $G = \epsilon_{am}\Delta f\text{CO}_2 + f_m(\delta_a^e - \delta_a)$ were calculated for each of these sites from atmospheric measurements of δ_a , hourly averaged measurements of f_m and SST, and with an assumed value of $\delta_m = 1.8 \text{ ‰}$ (Francois et al., 1993), and ϵ_{am} of -2.2 ‰ (Zhang et al., 1995).

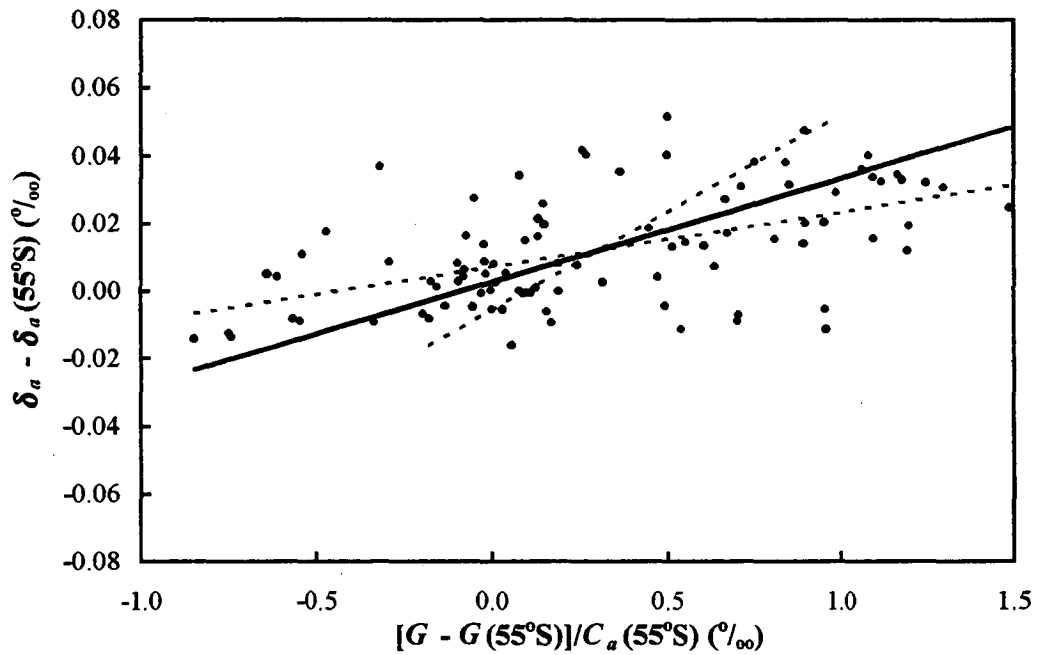


Fig. 5.12 Atmospheric $\delta^{13}\text{C}$ normalised to 55°S , against normalised values of $G/C_a(55^\circ\text{S})$, from sites between 44°S and 60°S . Values of $G = \epsilon_{am}\Delta f\text{CO}_2 + f_m(\delta_a^e - \delta_a)$ were calculated from measurements of δ_a at each sample site, hourly averaged measurements of f_m and SST, and with an assumed value of $\delta_m = 1.8 \text{ ‰}$, and ϵ_{am} of -2.2 ‰ . The dashed lines represent the linear regressions (Y on X and X on Y) and the solid line the geometric mean functional regression (Teissier, 1948; Ricker, 1973).

The geometric mean functional regression to the data presented in Figure 5.12 was

$$\begin{aligned}\delta_a - \delta_a(55^\circ\text{S}) &= (0.031 \pm 0.003)(G - G(55^\circ\text{S}))/C_a(55^\circ\text{S}) + (0.003 \pm 0.002) \\ r^2 &= 0.28, \quad n = 92.\end{aligned}\tag{5.21}$$

The error in the geometric mean regression coefficient (i.e. $C_a(55^\circ\text{S})d(\delta_a - \delta_a(55^\circ\text{S}))/d(G - G(55^\circ\text{S}))$) in equation 5.21 is due to the variation of $K/D(z_G)$ in time and space, and also to the variation in δ_m over the study region. As described in Section 5.3, attempts were again made to calculate K using first hourly averaged shipboard wind speeds and then SSMI 10 m 1988-91 mean wind speeds (Halpern et al., 1994a) without any improvement in accuracy of the estimate of $K/D(z_G)$. The error in the geometric mean regression coefficient due to the uncertainty in δ_m was estimated as follows.

Francois et al. (1993) presented values of $\delta^{13}\text{C-DIC}$ in surface waters of the Southern Indian Ocean during the austral summer of 1991. The mean value for $\delta^{13}\text{C-DIC}$ over the region $44^\circ - 60^\circ\text{S}$, $52^\circ - 80^\circ\text{E}$, was 1.8 ‰ with a standard deviation of $\pm 0.3 \text{ ‰}$. The expected range in values of

$C_a(55^\circ\text{S})d(\delta_a - \delta_a(55^\circ\text{S}))/d(G - G(55^\circ\text{S}))$ over the region $44^\circ - 60^\circ\text{S}$, $60^\circ - 150^\circ\text{E}$, can be determined by substituting δ_m values of 1.5 ‰ and 2.1 ‰ into the relationship for $(G - G(55^\circ\text{S}))/C_a(55^\circ\text{S})$.

The geometric mean functional regression to $\delta_a - \delta_a(55^\circ\text{S})$ against $(G - G(55^\circ\text{S}))/C_a(55^\circ\text{S})$, where δ_m was assigned a value of 1.5 ‰ , was

$$\begin{aligned}\delta_a - \delta_a(55^\circ\text{S}) &= (0.027 \pm 0.003)(G - G(55^\circ\text{S}))/C_a(55^\circ\text{S}) + (0.005 \pm 0.002) \\ r^2 &= 0.24, \quad n = 92.\end{aligned}\tag{5.22}$$

The geometric mean functional regression to $\delta_a - \delta_a(55^\circ\text{S})$ against

$(G - G(55^\circ\text{S}))/C_a(55^\circ\text{S})$, where δ_m was assigned a value of 2.1 ‰ , was

$$\begin{aligned}\delta_a - \delta_a(55^\circ\text{S}) &= (0.034 \pm 0.003)(G - G(55^\circ\text{S}))/C_a(55^\circ\text{S}) + (0.0006 \pm 0.002) \\ r^2 &= 0.32, \quad n = 92.\end{aligned}\tag{5.23}$$

Equations 5.21 to 5.23 suggest that over ice-free regions of the Southern Ocean, assuming $\delta_m = 1.8 \pm 0.3 \text{ ‰}$, then

$$C_a(55^\circ\text{S}) \frac{d(\delta_a - \delta_a(55^\circ\text{S}))}{d(G - G(55^\circ\text{S}))} = 12K/D(z_G) = 0.031 \pm 0.006 \tag{5.24}$$

Equations 5.9 and 5.24 imply that on average

$$D(z_N)/D(z_G) = (0.031 \pm 0.006)/(0.012 \pm 0.001) = 2.6 \pm 0.5. \tag{5.25}$$

The effective vertical diffusion coefficient at height z_N , $D(z_N)$, exceeding $D(z_G)$ (equation 5.25), is a direct result of the difference in atmospheric profiles of $^{12}\text{CO}_2$ and $^{13}\text{CO}_2$, and indicates that the effective mixing height of an anomaly in atmospheric $\delta^{13}\text{C}$ caused by fractionation during gross air-sea exchange, z_G , is higher than the effective mixing height of an anomaly in atmospheric CO_2 mixing ratios due to net air-sea exchange, z_N . The perturbation in concentrations of atmospheric $^{13}\text{CO}_2$ at 20 m a.s.l. due to air-sea exchange is therefore generally greater than the perturbation of atmospheric CO_2 mixing ratios at the same site. This implies that fractionation during gross air-sea exchange of CO_2 has a more measurable effect on $^{13}\text{CO}_2/^{12}\text{CO}_2$ at 20 m a.s.l., than the effect of net air-sea exchange on the atmospheric CO_2 mixing ratio, due to the difference in signal-to-noise ratios. The following example illustrates why this is the case.

Suppose that over reservoir a , $\Delta f\text{CO}_2 = 0$, implying that net air-sea transfer between m and a is zero. It follows that $C_a = C_b$ and $z_N = 0$. However, over the same region of ocean it is probable that $z_G > 0$, since, provided that the wind speed is greater than zero and $\delta_a^e \neq \delta_a$, the gross sea-to-air exchange term in equation 5.17, $12AK f_m(\delta_a^e - \delta_a)$, is non-zero. In the case of no net air-sea transfer, the $^{13}\text{C}/^{12}\text{C}$ ratio of atmospheric CO_2 is still strongly affected by gross sea-to-air transfer via air-sea isotopic disequilibrium and air-sea fractionation. Over a number of transects there will be a range of oceanic fugacities, f_m , but, in general, z_G will exceed z_N , and $D(z_N)$ will be greater than $D(z_G)$.

How does the meridional gradient in atmospheric $\delta^{13}\text{C}$ measurements obtained from our shipboard air samples compare with results from models? Keeling et al. (1989) modeled the zonally averaged north-south profile of atmospheric $\delta^{13}\text{C}$ by assuming a temperature-dependent fractionation between the atmosphere and oceans (Mook et al., 1974), a constant global average value of $\delta^{13}\text{C}$ -DIC in the surface ocean of 1.5512‰ , and simulating atmospheric mixing using a three-dimensional transport model. For the year 1980, Keeling et al. (1989) obtained a meridional gradient for annual mean atmospheric $\delta^{13}\text{C}$ between 40°S and 60°S of approximately -0.0011‰ per degree of latitude south, using a constant air-sea gas exchange coefficient of $7.9377 \times 10^{11} \text{ g C m}^{-2} \text{ yr}^{-1}$. Using Liss and Merlivat's (1986) relationship to calculate variable values of the air-sea exchange coefficient, Keeling et al. (1989) obtained a gradient of -0.0017‰ per degree of latitude south.

The geometric mean functional regression to $\delta_a - \delta_a(55^\circ\text{S})$ against latitude for $44^\circ - 60^\circ\text{S}$ was

$$\begin{aligned} \delta_a - \delta_a(55^\circ\text{S}) &= (-0.0036 \pm 0.0003) \text{ latitude}(^\circ\text{S}) - (0.199 \pm 0.001) \\ r^2 &= 0.42, \quad n = 99. \end{aligned} \tag{5.26}$$

For our sampling sites between 44°S and 60°S, atmospheric $\delta^{13}\text{C}$ at 20 m a.s.l. (normalised to suppress seasonal/interannual variations) varied -0.0036 ± 0.0003 ‰ per degree of latitude south, during the years 1992-94. This geometric mean functional regression coefficient is effectively an average value for the period 17 October 1992 to 28 February 1994, and is a factor of 2.1 steeper than the meridional gradient predicted by Keeling et al. (1989) for 1980 (using a variable air-sea exchange coefficient) over the same latitude range.

The difference in meridional gradient in atmospheric $\delta^{13}\text{C}$ between 1980 and 1992-94 may be due to a number of causes. Keeling et al.'s (1989) estimates of air-sea gas exchange coefficients, using Liss and Merlivat's (1986) equation, may have been too low for 1980. Wanninkhof's (1992) estimates for K at 20°C are, on average, 1.8 times Liss and Merlivat's (1986) estimates over a range of 10 m wind speeds from 3 m s⁻¹ to 13 m s⁻¹ (Figure 1.2). If the value of $\delta^{13}\text{C}$ in the surface ocean of 1.5512 ‰, chosen by Keeling et al. (1989) to represent all oceans during 1980, was less than the mean 1992-94 value of $\delta^{13}\text{C}$ -DIC of the surface ocean over 44°S to 60°S, then this may explain some of the discrepancy in meridional gradients in atmospheric $\delta^{13}\text{C}$.

5.6 EFFECT OF MARINE PRODUCTIVITY ON ATMOSPHERIC $\delta^{13}\text{C}$ OVER THE ASIZ

Over regions of the ocean with high phytoplankton productivity, one expects to see relatively high levels of $\delta^{13}\text{C}$ -DIC in surface waters (Section 1.4), and therefore higher values of δ_a^e . Areas of ocean that have experienced strong phytoplankton growth are characterised by low oceanic fugacities and negative $\Delta f\text{CO}_2$ values (Section 3.3).

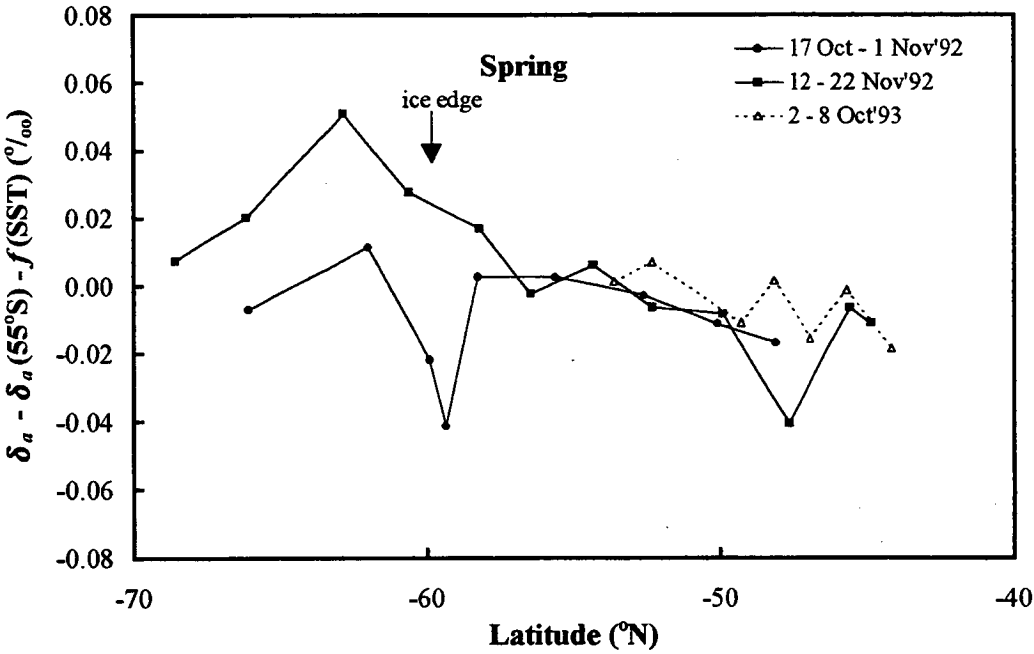
Equation 5.17 implies that an increase in the rate of change of atmospheric $\delta^{13}\text{C}$ caused by an increase in $\delta^{13}\text{C}$ -DIC, linked to high phytoplankton growth (via $f_m(\delta_a^e - \delta_a)$), is accentuated by the corresponding decrease in oceanic $f\text{CO}_2$ (via $\epsilon_{am}(f_m - f_a)$).

Therefore, over highly productive regions of the Southern Ocean one expects to see higher levels of atmospheric $\delta^{13}\text{C}$ compared with regions with similar sea surface temperatures but low productivity.

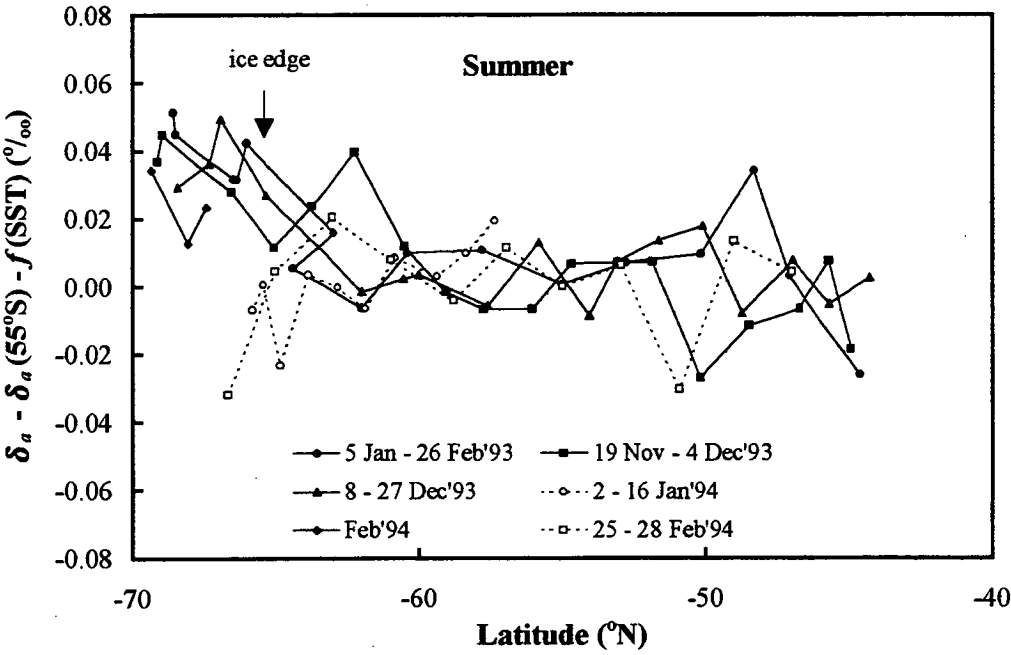
During summer, the region 60° - 70°S, 60° - 105°E, experienced levels of $\Delta f\text{CO}_2$ which were significantly more negative than those measured elsewhere over the study region (Figures 3.1(c)-(f)). The low fugacities in the surface ocean were associated with very high concentrations of chlorophyll *a* (Section 3.3), and therefore, phytoplankton productivity. It is therefore to be expected that values of $\delta_a - \delta_a(55^\circ\text{S})$, detrended for the temperature dependence, should be enhanced over the region 60° - 70°S, 60° - 105°E, compared with other areas. Figure 5.13 suggests that low levels of f_m and high levels of δ_m have resulted in higher levels of δ_a over the region west of 105°E (filled symbols) compared with transects east of 105°E (unfilled symbols), for the period November to February. It appears from Figure 5.13(b) that the high productivity of the western region of the ASIZ during summer had a more obvious impact on levels of atmospheric $\delta^{13}\text{C}$ than it had on CO_2 mixing ratios in the same air samples (Figure 5.3(b)).

It is also possible that the anomalously high values of atmospheric $\delta^{13}\text{C}$ south of 60°S (Figure 5.13) may have partially been due to air coming off dense pack ice or the continent which had not recently experienced exchange with the ocean. At the edge of the Antarctic sea-ice or land mass, the modeling results of Keeling et al. (1989) indicated a sharp reversal in the decrease of surface atmospheric $\delta^{13}\text{C}$ with increasing latitude. In this thesis, the reversal in the meridional trend in δ_a occurred during summer at the northernmost edge of the ASIZ, rather than the actual summer ice edge (Figure 5.13(b)), tending to discount the possibility that the positive meridional trend in δ_a south of 60°S was wholly due to a lack of gross air-sea exchange.

(a)



(b)



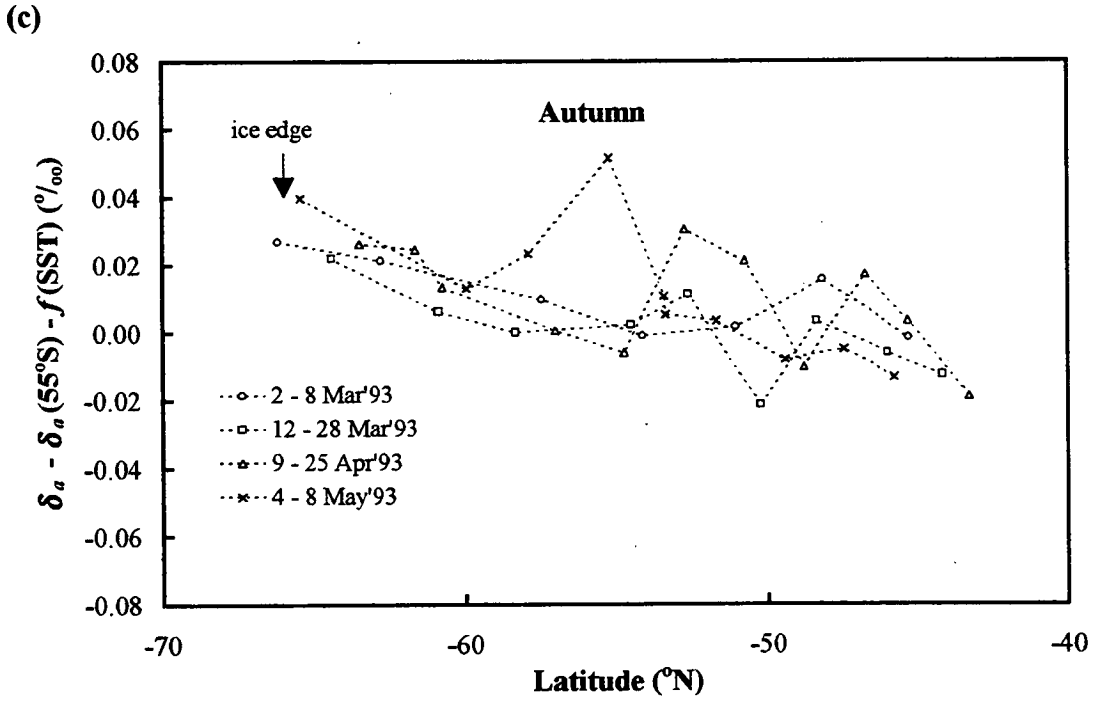


Fig. 5.13 Atmospheric $\delta^{13}\text{C}$, normalised to 55°S and detrended for the effect of sea surface temperature ($\delta_a - \delta_a(55^\circ\text{S}) - [0.0041(\text{SST} - \text{SST}(55^\circ\text{S})) - 0.002]$), during (a) Spring (17 October to 22 November 1992, 2 to 8 October 1993), (b) Summer (5 January to 26 February 1993, 19 November to 27 December 1993, 2 January to 28 February 1994), and (c) Autumn (2 to 28 March 1993, 9 April to 8 May 1993). The filled symbols correspond to cruises into the ASIZ to the west of 105°E and the unfilled symbols denote cruises east of 105°E .

An estimate may be obtained for the average increase in $\delta^{13}\text{C}$ -DIC in the surface ocean over the region $60^\circ - 70^\circ\text{S}$, $60^\circ - 105^\circ\text{E}$, required to produce the anomalously high summertime values of atmospheric $\delta^{13}\text{C}$, normalised to suppress seasonal/interannual variations and changes in sea surface temperature (Figure 5.13(b)).

Define the anomaly in atmospheric $\delta^{13}\text{C}$ due to marine productivity as

$$\Delta\delta_a = \delta_a - \delta_a' \quad (5.27)$$

where

$$\begin{aligned}\delta_a' &= \text{atmospheric } \delta^{13}\text{C that would be in reservoir } a \text{ for no algal production} \\ &\text{in reservoir } m \\ &\approx \delta_a(55^\circ\text{S}) + [0.0041(\text{SST} - \text{SST}(55^\circ\text{S})) - 0.002] \text{ } \text{‰} \\ &\text{(from equation 5.14).}\end{aligned}$$

Making the approximation that during the summer months of the study period the atmosphere was in equilibrium with the ocean, then $d(\delta_a - \delta_a')/dt \approx 0$. By definition, $\delta_a(55^\circ\text{S}) = \delta_a'(55^\circ\text{S})$, so that from equation 5.20:

$$\delta_a - \delta_a' \approx (12K/D(z_G))(G - G')/C_a(55^\circ\text{S}) \quad (5.28)$$

where

$$\begin{aligned}G' &= G \text{ for low marine productivity} \\ &= \varepsilon_{am}(f_m' - f_a') + f_m'(\delta_a^{e'} - \delta_a'), \text{ with } f_m', f_a' \text{ and } \delta_a^{e'} \text{ relating to regions} \\ &\text{of low marine productivity.}\end{aligned}$$

In areas of the Southern Indian Ocean of low marine productivity, $f_m' \approx f_a' \approx f_a$.

Hence, $G' = f_a(\delta_a^{e'} - \delta_a')$, and equation 5.28 may be rewritten as

$$\delta_a - \delta_a' \approx (12K/D(z_G))[\varepsilon_{am}(f_m - f_a) + f_m(\delta_a^e - \delta_a) - f_a(\delta_a^{e'} - \delta_a')]/C_a(55^\circ\text{S}). \quad (5.29)$$

Define the anomaly in $\delta^{13}\text{C-DIC}$ in the surface ocean due to marine productivity as

$$\Delta\delta_m = \delta_m - \delta_m' \quad (5.30)$$

Then from equation 1.15 and $\delta_a^e = [(\alpha_{ma}/\alpha_{am})(1 + \delta_m/1000) - 1] \times 1000 \text{ } \text{‰}$:

$$\begin{aligned}\delta_a^e &= \delta_a^{e'} + \Delta\delta_m(0.98947 + 0.104 \times 10^{-3} \text{ SST}) \\ &\approx \delta_a^{e'} + \Delta\delta_m\end{aligned} \quad (5.31)$$

Substituting equations 5.27 and 5.31 into equation 5.29 gives

$$\Delta\delta_a \approx (12K/D(z_G))[\varepsilon_{am}(f_m - f_a) + f_m(\delta_a^{e'} + \Delta\delta_m - \delta_a' - \Delta\delta_a) - f_a(\delta_a^{e'} - \delta_a')]/C_a(55^\circ\text{S}) \quad (5.32)$$

By rearranging equation 5.32, one obtains

$$\Delta\delta_m \approx [(D(z_G)/12K)C_a(55^\circ\text{S})\Delta\delta_a - (\varepsilon_{am} + \delta_a^{e'} - \delta_a')(f_m - f_a)]/f_m + \Delta\delta_a \quad (5.33)$$

The anomaly in $\delta^{13}\text{C}$ -DIC in the surface ocean due to marine productivity during the summer months, $\Delta\delta_m$, may be determined at each air sampling site within the south-western region $60^\circ - 70^\circ\text{S}$, $60^\circ - 105^\circ\text{E}$, if the mean value of $\delta^{13}\text{C}$ -DIC for no marine production, δ_m' , is known. Processing of water samples from the ASIZ will result in future estimates of baseline $\delta^{13}\text{C}$ -DIC in the surface ocean, but for now let δ_m' equal the mean value of surface $\delta^{13}\text{C}$ -DIC for the Southern Indian Ocean of $1.8 \pm 0.3 \text{ ‰}$ (Section 5.5). Equation 5.24 gives a mean value of $12K/D(z_G)$ over the Southern Ocean of 0.031 ± 0.006 . Substituting these values of δ_m' and $12K/D(z_G)$ into equation 5.33 gives a range of summertime values for $\Delta\delta_m$ over the region $60^\circ - 70^\circ\text{S}$, $60^\circ - 105^\circ\text{E}$, of $-0.48 \text{ ‰} < \Delta\delta_m < 1.77 \text{ ‰}$, with a mean of 0.72 ‰ ($n = 28$). Future analysis of surface water samples for $\delta^{13}\text{C}$ -DIC, which were collected simultaneously with air at all sampling sites, will indicate if the mean values of $\delta_m' = 1.8 \text{ ‰}$ and $\Delta\delta_m = 0.72 \text{ ‰}$ are reasonable estimates, thereby verifying the hypothesis that the high summer productivity in the south-western region affects ratios of $^{13}\text{C}/^{12}\text{C}$ in atmospheric CO_2 far more than it affects concentrations of atmospheric CO_2 .

5.7 CONCLUSIONS

Atmospheric CO₂ mixing ratios and $\delta^{13}\text{C}$ values, obtained from shipboard air samples collected during the period 17 October 1992 and 28 February 1994, between Tasmania and the Antarctic coast (60°E to 150°E), have been presented. The atmospheric measurements exhibited distinctly different characteristics north of the approximate maximum ice edge at 60°S, compared with south of this latitude.

For all months sampled (August to May), except January 1993, normalised CO₂ mixing ratios increased from north to south over the region 44° - 55°S, 85° - 160°E, suggesting net uptake of atmospheric CO₂ by this region of ocean. South of 55°S, between 60°E and 105°E, there was wide scatter in summertime values of atmospheric CO₂ mixing ratios, normalised to remove seasonality, with high values during November to early January, and below average values during January to February. The large variation in mixing ratios may be due to the wide variation in net air-sea transfer of CO₂ over this western region, as illustrated in Chapter 4.

In spite of low levels of oceanic $f\text{CO}_2$ in the ASIZ having little impact on atmospheric $\delta^{13}\text{C}$ values, the high marine productivity in the vicinity of Prydz Bay (south of 60°S, 70°E to 105°E) appears to be linked to consistently high atmospheric $^{13}\text{CO}_2/^{12}\text{CO}_2$ ratios, by way of higher levels of $^{13}\text{C}/^{12}\text{C}$ in dissolved inorganic carbon of the surface ocean. Measurements of atmospheric $\delta^{13}\text{C}$, atmospheric CO₂ mixing ratios, $\Delta f\text{CO}_2$ and sea surface temperature, together with an assumed mean value of $\delta^{13}\text{C}$ -DIC in the mixed layer of the Southern Ocean of 1.8 ‰, give a mean value for the summer anomaly in surface $\delta^{13}\text{C}$ -DIC over the region 60° - 70°S, 60° - 105°E, of 0.7 ‰, with a range of values from individual sampling sites of -0.5 ‰ to 1.8 ‰. This implies that the average summer value of $\delta^{13}\text{C}$ -DIC in the mixed layer of the Prydz Bay region was approximately 2.5 ‰ during 1992-94. The effect of the high productivity in the Prydz Bay region is therefore more clearly evident in the ratios of $^{13}\text{C}/^{12}\text{C}$ in atmospheric CO₂, than it is in the CO₂ concentrations.

Elsewhere over the study area of the Southern Ocean (south of 44°S, 105°E to 160°E), atmospheric $\delta^{13}\text{C}$ values were dominated by a linear dependence on sea surface temperature ($0.0041 \pm 0.0003 \text{ } \text{‰} \text{ } ^\circ\text{C}^{-1}$), due to equilibrium isotopic fractionation of CO_2 during gross sea-to-air exchange. For sample sites between 44°S and 60°S, where $\delta^{13}\text{C}$ -DIC in the surface ocean was likely to have been $1.8 \pm 0.3 \text{ } \text{‰}$, the meridional gradient in atmospheric $\delta^{13}\text{C}$ at 20 m a.s.l. was $-0.0036 \pm 0.0003 \text{ } \text{‰}$ per degree of latitude south. This meridional gradient is effectively an average value for the period 17 October 1992 to 28 February 1994, and is a factor of 2.1 steeper than the gradient predicted by Keeling et al. (1989) for 1980, assuming a mean $\delta^{13}\text{C}$ -DIC in the surface ocean of $1.55 \text{ } \text{‰}$. Keeling et al. (1989) used Liss and Merlivat's (1986) relationship to determine air-sea exchange coefficients over the latitude range 44°S and 60°S, which may have been partially responsible for the smaller gradient.

The ratio of the mean air-sea gas exchange coefficient to the mean effective vertical diffusion coefficient (for atmospheric CO_2) over the region 44° - 60°S, 60° - 160°E, was estimated as 0.031 ± 0.006 from atmospheric $\delta^{13}\text{C}$ data (assuming $\delta^{13}\text{C}$ -DIC in the surface ocean was $1.8 \pm 0.3 \text{ } \text{‰}$), and 0.012 ± 0.001 from atmospheric CO_2 mixing ratios. The dissimilarity between mean effective vertical diffusion coefficients for CO_2 at two different heights, determined from measurements of $^{13}\text{C}/^{12}\text{C}$ and mixing ratios of CO_2 at 20 m a.s.l., clearly demonstrates that the vertical atmospheric profiles of $^{13}\text{CO}_2$ and $^{12}\text{CO}_2$ were very different over the Southern Ocean. The implication is that the effective mixing height of an anomaly in $\delta^{13}\text{C}$ due to isotopic fractionation during gross air-sea exchange of CO_2 , will generally exceed the effective mixing height of an anomaly in atmospheric CO_2 due to net air-sea exchange. The perturbation in concentrations of atmospheric $^{13}\text{CO}_2$ at 20 m a.s.l. due to air-sea exchange is therefore generally greater than the perturbation of atmospheric CO_2 mixing ratios at the same site. It has been demonstrated that at current levels of measurement precision the impact on the atmosphere from air-sea exchange of CO_2 can be measured more easily in the ratio of $^{13}\text{CO}_2/^{12}\text{CO}_2$ than in the concentration of CO_2 .

CHAPTER SIX:

SUMMARY

The lack of in situ measurements of atmospheric and oceanic carbon dioxide over the Antarctic Seasonal Ice Zone and the complexity of the air-sea gas exchange system over the region presents challenges to gaining a more thorough understanding of the global carbon cycle. The hazardous conditions and inaccessibility of waters south of the Polar Front mean that few scientific vessels have ventured into this area. In particular, few measurements of the fugacity of CO_2 in surface waters, necessary for the calculation of air-sea transfer of carbon dioxide, have been collected within areas of pack ice.

The Antarctic Seasonal Ice Zone is potentially a large contemporary sink for atmospheric CO_2 due to the formation of bottom water along the Antarctic coast, resulting in carbon being out of contact with the atmosphere for periods as long as several centuries (Maier-Reimer and Hasselmann, 1987). The amount of CO_2 gas removed from the polar atmosphere by exchange with the surface ocean has been estimated on annual timescales by inverse modeling using sparse measurements of atmospheric CO_2 concentrations (e.g. Law et al., 1992; Conway et al., 1994). The scarcity of $\Delta f\text{CO}_2$ measurements south of 55°S has meant that these estimates of carbon uptake by the Southern Ocean could not be verified (Chapter 1).

This thesis presents estimates of the net uptake of atmospheric CO_2 , from October 1992 to March 1993, by a region ($55^\circ - 70^\circ\text{S}$, $60^\circ - 150^\circ\text{E}$) representing approximately 19% of the Antarctic Seasonal Ice Zone. About one half of this study region is influenced by coastal and ice edge algal blooms in spring and summer in the vicinity of Prydz Bay ($60^\circ - 105^\circ\text{E}$), while the eastern half of the region ($105^\circ - 150^\circ\text{E}$) includes little seasonal sea ice and a much smaller, shallow coastal zone. The calculations have taken into account the presence of sea-ice, and used $\Delta f\text{CO}_2$ data from six voyages of

the *RSV Aurora Australis* from 4 October 1991 to 28 February 1994, along with the Wanninkhof (1992) equation for the air-sea gas exchange coefficient.

The net air-sea fluxes of carbon were calculated using both surface wind speeds measured on the ship, and also six-hourly surface wind speeds from GASP analyses. Over the three month period 1 January to 31 March 1993 the average net transfer estimates from shipboard and GASP wind speeds were -15.2×10^{-3} Gt C/90 d and -14.3×10^{-3} Gt C/90 d, respectively, over an average area of open water of 6.00×10^{12} m² (Note: 1 Gt C = 10^{15} g C = $(10^{15}/12)$ mol C). The close agreement between these two fluxes does not imply that the two different methods used here to estimate gas transfer will always necessarily give similar results. From the difference between the two wind speed data sets it would have been expected that the net transfer estimate obtained using GASP wind speeds should have been 140% of the transfer calculated from shipboard wind speeds. The observed close agreement between the two transfer estimates is due to the difference in data interpolation techniques almost cancelling out the effect of using different wind speed data sets.

Over the six month period of 1 October 1992 to 31 March 1993 the ocean south of 55°S, between 60°E and 150°E (average area 5.29×10^{12} m²), sequestered $-25 \pm 13 \times 10^{-3}$ Gt C/182 d (calculated using surface wind speeds from GASP analyses). It is estimated that any reduction in gas transfer velocity, caused by the dampening effect of sea-ice on ocean turbulence, would have made very little difference to the total transfer value. The small effect of reduced wind fetch on total flux over the study region is due to the relatively small area of pack ice during the summer months and relatively low wind speeds close to the coast compared with the area of ocean and wind speeds north of the summer ice edge.

Over the study region, the ocean sink was most pronounced west of 105°E ($-26 \pm 13 \times 10^{-3}$ Gt C/182 d over an area 2.55×10^{12} m²), where it was associated with intense summer phytoplankton blooms (chlorophyll *a* concentrations as high as 17 mg m⁻³). South of 55°S, in January and February, there was a definite contrast between hourly averaged $\Delta f\text{CO}_2$ values measured west of 105°E

$(-201 \mu\text{atm} < \Delta f\text{CO}_2 < 23 \mu\text{atm}, \text{mean} = -43 \mu\text{atm})$ compared with east of 105°E $(-75 \mu\text{atm} < \Delta f\text{CO}_2 < 32 \mu\text{atm}, \text{mean} = 2 \mu\text{atm})$.

There were distinct differences between net air-sea transfer over the northern region $55^\circ - 60^\circ\text{S}$, $60^\circ - 150^\circ\text{E}$, and the southern region $60^\circ - 70^\circ\text{S}$, $60^\circ - 150^\circ\text{E}$. Over the region $55^\circ - 60^\circ\text{S}$ ($2.96 \times 10^{12} \text{ m}^2$ of open water), the ocean sequestered $-19 \pm 9 \times 10^3 \text{ Gt C}$ during 1 October 1992 to 31 March 1993, and only $-6.4 \pm 3.7 \times 10^3 \text{ Gt C}$ south of 60°S ($2.33 \times 10^{12} \text{ m}^2$ of open water). During December 1992 to February 1993, the ocean south of 60°S was a relatively small net sink for atmospheric CO_2 compared with the region 55°S to 60°S , mainly due to higher surface wind speeds over the northern region and to oceanic $f\text{CO}_2$ generally exceeding atmospheric fugacities over the south-western region ($60^\circ - 70^\circ\text{S}$, $105^\circ - 150^\circ\text{E}$).

The estimates for average net air-sea flux per unit area, calculated in this study using GASP wind speeds, agree relatively closely with flux estimates made by Takahashi (1989) and Tans et al. (1990), using climatological wind speeds, and Metzl et al. (1995), using shipboard wind speeds. There is less agreement with flux estimates made by Robertson and Watson (1995) using shipboard wind speeds, possibly due to their use of a relatively small wind speed data set, which could have had a preponderance of high wind speeds and a non-Rayleigh distribution. The frequency distribution of any set of wind speeds should be determined before applying equations for air-sea gas exchange coefficients which assume a Rayleigh distribution. Care should also be taken when interpolating or extrapolating from oceanic $f\text{CO}_2$ data over the Antarctic Seasonal Ice Zone due to the high spatial and temporal variability throughout this region. More oceanic $f\text{CO}_2$ data is required south of 55°S , particularly during April to September (Table 1.1) when high wind speeds over areas of open water may cause strong net fluxes of CO_2 , and any small error in overall average $f\text{CO}_2$ will cause a large error in estimated flux.

Additional information on air-sea exchange of CO_2 south of 44°S is obtained from air samples collected on six *RSV Aurora Australis* cruises in the Southern Ocean between 17 October 1992 and 28 February 1994. Mixing ratios of atmospheric CO_2 in these air

samples, when normalised to suppress seasonal and interannual variations, exhibited changes with latitude which were linked to net air-sea exchange of carbon. In contrast, meridional variations in normalised $\delta^{13}\text{C}$ values from the same air samples were dominated by the isotopic fractionation associated with gross air-sea exchange of carbon. The difference in the effect of net air-sea carbon flux on atmospheric CO_2 mixing ratios compared with the effect of gross flux on the $^{13}\text{C}/^{12}\text{C}$ ratio in atmospheric CO_2 is demonstrated by a study of two different regions of the Southern Ocean: $44^\circ - 60^\circ\text{S}$, $85^\circ - 160^\circ\text{E}$, and $60^\circ - 70^\circ\text{S}$, $60^\circ - 150^\circ\text{E}$. Atmospheric CO_2 concentrations and $^{13}\text{CO}_2/^{12}\text{CO}_2$ ratios exhibited distinctly different characteristics north of the approximate maximum ice edge along the transects studied, compared with south of this latitude (60°S).

For all months sampled (August to May), except January 1993, normalised CO_2 mixing ratios increased from north to south over the region $44^\circ - 55^\circ\text{S}$, $85^\circ - 160^\circ\text{E}$, suggesting net uptake of atmospheric CO_2 by the mid-latitude region to the south of Tasmania. South of 55°S , between 60°E and 105°E , there was wide scatter in summertime values of atmospheric CO_2 mixing ratios, normalised to suppress seasonality, with relatively high values during November to early January, linked to relatively small net ocean uptake of carbon during this time (Table 4.1(b)), and below average values during January to February, linked to much stronger oceanic uptake of CO_2 .

Over the ice-free region of the Southern Ocean between 44°S and 60°S , from 85°E to 160°E , atmospheric $\delta^{13}\text{C}$ values were dominated by a linear dependence on sea surface temperature ($0.0041 \pm 0.0003 \text{ ‰ } ^\circ\text{C}^{-1}$ - Chapter 5), due to “equilibrium” fractionation of CO_2 during gross air-sea exchange (Chapter 1). The temperature effect was reflected in the observed meridional gradient in atmospheric $\delta^{13}\text{C}$ of $-0.0036 \pm 0.0003 \text{ ‰}$ per degree of latitude south. This linear relationship between atmospheric $\delta^{13}\text{C}$ and sea surface temperature will be of use in inverse modeling of the net carbon sink over the Southern Ocean, where measurements of atmospheric $\delta^{13}\text{C}$ from stations are very scarce (Chapter 1).

The relatively strong net ocean uptake of atmospheric CO_2 over the region $60^\circ - 70^\circ\text{S}$, $60^\circ - 105^\circ\text{E}$, during summer (Table 4.1(b)) is estimated to have had little impact on atmospheric $\delta^{13}\text{C}$ values. However, the intense marine productivity in this south-western region appears to have caused anomalously high atmospheric $^{13}\text{CO}_2/^{12}\text{CO}_2$ ratios, by way of gross sea-to-air exchange transmitting the effect of high values of $^{13}\text{C}/^{12}\text{C}$ in dissolved inorganic carbon of the surface ocean to the atmosphere.

Measurements of atmospheric $\delta^{13}\text{C}$, atmospheric CO_2 mixing ratios, $f\text{CO}_2$ in the surface ocean and sea surface temperature, together with an assumed mean value of $\delta^{13}\text{C}$ -DIC in the mixed layer of the Southern Ocean of 1.8‰ , gave a mean value for the summer anomaly in surface $\delta^{13}\text{C}$ -DIC over the region $60^\circ - 70^\circ\text{S}$, $60^\circ - 105^\circ\text{E}$, of 0.7‰ , with a range of values from individual sampling sites of -0.5‰ to 1.8‰ .

This implies that the average summer value of $\delta^{13}\text{C}$ -DIC in the mixed layer of the south-western region was approximately 2.5‰ during 1992-94. Future analysis of $\delta^{13}\text{C}$ -DIC in the surface water samples which were collected simultaneously with air at all sampling sites will indicate if the mean summer value of $\delta^{13}\text{C}$ -DIC was 1.8‰ over the relatively unproductive region of $60^\circ - 70^\circ\text{S}$,

$105^\circ - 150^\circ\text{E}$, and 2.5‰ over the highly productive region west of 105°E . The actual measurements of $\delta^{13}\text{C}$ -DIC will verify the hypothesis that at current measurement precision levels the high summer productivity in the Prydz Bay region is clearly reflected in ratios of $^{13}\text{C}/^{12}\text{C}$ in atmospheric CO_2 .

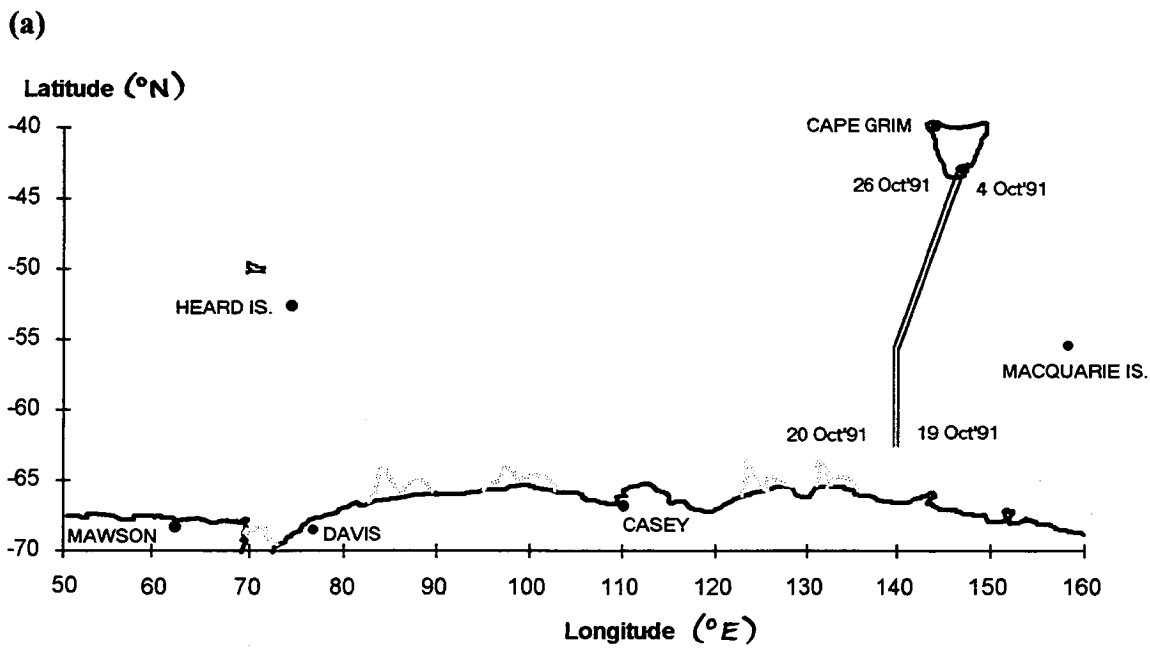
The effect of air-sea gas exchange on the concentration and $\delta^{13}\text{C}$ of atmospheric CO_2 at 20 m a.s.l. is modeled using a simple atmospheric box model and “effective vertical diffusion coefficients” for CO_2 at two different heights, z_N and z_G , reflecting the different vertical atmospheric profiles of CO_2 and $^{13}\text{CO}_2$, respectively. The ratio of the mean air-sea gas exchange coefficient to the mean effective vertical diffusion coefficient over the region $44^\circ - 60^\circ\text{S}$, $60^\circ - 160^\circ\text{E}$, is estimated as 0.031 ± 0.006 from atmospheric $\delta^{13}\text{C}$ data (assuming $\delta^{13}\text{C}$ -DIC in the surface ocean was $1.8 \pm 0.3\text{‰}$), and 0.012 ± 0.001 from atmospheric CO_2 mixing ratios. The ratio of the effective vertical diffusion coefficient for atmospheric CO_2 at height z_N to that at height z_G is thereby estimated as 2.6 ± 0.5 , which implies that the effective mixing height of an anomaly in $\delta^{13}\text{C}$ due to isotopic fractionation during gross air-sea exchange of CO_2

(z_G), will generally exceed the effective mixing height of an anomaly in atmospheric CO_2 due to net air-sea exchange (z_N). Physically, this means that the magnitude of the perturbation in the atmospheric concentration of $^{13}\text{CO}_2$ at 20 m a.s.l. due to air-sea exchange is generally much greater than the magnitude of the anomaly in atmospheric concentration of CO_2 .

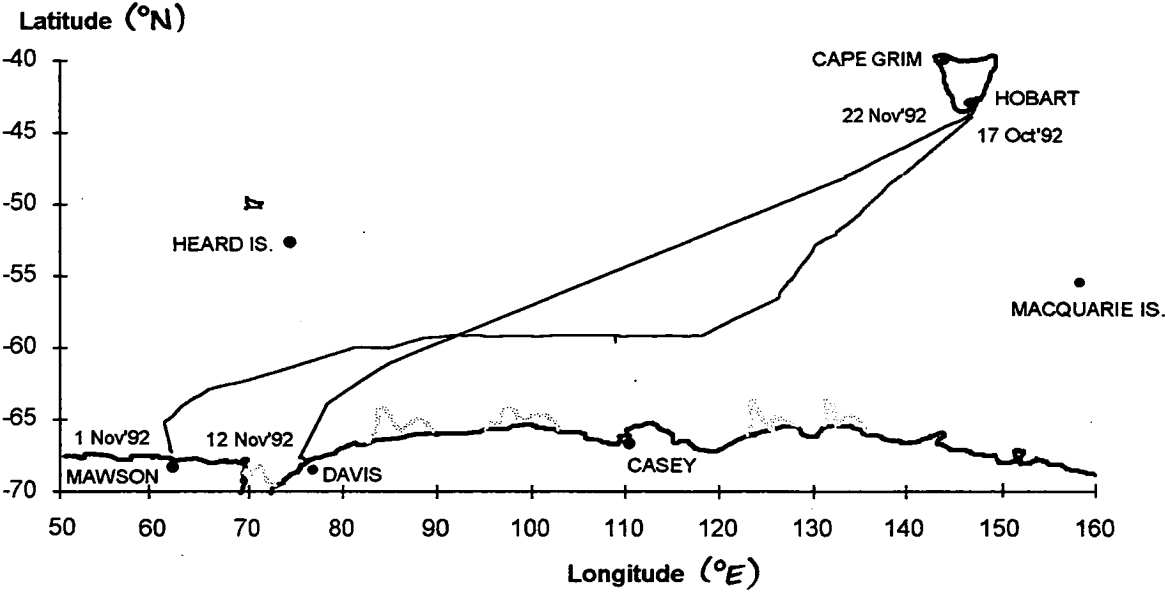
Analysis of 360 air samples collected over the Southern Ocean has clearly demonstrated that the impact of fractionation during gross air-sea exchange of CO_2 on atmospheric ratios of $^{13}\text{CO}_2/^{12}\text{CO}_2$ can be measured more easily than the impact of net CO_2 flux on atmospheric mixing ratios of CO_2 . Long-term changes in sea surface temperature and productivity over the ASIZ, and therefore net ocean uptake, can be more accurately determined from ratios of $^{13}\text{CO}_2/^{12}\text{CO}_2$ in baseline air samples from a coastal Antarctic station (such as Mawson or Davis), than from mixing ratios of CO_2 in the same samples.

APPENDIX A
SOUTHERN OCEAN CRUISES

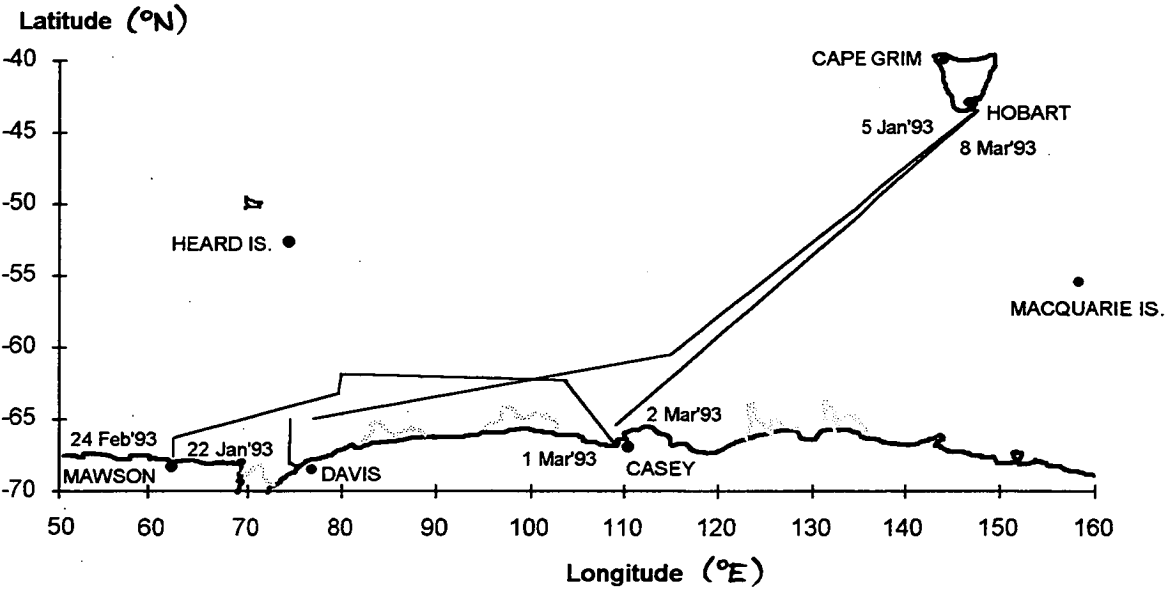
Figure A.1 present the Southern Ocean transects of the *RSV Aurora Australis* from 4 October, 1991, to 28 February, 1994. Atmospheric and oceanic CO₂ data from these transects have been used in chapters 3, 4 and 5. A summary of the start/end dates for each transect and data collection details are given in Table A.1.



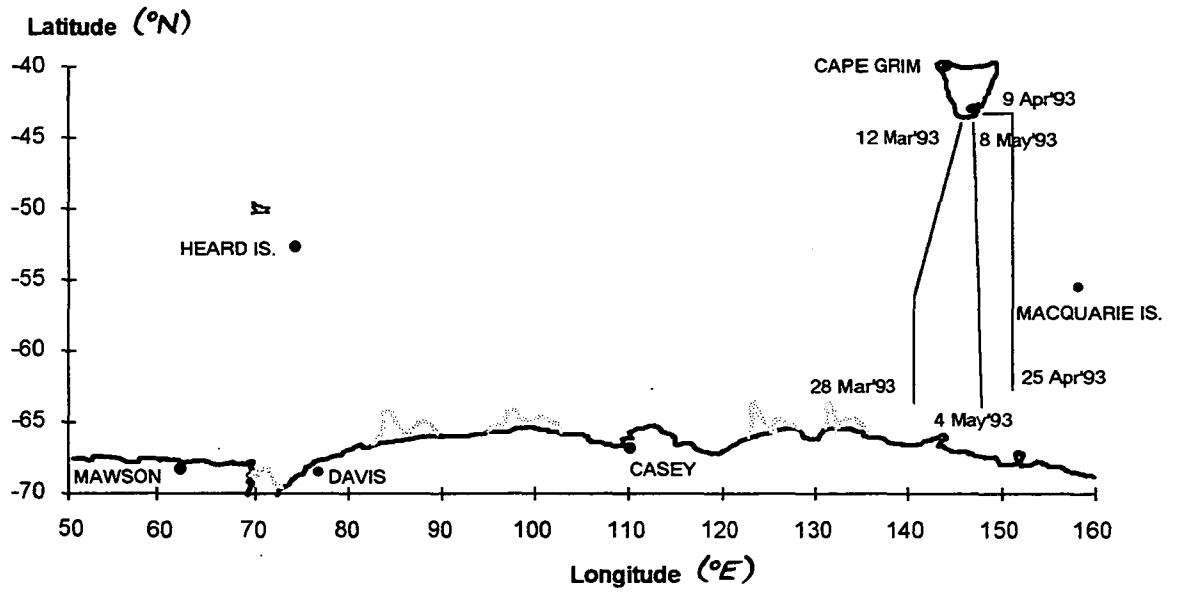
(b)



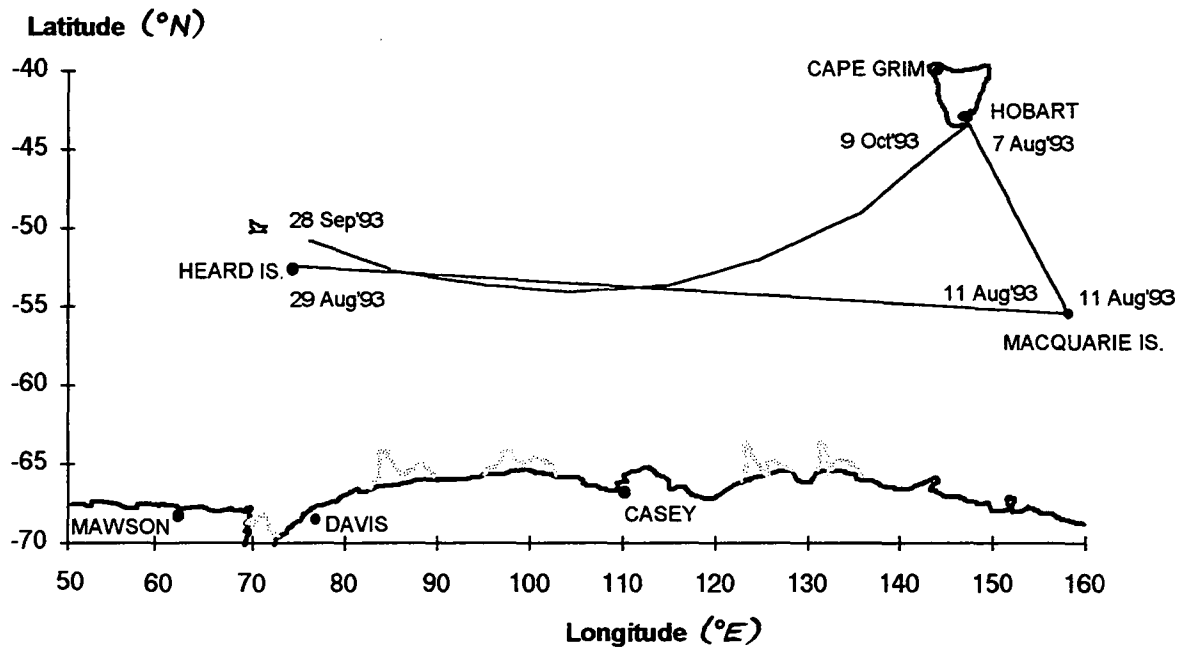
(c)



(f)



(g)



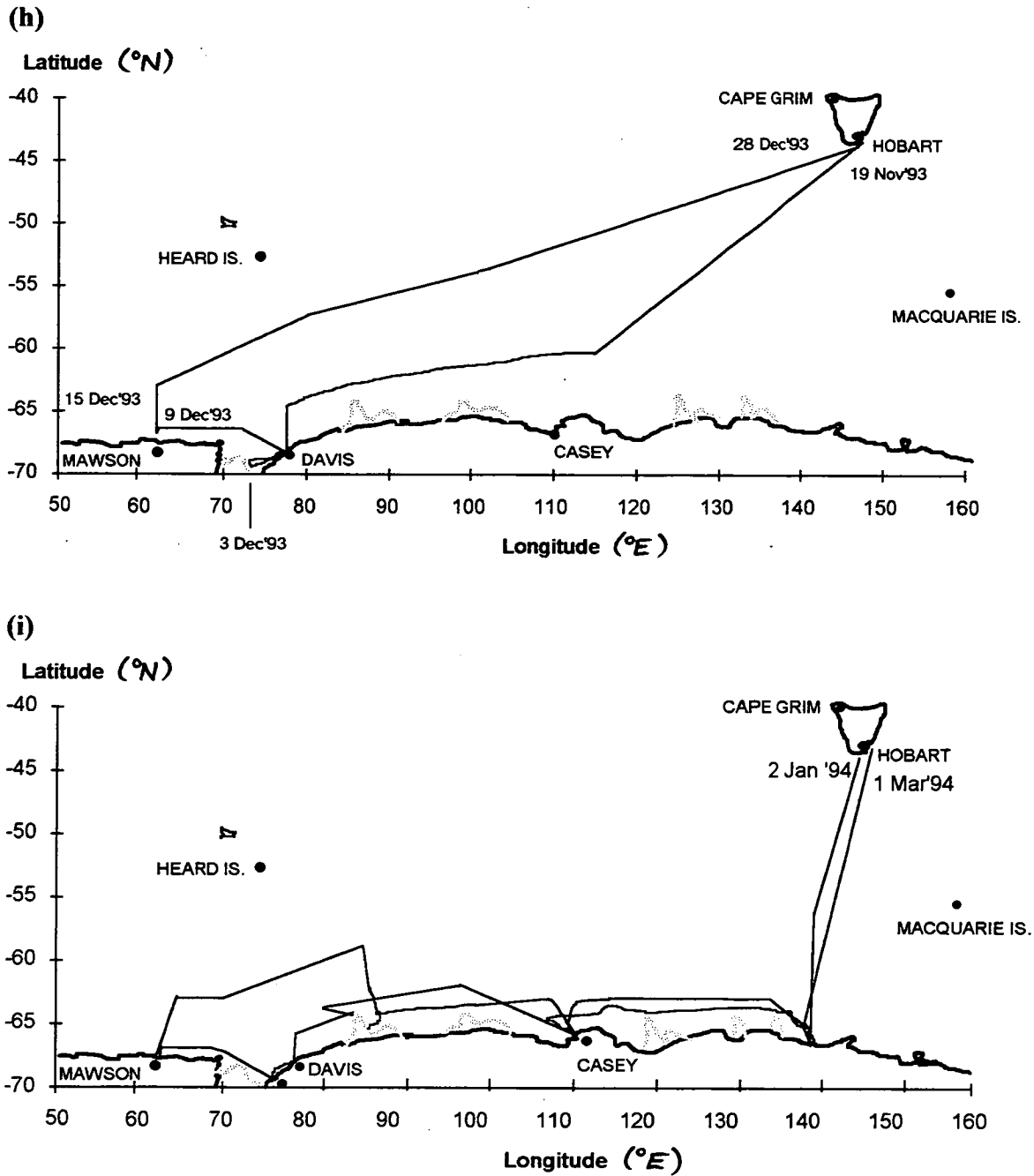


Fig. A.1 Southern Ocean transects on *RSV Aurora Australis* where oceanic fugacity of CO_2 , f_m , was recorded continuously during the periods (a) 4 to 26 October, 1991; (b) 19 October to 1 November, 1992; and 12 to 22 November, 1992; (c) 5 to 22 January, 1993; 24 February to 8 March, 1993; (d) 15 January to 7 February, 1993; (e) 7 to 25 February, 1993; (f) 12 to 28 March, 1993; 9 to 25 April, 1993; and 4 to 8 May, 1993; (g) 7 August to 8 October, 1993; (h) 19 November to 28 December, 1993; and (i) 2 January to 1 March, 1994. Air samples were collected between one and three degrees of latitude along the cruise tracks, except in Figures (d) and (e) where air was sampled at the sites marked with the larger circles.

Voyage ID	Transect dates	Transect lat/long	No. of sampling sites	No. air flasks filled at each site
V1_92	17 Oct'92 - 1 Nov'92	44.3°S, 145.9°E - 66.1°S, 61.5°E	11	2
V1_92	12 Nov'92 - 22 Nov'92	68.5°S - 77.9°E - 45.5°S, 141.2°E	12	2
V7_93	5 Jan'93 - 22 Jan'93	44.5°S, 145.8°E - 68.5°S, 75°E	12	2
V7_93	29 Jan'93 - 26 Feb'93	66°S, 70.5°E - 63°S, 80°E	4	2
V7_93	2 Mar'93 - 8 Mar'93	66.2°S, 109.8°E - 45.2°S, 145°E	8	2
V9_93	12 Mar'93 - 28 Mar'93	44.1°S, 146.2°E - 64.4°S, 140°E	10	2
V9_93	9 Apr'93 - 25 Apr'93	43.3°S, 155°E - 63.4°S, 150.7°E	11	2
V9_93	4 May'93 - 8 May'93	65.4°S, 143.6°E - 44°S, 147.5°E	10	2
V1_93	7 Aug'93 - 11 Aug'93	43.8°S, 148°E - 54.25°S, 158.7°E	8	2
V1_93	13 Aug'93 - 31 Aug'93	54.15°S, 147°E - 52.6°S, 75.15°E	7	2
V1_93	2 Sep'93 - 26 Sep'93	around Heard Is.	10	2
V1_93	2 Oct'93 - 8 Oct'93	53.6°S, 106.4°E - 44.1°S, 146.3°E	8	2
V4_93	19 Nov'93 - 4 Dec'93	44.8°S, 145°E - 69.2°S, 75.6°E	18	2
V4_93	8 Dec'93 - 27 Dec'93	68.4°S, 77.1°E - 44.2°S, 144.2°E	18	2
V7_94	2 Jan'94 - 7 Feb'94	44°S, 146.3°E - 69.4°S, 76.4°E	28	2
V7_94	21 Feb'94 - 28 Feb'94	66.7°S, 140°E - 47°S, 146.4°E	11	1

Table A.1 Summary of air samples from the *RSV Aurora Australis* used in this thesis.

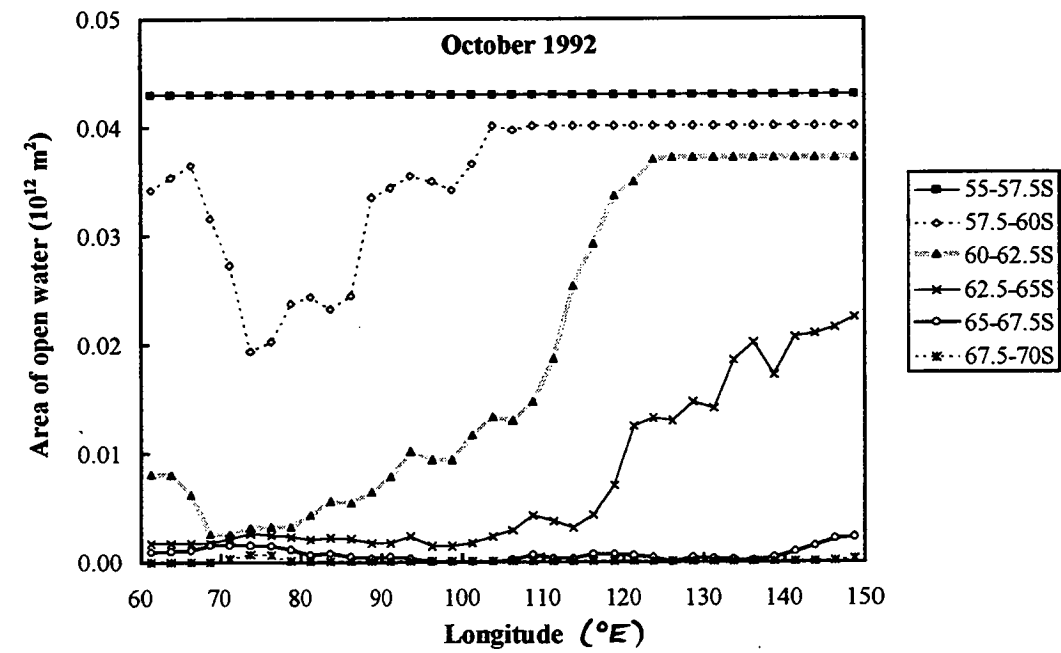
APPENDIX B

SOUTHERN OCEAN DATA

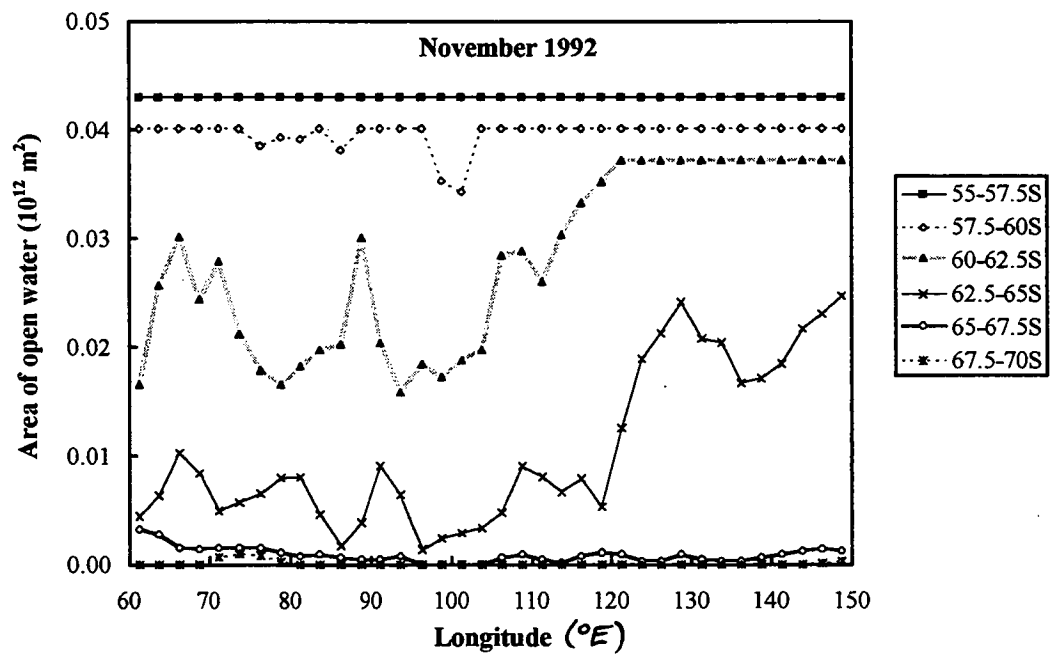
B.1 SOUTHERN OCEAN SEA-ICE DATA

The area of open water in each $2.5^{\circ} \times 2.5^{\circ}$ grid square over the region south of 55°S , between 60°E to 150°E , was estimated from U.S. Navy/NOAA Joint Ice Center weekly sea-ice maps. The weekly values were averaged to give an average monthly area of open water over the study region (Figure B.1).

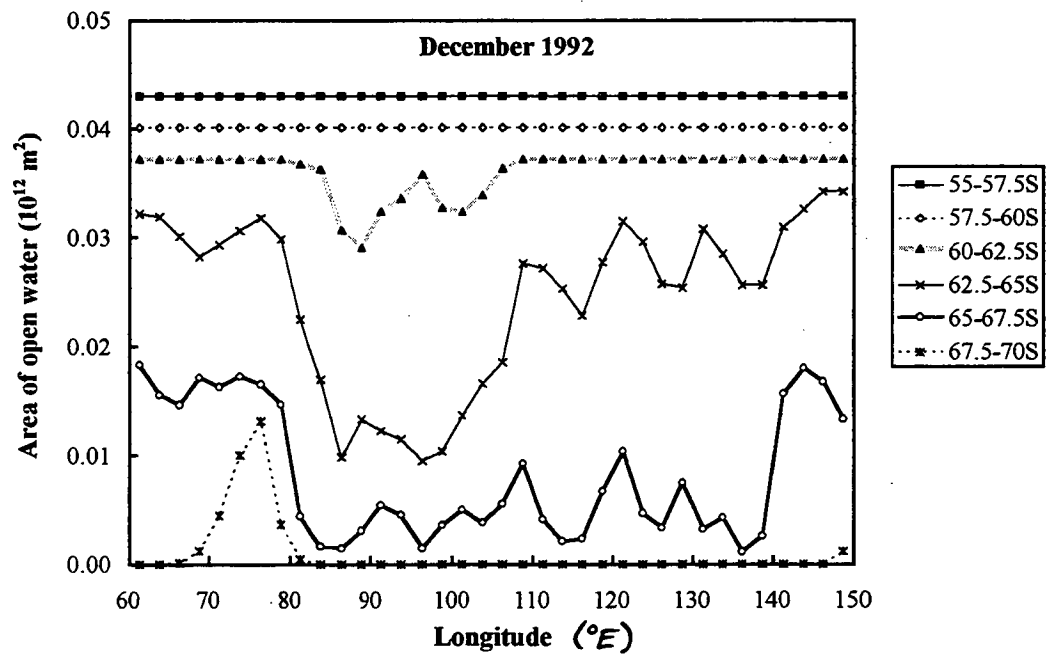
(a)



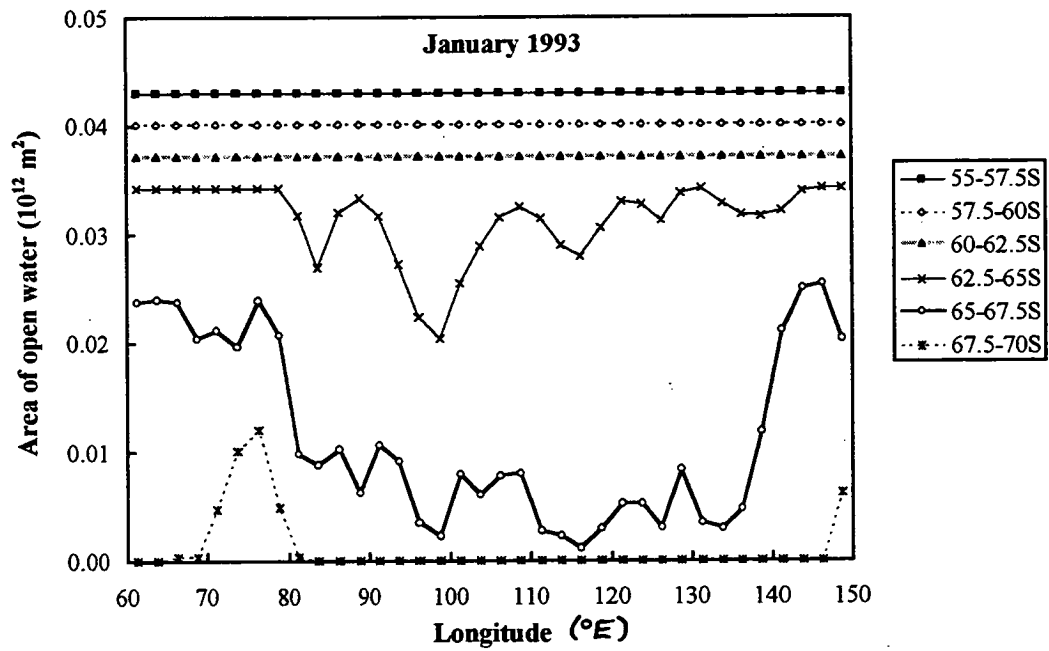
(b)



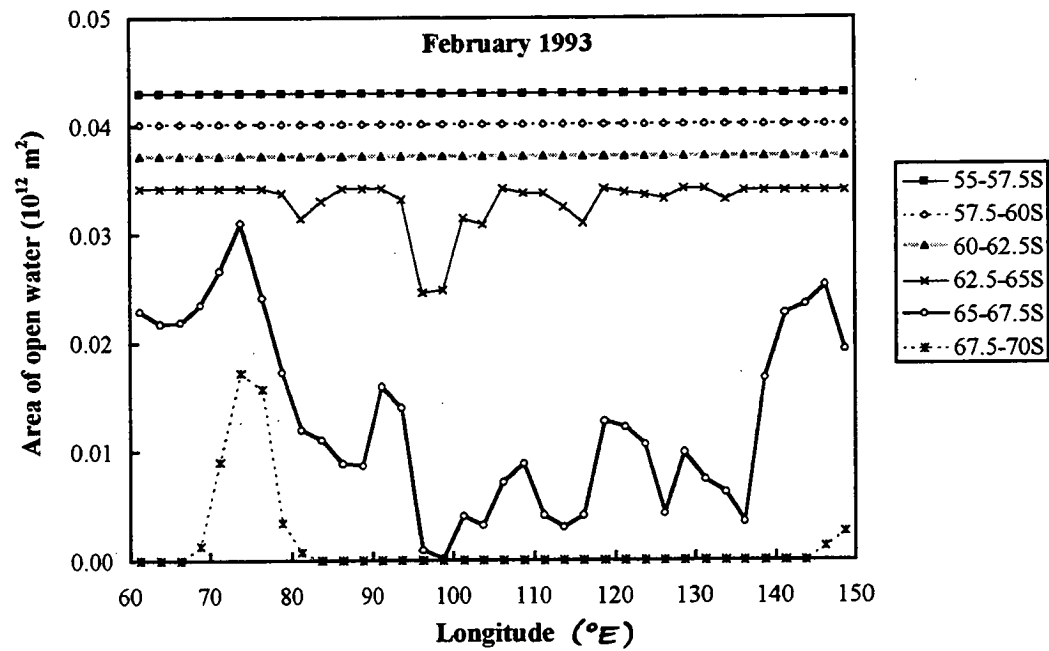
(c)



(d)



(e)



(f)

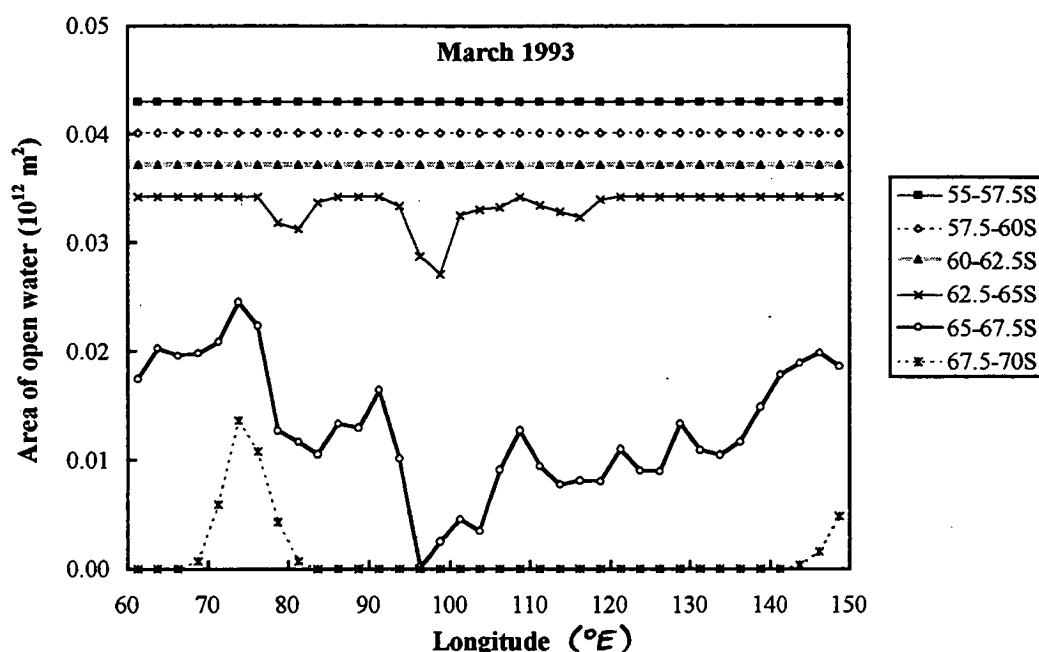
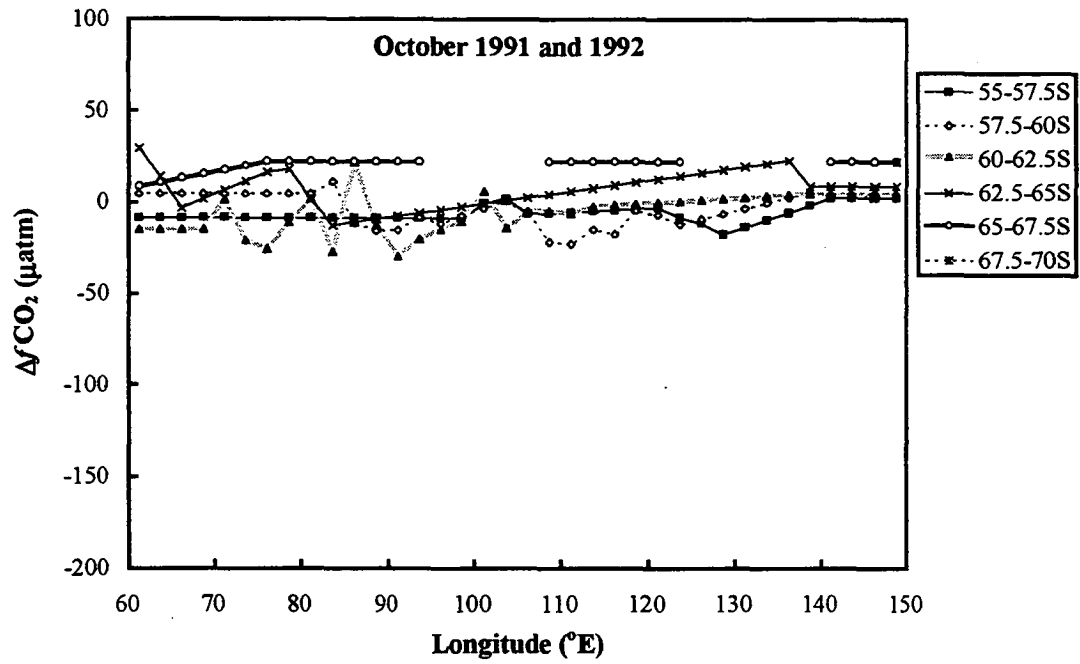


Fig. B.1 Average area of open water in each $2.5^{\circ} \times 2.5^{\circ}$ grid square, over the region south of 55°S , between 60°E and 150°E , for (a) October, 1992; (b) November, 1992; (c) December, 1992; (d) January, 1993; (e) February, 1993; and (f) March, 1993. These values were obtained from U.S. Navy/NOAA Joint Ice Center weekly sea-ice maps.

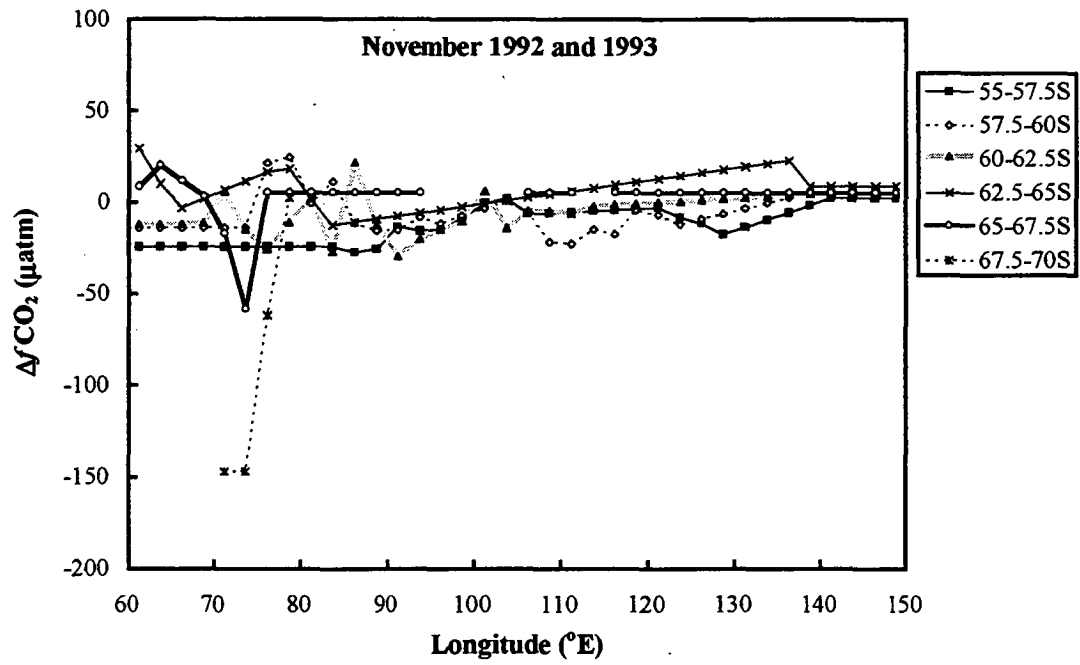
B.2 $\Delta f\text{CO}_2$ DATA OVER THE ASIZ

Oceanic and atmospheric $f\text{CO}_2$ values were obtained from six cruises of the *RSV Aurora Australis* between Hobart and Antarctica (Sections 2.2-2.6 and 3.2). The monthly averaged $\Delta f\text{CO}_2$ (= oceanic $f\text{CO}_2$ - atmospheric $f\text{CO}_2$) values for each $2.5^{\circ} \times 2.5^{\circ}$ grid square of the 55° - 70°S , 60° - 150°E , study region are presented in Figure B.2. Grid points without data were filled in by using average $\Delta f\text{CO}_2$ values from adjacent months. If data were not available from adjacent months the $\Delta f\text{CO}_2$ was linearly interpolated from known values at the same latitude (Section 4.3). The high spatial variability in $\Delta f\text{CO}_2$ meant that it was more accurate to use a mean value for the same grid point from an adjacent month than to interpolate between measurements made hundreds of kilometers from the grid point.

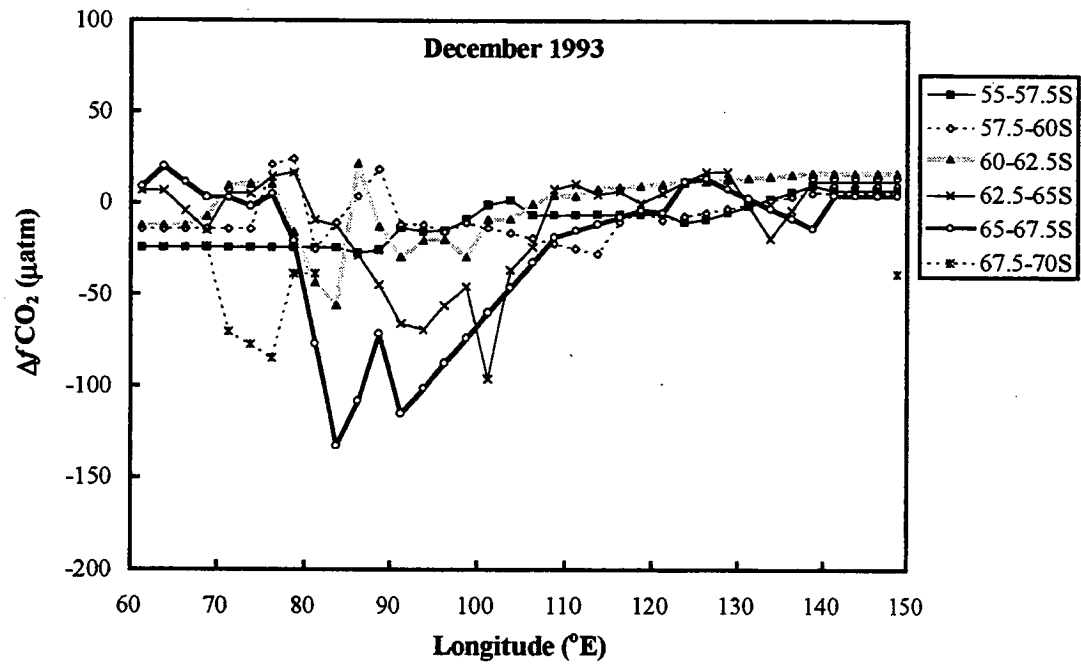
(a)



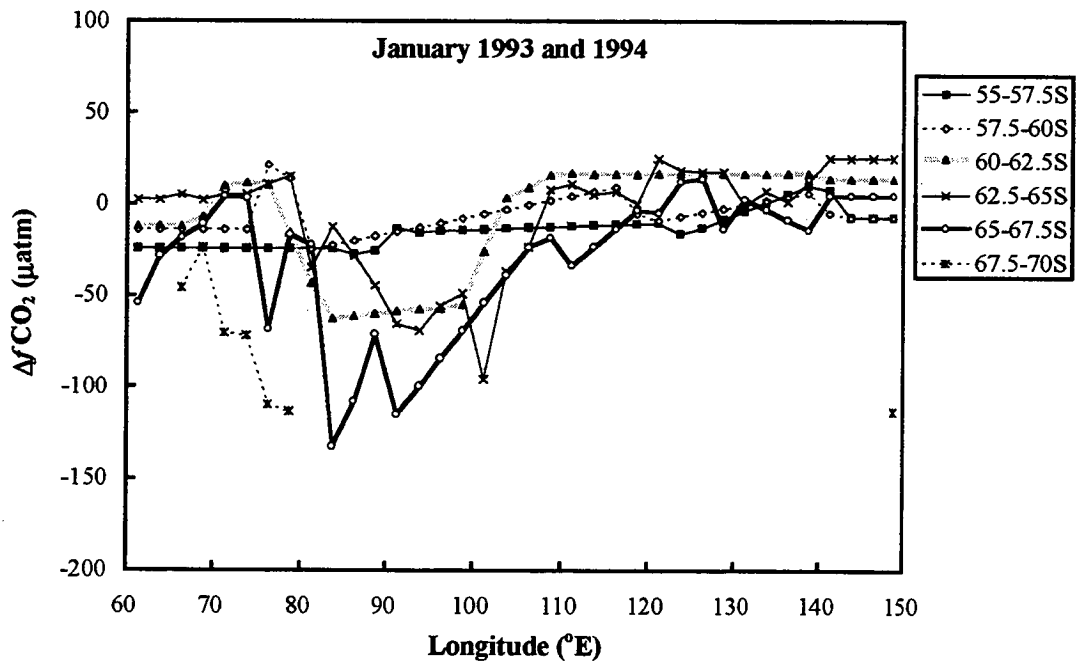
(b)



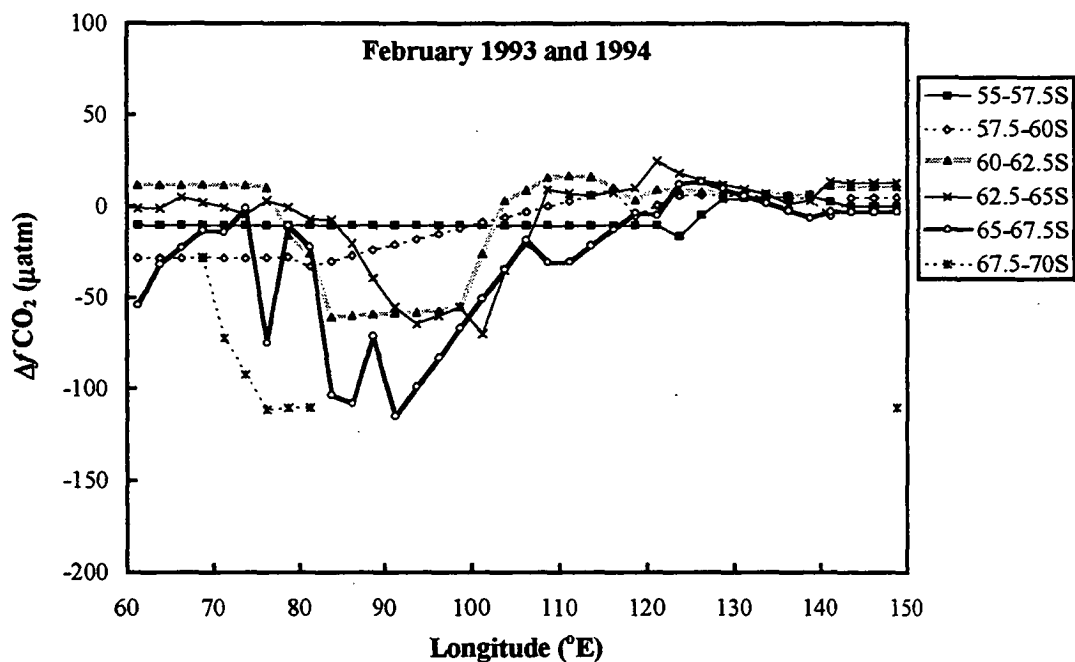
(c)



(d)



(e)



(f)

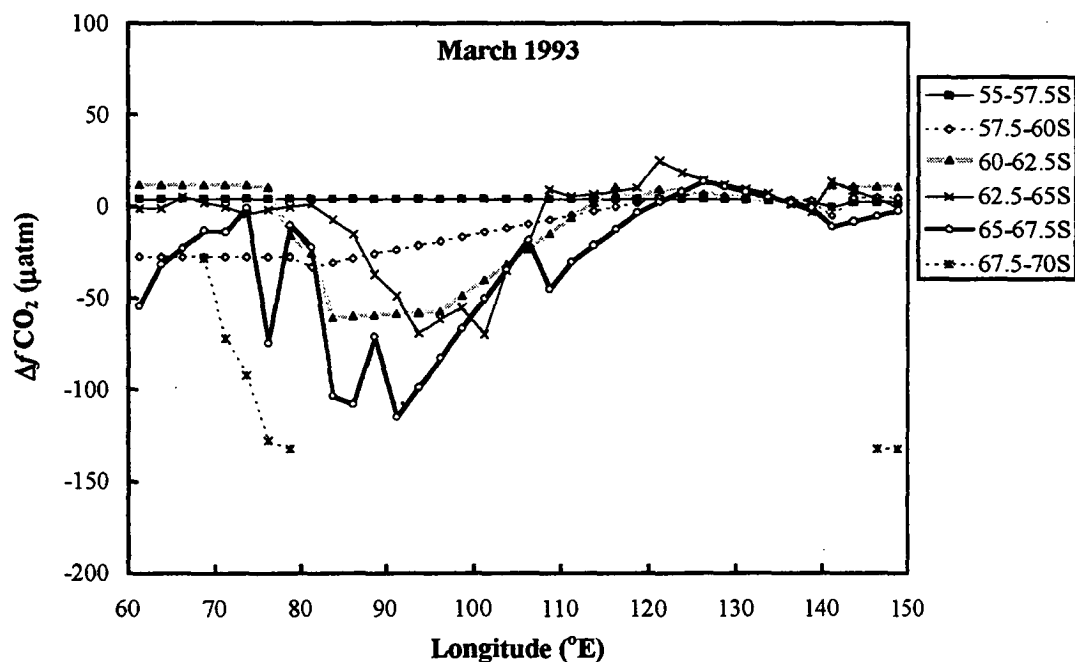
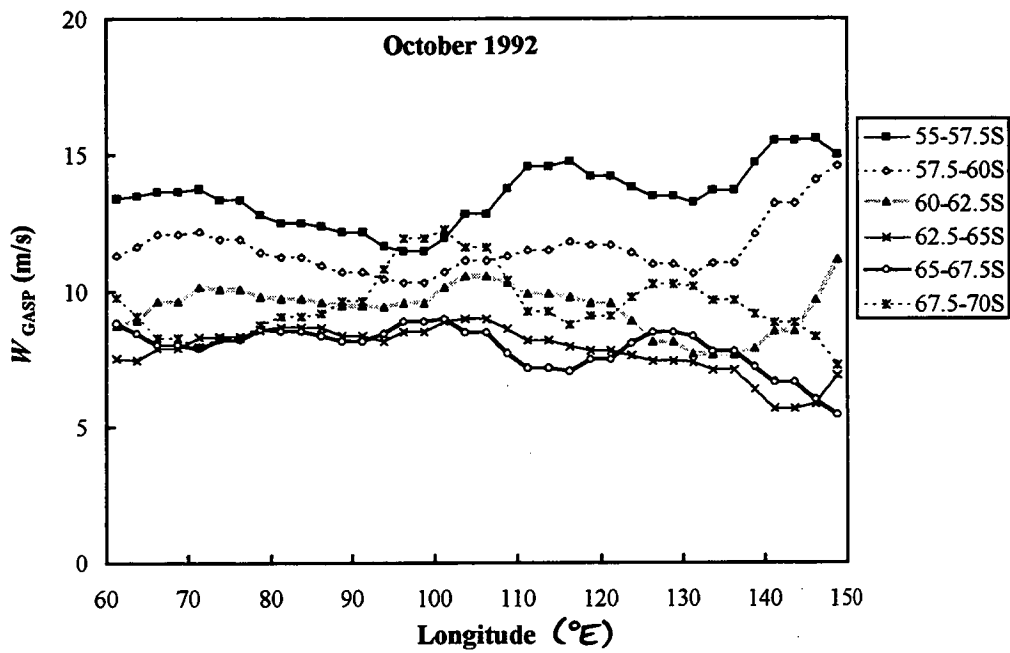


Fig. B.2 Mean $\Delta f\text{CO}_2$ for each $2.5^{\circ} \times 2.5^{\circ}$ grid square south of 55°S , between 60°E and 150°E , for (a) October, 1991 and 1992; (b) November, 1992 and 1993; (c) December, 1993; (d) January, 1993 and 1994; (e) February, 1993 and 1994; and (f) March, 1993.

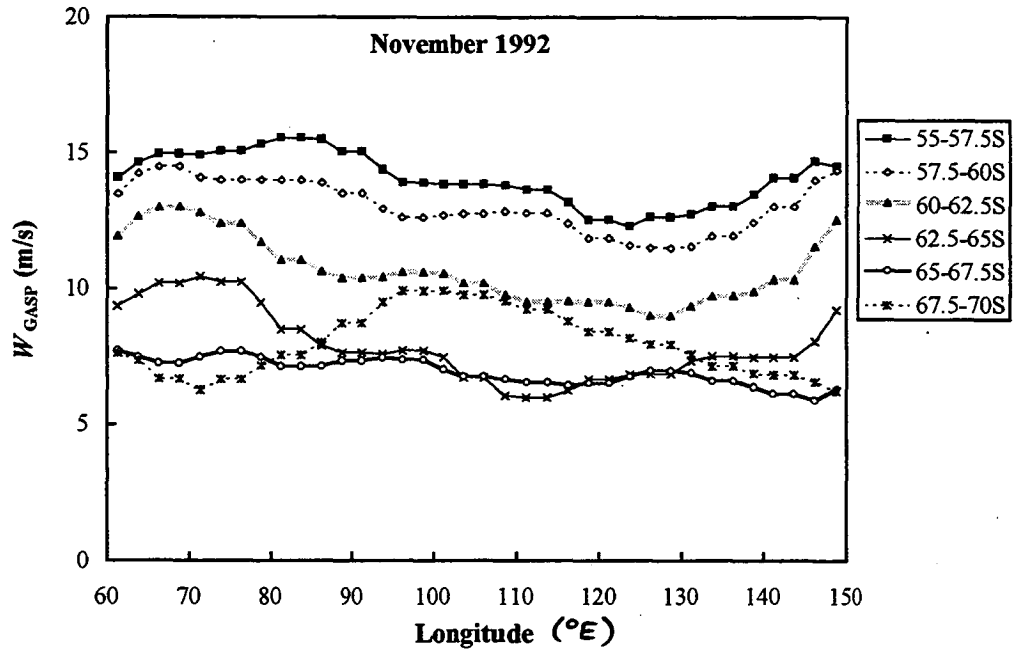
B.3 GASP WIND SPEEDS OVER THE ASIZ

Figure B.3 presents monthly mean surface wind speeds over the study region 55°-70°S, 60°-150°E, derived from 6-hourly GASP analyses (Section 4.3). The GASP model uses spot measurements from satellites, ships and stations in the few hours preceeding each six-hourly analysis, spatially averaged over $2.24^{\circ} \times 3.75^{\circ}$ grid squares.

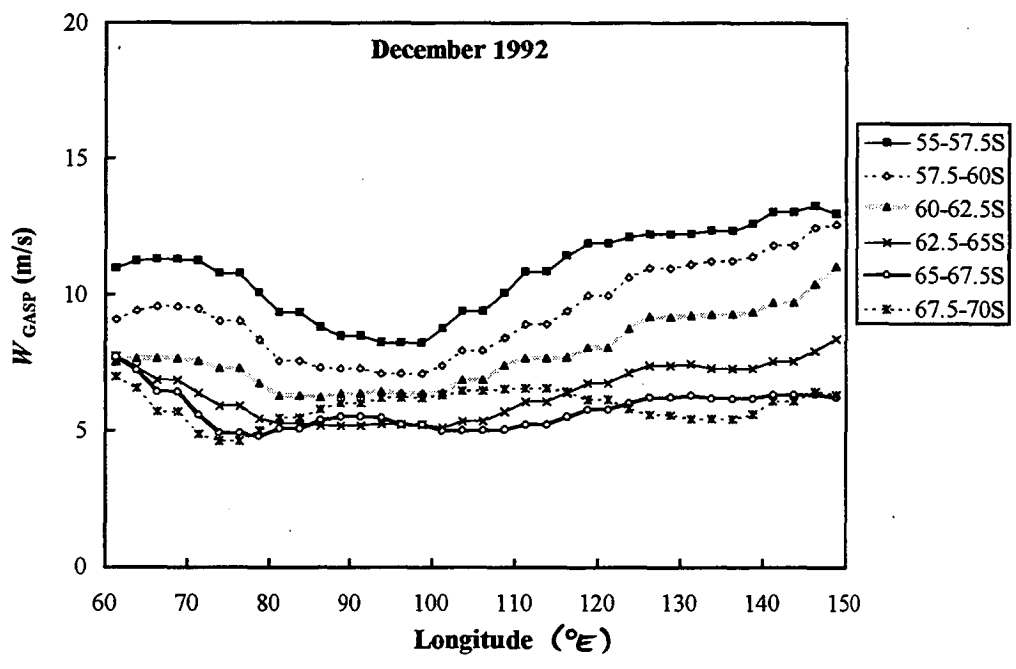
(a)



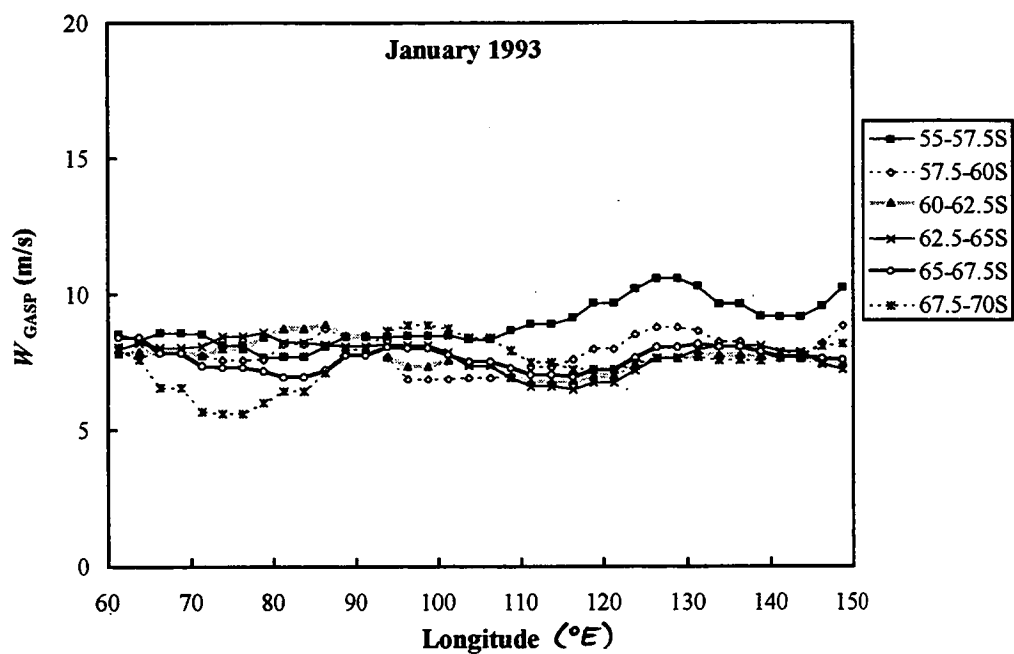
(b)



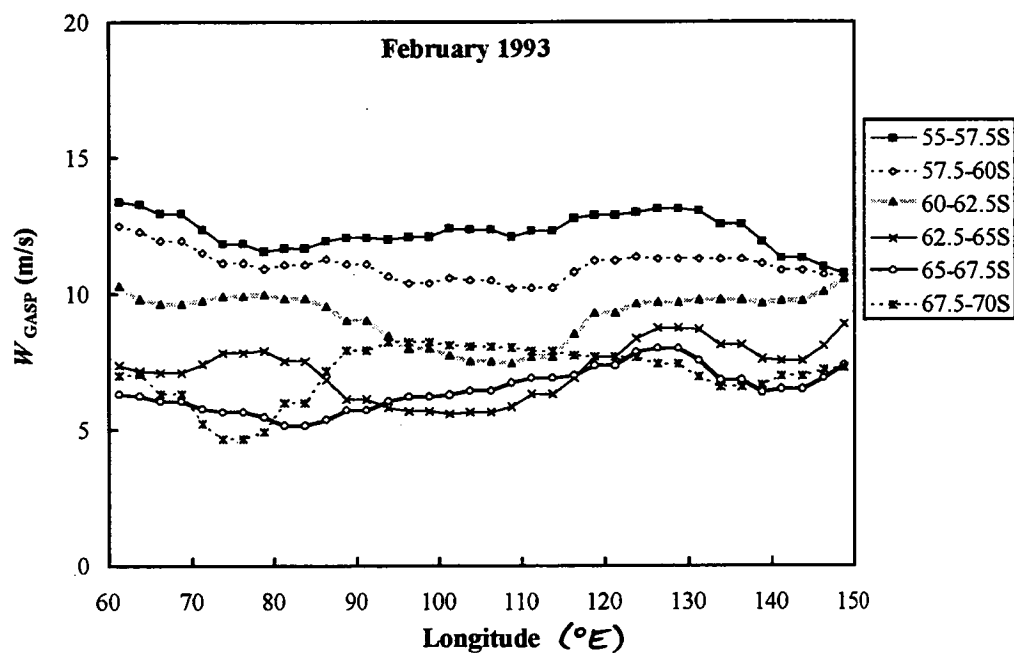
(c)



(d)



(e)



(f)

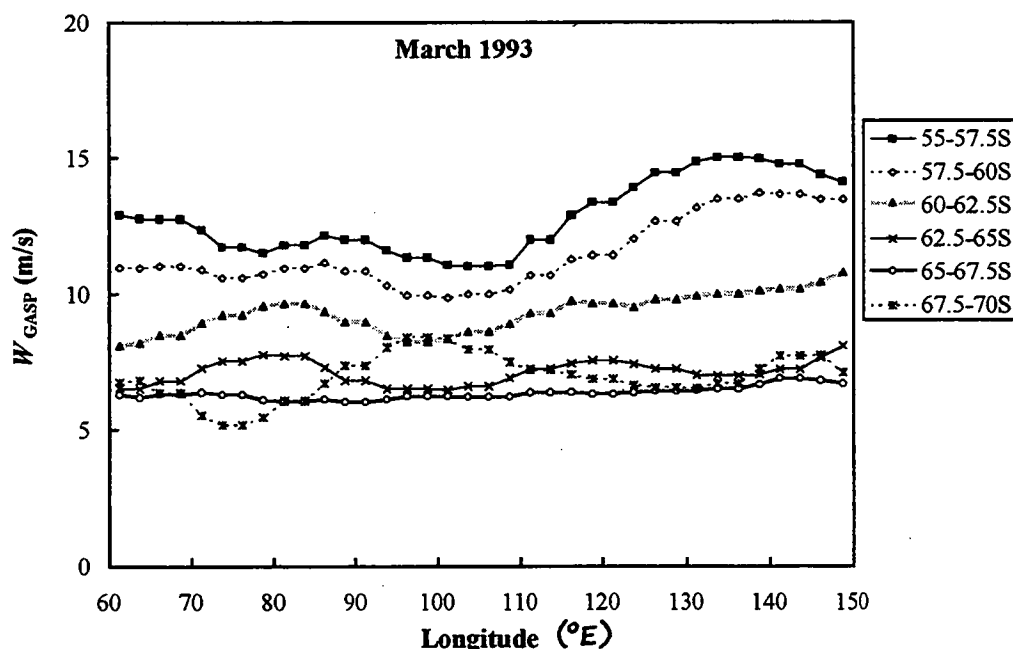


Fig. B.3 Mean GASP wind speeds for each $2.5^{\circ} \times 2.5^{\circ}$ grid square south of $55^{\circ}S$, between $60^{\circ}E$ and $150^{\circ}E$, for (a) October, 1992; (b) November, 1992; (c) December, 1992; (d) January, 1993; (e) February, 1993; and (f) March, 1993. The average monthly wind speed for each grid point was calculated using six-hourly surface wind speeds from GASP analyses.

B.4 CHLOROPHYLL *a*, SST AND fCO_2 DATA FROM A SPRING SOUTHERN OCEAN CRUISE

Surface chlorophyll *a* data was collected at regular intervals between Tasmania and the Antarctic coast on only one Southern Ocean cruise of the *RSV Aurora Australis* during the study period. From 19 November to 28 December 1993 water samples were collected every four hours, filtered on the ship for phytoplankton, and later analysed at the Australian Antarctic Division in Hobart for concentration of chlorophyll *a* in the original water sample (Section 2.8). Figure B.4 presents hourly mean values of temperature, chlorophyll *a* and fCO_2 , measured from the same seawater inlet at 7.5 m depth, during the Hobart to Prydz Bay transect from 19 November to 3 December 1993. Figure B.5 presents the same data for the Prydz Bay to Hobart transect from 4 to 28 December 1993.

On the southward transect (Figure B.4), the first significantly enhanced value of chlorophyll *a* concentration was observed at 57.6°S, but was not associated with any change in $f\text{CO}_2$ in the same seawater or any distinct change in sea surface temperature. Further south at 59°S, north of the ice edge at 60°S, the level of $f\text{CO}_2$ decreased sharply to a minimum of 301 μatm , associated with a chlorophyll *a* concentration of 1.50 mg m^{-3} . The ice edge was entered at 60°S and thereafter any increase in chlorophyll *a* concentration was immediately followed by a decrease in oceanic $f\text{CO}_2$ values in the same waters. Chlorophyll *a* concentration peaked on 3 December 1993 in open waters in Southern Prydz Bay at 17.2 mg m^{-3} (69.25°S, 74.70°E, SST = -1.18°C, $f_m = 197 \mu\text{atm}$).

On the northward transect (Figure B.5), the minimum hourly mean $f\text{CO}_2$ of 128 μatm occurred on 4 December 1993 at 69.26°S, 74.95°E, in open waters (SST = -0.60°C, Chl *a* = 14.0 mg m^{-3}), with a four-minute average $f\text{CO}_2$ recorded as low as 109 μatm . North of the ice edge (at 64.4°S), concentration of chlorophyll *a* was low until 57.7°S when it suddenly jumped to 2.56 mg m^{-3} fugacity dropped to 318 μatm with a sudden rise in sea surface temperature shortly afterwards at 57.3°S (Figure B.5(a)) of 0.96°C to 1.36°C suggesting a link with the Polar Front. The high chlorophyll *a* concentrations from this point to 51°S may have been associated with large eddies throughout the Polar Frontal Zone as suggested by the variation in SST.

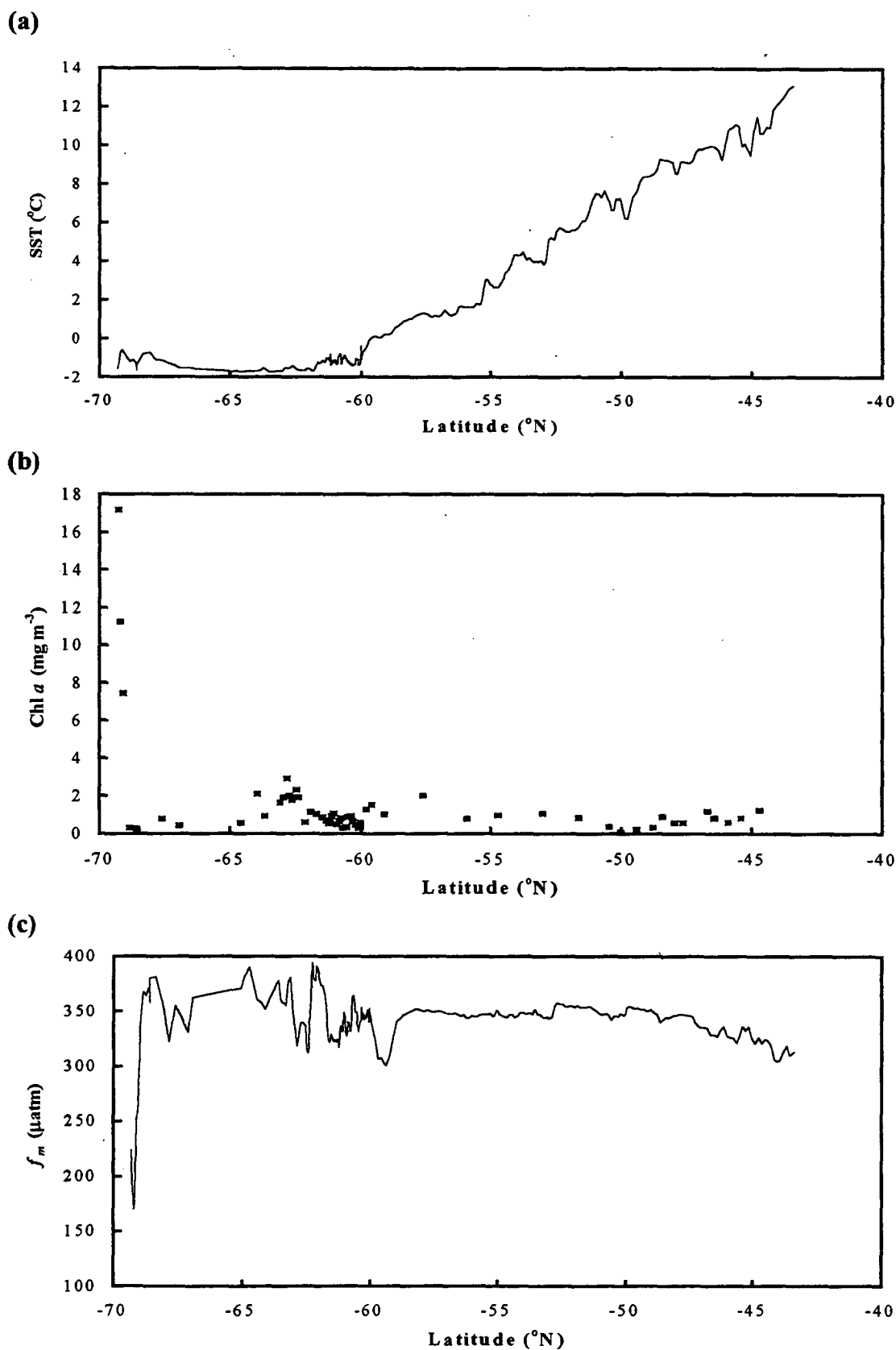


Fig. B.4 Hourly averaged surface ocean measurements of (a) sea surface temperature, (b) chlorophyll *a* concentration and (c) $f\text{CO}_2$ from the *RSV Aurora Australis* transect 19 November to 3 December 1993.

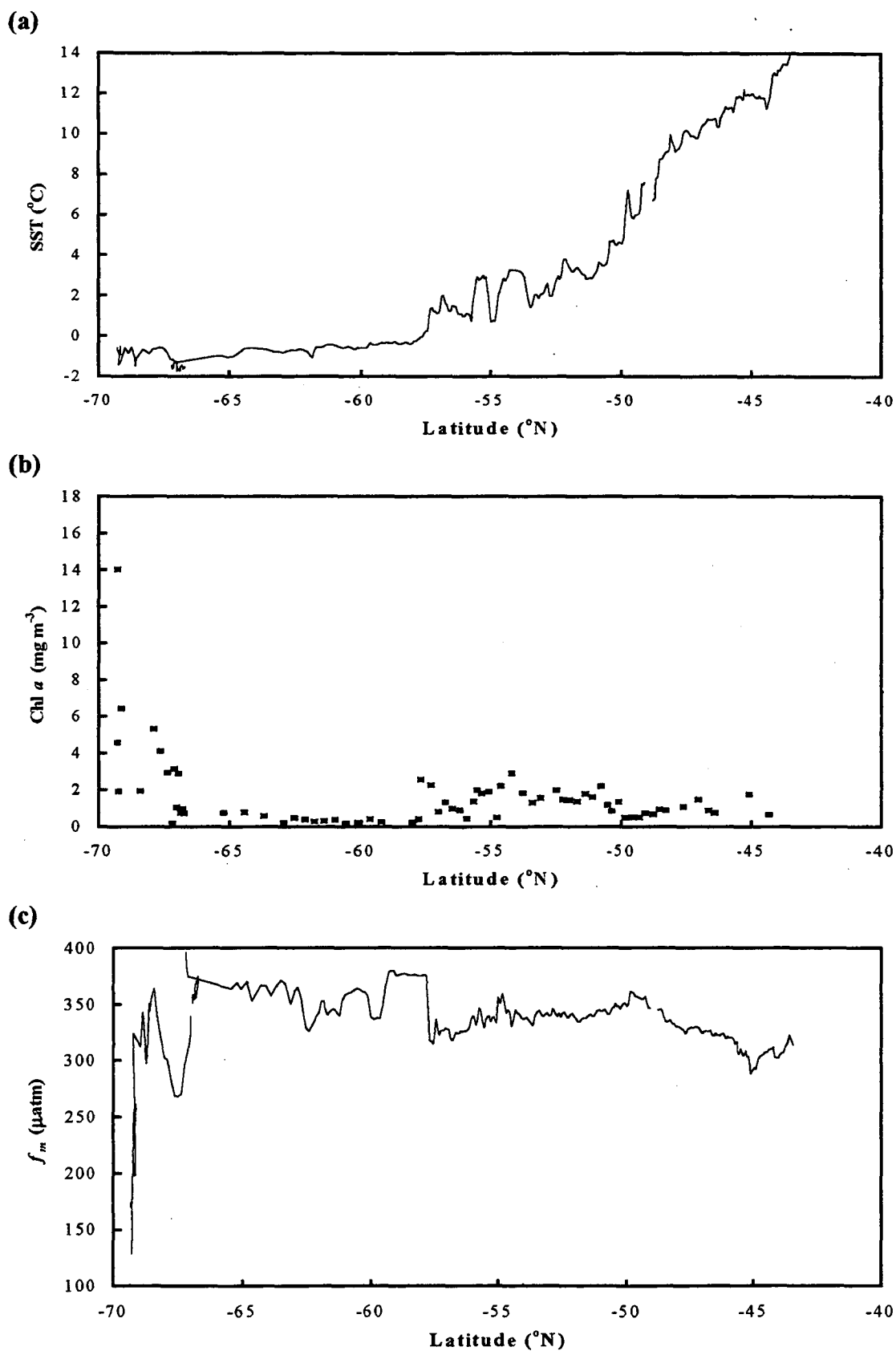


Fig. B.5 Hourly averaged surface ocean measurements of (a) sea surface temperature, (b) chlorophyll *a* concentration and (c) $f\text{CO}_2$ from the *RSV Aurora Australis* transect 4 to 28 December 1993.

REFERENCES

- Allison C.E., R.J. Francey and H.A.J. Meijer (1993) Recommendations for the reporting of stable isotope measurements of carbon and oxygen in CO₂ gas. Report of I.A.E.A. Consultants' Meeting on Stable Isotope Standards and Intercalibration, Vienna, Austria, 1-3 December, 1993.
- Allison C.E., R.J. Francey, R.L. Langenfelds and E.D. Welch (1994) Comparison of high precision Cape Grim CO₂ stable isotope measurements using two mass spectrometers, In: *Baseline Atmospheric Program (Australia) 1991*, ed. A.L. Dick and J.L. Gras, Department of the Environment, Sport and Territories and CSIRO, 10-19.
- Allison C.E. and R.J. Francey (1995) High precision stable isotope measurements of atmospheric trace gases. Report to I.A.E.A. Consultant's Meeting on Stable Isotope Standards and Intercalibration, Vienna, Austria, 1-3 December, 1993 (in press).
- Bacastow R. (1979) Dip in the atmospheric CO₂ level during the mid-1960's, *J. Geophys. Res.*, **84**, 3108-3114.
- Beardsmore D.J., G.I. Pearman and F.R. de Silva (1995) The CSIRO (Australia) atmospheric carbon dioxide monitoring program by infra-red gas analysis: Post 1981 developments and data, *CSIRO Division of Atmospheric Research Tech. Paper* (in prep.)
- Bolin B. (1960) On the exchange of carbon dioxide between the atmosphere and the sea, *Tellus*, **12**, 274-281.
- Broecker H.C. and T.-H. Peng (1974) Gas exchange rates between air and sea, *Tellus*, **24**, 21-35.
- Broecker W.S. and T.-H. Peng (1982) *Tracers in the Sea*, pp. 110-165, pub. Eldigio Press, Palisades, New York.
- Broecker W.S., T.-H. Peng, G. Östlund and M. Stuiver (1985) The distribution of bomb radiocarbon in the ocean, *J. Geophys. Res.*, **90**, 6953-6970.
- Broecker W.S. and T.-H. Peng (1993) What caused the glacial to interglacial CO₂ change?, in *The Global Carbon Cycle, NATO ASI Series*, edited by M. Heimann, Vol. I 15.

- Budd W.F. (1980) The importance of the Antarctic region for studies of the atmospheric carbon dioxide concentration, In: *Carbon Dioxide and Climate: Australian Research*, pp. 115-128, pub. Australian Academy of Science, Canberra, Australia.
- Butler J.H., J.W. Elkins, C.M. Brunson, K.B. Egan, T.M. Thompson, T.J. Conway and B.D. Hall (1988) Trace Gases in and over the West Pacific and East Indian Oceans during the El Niño-Southern Oscillation event of 1987, *NOAA Data Report, ERL ARL-16*, National Oceanic and Atmospheric Administration, U.S.A., 49 pp.
- Chipman D.W., T. Takahashi and S.C. Sutherland (1986) Carbon chemistry of the South Atlantic Ocean and the Weddel Sea: The results of the Atlantic Long Lines (AJAX) Expeditions, October 1983-February 1984, *Tech. Rep. to the N.S.F.*, Lamont-Doherty Geological Observatory, Palisades.
- Chipman D.W., T. Takahashi, D. Breger and S.C. Sutherland (1992) Investigation of carbon dioxide in the South Atlantic and Northern Weddell Sea areas (WOCE sections A-12 and A-21) during the meteor expedition 11/5, January-March, 1990, *Tech. Rep. to the Office of Health and Environmental Res. U.S. Dept. of Energy*, Lamont-Doherty Geological Observatory, Palisades.
- Ciais P., P.P. Tans, J.W.C. White, M. Troler, R.J. Francey, J.A. Berry, D.R. Randall, P.J. Sellers, J.G. Collatz and D.S. Schimel (1995a) Partitioning of ocean and land uptake of CO₂ as inferred by $\delta^{13}\text{C}$ measurements from the NOAA Climate Monitoring and Diagnostics Laboratory Global Air Sampling Network, *J. Geophys. Res.*, **100**(D3), 5051-5070.
- Ciais P., P.P. Tans, M. Troler, J.W.C. White and R.J. Francey (1995b) A large Northern Hemisphere terrestrial CO₂ sink indicated by the $^{13}\text{C}/^{12}\text{C}$ ratio of atmospheric CO₂, *Science*, **269**, 1098-1102.
- Comiso J.C., C.R. McClain, C.W. Sullivan, J.P. Ryan, and C.L. Leonard (1993) Coastal zone color scanner pigment concentrations in the Southern Ocean and relationships to geophysical surface features, *J. Geophys. Res.*, **98**(C2), 2419-2451.
- Conway T.J., Tans P.P., Waterman L.S., Thoning K.W., Kitzis D.R., Masarie K.A. and Zhang N. (1994) Evidence for interannual variability of the carbon cycle from the National Oceanic and Atmospheric Administration/Climate Monitoring and Diagnostics Laboratory Global Air Sampling Network, *J. Geophys. Res.*, **99**(D11), 22,831-22,855.
- Copin-Montégut C. (1985) A method for the continuous determination of the partial pressure of carbon dioxide in the upper ocean, *Mar. Chem.*, **17**, 13-21.
- Copin-Montégut C. (1988) A new formula for the effect of temperature on the partial pressure of CO₂ in seawater, *Mar. Chem.*, **25**, 29-37.

- Copin-Montégut C. (1989) Corrigendum to Copin-Montegut C., 1988. A new formula for the effect of temperature on the partial pressure of CO₂ in seawater, *Mar. Chem.*, 25: 29-37, *Mar. Chem.*, 27, 143-144.
- Craig H. (1953) The geochemistry of the stable carbon isotopes, *Geochim. Cosmochim. Acta*, 3, 53-92.
- Craig H. (1957) Isotopic standards for carbon and oxygen and correction factors for mass spectrometric analysis of carbon dioxide, *Geochim. Cosmochim. Acta*, 12, 133-149.
- de Baar H.J.R., J.T.M. de Jong, D.C.E. Bakker, B.M. Löscher, C. Veth, U. Bathmann and V. Smetacek (1995) Importance of iron for plankton blooms and carbon dioxide drawdown in the Southern Ocean, *Nature*, 373, 412-415.
- Dickson A.G. and F.J. Millero (1987) A comparison of the equilibrium constants for the dissociation of carbonic acid in seawater media, *Deep-Sea Res.*, 34: 1733-1743.
- Enting I.G. and J.V. Mansbridge (1991) Latitudinal distribution of sources and sinks of CO₂: Results of an inversion study, *Tellus*, 43B, 156-170.
- Enting I.G., C.M. Trudinger, R.J. Francey and H. Granek (1993) Synthesis inversion of atmospheric CO₂ using the GISS Tracer Transport Model, *CSIRO Aust. Div. Atmos. Res. Tech. Pap. No. 29*, 45 pp.
- Enting I.G., C.M. Trudinger and R.J. Francey (1995) A synthesis inversion of the concentration and $\delta^{13}\text{C}$ of atmospheric CO₂, *Tellus*, 47B, 35-52.
- Esbensen S.K. and Y. Kushnir (1981) The heat budget of the global ocean, An atlas based on estimates from surface marine observations, *Rep. 29*, Climate Research Institute, Oregon State University, Corvallis, Oregon.
- Farquar G.D., M.H. O'Leary and J.A. Berry (1982) On the relationship between carbon isotope discrimination and the intercellular carbon dioxide concentration in leaves, *Aust. J. Plant Physiol.*, 9, 121-137.
- Fleagle R.G. and J.A. Businger (1980) An introduction to Atmospheric Physics, International Geophysics Series, Vol. 25, 2nd Ed., Academic Press, New York, pp. 432.
- Francey R.J. (1985) Cape Grim isotope measurements - A preliminary assessment, *J. Atmos. Chem.*, 3, 247-260.
- Francey R.J., C.E. Allison, L.P. Steele, R.L. Langenfelds, E.D. Welch, J.W.C. White, M. Troler, P.P. Tans and K.A. Masarie (1994) Intercomparison of stable isotope measurements of CO₂, *Climate Monitoring and Diagnostics Laboratory No. 22, Summary Report 1993*, NOAA, Boulder, Colorado, 106-110.

- Francey R.J., P.P. Tans, C.E. Allison, I.G. Enting, J.W.C. White and M. Troler (1995) Changes in oceanic and terrestrial carbon uptake since 1982, *Nature*, **373**, 326-330.
- Francey R.J., L.P. Steele, R.L. Langenfelds, M. Lucarelli, C.E. Allison, D. Beardsmore, S. Coram, N. Derek, F. de Silva, D. Etheridge, P. Fraser, R. Henry, B. Turner and E.D. Welch (1996) Global Atmospheric Sampling Laboratory (GASLAB): supporting and extending the Cape Grim trace gas programs, In: *Baseline Atmospheric Program (Australia) 1993*, ed. R.J. Francey, A.L. Dick and N. Derek, Department of the Environment, Sport and Territories and CSIRO (in press).
- Francois R., M.A. Altabet, R. Goericke, D.C. McCorkle, C. Brunet and A. Poisson (1993) Changes in the $\delta^{13}\text{C}$ of surface water particulate organic matter across the Subtropical Convergence in the SW Indian Ocean, *Glob. Biogeochem. Cyc.*, **7**, 627-644.
- Geoffrey S.W. and G.F. Humphrey (1975) New spectrophotometric equations for determining Chlorophyll *a*, *b*, *c*1, *c*2 in higher plants, algae and natural phytoplankton, *Biochem. Physiol. Pflanzen*, **167**, 191-194.
- Gill A.E. (1982) Atmosphere-ocean dynamics, International Geophysics Series, Vol. 30, Academic Press, Inc., San Diego, 662 p.
- Gordon L.I. (1973) A study of carbon dioxide partial pressures in surface waters of the Pacific Ocean, PhD thesis, Oregon State University, USA.
- Goyet C., F.J. Millero, A. Poisson and D.K. Shafer (1993) Temperature dependence of CO_2 fugacity in seawater, *Marine Chem.*, **44**, 205-219.
- Halpern D. (1993) SSMI wind speed measurements over the Southern Hemisphere oceans, In: Preprints of the Fourth International Conference on Southern Hemisphere Meteorology and Oceanography, American Met. Soc., USA, p. 19-20.
- Halpern D., A. Hollingsworth and F. Wentz (1994a) ECMWF and SSM/I Global Surface Wind Speeds, *J. Atmos. Oceanic Tech.*, **11**, 780-788.
- Halpern D., W. Knauss, O. Brown, M. Freilich and F. Wentz (1994b) An atlas of monthly mean distributions of SSMI surface wind speed, ARGOS buoy drift, AVHRR/2 sea surface temperature, AMI surface wind components, and ECMWF surface wind components during 1992, *JPL Publication 94-4*, published by National Aeronautics and Space Administration, Jet Propulsion Laboratory, California Institute of Technology, Pasadena, California, 143 pp.
- Hashida G., T. Nakazawa, S. Aoki, S. Murayama, T. Yamanouchi, M. Tanaka, A. Shimizu, M. Hayashi and K. Iwai (1994) Measurements of the partial pressure of CO_2 in the air and surface sea water on board icebreaker "Shirase", In:

Proceedings of the International Symposium on Global Cycles of Atmospheric Greenhouse Gases, March 7-10, 1994, Sendai, Japan, Tohoku University, 192-195.

Hasse L. (1971) The sea surface temperature deviation and the heat flow at the sea-air interface, *Boundary Layer Meteorol.*, **1**, 368-379.

Heimann M. and C.D. Keeling (1989) A three-dimensional model of atmospheric CO₂ transport based on observed winds: 2. Model description and simulated tracer experiments, In: *Aspects of climatic variability in the Pacific and the Western Americas*, Geophys. Monogr. 55, edited by D.H. Peterson, pp. 237-275, AGU, Washington, D.C.

Hoover T.E. and D.C. Berkshire (1969) Effects of hydration in carbon dioxide exchange across an air-water interface, *J. Geophys. Res.*, **74**, 456-464.

Houghton J.T., B.A. Callander and S.K. Varney (Ed.) (1992) *Climatic Change 1992: The Supplementary Report to the IPCC Scientific Assessment*, Cambridge University Press, Cambridge, 200 pp.

Inoue H. and Y. Sugimura (1988) Distribution and variations of oceanic carbon dioxide in the western North Pacific, eastern Indian, and Southern Ocean south of Australia, *Tellus*, **40B**, 308-320.

Jacques G. and M. Fukuchi (1994) Phytoplankton of the Indian Ocean, In: *Southern Ocean ecology: the BIOMASS perspective*, edited by Sayed Z. El-Sayed, Cambridge University Press, 399 p.

Jähne B., G. Heinz and W. Dietrich (1987a) Measurement of the diffusion coefficients of sparingly soluble gases in water with a modified Barrer method, *J. Geophys. Res.*, **92**(C10), 10,767-10,776.

Jähne B., K.O. Münnich, R. Börsinger, A. Dutzi, W. Huber and P. Libner (1987b) On the parameters influencing air-water gas exchange, *J. Geophys. Res.*, **92**(C2), 1937-1949.

Jähne B., P. Libner, R. Fischer, T. Billen and E.J. Plate (1989) Investigating the transfer process across the free aqueous viscous boundary layer by the controlled flux method, *Tellus*, **41B**, 177-195.

Keeling C.D. (1961) The concentration and isotopic abundance of carbon dioxide in rural and marine air, *Geochim. Cosmochim. Acta*, **24**, 277-298.

Keeling C.D., S.C. Piper and M. Heimann (1989) A three-dimensional model of atmospheric CO₂ transport based on observed winds: 4. Mean annual gradients and interannual variations, In: *Aspects of climatic variability in the Pacific and the Western Americas*, Geophys. Monogr. 55, edited by D.H. Peterson, pp. 305-363, AGU, Washington, D.C.

- Keir R.S. (1993) Are atmospheric CO₂ content and Pleistocene climate connected by windspeed over a polar Mediterranean Sea? *Global and Planet. Change*, **8**, 59-68.
- Law R., I. Simmonds and W.F. Budd (1992) Application of an atmospheric tracer model to high southern latitudes, *Tellus*, **44B**, 358-370.
- Liss P.S. (1973) Processes of gas exchange across an air-water interface, **20**, 221-238.
- Liss P.S. and L. Merlivat (1986) Air-sea gas exchange rates: introduction and synthesis, In: *The Role of Air-Sea Exchange in Geochemical Cycling*, ed. P. Buat-Menard, pp. 113-127, D. Reidel, Norwell, Mass.
- Maier-Reimer E. and K. Hasselmann (1987) Transport and storage of CO₂ in the ocean - an inorganic ocean-circulation carbon cycle model, *Climate Dynamics*, **2**, 63-90.
- Merlivat L. and L. Memery (1983) Gas exchange across an air-water interface: Experimental results and modelling of bubble contribution to transfer, *J. Geophys. Res.*, **88**, 707-724.
- Metzl N., C. Beauverger, C. Brunet, C. Goyet and A. Poisson (1991) Surface water carbon dioxide in the southwest Indian sector of the Southern Ocean: a highly variable CO₂ source/sink region in summer, *Marine Chemistry*, **35**, 85-95.
- Metzl N., A. Poisson, F. Louanchi, C. Brunet, B. Schauer and B. Bres (1995) Spatio-temporal distributions of air-sea fluxes of CO₂ in the Indian and Antarctic oceans - A first step, *Tellus*, **47B**, 56-69.
- Milne P.J. and J.D. Smith (1980) Measurement of dissolved carbonate parameters in Antarctic coastal waters, In: *Carbon Dioxide and Climate: Australian Research*, Ed. G.I. Pearman, Pub. Australian Academy of Science, Canberra.
- Mook W.G., J.C. Bommerson and W.H. Staverman (1974) Carbon isotope fractionation between dissolved bicarbonate and gaseous carbon dioxide, *Earth Plan. Sci. Let.*, **22**, 169-176.
- Muench, R.D. (1990) Mesoscale phenomena in the polar oceans, In: *Polar Oceanography, Part A: Physical Science*, Ed. Walker O. Smith, Jr., Academic Press, Inc., San Diego, 223-285.
- Murphy P.P., R.A. Feely, R.H. Gammon, D.E. Harrison, K.C. Kelly and L.S. Waterman (1991) Assessment of the air-sea exchange of CO₂ in the Southern Pacific during austral autumn, *J. Geophys. Res.*, **96**(C11), 20455-20465.
- Parkinson C.L. (1992) Interannual variability of monthly Southern Ocean sea ice distributions, *J. Geophys. Res.*, **97**(C4), 5349-5363.

- Pearman G.I. and P. Hyson (1986) Global transport and inter-reservoir exchange of carbon dioxide with particular reference to stable isotopic distributions, *J. Atmos. Chem.*, **4**, 81-124.
- Peng T-H., W.S. Broecker, G.G. Mathieu and Y.-H. Li (1979) Radon evasion rates in the Atlantic and Pacific Oceans as determined during the GEOSECS program, *J. Geophys. Res.*, **84**, 2471-2486.
- Plumb R.A. and J.D. Mahlman (1987) The zonally averaged transport characteristics of the GFDL General Circulation/Transport Model, *J. Atmos. Sci.*, **44**, 298-327.
- Poisson A., N. Metzl, C. Brunet, B. Schauer, B. Bres, D. Ruiz-Pino and F. Louanchi (1993) Variability of sources and sinks of CO₂ in the Western Indian and Southern Oceans during the year 1991, *J. geophys. Res.*, **98**(C12), 22759-22778.
- Ricker W.E. (1973) Linear Regressions in Fishery Research, *J. Fish. Res. Board Can.*, **30**, 409-434.
- Robertson J.E. and A.J. Watson (1992) Thermal skin effect of the surface ocean and its implications for CO₂ uptake, *Nature*, **358**, 738-740.
- Robertson J.E. and A.J. Watson (1995) A summertime sink for atmospheric carbon dioxide in the Southern Ocean between 88° W and 80° E, *Deep Sea Res. II*, **42**, 1081-1091.
- Sakshaug E. and H.R. Skjoldal (1989) Life at the ice edge, *AMBIO*, **18**, 60-67.
- Sarmiento J.L. and E.T. Sundquist (1992) Revised budget for the oceanic uptake of anthropogenic carbon dioxide, *Nature*, **356**, 589-593.
- Schneider B. and J. Morlang (1995) Distribution of the CO₂ partial pressure in the Atlantic ocean between Iceland and the Antarctic peninsula, *Tellus*, **47B**, 93-102.
- Siegenthaler U. (1986) Carbon dioxide: Its natural cycle and anthropogenic perturbation, In: *The Role of Air-Sea Exchange in Geochemical Cycling*, ed. P. Buat-Menard, pp. 209-247, D. Reidel, Norwell, Mass.
- Skirrow G. (1975) The dissolved gases - Carbon dioxide. In: *Chemical Oceanography, Vol. 2.*, Ed. J.P. Riley and G. Skirrow, Academic Press, London, pp. 1-192.
- Smethie W.M., T.T. Takahashi, D.W. Chipman and J.R. Ledwell (1985) Gas exchange and CO₂ flux in the tropical Atlantic Ocean determined from ²²²Rn and pCO₂ measurements, *J. Geophys. Res.*, **90**, 7005-7022.

- Smith W.O. and D.M. Nelson (1986) The importance of ice-edge phytoplankton blooms in the Southern Ocean, *BioScience*, **36**, 251-257.
- Sullivan C.W., K.R. Arrigo, C.R. McClain, J.C. Comiso and J. Firestone (1993) Distributions of phytoplankton blooms in the Southern Ocean, *Nature*, **262**, 1832-1837.
- Sundquist E.T. (1993) The global carbon dioxide budget, *Science*, **259**, 934-941.
- Takahashi T. (1961) Carbon dioxide in the atmosphere and in Atlantic Ocean water, *J. Geophys. Res.*, **66** (2), 477-494.
- Takahashi T. (1989) The carbon dioxide puzzle, *Oceanus*, **32**, 22-29.
- Takahashi T., W.S. Broecker, A.E. Bainbridge and R.F. Weiss (1980) Carbonate chemistry of the Atlantic, Pacific and Indian Oceans: The results of the GEOSECS Expeditions, 1972-1978, *Tech. Report No. 1*, CU-1-80, Lamont Doherty Geological Observatory.
- Takahashi T. and D. Chipman (1982) Carbon Dioxide partial pressure in surface waters of the southern ocean, *Antarct. J. U.S.*, **17**, 103-104.
- Takahashi T., J. Olafsson, J.G. Goddard, D.W. Chipman and S.C. Sutherland (1993) Seasonal variation of CO₂ and nutrients in the high-latitude surface oceans: a comparative study, *Glob. Geochem. Cyc.*, **7**, 843-878.
- Tans P.P., I.Y. Fung and T. Takahashi (1990) Observational constraints on the global atmospheric CO₂ budget, *Science*, **247**, 1431-1438.
- Tans P.P., J.A. Berry and R.F. Keeling (1993) Oceanic ¹³C/¹²C observations: a new window on ocean CO₂ uptake, *Global Biogeochemical Cycles*, **7**, 353-368.
- Tans P.P., I.Y. Fung, and I.G. Enting (1995) Storage versus flux budgets: The terrestrial uptake of CO₂ during the 1980's, in *Biotic Feedbacks in the Global Climate System: Will the Warming Feed the Warming?*, edited by G.M. Woodwell and F.T. Mackenzie, pp. 351-366, Oxford University Press, New York.
- Teissier G. (1948) La relation d'allométrie: sa signification statistique et biologique, *Biometrics*, **4**, 14-48.
- Tilbrook B. and H.M. Beggs (1996) Data report on measurements of fugacity of carbon dioxide in surface waters measured on SRV Aurora Australis in the Southern Ocean between 1991 and 1995, (in prep.)
- Tréguer P. and G. Jacques (1992) Dynamics of nutrients and phytoplankton, and fluxes of carbon, nitrogen and silicon in the Antarctic Ocean, *Polar Biol.*, **12**, 149-162.

- Upstill-Goddard R.C., A.J. Watson, P.S. Liss and M.I. Liddicoat (1990) Gas transfer in lakes measured with SF₆, *Tellus*, **42B**, 364-377.
- Van Scoy K.A., K.P. Morris, J.E. Robertson and A.J. Watson (1995) Thermal skin effect and the air-sea flux of carbon dioxide: A seasonal high-resolution estimate, *Glob. Biogeochem. Cyc.*, **9**, 253-262.
- Wanninkhof R., J. Ledwell and W.S. Broecker (1985) Gas exchange wind speed relation measured with sulfur hexafluoride on a lake, *Science*, **227**, 1224-1226.
- Wanninkhof R. and L. Bliven (1991) Relationship between gas exchange, wind speed and radar backscatter in a large wind-wave tank, *J. Geophys. Res.*, **96**, 2785-2796.
- Wanninkhof R. (1992) Relationship between wind speed and gas exchange over the ocean, *J. Geophys. Res.*, **97**(C5), 7373-7382.
- Wanninkhof R. and K. Thoning (1993) Measurement of fugacity of CO₂ in surface water using continuous and discrete sampling methods, *Marine Chem.*, **44**, 189-204.
- Wanninkhof R., W. Asher, R. Weppernig, H. Chen, P. Schlosser, C. Langdon and R. Sambrotto (1993) Gas transfer experiment on Georges Bank using two volatile deliberate tracers, *J. Geophys. Res.*, **98**(C11), 20237-20248.
- Watson A.J., R.C. Upstill-Goddard and P.S. Liss (1991) Air-sea gas exchange in rough and stormy seas measured by a dual-tracer technique, *Nature*, **349**, 145-147.
- Weiss R.F. (1974) Carbon dioxide in water and seawater: the solubility of a non-ideal gas, *Marine Chemistry*, **2**, 203-215.
- Weiss R.F. and B.A. Price (1980) Nitrous oxide solubility in water and seawater, *Mar. Chem.*, **8**, 347-359.
- Wentz F.J., S. Peteherych and L.A. Thomas (1984) A model function for ocean radar cross sections at 14.6 Ghz, *J. Geophys. Res.*, **89**(C3), 3689-3704.
- Woodcock A.H. (1941) Surface cooling and streaming in shallow fresh and salt waters, *J. Marine Res.*, **4**, 153-161.
- Wright S.W. and J.D. Shearer (1984) Rapid extraction and high-performance liquid chromatography of chlorophylla and carotenoids from marine phytoplankton, *J. Chromatogr.*, **294**, 281-295.
- Zhang J., P.D. Quay and D.O. Wilbur (1995) Carbon Isotope fractionation during gas-water exchange and dissolution of CO₂, *Geochimica et Cosmochimica Acta*, **59**, 107-114.